

AD-A050 483

AEROSPACE CORP EL SEGUNDO CALIF IVAN A GETTING LABS F/G 3/2  
COMPILATION OF SCIENTIFIC RESULTS FROM THE SATELLITE OV1-17.(U)  
DEC 77 H R RUGGE F04701-77-C-0078  
TR-0078(3960-01)-1 SAMS0-TR-77-216 NL

UNCLASSIFIED

1 OF 4  
AD  
A050483



②  
B.S.

AD A 050483

## Compilation of Scientific Results from the Satellite OV1-17

H. R. RUGGE

Space Sciences Laboratory  
The Ivan A. Getting Laboratories  
The Aerospace Corporation  
El Segundo, Calif. 90245

Final Report

APPROVED FOR PUBLIC RELEASE;  
DISTRIBUTION UNLIMITED

Prepared for  
SPACE AND MISSILE SYSTEMS ORGANIZATION  
AIR FORCE SYSTEMS COMMAND  
Los Angeles Air Force Station  
P.O. Box 92960, Worldway Postal Center  
Los Angeles, Calif. 90009



THE AEROSPACE CORPORATION

DDC  
RECEIVED  
FEB 27 1978  
B

AD No.  
JDC FILE COPY



This final report was submitted by The Aerospace Corporation, El Segundo, CA 90245, under Contract No. F04701-77-C-0078 with the Space and Missile Systems Organization, Deputy for Advanced Space Programs, P.O. Box 92960, Worldway Postal Center, Los Angeles, CA 90009. It was reviewed and approved for The Aerospace Corporation by G. A. Paulikas, Director, Space Sciences Laboratory. Lieutenant Dara Batki, SAMSO/YCPT, was the project officer for Advanced Space Programs.

This report has been reviewed by the Information Office (OI) and is releasable to the National Technical Information Service (NTIS). At NTIS, it will be available to the general public, including foreign nations.

This technical report has been reviewed and is approved for publication. Publication of this report does not constitute Air Force approval of the report's findings or conclusions. It is published only for the exchange and stimulation of ideas.

Dara Batki  
Dara Batki, Lt. USAF  
Project Officer

Robert W. Lindemuth  
Robert W. Lindemuth, Lt Col, USAF  
Chief, Technology Plans Division

FOR THE COMMANDER

Leonard E. Baltzell  
Leonard E. Baltzell, Col, USAF  
Asst. Deputy for Advanced Space Programs

UNCLASSIFIED

SECURITY CLASSIFICATION OF THIS PAGE (When Data Entered)

19 REPORT DOCUMENTATION PAGE		READ INSTRUCTIONS BEFORE COMPLETING FORM	
1. REPORT NUMBER SAMSO TR-77-216	2. GOVT ACCESSION NO.	3. RECIPIENT'S CATALOG NUMBER	
4. TITLE (and Subtitle) COMPILATION OF SCIENTIFIC RESULTS FROM THE SATELLITE OV1-17		5. TYPE OF REPORT & PERIOD COVERED Final rept.	
7. AUTHOR(s) Hugo R./Rugge		6. PERFORMING ORG. REPORT NUMBER TR-0078(3960-01)-1	
9. PERFORMING ORGANIZATION NAME AND ADDRESS The Aerospace Corporation El Segundo, CA 90245		8. CONTRACT OR GRANT NUMBER(s) F04701-77-C-0078	
11. CONTROLLING OFFICE NAME AND ADDRESS Space and Missile Systems Organization Air Force Systems Command Los Angeles, CA 90009		10. PROGRAM ELEMENT, PROJECT, TASK AREA & WORK UNIT NUMBERS	
14. MONITORING AGENCY NAME & ADDRESS (if different from Controlling Office)		12. REPORT DATE 2 Dec 1977	
		13. NUMBER OF PAGES 317	
		15. SECURITY CLASS. (of this report) Unclassified	
16. DISTRIBUTION STATEMENT (of this Report) Approved for public release; distribution unlimited		15a. DECLASSIFICATION/DOWNGRADING SCHEDULE	
17. DISTRIBUTION STATEMENT (of the abstract entered in Block 20, if different from Report)			
18. SUPPLEMENTARY NOTES			
19. KEY WORDS (Continue on reverse side if necessary and identify by block number) OV1-17 Satellite Magnetosphere Protons Solar X-Rays Solar Protons			
20. ABSTRACT (Continue on reverse side if necessary and identify by block number) This compilation consists of all scientific papers published by The Aerospace Corporation Space Sciences Laboratory scientists as of October 1977 based on data obtained wholly, or in part, from experiments flown on the OV1-17 satellite. The total number of papers is severely limited because only three of the seven Aerospace experiments on board OV1-17 were able to obtain any useful data as a result of the inability of the satellite to achieve proper orientation. Even these three experiments received useful data for only relatively short time periods. In addition to the scientific papers, a brief description of the			

DD FORM 1473  
(FACSIMILE)

409 944

UNCLASSIFIED  
SECURITY CLASSIFICATION OF THIS PAGE (When Data Entered)DDC  
RECEIVED  
FEB 27 1978  
B



UNCLASSIFIED

SECURITY CLASSIFICATION OF THIS PAGE(When Data Entered)

19. KEY WORDS (Continued)

20. ABSTRACT (Continued)

OV1-17 satellite is included.

This compilation consists of all scientific reports published by The Aerospace Corporation Space Sciences Laboratory scientists as of October 1977 based on data obtained wholly or in part from experiments flown on the OV1-17 satellite. The total number of reports is seventy limited because only those of the seven Aerospace experiments on board OV1-17 were able to obtain any useful data as a result of the inability of the satellite to achieve proper orientation. Even these few experiments received useful data for only ten days short of the mission. In addition to the scientific papers, a brief description of the

UNCLASSIFIED

SECURITY CLASSIFICATION OF THIS PAGE(When Data Entered)



## PREFACE

The scientific data obtained from the OV1-17 satellite are the result of efforts of a large number of people, many of whom have never been recognized as authors or, perhaps, even in Acknowledgments in scientific papers. The OV1-17 satellite was designed, fabricated, and tested by the Convair Division of the General Dynamics Corporation, San Diego. The program was sponsored and directed by the Air Force Office of Aerospace Research (OAR) and was contractually monitored by the Air Force Space and Missile Systems Organization (SAMSO). Launch support was provided by the SAMSO/SESP (now the Space Test Program) organization. Orbital support was provided by the Eastern Test Range of the Air Force National Range Division. None of the results that were obtained by The Aerospace Corporation and other scientists would have been possible without the wholehearted cooperation of these groups. Additionally, the successfully analyzed Aerospace data were, in large part, the result of outstanding efforts by those engineers, technicians, and support personnel who participated in the design, fabrication, testing, and calibration of the experiments flown on the OV1-17 satellite.

ACCESSION for	
NTIS	White Section <input checked="" type="checkbox"/>
DDC	Buff Section <input type="checkbox"/>
UNANNOUNCED	<input type="checkbox"/>
JUSTIFICATION _____	
BY _____	
DISTRIBUTION/AVAILABILITY CODES	
Dist.	Avail. and/or SPECIAL
A	

# CONTENTS

PREFACE .....	1
I. INTRODUCTION .....	5
II. SOLAR X-RAY OBSERVATION OF FORBIDDEN LINES IN THE HELIUM ISOELECTRONIC SEQUENCE .....	11
III. FURTHER RESULTS ON O VII X-RAY CORONAL LINE EMISSION .....	47
IV. OBSERVATION OF AUTOIONIZING STATES IN THE SOLAR CORONA .....	59
V. RELATIVE INTENSITIES OF THE LYMAN LINES OF HYDROGEN-LIKE OXYGEN, MAGNESIUM, AND SILICON IN THE SOLAR CORONA .....	93
VI. RELATIVE CORONAL ABUNDANCES DERIVED FROM X-RAY OBSERVATIONS, I: SODIUM, MAGNESIUM, ALUMINUM, SILICON, SULFUR, AND ARGON .....	115
VII. RELATIVE CORONAL ABUNDANCES DERIVED FROM X-RAY OBSERVATIONS, III: THE EFFECT OF CASCADES ON THE RELATIVE INTENSITY OF Fe XVII LINE FLUXES AND A REVISED IRON ABUNDANCE .....	171
VIII. THE RELATIVE ABUNDANCE OF NEON AND MAGNESIUM IN THE SOLAR CORONA .....	217
IX. OBSERVATION AND ANALYSIS OF Fe XVIII SOLAR X-RAY EMISSION .....	239
X. POLAR CAP MEASUREMENTS OF SOLAR-FLARE PROTONS WITH ENERGIES DOWN TO 12.4 keV .....	291
XI. OBSERVATIONS OF RING CURRENT PROTONS AT LOW ALTITUDES .....	315
XII. OBSERVATIONS OF PRECIPITATING PROTONS WITH RING CURRENT ENERGIES .....	337

I. INTRODUCTION



## I. INTRODUCTION

A payload of twelve experiments was launched in March 1969 onboard the U.S. Air Force OV1-17 satellite. The major purpose of this payload was to conduct a number of investigations concerning the earth's atmosphere and magnetosphere, the sun, and environmental effects of space.

The payload consisted of seven experiments supplied by the Space Sciences Laboratory of The Aerospace Corporation and one experiment each supplied by the Space Sciences Laboratory of the University of California, Berkeley, the Air Force Materials Laboratory, and the Air Force Aerospace Research Laboratory. The Air Force Geophysics Laboratory had two experiments on board the OV1-17 satellite as well.

The seven Aerospace experiments were designed to make measurements primarily of: (1) solar x-rays, (2) energetic precipitating protons and electrons, (3) low-energy precipitating protons and electrons, (4) the  $O_2$  and  $O_3$  altitude distribution in the earth's upper atmosphere, (5) far ultraviolet atmospheric radiation, (6) earth horizon ultraviolet dayglos, and (7) earth horizon visible nightglow. The other experiments onboard were designed to make measurements of: (1) dc and low-frequency electric fields, (2) property changes of thermal control coatings, (3) CdS solar cell efficiency, (4) extremely-low-frequency (ELF) propagation in the ionosphere, and (5) radar meteor trail calibrations.

The OV1-17 satellite was launched at 0747 UT on 18 March 1969 in a triple configuration along with the OV1-18 and OV1-19 satellites onboard Atlas Boost Vehicle 104F from Vandenberg Air Force Base. The initial orbital parameters were:

Perigee	217 nmi
Apogee	253 nmi
Inclination	99.2°
Period	93.2 min

The satellite was to have been three-axis stabilized with one axis always pointing to the center of the earth. A sophisticated "Vertistat" gravity gradient deployable boom system was included on board the satellite to accomplish this goal. Unfortunately, for reasons not entirely clear, even at this time, the gravity gradient stabilization of the OV1-17 satellite was not achieved. The "Vertistat" primary and damper booms deployed satisfactorily. However, the vehicle did not "capture" but spun about an axis approximately normal to the orbit plane. The spin rate slowly increased from 0.04 rpm to 0.45 rpm over a five month period, despite efforts to diagnose the cause of the spin and to correct it.

The effect of this unexpected spin-up of the satellite on the ability of many of the experiments on board to obtain useful data was extremely serious. Of the seven Aerospace experiments on board, only three were able to usefully analyze any of the data obtained. Only minimal amounts of useful data were obtained by these experiments compared to the amount of data originally anticipated.

The three Aerospace experiments that were able to analyze some of the data obtained were those that measured solar x-rays and energetic and low-energy precipitating electrons and protons. The experiments are described briefly in some of the scientific papers included in this report.

The OV1-17 satellite is shown in Figure 1. It consisted of a cylindrical section 27 inches in diameter and 32 inches long, which served as the container for the scientific payload. A faceted dome containing solar cells was attached to each end of the cylinder, which made the overall length of the satellite 54 inches. The total weight of the satellite was approximately 315 pounds.

Figure 2 shows the OV1-17, -18, and -19 satellites mounted in launch configuration on a common truss assembly that is attached directly to the Atlas booster.

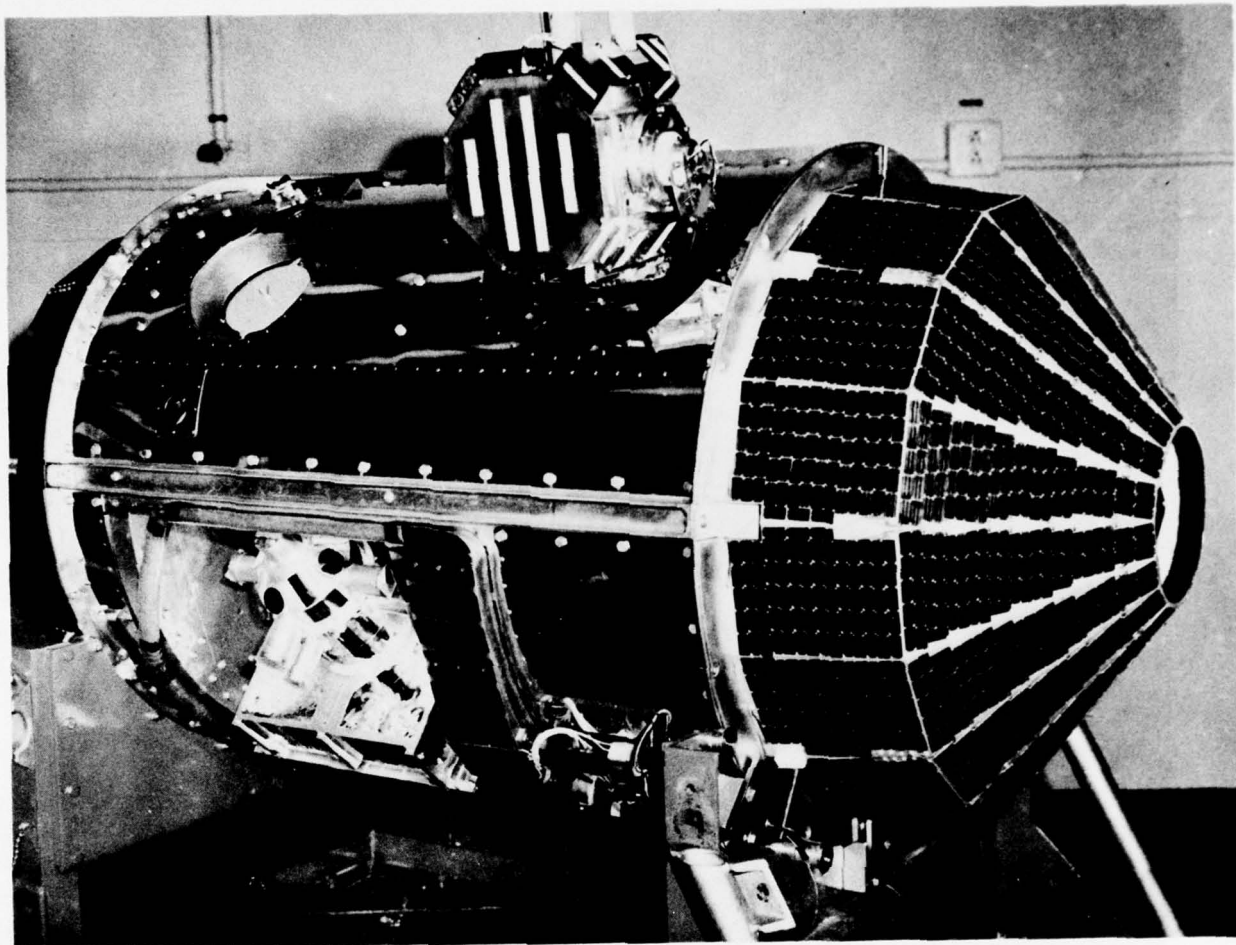


Figure 1. The OV1-17 satellite. Two of the three Aerospace experiments that were able to obtain some useful data from the unstabilized satellite are visible. The solar biaxially pointed x-ray experiment is near the top center of the figure and the energetic precipitating proton and electron experiment with its many "fingers" containing geiger tubes and semi-conductor detectors (the Urchin) is visible at the lower left of the spacecraft. In flight, the Urchin was extended on a short boom.



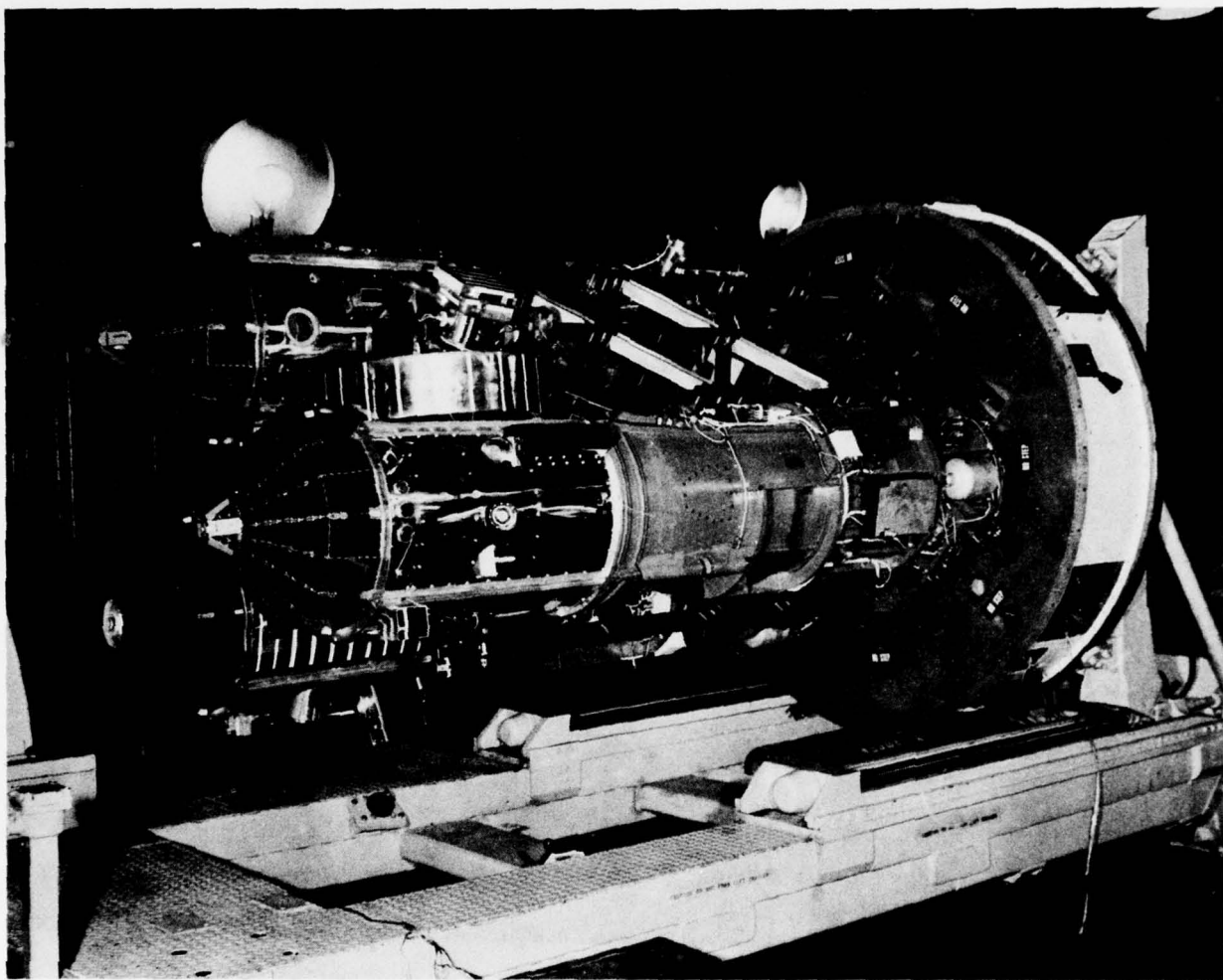


Figure 2. The OV1-17, OV1-18, and OV1-19 satellites mounted on the support truss. OV1-17 is the uppermost satellite. The x-ray solar pointer can be seen in this view.

The purpose of this report is to provide a compilation of information published up to October 1977 that is the result of analyses of the data from the three Aerospace experiments that were able to obtain any useful data from the unstabilized spacecraft. This compilation will clearly contain the majority of the information to be obtained from these experiments. However, analysis of data from one of these experiments (solar x-rays) is still continuing.

## II. SOLAR X-RAY OBSERVATION OF FORBIDDEN LINES IN THE HELIUM ISOELECTRONIC SEQUENCE\*

A. B. C. Walker, Jr., and H. R. Rugge

### ABSTRACT

The  $1s^2\ ^1S_0 - 1s2p\ ^1P_1$  resonance and the  $1s^2\ ^1S_0 - 1s2p\ ^3P_1$  intercombination lines in the helium-like ions of carbon, oxygen, neon, and magnesium observed in the solar corona are accompanied by strong, longer wavelength satellites. Gabriel and Jordan identify these longer wavelength satellites as due to single-photon decay of the  $1s2s\ ^3S_1$  level, and point out that the intensity ratio of the  $^3P_1$  and  $^3S_1$  lines is a sensitive function of electron density at typical coronal densities. We have observed these three lines in oxygen, neon, aluminum, silicon, and sulphur with a scanning Bragg crystal spectrometer, which was orbited on the satellite OV1-17 (1969-025A), launched on 18 March 1969. In this report, we present the relative intensities of each of the three lines and discuss the coronal densities that they predict.

\*This paper has also been published as TR-0066(9260-02)-4, The Aerospace Corporation, El Segundo, California (15 November 1969) and in Astronomy and Astrophysics 5, 4-11 (1970).

Forbidden Lines in the Helium  
Isoelectronic Sequence



## CONTENTS

ABSTRACT .....	11
I. INTRODUCTION .....	15
II. EXPERIMENTAL DETAILS .....	17
III. EXPERIMENTAL DATA .....	19
IV. IDENTIFICATION OF LINES .....	25
V. THEORY .....	33
VI. DISCUSSION OF LINE RATIOS .....	37
VII. DISCUSSION OF THE RESULTS .....	41
ACKNOWLEDGMENTS .....	43
REFERENCES .....	45

## TABLES

1. Extrapolated Wavelengths of Lines in the HeI Isoelectronic Sequence .....	26
2. Lines Observed in the EDDT Scan .....	27
3. Intensities of OVII and NeIX Lines .....	29
4. Line Ratios and Predicted Densities (20 March 1969) .....	30

## FIGURES

1.	Solar X-Ray Spectrum Observed with an EDDT Spectrometer; Obtained at 0604 UT on March 20, 1969 . . . . .	20
2.	Solar X-Ray Spectrum Observed with a KAP Spectrometer; Obtained at 0615 UT on March 20, 1969 . . . . .	21
3.	Solar X-Ray Spectrum Between 4 and 8.5 Å During a Period of High Solar Activity . . . . .	22
4.	Dependence of the Ratio of the Forbidden to Intercombination Line Intensities (R) for Helium-Like Ions on Electron Density. . . . .	35

## I. INTRODUCTION

Long-wavelength satellites to the  $1s^2\ ^1S_0 - 1s2p\ ^1P_1$  and  $^3P_1$  lines in helium-like ions have been observed in laboratory plasmas (Edlen and Tyren 1939; Jahoda, Ribe, Sawyer, and Stratton 1961; Roth and Elton 1968) and in the solar corona (Austin, Purcell, Tousey, and Widing 1966; Fritz, Kreplin, Meekins, Unzicker, and Friedman 1967; Rugge and Walker 1968; Walker and Rugge 1969; Jones, Freeman, and Wilson 1968; Meekins, Kreplin, Chubb, and Friedman 1969; Evans and Pounds 1969). Gabriel and Jordan (1969a) point out that the laboratory and coronal satellites have different origins. The laboratory lines are due to transitions in doubly excited lithium-like ions. In the solar corona, the strong satellite line that is observed is due to the single-photon decay of the metastable  $1s2s\ ^3S_1$  level. Griem (1969) calculates the transition probability for magnetic dipole radiation from the  $^3S_1$  level and finds that single-photon emission rather than two-photon emission (Dalgarno, Drake, and Victor 1969; Bely and Faucher 1969) is the dominant mode of decay for  $Z \leq 20$ .

In a subsequent article, Gabriel and Jordan (1969b) point out that collisional interchange between the  $^3S$  and  $^3P$  levels may take place such that the relative intensities of these two lines are density dependent. These authors calculate the density dependence of the intensity ratio ( $^3S/^3P$ ), which they call  $R$ , for CV, OVII, NeIX, MgXI, and SiXIII, and use the measured values to compute electron density in the coronal regions responsible for these emissions.

We have obtained spectral scans of coronal emissions in the wavelength region between 1.5 and 25 Å with three crystal spectrometers on board the satellite OV1-17 (1969-025A), which was launched in March of 1969. We have observed the forbidden  $1s^2\ ^1S_0 - 1s2s\ ^3S_1$  transition in OVII, NeIX, AlXII, SiXIII, and SXV. A large EUV background makes the identification of this line in NaX and MgXI difficult. We have, however, observed this line in NaX and MgXI on an earlier flight (Rugge and Walker 1968).



In this report, we discuss the identification of these lines and present the observed values of wavelength and the relative fluxes for the resonance, intercombination, and forbidden lines.

Long-wavelength transitions in the  $1s^2$  -  $1s2p$  and  $1s^2$  -  $1s3p$  series in helium-like ions have been observed in laboratory plasmas (Eden and Tully 1973; Jahnke, Kuhn, Sawyer, and Straton 1961; Roth and Eron 1968) and in the solar corona (Auer, Forcell, Towner, and Widing 1966; Frits, Kruip, Mackinnon, Jahnke, and Friedman 1967; Ruge and Walker 1968; Walker and Ruge 1967; Jones, Freeman, and Wilson 1968; Mackinnon, Kruip, and Friedman 1969; Evans and Bould 1969). Gabriel and Jordan (1970) point out that the laboratory and coronal satellites have similar structure. The laboratory lines are due to transitions in doubly excited helium-like ions. In the solar corona, the strong satellite line that is observed is due to the singlet-photon decay of the metastable  $1s2s^3S_1$  level. Jordan (1969) calculates the transition probability for magnetic dipole radiation from the  $2s$  level and finds that singlet-photon emission rather than two-photon emission (DeJure, Drake, and Victor 1969; Reyl and Fischer 1969) is the dominant mode of decay for  $2s$  and  $3s$ .

In a subsequent article, Gabriel and Jordan (1970b) point out that collisional interchange levels are the  $2s$  and  $3s$  levels may take place such that the relative intensities of these two lines are density dependent. These authors calculate the density dependence of the intensity ratio ( $I_{2s}/I_{3s}$ ) which they call  $R$ , for CV, OVII, NeIX, MgXI, and SiXII, and use the measured values to compare electron density in the coronal regions responsible for these emissions.

We have obtained spectra of coronal emissions in the wavelength region between 15 and 35 Å with three crystal spectrometers on board the satellite OVI-17 (4989-5025 Å), which was launched in March of 1969. We have observed the forbidden  $1s^2$  -  $1s2s^3S_1$  transition in OVII, NeIX, SiXII, SiXIII, and SXV. A large EUV background makes the identification of this line in NeIX and MgXI difficult. We have, however, observed this line in NeIX and MgXI on an earlier flight (Ruge and Walker 1968).

## II. EXPERIMENTAL DETAILS

The OVI-17 crystal spectrometer is mounted on a compact solar pointer (Chater and Howey 1967), which points at the center of the solar disk with an accuracy of a few seconds of arc. The spectrometer uses three crystals: KAP( $2d = 26.63 \text{ \AA}$ ), EDDT( $2d = 8.81 \text{ \AA}$ ), and LiF( $2d = 4.03 \text{ \AA}$ ). The KAP crystal is mounted above the other crystals, and the spectrum is recorded by a Bendix M312 detector with a CsI cathode that is mounted behind a thin formvar and aluminum filter. The EDDT and LiF crystals are mounted back to back at right angles to the KAP crystal, and the spectra from these crystals is recorded in a proportional counter with a 1-mil thick beryllium window. All crystals are rigidly constrained to rotate together.  $\text{Fe}^{55}$  sources are mounted at one end of each crystal holder and provide the in-flight calibration of both detectors. The events recorded by each detector are stored in scalers and sampled every 0.11 sec, which corresponds to 1.9 arc min of crystal travel. The spectrometer is driven by a synchronous motor and scans continuously.

The response of a crystal spectrometer to discrete sources on the disk and the determination of absolute efficiency are discussed by Walker and Rugge (1969). In this paper, we report only relative line intensities, and we ignore the small changes in efficiency between the closely spaced wavelengths of each group of lines observed with the EDDT spectrometer. For the data obtained with the KAP spectrometer, we make use of the calibration curve of the similar OVI-10 spectrometer (Walker and Rugge 1969) to correct the relative intensities of each group of lines. A shaft-angle encoder that changes levels every 15 arc sec of crystal travel is used for accurate wavelength determination and has been calibrated against a number of x-ray lines in the laboratory.

### III. EXPERIMENTAL DATA

Figure 1 shows a single-scan spectrum obtained with the EDDT spectrometer at 0604 UT on 20 March 1969. A number of lines of interest are identified on the scan. A list of identification is given in Table 2, which is discussed in the next section. The sun was quiet at this time; no flares were recorded for the previous 6-hr period (ESSA 1969). The three groups of lines resulting from the  $1P$ ,  $3P$ , and  $3S$  transitions in AlXII, SiXIII, and SXV are identified, along with several other prominent lines.

Figure 2 is a single-scan spectrum obtained with the KAP spectrometer at 0615 UT. The steep rise in counting rate at short wavelengths is due to EUV radiation that is specularly reflected from the crystal. The groups of lines resulting from the  $1P$ ,  $3P$ , and  $3S$  transitions in OVII and NeIX are identified as are several other prominent lines.

Figure 3 shows spectra obtained before and after two class 1B flares (ESSA 1969) that were observed at 1551 UT and approximately 1630 UT on 20 March 1969. The sun was quite active during this period, with class 1N flares being reported at 1450, 1555, and 1625 UT. The spectra obtained at 1642 and 1529 UT are considerably enhanced over the spectrum obtained at 0604 UT, with the SXV  $1s^2 - 1s2p, 1s2s$   $1P$ ,  $3P$ , and  $3S$  lines and the SXVI Ly $\alpha$  line at 4.73 Å clearly visible.

Fritz, et al. (1967), report several lines between 7.7 and 7.9 Å, which we identify from our spectra as the AlXII  $1s^2 - 1s2p, 1s2s$  lines, and the MgXI  $1s^2 - 1s3p$  transition. Their assigned wavelengths are slightly different from ours, and their identifications also differ. They report only two of the three lines that we observe and identify as the SiXIII  $1s^2 - 1s2p, 1s2s$  lines, and they do not report the three weak lines that we identify as the SXV  $1s^2 - 1s2p, 1s2s$  lines. The unidentified line which they observe at 7.05 Å probably corresponds to the MgXI Ly $\beta$  line that we observe at the predicted wavelength of 7.11 Å.



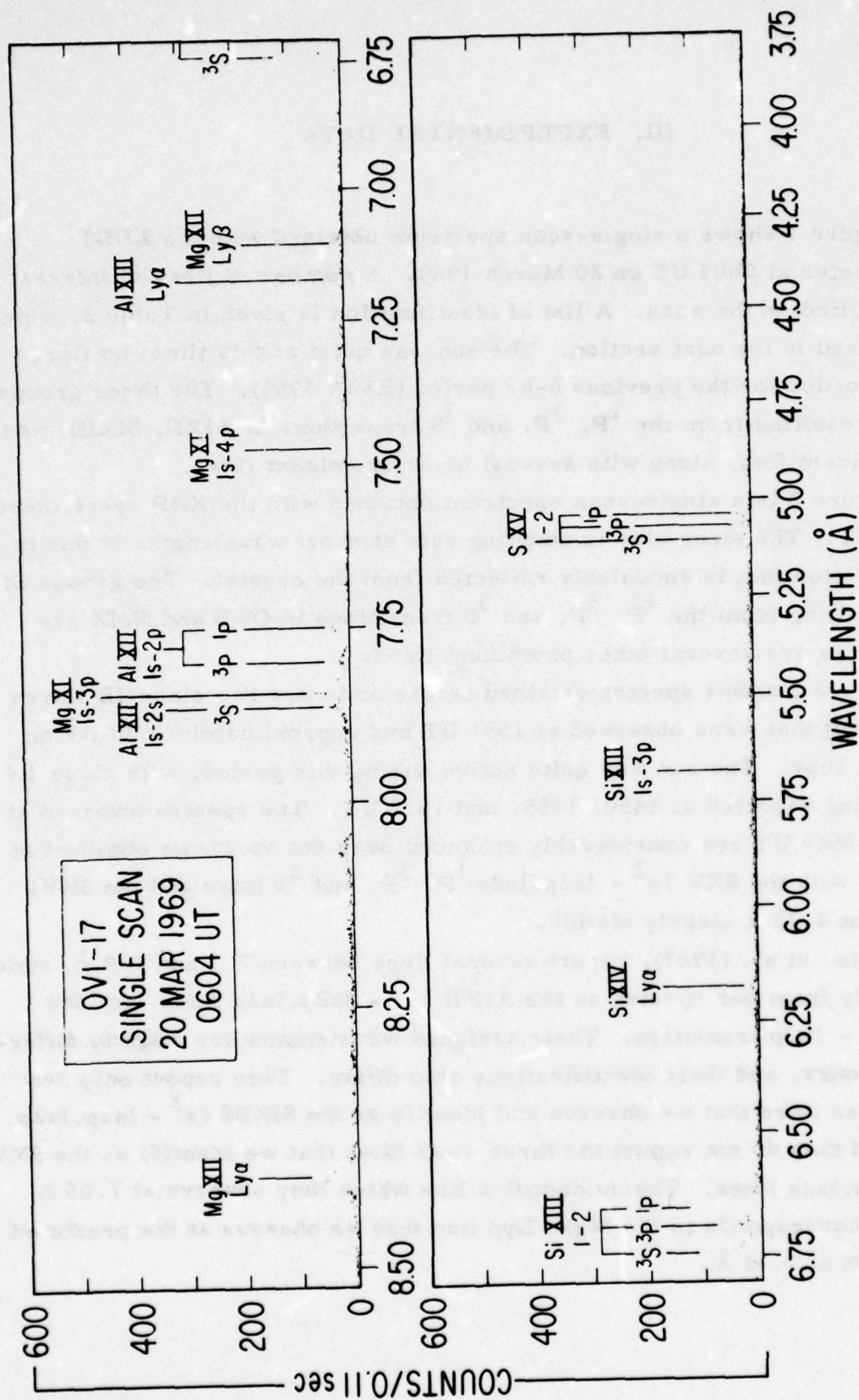


Figure 1. Solar X-Ray Spectrum Observed with an EDDT Spectrometer, Obtained at 0604 UT on March 20, 1969. No flares were reported near this time.

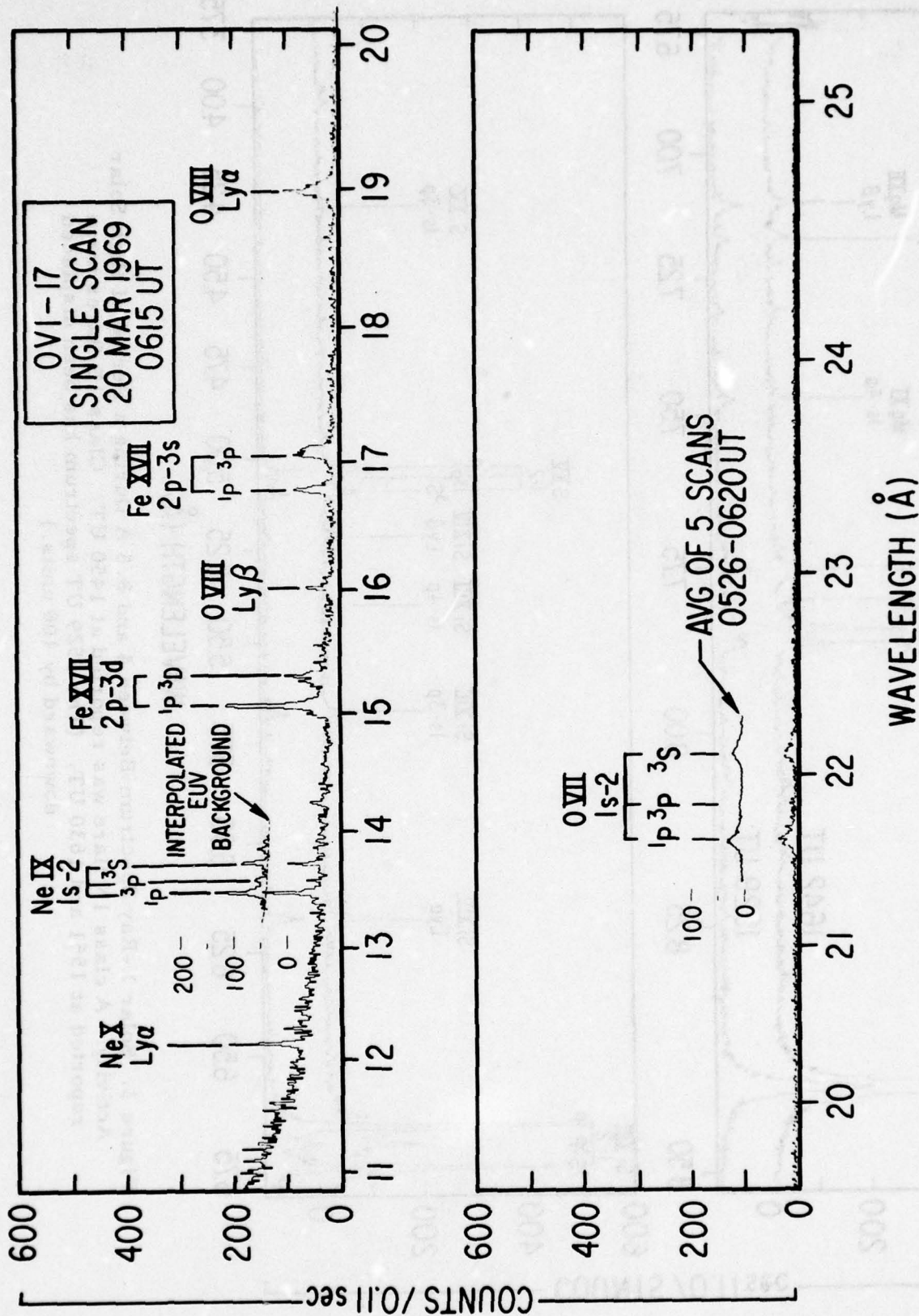


Figure 2. Solar X-Ray Spectrum Observed with a KAP Spectrometer, Obtained at 0615 UT on March 20, 1969. No flares were reported near this time. The average of five scans taken between 0526 and 0620 UT are shown for the NeIX and OVII resonances, intercombination, and forbidden lines.





Meekins, et al. (1969), observe three lines near the position of the silicon XIII triplet which we observe, but do not identify them as the silicon XIII triplet. They also observe three lines near the position of the Al XII triplet, but identify only the Al XII resonance line. The SXV line which they observe near  $5.1 \text{ \AA}$  is not resolved into three components in their spectrum.

We do not discuss in this report the interpretation of lines other than the helium-like  $^1\text{P}$ ,  $^3\text{P}$ , and  $^3\text{S}$  lines. We do, however, observe other lines corresponding to the prominent lines which Meekins, et al., report. If the emission lines that Meekins identifies as K lines are present in our spectra, they are considerably weaker than in the spectra which he has presented.

#### IV. IDENTIFICATION OF LINES

We do not discuss the identification of lines from the KAP spectrometer in detail here (see for example Rugge and Walker 1968). Unfortunately, precise wavelengths have not been measured in the laboratory for a number of the lines observed by the EDDT spectrometer. To obtain the wavelengths of lines originating in hydrogen-like spectra, we use the calculations of Garcia and Mack (1965). For lines of the helium-like isoelectronic series, the *Atomic Energy Level Tables* of Moore (1949) are used. We use these published values to extrapolate the wavelengths of the transitions of interest in other ions of astrophysical interest. The results of these extrapolations are given in Table 1. The values taken from Moore are denoted by an asterisk. The prominent lines observed in the EDDT spectrum are listed in Table 2. The wavelengths listed as observed with the EDDT spectrometer were determined by using the MgXII Ly $\alpha$  line at 8.421 Å as a standard. All other wavelengths were assigned using the position of this line and the precisely known scanning rate of the spectrometer. The wavelength of the MgXII line was confirmed to be correct to within the accuracy of spectrometer calibration (0.005 Å) using the geometry of the spectrometer and the precisely known wavelengths of the FeXVII 17.051 Å and OVIII 18.969 Å lines observed with the KAP spectrometer. The intensity in counts given in Table 2 is the integral number of counts under each line that is proportional to the line intensity (Walker and Rugge 1969).

Table 3 lists the intensities and positions of the OVII and NeIX resonance, intercombination, and forbidden lines. Because of the low counting rates in the KAP data, we have averaged 5 scans near 13.6 and 22 Å in order to improve the accuracy of the derived fluxes. These averaged spectra are shown superimposed on Fig. 2. Table 4 lists the calculated values of R, the ratio of the forbidden to intercombination lines and of G, the ratio of the sum of the forbidden and intercombination lines G to the resonance line.

Table 1. Extrapolated Wavelengths of Lines in the  
HeI Isoelectronic Sequence

Upper Level	Ion									
	CV	NVI	OVII	FVIII	NeIX	NaX	MgXI	AlXII	SiXIII	SXV
1s2p $^3S_1$	41.472*	29.543*	22.098*	17.153*	13.701	11.192	9.314	7.871	6.739	5.100
1s2p $^3P_1$	40.731*	29.084*	21.084*	16.951*	13.554	11.084	9.231	7.807	6.687	5.065
1s2p $^1P_1$	40.270*	28.787*	21.602*	16.807*	13.447	11.002	9.168*	7.756	6.646	5.0360
1s3p $^3P$	35.073	24.963	18.669*	14.488	11.568	9.450	7.863	6.645	5.688	4.304
1s3d $^3D$	34.998*	24.917	18.639*	14.467*	11.553	9.438	7.854	6.638	5.683	4.301
1s3p $^1P$	34.973*	24.898*	18.627*	14.458*	11.547	9.433	7.850	6.635	5.680	4.299

\*Values are taken from Moore.



Table 2. Lines Observed in the EDDT Scan

Observed Wavelength	Predicted Wavelength	Ion and Transition	Line Intensity, counts			
			20 Mar 0604 UT	20 Mar 1529 UT	20 Mar 1642 UT	20 Mar 1704 UT
8.421	8.421	MgXII $1s^2 S_{1/2} - 2p^2 P_{1/2, 3/2}$	591	3190	8610	4054
8.068		Not Identified				
7.873	7.871	AlXII $1s^2 1S_0 - 1s2s^3 S_1$	87	280	483	270
	7.863	MgXI $1s^2 1S_0 - 1s3p^3 P_{2,1}$				
7.850	7.854	MgXI $1s^2 1S_0 - 1s3d^3 D_{2,1}$	276	864	1067	765
	7.850	MgXI $1s^2 1S_0 - 1s3p^1 P_1^*$				
7.827		Not Identified				
7.805	7.807	AlXII $1s^2 1S_0 - 1s2p^3 P_{2,1}$	47	118	206	119
7.776		Not Identified				
7.759	7.756	AlXII $1s^2 1S_0 - 1s2p^1 P_1$				
7.474	7.47	MgXI $1s^2 1S_0 - 1s4p^1 P_1$				
7.316	7.31	MgXI $1s^2 1S_0 - 1s5p^1 P_1$	117	357	614	428
7.233		Not Identified				
7.179	7.173	AlXIII $1s^2 S_{1/2} - 2p^2 P_{1/2, 3/2}$				
7.111	7.106	MgXII $1s^2 S_{1/2} - 3p^2 P_{1/2, 3/2}$				

\* Transition is expected to be the strongest of the group.

Table 2. Lines Observed in the EDDT Scan (continued)

Observed Wavelength	Predicted Wavelength	Ion and Transition	Line Intensity, counts			
			20 Mar 0604 UT	20 Mar 1529 UT	20 Mar 1642 UT	20 Mar 1704 UT
6.739	6.739	SiXIII $1s^2 1S_0 - 1s2s^3S_1$	381	1115	2018	1560
6.727	6.72	See §IV		258		
6.684	6.687	SiXIII $1s^2 1S_0 - 1s2p^3P_{2,1}$	216	566	908	585
6.652	6.646	SiXIII $1s^2 1S_0 - 1s2p^1P_1$	532	1768	3186	2387
6.184	6.182	SiXIV $1s^2 S_{1/2} - 2p^2P_{1/2, 3/2}$				
5.810		Not Identified				
5.680	5.688	SiXIII $1s^2 1S_0 - 1s3p^3P_{2,1}$				
	5.683	SiXIII $1s^2 1S_0 - 1s3d^3D_{2,1}$				
	5.680	SiXIII $1s^2 1S_0 - 1s3p^1P_1^*$				
5.401	5.40	SiXIII $1s^2 1S_0 - 1s4p^1P$				
5.219	5.217	SiXIV $1s^2 S_{1/2} - 3p^2P_{1/2, 3/2}$				
5.100	5.100	SXV $1s^2 1S_0 - 1s2s^3S_1$	38	152	297	136
5.080	5.08	See §IV				
5.065	5.065	SXV $1s^2 1S_0 - 1s2p^3P_{2,1}$	38	102	168	75
5.039	5.036	SXV $1s^2 1S_0 - 1s2p^1P_1$	68	213	420	151
4.734	4.729	SXVI $1s^2 S_{1/2} - 2p^2P_{1/2, 3/2}$				

\*Transition is expected to be the strongest of the group.

Table 3. Intensities of OVII and NeIX Lines

Observed Wavelength	Predicted Wavelength	Ion and Transition		0526 - 0620 UT	
				Counts	Corrected Intensity*
22.103	22.097	OVII	$1s^2 1S_0 - 1s2s^3S_1$	1178	1341
21.811	21.804	OVII	$1s^2 1S_0 - 1s2p^3P_{2,1}$	354	364
21.606	21.602	OVII	$1s^2 1S_0 - 1s2p^1P_1$	1849	1849
13.700	13.701	NeIX	$1s^2 1S_0 - 1s2s^3S_1$	784	814
13.556	13.554	NeIX	$1s^2 1S_0 - 1s2p^3P_{2,1}$	384	387
13.455	13.447	NeIX	$1s^2 1S_0 - 1s2p^1P_1$	1680	1680

\* Normalized to the  $1P_1$  line intensity



Table 4. Line Ratios and Predicted Densities (20 March 1969)\*

Ion	0604 UT			1529 UT			1642 UT			1704 UT			Approx Temp of Line Forma- tion 10 <sup>6</sup> °K
	R	G	N <sub>e</sub> (cm <sup>-3</sup> )	R	G	N <sub>e</sub> (cm <sup>-3</sup> )	R	G	N <sub>e</sub> (cm <sup>-3</sup> )	R	G	N <sub>e</sub> (cm <sup>-3</sup> )	
OVII	3.7	0.9	2 × 10 <sup>8</sup>										1.8
NeIX	2.1	0.7	1.5 × 10 <sup>10</sup>										3.5
AlXII	1.85	1.1	2 × 10 <sup>11</sup>	2.4	1.1	<10 <sup>11</sup>	2.35	1.1	<10 <sup>11</sup>	2.25	0.9	<10 <sup>11</sup>	7.3
SiXIII	1.75	1.1	3.5 × 10 <sup>11</sup>	2.0	0.95	2 × 10 <sup>11</sup>	2.2	0.9	<10 <sup>11</sup>	2.7	0.9	<10 <sup>11</sup>	8.9
SXV	1.0	1.1	4 × 10 <sup>12</sup>	1.5	1.2	~10 <sup>12</sup>	1.75	1.1	<5 × 10 <sup>11</sup>	1.8	1.4	<5 × 10 <sup>11</sup>	12.2

\* F = 0.50

Jones, et al., report a line at 22.03 Å in addition to the OVII forbidden line at 22.09 Å. Unfortunately, the rocking curve of KAP is too broad to resolve these two lines in our spectra. However, we observe lines near the SiXIII and SXV forbidden lines at 6.727 Å and 5.085 Å, respectively. The presence of the MgXI 1s - 3p line prevents the observation of a similar line between the AlXII forbidden and intercombination lines. We point out the close agreement between the wavelength of the 22.03 Å line of Jones, et al., and the calculated wavelengths of the  $1s^2 2s^2 S^e - 1s2s2p^2 P^o$  line in OVI (Gabriel and Jordan 1969a). We extrapolate the wavelength of this line for SiXIII and SXV and find that the lines we observe at 6.727 Å and 5.085 Å are sufficiently near the proper wavelength to be identified with this line. Gabriel and Jordan (1969a) point out that this line is observed in low density plasmas and can be formed by dielectronic recombination (Burgess 1965). The  $1s^2 2p^2 P^o - 1s2p^2 D^e$  line, which can also be formed by dielectronic recombination, is too close to the forbidden line to be observed in any of the solar spectra so far published.

If these lines are indeed due to transitions in excited lithium-like ions, it remains to be determined whether these levels are formed by dielectronic recombination in helium-like ions, or by direct excitation of lithium-like ions (i.e.,  $K\alpha$  type transitions). The observation of the  $1s^2 2p^2 P^o - 1s2p^2 D^e$  line would strongly imply dielectronic recombination, because the formation of the doubly excited  $2D^e$  state by excitation at coronal densities is very improbable. The observation of the  $1s^2 2p^2 P^o - 1s2p^2 P^e$  lines, which cannot be formed by dielectronic recombination (Gabriel and Jordan 1969a) would be strong evidence for  $K\alpha$  type transitions.

## V. THEORY

Gabriel and Jordan (1969b) point out that, for long-lived levels such as  $1s2s\ ^3S$ , collisional and radiative coupling to adjacent levels such as  $1s2p\ ^3P$  becomes important. They derive the observed ratio of the  $^3S$  to the  $^3P$  line intensities.

$$R = \frac{A(2^3S - 1^1S)}{[N_e C(2^3S - 2^3P) + \emptyset] (1 + F) + A(2^3S - 1^1S)} \left( \frac{1 + F}{B} - 1 \right), \quad (1)$$

where the  $C$ 's are collisional excitation rates, the  $A$ 's are transition probabilities,  $N_e$  is the electron density, and  $\emptyset$  is the photo-excitation rate (which is negligible for all important coronal ions except CV). The quantity  $F$  is defined as<sup>1</sup>

$$F = \frac{C(1^1S - 2^3S)}{C(1^1S - 2^3P)},$$

and  $B$  is the effective branching ratio from the  $^3P$  states to the ground state

$$B = \frac{1}{3} \frac{A(2^3P_1 \rightarrow 1^1S)}{A(2^3P_1 - 1^1S) + A(2^3P - 2^3S)} + \frac{5}{9} \frac{A(2^3P_2 \rightarrow 1^1S)}{A(2^3P_2 - 1^1S) + A(2^3P - 2^3S)}.$$

Gabriel and Jordan evaluate Eq. (1) for CV, OVII, NeIX, MgXI, and SiXIII. They assume that the temperature dependence of the ratio of the collisional excitation rates is negligible and calculate the value of  $C(2^3S - 2^3P)$  at

<sup>1</sup>In the calculation of  $F$ , a rigorous treatment should include all processes other than the exchange between the  $^3P$  and  $^3S$  levels, which may populate either level.



the temperature at which the collisional excitation of the resonance line is a maximum. The ionization equilibrium calculations of Jordan (1969) were used to calculate this temperature. We extend the calculations of R to AlXII and SXV. The values of  $A(2^3P - 2^3S)$  were obtained from Weise, et al. (1966), of  $A(2^3P_1 - 1^1S)$  from Drake and Dalgarno (1969), of  $A(2^3P_2 - 1^1S)$  from Garstang (1967), and of  $A(2^3S - 1^1S)$  from Griem (1969). The values of  $C(2^3S - 2^3P)$  were calculated from the formula given by Van Regemorter (1962). The temperatures at which the collisional excitation rates were evaluated are given in Table 4. The dependence of R on  $N_e$  is shown in Fig. 4.

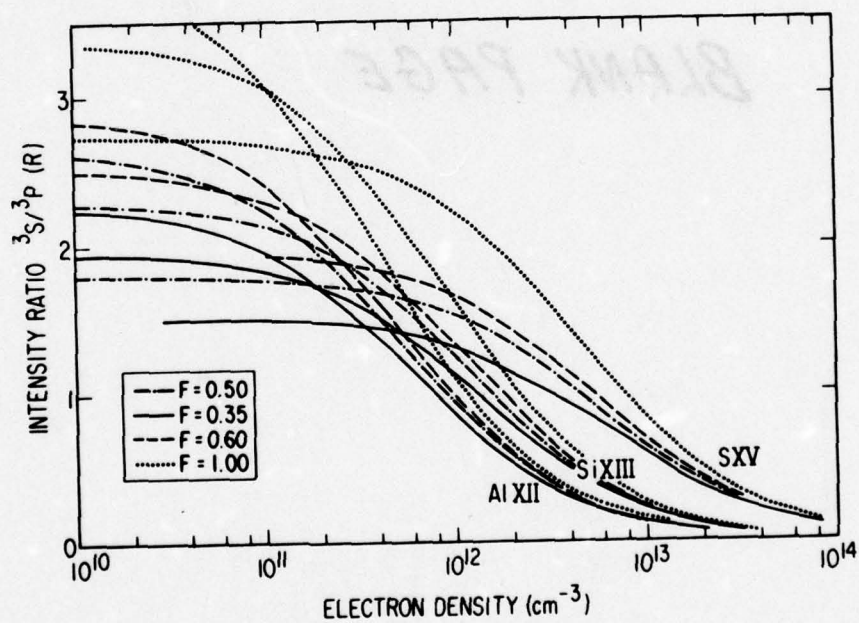
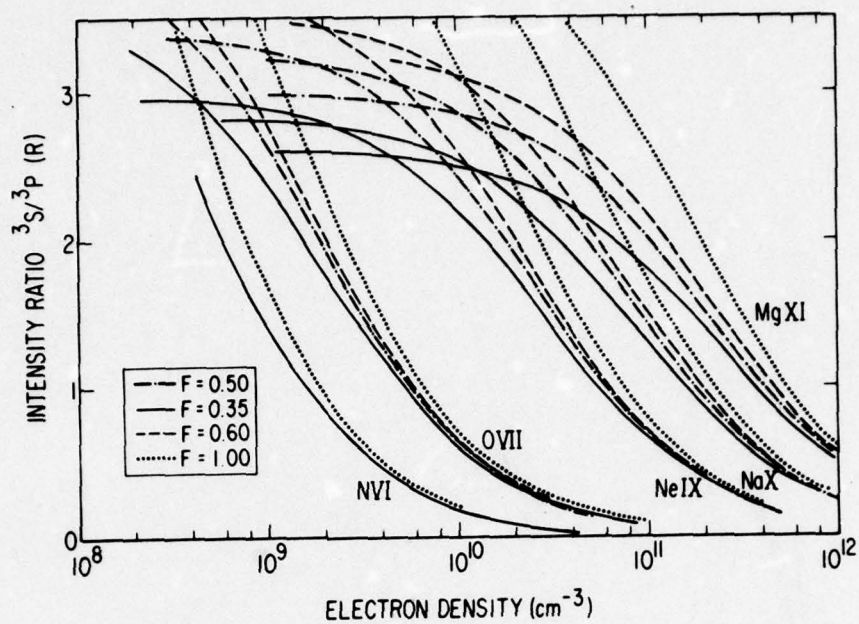


Figure 4. Dependence of the Ratio of the Forbidden to Intercombination Line Intensities R for Helium-Like Ions on Electron Density

## VI. DISCUSSION OF THE LINE RATIOS

In order to utilize Eq. (1) in the determination of coronal densities, the ratio of the collisional excitation cross sections  $F$  must be determined. Using a ratio  $R$  of 3.6 for the OVII lines derived from several scans from our previous work (Rugge and Walker 1968) and assuming that the OVII emission arises from the quiet corona for the highest ratio, Gabriel and Jordan (1969b) deduce that  $F \approx 0.35$ . We have studied the value of  $R$  and  $G$  for OVII as a function of the daily 2800-MHz solar radio flux from data taken over a 5-month time period by the OV1-10 satellite in late 1966 and early 1967 (Rugge and Walker 1969), which included the data used by Gabriel and Jordan. We find mean values of  $R \approx 3.3$  and  $G \approx 1.1$  essentially independent of the solar radio flux, with the x-ray fluxes increasing linearly by about a factor of two while the radio flux increased from 100 to 200 flux units. The measured values of  $R$  vary by up to  $\pm 20\%$ , which is only slightly more than the experimental uncertainties in the x-ray fluxes. This suggests that only slight changes in density take place in the emitting regions. Much larger density changes are suggested by the other OVII data cited by Gabriel and Jordan (1969b). Our present measurement of  $R \approx 3.7$  for the OVII ratio in the averaged scans shown in Fig. 2 is in agreement with the average OV1-10 results cited above. Thus, our present data, using the assumption of Gabriel and Jordan, also leads to a value of  $F \approx 0.35$ .

However, our values of  $R$  determined for AlXII, SiXIII, and SXV cannot be obtained with a value of  $F$  as small as 0.35. Because of the increasing importance of the magnetic quadrupole  $1^1S_0 - 2^3P_2$  transition in the heavier ions, the maximum value of  $R$  for a particular  $F$  decreases with increasing  $Z$  (see Fig. 4). The maximum value of  $R[R_{\max} = (1 + F)/B - 1]$  for a particular ion occurs when

$$N_e C(2^3S - 2^3P)(1 + F) \ll A(2^3S - 1^1S) \quad (2)$$

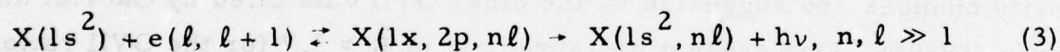


If we assume that the maximum SXV and SiXIII ratios were observed for radiation originating in a region satisfying Eq. (2), then we would predict  $0.5 \lesssim F \lesssim 0.55$ .

Using a value of  $F = 0.5$ , we calculate the electron densities given in Table 4. The density entries in Table 4 shown as less than a given density were derived from ratios which lie on the insensitive part of the line ratio  $R$  vs density plot. In addition to direct collisional excitation, the values of  $F$ , determined empirically by Gabriel and Jordan and by us, include the effects of other population mechanisms, such as cascades and radiative recombination, which can modify the ratio determined for direct excitation from the ground state alone.

Gabriel and Jordan point out that  $G$ , the ratio of the sum of the forbidden and intercombination lines to the resonance line, should be a constant for each ion. Our measured values of  $G$  are listed in Table 4. The measured values cluster near  $G \approx 1$  for all  $Z$ .

One might expect that dielectronic recombination of the  $^1P$  state would contribute to the flux in that line by the process



Because the transition probability for the  $1s2s\ ^3S$  and  $1s2p\ ^3P$  states is smaller than that for the  $1s2p\ ^1P$ , this process should be less important for these lines. Because  $n$  and  $\ell$  are large in most cases (Burgess 1965), the wavelength of the resultant photon would be too close to that of the resonance line to be resolvable. The relative intensity of the line radiation resulting from stabilizing transitions after dielectronic recombination (Tucker and Gould 1966) to the collisionally excited line radiation evaluated at the temperature at which the latter reaches a maximum increases from 0.185 for OVII to 0.435 for SXV.<sup>2</sup> This suggests that if  $F$  is independent of nuclear

<sup>2</sup>Jordan (private communication) finds ratios about a factor of two smaller using Burgess' (1965) theory.

charge, then  $G(\text{SXV})/G(\text{OVII}) = 0.83$ . Our observations do not support this result, suggesting that  $F$  may not be independent of  $Z$ . It is also possible that radiative recombination may be important for some conditions and may favor the triplet state, resulting in a higher value of  $G$ .

BLANK PAGE

## VII. DISCUSSION OF THE RESULTS

We find that for undisturbed periods (i.e., the 0604 UT spectrum), the electron density predicted by the Gabriel-Jordan theory increases with temperature. We find a density of  $\approx 2 \times 10^8 \text{ cm}^{-3}$  from the OVII intensity ratios. This value is somewhat lower than the typical active region densities given by Newkirk (1967), but is certainly reasonable. While the densities found for the AlXII, SiXIII, and SXV lines are somewhat greater than those suggested by Newkirk for condensations with lifetimes greater than a few hours, they may be reasonable for small regions at or near the time of flares.

An unexpected result is the apparent decrease in electron density after the group of flares between 1500-1600 UT on 20 March 1969. This may be real, or it may indicate a breakdown of one or more of the assumptions of the theory during times of considerable change in the condition of the active regions giving rise to these emissions.



#### ACKNOWLEDGMENTS

The authors are deeply indebted to W. T. Chater and C. K. Howey, who designed the solar pointer without which this experiment would have been impossible. Chater and Howey were also responsible in part for the design of the Bragg crystal spectrometer and its drive mechanism. The exacting demands of the fabrication and assembly of the experiment were met by E. Irwin, R. L. Owens, and L. Bellocchio. The authors would like to acknowledge the support and encouragement of Drs. G. A. Paulikas and R. A. Becker. The authors are grateful to the Office of Aerospace Research for the construction and operation of the OV1-17 satellite. They would also like to thank the Aerospace Computing Center and Mrs. G. Boyd for their aid in reducing the raw satellite data to the form in which it is presented herein.

REFERENCES

- Austin, W.E., Purcell, J.D., Tousey, R., and Widing, K.G. 1966, Astrophys. J. 145, 373.
- Bely, O. and Faucher, P. 1969, Astr. and Astrophys. 1, 37.
- Burgess, A. 1965, Smithsonian Astrophysical Observatory Spec. Rep. No. 174, p. 47.
- Chater, W.T. and Howey, C.K. 1967, Trans. AGU, 48, 151.
- Dalgarno, A., Drake, G.W.F., and Victor, G.A. 1969, Phys. Rev. 180, 25.
- Drake, G.W.F., and Dalgarno, A. 1969, Astrophys. J. 157, 459.
- Edlen, B. and Tyren, F. 1939, Nature, 143, 940.
- ESSA Research Lab., Solar Geophys. Data 1969, IER-FB-296.
- Evans, K. and Pounds, K.A. 1969 (to be published).
- Flemberg, H. 1942, Ark. Mat. Astr. Fys. 28A, 34.
- Fritz, G. Kreplin, R.W., Meekins, J.F., Unzicker, A.E., and Friedman, H. 1967, Astrophys. J. 148, L133.
- Gabriel, A.H. and Jordan, C., 1969a, Nature 221, 947.
- Gabriel, A.H. and Jordan, C., 1969b, "Interpretation of Solar Helium Like Line Intensities," Mon. Not. Roy. Astr. Soc. (in press).
- Garcia, J.D., and Mack, J.E., 1965, Opt. Soc. Am. 55, 654.
- Garstang, R.H., 1967, Astrophys. J. 148, 579.
- Griem, H.R. 1969, Astrophys. J. 156, L103.
- Jahoda, F.C., Ribe, F.L., Sawyer, G.A., and Stratton, T.F. 1961, Proceedings Fifth International Conference on Ionization Phenomena in Gases, Munich 1961 (Amsterdam: North Holland Publishing Co.) p. 1987.

#### REFERENCES (Continued)

- Jones, B.B., Freeman, F.F., and Wilson R. 1968, Nature 219, 252.
- Jordan, C. 1969, Mon. Not. Roy. Astr. Soc. 142, 501.
- Meekins, J.F., Kreplin, R.W., Chubb, T.A., and Friedman, H. 1968, Science 162, 891.
- Moore, C.E., 1949, Atomic Energy Levels, NBS Circular 467 (U.S. Government Printing Office).
- Newkirk, G., Jr., 1967, Ann. Rev. Astron. and Astrophys. 5 (Palo Alto: Annual Review, Inc.) p. 213.
- Roth, N.V. and Elton, R.C. 1968, NRL Report 6638.
- Rugge, H.R. and Walker, A.B.C., Jr. 1968, Space Res. VIII (Amsterdam: North Holland Publishing Co.) p. 439.
- Rugge, H.R. and Walker, A.B.C., Jr. 1969 (to be published).
- Tucker, W.J. and Gould, R.J. 1966, Astrophys. J. 144, 244.
- Tyren, F. 1940, Nova Act. Reg. Soc. Sci. 12, 25.
- Walker, A.B.C., Jr., and Rugge, H.R. 1969, Solar Flares and Space Research (Amsterdam: North Holland Publishing Co.) p. 102.
- Weise, W.L., Smith, M.W., and Glennon, B.M., 1966, Atomic Transition Probabilities, NSRDS-NBS 4 (U.S. Government Printing Office).
- Van Regemorter, H. 1962, Astrophys. J. 136, 906.



### III. FURTHER RESULTS ON O VII X-RAY CORONAL LINE EMISSION\*

H. R. Rugge and A. B. C. Walker, Jr.

#### ABSTRACT

Measurements of the intensity ratio of O VII solar x-ray emission lines were made during a three-day period in 1969. The results are essentially the same as obtained from a different satellite during an extended period in 1966/1967. These results lead to an upper bound on the coronal electron density from the regions emitting the O VII radiation of  $\approx 5 \times 10^9 \text{ cm}^{-3}$ .

---

\* This paper has also been published as TR-0059(9260-02)-4, The Aerospace Corporation, El Segundo, California (14 December 1970) and in Solar Physics 18, 244-246 (1971).

CONTENTS

ABSTRACT .....	47
FURTHER RESULTS ON O VII X-RAY CORONAL LINE EMISSION .....	51
REFERENCES .....	57
Table 1. Solar Activity Parameters and O VII Line Intensity Ratios .....	54

# FURTHER RESULTS ON O VII X-RAY CORONAL LINE EMISSION

In a recent publication (Rugge and Walker, 1971) we reported on the relative intensities of the solar x-ray resonance ( $1s^2\ ^1S_0 - 1s2p\ ^1P_1$ ), intercombination ( $1s^2\ ^1S_0 - 1s2p\ ^3P_1$ ) and forbidden ( $1s^2\ ^1S_0 - 1s2s\ ^3S_1$ ) lines of helium-like O VII for a 90-day period in 1966/1967. These relative intensities were used to determine the ratio of the forbidden to the intercombination line intensity, R, which, utilizing the theory of Gabriel and Jordan (Gabriel and Jordan 1969, 1970; Freeman, et. al., 1970), gave an upper limit on the solar coronal electron density in regions emitting the O VII x-radiation. It is the purpose of this note to report similar measurements for O VII for a brief period in 1969, near the peak of the present solar cycle. The results for this time period are identical, within the uncertainties, to those obtained earlier.

The instrumentation used for this study consisted of a scanning KAP Bragg crystal spectrometer which has been described briefly elsewhere (Walker and Rugge, 1970). It was similar to that used on the OV1-10 satellite (Rugge and Walker, 1968), which gathered the previous data, but with spectral resolution improved by a factor of five. Thus, the resonance (21.60A) intercombination (21.80A) and forbidden (22.10A) lines of O VII are all clearly resolved in the present data. These data were gathered on the OV1-17 satellite (1969-25A) launched 18 March, 1969. Data were obtained for only



a three-day period because of a malfunction of the spectrometer motor. The individual scans of the spectrometer taken during this period have been summed to produce an average spectrum for each orbit of the satellite. The average relative intensities for each orbit are used to calculate the line intensity ratios which are compared to our previous results.

We previously obtained data on the relative intensities of the O VII lines for 90 days ( $\approx 3$  solar revolutions) from Dec. 1966 to Feb. 1967, a period on the rising portion of the present solar cycle. During this period the 2800 MHz solar radio flux varied between 110 and 204 ( $\times 10^{-22} \text{ w m}^{-2} \text{ Hz}^{-1}$ ) and the Zurich Relative Sunspot Number between 34 and 191. Throughout this period there was no systematic variation in R over the considerable range of solar activity encountered and there appeared to be little, if any, true change within the uncertainty in R at any time. Because of this it was assumed, using the Gabriel and Jordan theory, that the electron density in the regions emitting the O VII lines was at all times near or below a value at which R is not sensitive to the density. This allowed an upper bound of  $\approx 5 \times 10^9 \text{ cm}^{-3}$  to be placed on this density. In addition, following Gabriel and Jordan (1969), we calculated the quantity they called G, the ratio of the sum of the intercombination and forbidden line intensities to the resonance line intensity; G was also found to be effectively constant with solar activity with some indication of a slightly smaller

value for higher solar activity. The average value of  $R$  over the 90-day period was  $\bar{R} \approx 3.35$  and for the time of higher solar activity,  $\bar{G} \approx 1.08$ .

The present data have been used to compute the ratios  $R$  and  $G$  for each orbit in the same manner as for the OV1-10 data. The line intensities were obtained by integrating under each spectral line and subtracting the contribution from continuum and background. The ratios were calculated after correction for the relative efficiency of the spectrometer at the appropriate wavelengths. The values calculated are presented in Table 1. The uncertainties are primarily due to the background subtraction and counting statistics. Also presented in Table 1 are the starting time of each orbit, the "daily" 2800 MHz solar radio flux and the Zurich Relative Sunspot Number. As can be seen, solar activity was somewhat higher than at any time during the 1966/1967 period discussed above and was fairly constant over the 3-day period. Class 1 flares were reported during two of the orbits. However, all values of  $R$  in Table 1 are consistent with  $R$  being constant and equal to the average value of  $R = 3.21 \pm 0.18$ . The average value of  $G$  is  $0.99 \pm 0.06$ . These values are essentially the same as the values obtained during the 1966/1967 measurements. This lack of variation of  $R$  implies an upper bound on the coronal electron density in those regions emitting the O VII x-radiation of  $N_e \leq 5 \times 10^9 \text{ cm}^{-3}$ .

TABLE 1

Solar Activity Parameters and O VII Line Intensity Ratios

Date (1969)	2800 MHz "daily" solar radio flux ( $10^{-22} \text{ W m}^{-2} \text{ Hz}^{-1}$ )	Zurich Relative Sunspot Number	R	G
0500 UT 20 March	215	196	$3.19 \pm 0.42$	$1.00 \pm 0.14$
1530 UT 20 March			$2.84 \pm 0.33$	$0.91 \pm 0.11$
0400 UT 21 March	232	204	$3.56 \pm 0.46$	$1.03 \pm 0.14$
1430 UT 21 March			$3.66 \pm 0.37$	$0.97 \pm 0.11$
0400 UT 22 March	224	207	$3.46 \pm 0.88$	$1.35 \pm 0.35$
1600 UT 22 March			$2.56 \pm 0.61$	$1.14 \pm 0.28$
			$\bar{R} = 3.21 \pm 0.18$	$\bar{G} = 0.99 \pm 0.06$



The present higher resolution data indicate the (identical) method used in integrating both the present and previous pertinent line intensities may systematically overestimate the flux in the inter-combination line (due to the extended wings of the resonance line caused by the rocking curve width of the KAP crystal) by about 15%. This results in a (corrected)  $\bar{R}$  for the 1966/1967 data of  $\approx 3.92$  and  $\bar{R} \approx 3.78$  for the present data.  $\bar{G}$  is reduced by about 3% in both cases. The upper limit on the electron density is not affected since it is established by the constancy of  $R$ ; however, the parameter  $F$  in the theory (see Gabriel and Jordan, 1969, and Rugge and Walker, 1971) is affected. The previous value for  $R$  (1966/1967 data) implied  $F \approx 0.27$ ; the corrected value implies  $F \approx 0.44$  in closer agreement with values of  $F$  found for higher members of the isoelectronic sequence (Walker and Rugge, 1970).

In summary, measurements of the intensity ratio of O VII x-ray emission lines made for an extended period in 1966/1967 during the rising portion of the solar cycle and during a brief period in 1969, near the peak of the solar cycle, have given essentially the same result leading to an upper bound on the electron density of  $\approx 5 \times 10^9 \text{ cm}^{-3}$ . It seems reasonable to speculate that this density limit would not be exceeded during other parts of this solar cycle.

### References

Freeman, F. F., Gabriel, A. H., Jones, B. B. and Jordan, C.:  
1970, The Royal Society (to be published).

Gabriel, A. H., and Jordan, C.: 1969, Monthly Notices Roy.

Astron. Soc. 145, 241.

Gabriel, A. H. and Jordan, C.: 1970, Physics Letters 32A, 166.

Rugge, H. R. and Walker, A. B. C., Jr.: 1968, Space Research VIII

Ed. A. P. Mitra, L. G. Jacchia, W. S. Newman, North Holland  
Publishing Co., Amsterdam, pg. 439.

Rugge, H. R. and Walker, A. B. C., Jr.: 1970 Solar Phys. (to  
be published).

Walker, A. B. C., Jr. and Rugge, H. R.: 1970, Astron. and  
Astrophys. 5, 4.

PRECEDING PAGE DELETED FILMED

IV. OBSERVATION OF AUTOIONIZING STATES  
IN THE SOLAR CORONA\*

A. B. C. Walker, Jr., and H. R. Rugge

ABSTRACT

We have observed weak satellites to the lines of the principal series of the helium and hydrogen like ions of magnesium, aluminum, silicon and sulphur in the solar spectrum. These lines coincide in wavelength with the extrapolated positions of transitions from the  $2s2p^3P$  and  $2p^2^1D$  autoionizing levels in helium like ions, and the  $1s2s2p^2P$ ,  $1s2s3p^2P$  and  $1s2p3p^2S$  or  $^2D$  autoionizing levels in lithium like ions. The observed ratio of the intensity of the  $1s2p^1P - 2p^2^1D$  line in Mg XI relative to the intensity of the Mg XII Lyman- $\alpha$  line is found to be  $5 \times 10^{-3}$ , compared to a predicted ratio which varies from  $16 \times 10^{-3}$  at  $6 \times 10^6$  K to  $7.5 \times 10^{-3}$  at  $10^7$  K. These observations provide direct evidence of dielectronic recombination in the corona.

\*This paper has also been published as TR-0059(9260-02)-2, The Aerospace Corporation, El Segundo, California (20 November 1970) and in The Astrophysical Journal 164, 181-190 (1971).



## CONTENTS

ABSTRACT .....	59
I. INTRODUCTION .....	63
II. THE LITHIUM LIKE IONS .....	65
III. THE HELIUM LIKE IONS .....	75
IV. DISCUSSION .....	81
V. CONCLUSIONS .....	85
ACKNOWLEDGMENTS .....	87
REFERENCES .....	89

## FIGURES

1. Enlargement of the spectrum near the Al XII $1s^2 \ ^1S - 1s2p \ ^1P$ and Mg XI $1s^2 \ ^1S - 1s3p \ ^1P$ lines obtained at 1642 UT on March 20, 1969 from the OV1-17 satellite .....	67
2. Enlargement of the spectrum near the Si XIII $1s^2 \ ^1S - 1s3p \ ^1P$ line obtained at 1642 UT on March 20, 1969 from the OV1-17 satellite .....	68
3. Enlargement of the spectrum near the Si XIII $1s^2 \ ^1S - 1s2p \ ^1P$ line obtained at 1529 UT on March 20, 1969 from the OV1-17 satellite .....	69
4. Extrapolation of the wave numbers of the lithium like satellite lines relative to the helium $1s^2$ $^1S - 1s2p \ ^1P$ and $1s^2 \ ^1S - 1s3p \ ^1P$ lines, based on laboratory observations and theoretical calculations .....	70

## FIGURES (Continued)

5.	Extrapolation of the wave numbers of the helium like satellite lines relative to the Lyman-alpha line, based on laboratory observations and theoretical calculations . . . . .	77
6.	Enlargement of the spectrum near the Mg XII Lyman-alpha line obtained at 1642 UT on March 20, 1969 from the OV1-17 satellite . . . . .	79

## TABLES

I.	Doubly Excited States for Configurations with $n \leq 3$ . . . . .	72
II.	Transitions from the $2s2p$ and $2p^2$ Levels Originating from Autoionizing States . . . . .	76

## I. INTRODUCTION

The importance of resonances in atomic cross sections in astrophysical plasmas has become increasingly appreciated since Burgess (1964) pointed out the importance of dielectronic recombination in the solar corona. The formation of doubly excited autoionizing states also plays an important role in collisional and photoionization (Goldberg 1966), and should have an important effect on the spectrum of the high temperature corona.

We reported earlier on the observation, from the satellite OV1-17 (1969-025A), of the  $1s^2 2s^2 S - 1s2s2p^2 P$  satellite line to the helium like resonance line from the  $1s2s2p^2 P$  autoionizing level in Ne VIII, Si XII, and S XIV. We have now identified additional lines due to the decay of autoionizing levels in both helium like and lithium like ions in the corona. We have observed lines from the  $1s2s3p$  and  $1s2p3p$  configurations of the lithium like ions of magnesium, aluminum and silicon. We have also identified the line at 6.265 Å observed by Meekins, et al. (1970) as due to the decay of the  $2p^2 1D$  level in Si XIII, and two weak lines in our own spectra at 8.518 Å and 8.550 Å as due to the decay of the  $2s2p^3 P$  and  $2p^2 1D$  levels in Mg XI. Neupert and Swartz (1970 a, b) have also observed lines from the  $1s2s2p$  configuration in silicon, sulphur, argon, and iron from the OSO V satellite. A theoretical extrapolation formula for the level width of the  $2p^2 1D$  level has been used to show that the intensity of the  $1s2p^1 P - 2p^2 1D$  line in Mg XI is consistent with the formation of the



upper level by dielectronic recombination. The decay of the  $2p^2\ ^3P$  level, which is not autoionizing and has been observed in the laboratory, has not been observed in Mg XI, further reinforcing the interpretation of dielectronic recombination as the mechanism for the formation of doubly excited levels in the corona. The direct observation of dielectronic recombination is of great importance because of the role of this process in determining the ionization balance in the high temperature corona.

Historically, doubly excited states were first detected in the laboratory in helium by Compton and Boyce (1928). Theoretical efforts were directed initially at the study of those states which were metastable to autoionization, and could therefore explain the narrow natural width of the observed lines. Wu (1944) was able to identify the line observed at 320.4 Å in helium as due to the transition  $1s2p\ ^3P - 2p^2\ ^3P$ .

A number of transitions from doubly excited levels have now been observed and identified in the spectra of highly ionized atoms in the laboratory. A number of theoretical studies of the properties of these levels have also been made, especially in helium like ions. The line identifications which we have made are based on wavelength comparisons of the observed lines with extrapolated wavelengths obtained from these theoretical and experimental results. The origin of the laboratory satellites has been discussed by Gabriel and Jordan (1969) and by Gabriel, Jordan and Paget (1969), who show that at low densities ( $10^{16}\text{ cm}^{-3}$ ) these lines result from stabilizing transitions following dielectronic recombination. At higher densities the observation of lines such as  $1s^2\ 2p^2\ ^2P - 1s2p^2\ ^2P$ , with upper levels which can autoionize only by second order processes, indicates that inner shell excitation may be important.

## II. THE LITHIUM-LIKE IONS

In their pioneering work on the EUV and soft x-ray spectra of highly ionized elements Edlén and Tyrén (1939) observed satellites to the helium and hydrogen like resonance lines of carbon. They ascribed these lines to transitions from doubly excited configurations with two electrons in the  $n = 2$  level, to singly excited configurations.

Satellite lines to the helium like resonance lines arising from doubly excited configurations of the lithium like ion have been observed in the laboratory more recently by Flemberg (1942), Edlén (1947), Sawyer, Jahoda, Ribe and Stratton (1962), Roth and Elton (1968), Peacock, Speer and Hobby (1969), Gabriel and Jordan (1969), and Gabriel, Jordan and Paget (1969). Gabriel and Jordan (1969) have classified all of the lines expected from the configurations  $1s2s2p$  and  $1s2p^2$  by comparing the positions of the observed laboratory satellites with the wavelengths computed by the Charlotte Froese Hartree-Fock program including configuration mixing. The identifications of the  $1s^2 2s^2 S - 1s2s2p^2 P$  lines in several ions in the solar spectrum by Walker and Rugge, and by Neupert and Swartz were based on this work. Peacock, et al. have calculated the expected position of several of the lithium like lines in neon and argon, including lines from the  $1s2s3p$  and  $1s2p3p$  configurations, using a Hartree-Fock-Slater program developed by Cowan (1968).

Figure 1 shows the Mg X  $1s^2 2s^2 S - 1s2s3p^2 P$  and  $1s^2 2p^2 P - 1s2p3p^2 S$  or  $^2 D$  lines<sup>1</sup> and the Al XI  $1s^2 3p^2 P - 1s2p3p^2 D$  or  $^2 S$  line. Figure 2 shows the unresolved  $1s^2 2s^2 S - 1s2s3p^2 P$  and  $1s^2 2p^2 P - 1s2p3p^2 S$ ,  $^2 D$  lines in Si XII. Figure 3 shows the  $1s^2 2s^2 S - 1s2s2p^2 P$  and  $1s^2 2s^2 S - 1s2s2p^4 P$  lines in Si XII. These spectra were obtained during a period of high solar activity on March 20, 1969. The complete spectra between 3.75 and 8.5 Å are shown in Figure 3 of Walker and Rugge (1970), and a partial list of the observed lines is given in Table I of that paper. In Figure 4 we have indicated how the wave numbers of the lines identified with the  $1s2s2p$  level relative to the wave numbers of the  $1s^2 1S - 1s2p^1 P$  resonance line compare with the relative wave numbers predicted by extrapolations based on the data given by Gabriel and Jordan. The identification of lines due to this configuration is quite certain.

The position and identification of the lines of the  $1s2s3p$  and  $1s2p3p$  configurations are less certain. Calculations of the energy of the doubly excited states of helium, with one electron in an  $n = 3$  state or higher (see for example Fano (1969) and Altick and Moore (1965)) indicate that configuration mixing is extremely important for these states. We might expect that this would also be the case for lithium-like ions. In view of this, we regard the multiplet assignments of the  $1s2s3l$ , and  $1s2p3l$  configurations as not yet definitively established. We have used the

<sup>1</sup>We probably observe the  $^2 P - ^2 D$  line to the long wavelength side of the  $^2 S - ^2 P$  line by analogy with  $1s2p^2 D$  and  $1s2s2p^2 P$ . The  $^2 P - ^2 S$  line is probably closer to the resonance line, and evidently too weak to observe.



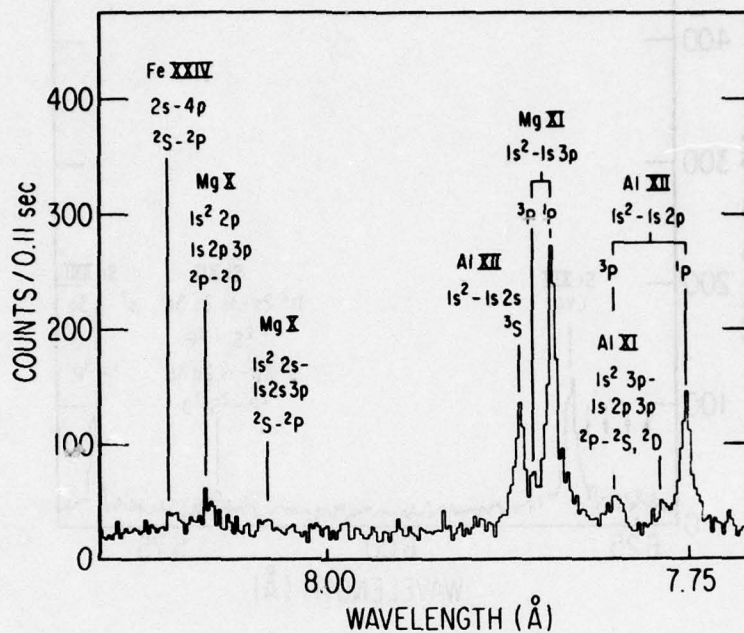
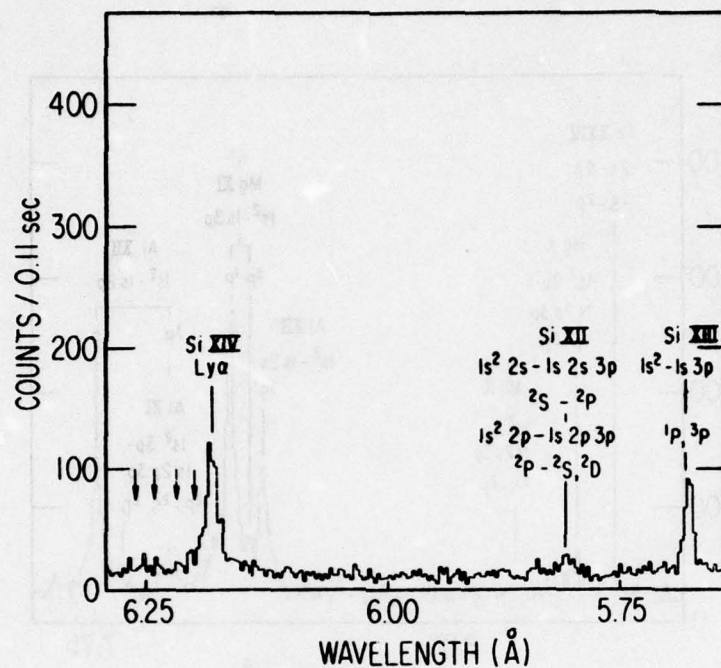
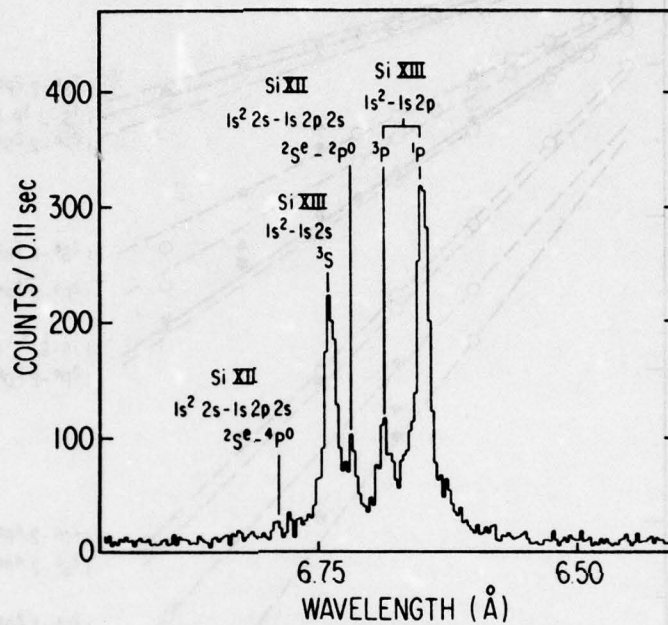


Figure 1. Enlargement of the spectrum near the Al XII  $1s^2 1S-1s2p^1P$  and Mg XI  $1s^2 1S-1s3p^1P$  lines obtained at 1642 UT on March 20, 1969 from the OV1-17 satellite. The 1-3 transitions from the  $1s2s3p$  and  $1s2p3p$  levels in Mg X and the 1-2 transitions from the  $1s2p3p$  level in Al XI are shown.



**Figure 2.** Enlargement of the spectrum near the Si XIII  $1s^2 1S - 1s3p^1P$  line obtained at 1642 UT on March 20, 1969 from the OVI-17 satellite. The Si XII 1-3 transitions from the  $1s2s3p$  and  $1s2p3p$  levels in Si XII are shown. The Si XIV Lyman- alpha line and the positions of four Si XIII satellite lines are also indicated.



**Figure 3.** Enlargement of the spectrum near the Si XIII  $1s^2 1S-1s2p^1P$  line obtained at 1529 UT on March 20, 1969 from the OV1-17 satellite. The lines from the  $1s2s2p^2P$  and  $1s2s2p^4P$  levels in Si XII are shown.



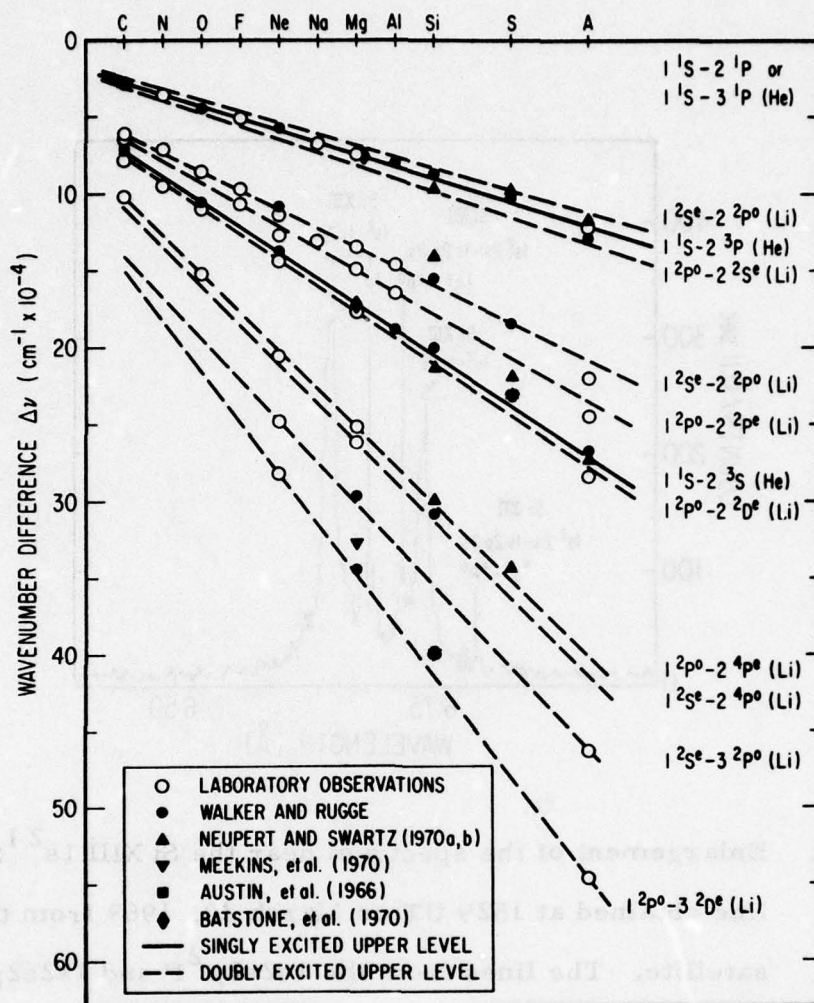


Figure 4. Extrapolation of the wave numbers of the lithium like satellite lines relative to the helium  $1s^2\ ^1S - 1s2p\ ^1P$  and  $1s^2\ ^1S - 1s3p\ ^1P$  lines, based on laboratory observations and theoretical calculations. The solar observations of the  $1s^2\ ^1S - 1s2p\ ^3P$  and  $1s^2\ ^1S - 1s2s\ ^3S$  lines and of several of the satellite lines are compared with extrapolated curves. The ion in which each transition occurs is shown in parenthesis.

wave numbers of the Ne VIII and A XVI lines observed by Peacock, et al. relative to the wave numbers of the  $1s^2 1S - 1s3p^1P$  line to interpolate relative wave numbers for the Mg X, Al XI, and Si XII lines. The relative wave numbers for the observed solar lines are compared with the interpolated curve in Figure 4. The lines which we observed at 8.068 A and 5.810 A have also been reported by Meekins, et al. (1968, 1970) and previously by us (Walker and Rugge 1970). In Table I we have listed all of the doubly excited states for configurations with  $n \leq 3$ , which would result, for pure L-S coupling, in satellite lines to the  $1s^2 1S - 1s2p^1P$  and  $1s^2 1S - 1s3p^1P$  lines. We have listed only those states which are autoionizing (i. e. couple to a  $1s^2$  continuum) and which can decay to a lower state by an electric dipole transition. Garcia and Mack (1965) have tabulated these states and discussed the selection rules for autoionization. We have also listed other autoionizing configurations which could be mixed with the configurations satisfying the selection rules for autoionization. For the  $1s2p^2$  and  $1s2s2p$  configurations we have included 3 levels which are not autoionizing because one of these is observed as a weak line by both Walker and Rugge (1970) and Neupert and Swartz (1970 a, b). Some inner shell excitation is to be expected for lithium like ions, even under conditions of thermal equilibrium. The lithium like ion population equilibrium curve has a high temperature tail (Jordan (1969)) and, for example, in silicon accounts for 1% of the population at  $4 \times 10^6$  K. The wavelengths listed in Table I are those observed by us for the spectra shown in Figures 1, 2 and 3 of this paper (and in Figure 3 of Walker and Rugge (1970)). Note that the Mg X line at 8.068 A is distinct from the line at 8.092A,

Table I. Doubly Excited States for Configurations with  $n \leq 3$

Transition	Other Autoionizing Configurations	Mg Obs.	Mg Pred.	Al Obs.	Al Pred.	Si Obs.	Si Pred.	S Obs.	S Pred.
$1s^2 1S - 1s2p^1 P_1^*$				7.759	7.756	6.649	6.646	5.039	5.036
$1s^2 n l^2 L - 1s2p n l^2 (L \pm 1)$	$1s2sn(l \pm 1)$								
$1s^2 3p^2 P - 1s2p3p^2 D$	$1s2s3d$	7.776	7.787						
$1s^2 3p^2 P - 1s2p3p^2 S$	$1s2s3s$								
$1s^2 3d^2 D - 1s2p3d^2 P$	$1s2p3s, 1s2s3p$								
$1s^2 3d^2 D - 1s2p3d^2 F$									
$1s^2 3s^2 S - 1s2p3s^2 P$	$1s2s3p, 1s2p3d$								
$1s^2 2s^2 S - 1s2s2p^2 P$									
$1s^2 1S - 1s2p^3 P^*$				7.807	7.807	6.684	6.687	5.065	5.062
$1s^2 2p^2 P - 1s2p^2 2S$	$1s2s^2$								
$1s^2 2s^2 S - 1s2s2p^2 P$									

\*Not an autoionizing level  
 †This line is probably due to  $1s2p3p^2 D$ , with the  $2S$  transition closer to the resonance line, and too weak to be observed.



Table I. Doubly Excited States for Configurations with  $n \leq 3$  (Continued)

Transition	Other Autoionizing Configurations		Mg		Al		Si		S	
	Obs.	Pred.	Obs.	Pred.	Obs.	Pred.	Obs.	Pred.	Obs.	Pred.
$1s^2 2p^2 P - 1s2p^2 2P^*$					7.856		6.726		5.090	
$1s^2 1S - 1s2s^3 S^*$				7.873	7.871		6.739		5.100	5.100
$1s^2 2p^2 P - 1s2p^2 2D$					7.872		6.740		5.101	
$1s^2 2p^2 P - 1s2p^2 4P^*$					7.926		6.782		5.124	
$1s^2 2s^2 S - 1s2s2p^4 P^*$					7.930		6.788		5.126	
$1s^2 1S - 1s3p^1 P^*$			7.850	7.850	6.635		5.680		5.680	
$1s^2 n^2 L - 1s3pnl^2 (L \pm 1)$ $1s3d n (L \neq 0, 1, 2)$							5.680			
$1s^2 1S - 1s3p^3 P^*$			7.864	7.863	6.645		5.688		5.688	
$1s^2 2s^2 S - 1s2s3p^2 P$			8.034	8.039			5.797			
$1s^2 2p^2 P - 1s2p3p^2 S^{\dagger}$ or							5.810		5.817	
$1s^2 2p^2 P - 1s2p3p^2 D^{\dagger}$			8.068	8.073						

\* Not an autoionizing level

which we identify as the  $2^2S - 4^2P$  transition in Fe XXIV, based on the calculated wavelengths given by Chapman (1969). This identification was originally suggested by Meekins, et al. (1968).

Using the extrapolated position of the  $1s^2 2p - 1s2p3p$  line we can establish the wave number of the upper level,  $1s2p3p$ . This level may also decay by  $1s^2 3p - 1s2p3p$ . We were able to calculate the position of this line since the other levels involved are singly excited levels and their wave numbers may be obtained from the tables of Moore (1949). The position of this satellite line lies very near to that of the  $1s^2 1S - 1s2p^1P$  line. The dispersion of the spectrometer is not sufficient to resolve the satellite line from the  $1P$  line for silicon or sulphur, however, in aluminum we do observe a line at 7.776 Å, very near to the extrapolated wavelength of 7.787 Å.

If this line is indeed due to the  $1s^2 3p - 1s2p3p$  transition there may well be contributions to it due to the decay of other levels with configurations  $1s2l3l$ .

### III. THE HELIUM LIKE IONS

There have been a considerable number of studies of the doubly excited levels in helium. Much of this work has been stimulated by the resonances in the  $e^- - H$  and  $e^- - He^+$  excitation cross sections caused by coupling to these levels. This work has been recently reviewed by Burke (1968). Burke also summarizes the results of the calculation of the energy of the  $2s^2$ ,  $2s2p$ , and  $2p^2$  levels in helium. Chan and Stewart (1967) have calculated the energy of the  $2s2p^{1,3}P$  levels for  $H^-$ , He I, Li II, Be III, and B IV. Perrott and Stewart (1968a, b) have calculated the energies of the  $2p^2\ ^1D$  and  $2s^2\ ^1S$  levels in  $H^-$ , He I, Li II, Be III and B IV. Goldsmith (1969) has observed satellites to the Be IV Lyman- $\alpha$  line which he has identified as transitions from the  $2s2p\ ^3P$  and  $2p^2\ ^3P, ^1D$  levels in Be III. Peacock, et al. have observed two satellites to the Ne X Lyman- $\alpha$  line which they have identified as due to transitions from the  $2s2p\ ^3P$  and  $2p^2\ ^1D$  levels, and Feldman and Cohen (1969) have observed these lines in C V. In Table II we have listed those transitions from the  $2s2p$  and  $2p^2$  levels which originate from autoionizing states and which can decay to a stable configuration by a dipole transition. Other autoionizing configurations which could be mixed with the configurations satisfying the dipole selection rules are listed in the second column. In Figure 5, we have used the theoretical and experimental results discussed above to extrapolate the wave numbers of these lines relative to the Lyman- $\alpha$  line to obtain relative wave numbers for higher members of the isoelectronic sequence. Roth and Elton (1968) have reported two lines



Table II. Transitions from the  $2s2p$  and  $2p^2$  Levels Originating from Autoionizing States

Transition	Other Autoionizing Configuration	Mg Obs.	Mg Pred.	Si Obs.	Si Pred.
$1s^2S - 2p^2P$		8.421	8.421	6.184	6.182
$1sn\ell^3,^1L - 2pn\ell^3,^1(L \pm 1)$	$2s, n(\ell \pm 1)^3,^1(L \pm 1)$				
$1s2p^1P - 2p^2^1S$			8.449		6.200
$1s2s^1S - 2s2p^1P$			8.488		6.224
$1s2s^3S - 2s2p^3P$		8.518	8.519		6.244
$1s2p^1P - 2p^2^1D$		8.550	8.548	6.265*	6.263

\* Meekins et al (1970)

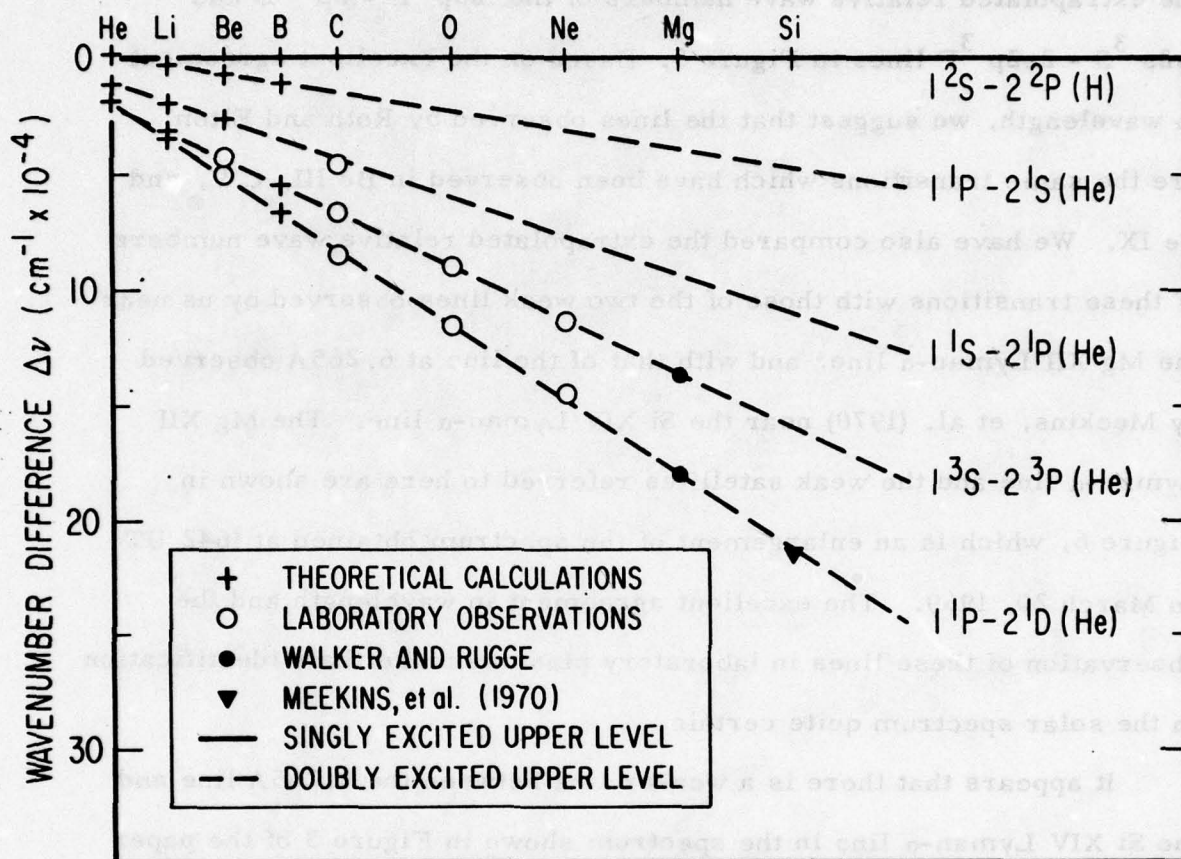


Figure 5. Extrapolation of the wave numbers of the helium like satellite lines relative to the Lyman-alpha line, based on laboratory observations and theoretical calculations. The solar observations of the satellite lines are compared to the extrapolated curves. The ion in which each line occurs is shown in parenthesis.

near the O VIII Lyman- $\alpha$  line, which they have identified only as O VIII satellites. We have compared the relative wave numbers of these lines with the extrapolated relative wave numbers of the  $1s2p\ ^1P - 2p^2\ ^1D$  and  $1s2s\ ^3S - 2s2p\ ^3P$  lines in Figure 5. Based on the excellent agreement in wavelength, we suggest that the lines observed by Roth and Elton are the same transitions which have been observed in Be III, C V, and Ne IX. We have also compared the extrapolated relative wave numbers of these transitions with those of the two weak lines observed by us near the Mg XII Lyman- $\alpha$  line, and with that of the line at 6.265A observed by Meekins, et al. (1970) near the Si XIV Lyman- $\alpha$  line. The Mg XII Lyman- $\alpha$  line and the weak satellites referred to here are shown in Figure 6, which is an enlargement of the spectrum obtained at 1642 UT on March 20, 1969. The excellent agreement in wavelength and the observation of these lines in laboratory plasmas make their identification in the solar spectrum quite certain.

It appears that there is a weaker line between the 6.265A line and the Si XIV Lyman- $\alpha$  line in the spectrum shown in Figure 3 of the paper by Meekins, et al. (1970). This line has not been listed in Table 2 of their paper, but may be another transition of doubly excited Si XIII. In Figure 2 we show the spectrum near Si XIV Lyman- $\alpha$  obtained at 1642 UT on March 20, 1969. We have indicated the position of the four satellite lines listed in Table II. There is some indication of several weak lines near the expected positions of the Si XIII lines; however, the counting statistics are too poor to allow the lines to be reliably recognized.



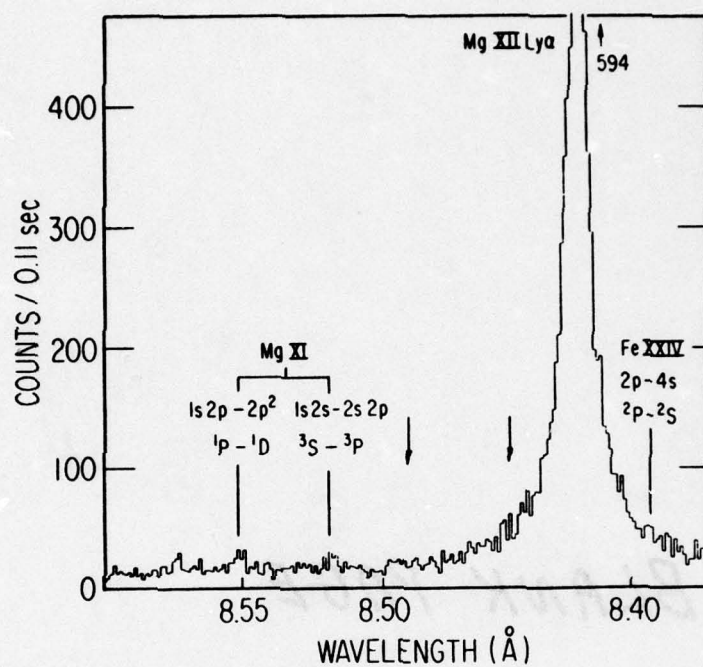


Figure 6. Enlargement of the spectrum near the Mg XII Lyman-alpha line obtained at 1642 UT on March 20, 1969 from the OV1-17 satellite. The two weak satellite lines due to the  $2s2p^3P$  and  $2p^2^1D$  levels are shown.

#### IV. DISCUSSION

The rate coefficient for the process of dielectronic recombination, which we presume is the process responsible for the formation of the doubly excited states which we have observed, has been derived by Shore (1969). The rate for recombination to a particular singly excited state  $s$ , through a doubly excited state  $d$  is given by:

$$R = 17.12 N_e N(i) \frac{\exp(-\epsilon/kT)}{T^{3/2}} \frac{\omega_d}{\omega_e \omega_i} \frac{A^{\text{rad}}(d \rightarrow s) A^{\text{auto}}(d \rightarrow i\epsilon)}{\Gamma^{\text{rad}}(d) + \Gamma^{\text{auto}}(d)} \text{ cm}^{-3} \text{ sec}^{-1} \quad (1)$$

The state  $i$  is the initial state of the unrecombined ion, which will be assumed to be the ground state;  $\epsilon$  is the energy of the electron before capture;  $\omega_d, \omega_i$ , and  $\omega_e$  are statistical weights;  $A^{\text{rad}}$  and  $A^{\text{auto}}$  are the transition probabilities of the state  $d$  for radiative decay to state  $s$ , and autoionization to state  $i\epsilon$ , and  $\Gamma^{\text{rad}}$  and  $\Gamma^{\text{auto}}$  are the total widths for all modes of radiative decay or autoionization. Perrott and Steward (1968a, b) have calculated the autoionization widths of the  $2p^2 \ ^1D$ ,  $\ ^1S$  and  $2s^2 \ ^1S$  states of the helium like ions up to B IV. They have also given formulas for the extrapolation of these widths to higher  $Z$ . The autoionization width  $\Gamma$  is not strongly dependent on  $Z$ . In order to compute  $R$  we must also know  $A^{\text{rad}}$  and  $\Gamma^{\text{rad}}$ . Knox and Rudge (1969) have calculated the transition probability of doubly excited triplet states to the  $1s2s \ ^3S$  state of helium. For the transition  $1s2s \ ^3S - 2s2p \ ^3P$  their result is  $6.1 \times 10^9 \text{ sec}^{-1}$ .

The value of  $A^{\text{rad}}$  for the transition  $1s2p\ ^1P - 2p^2\ ^1D$  may be deduced to be approximately twice that of  $1s2s\ ^3S - 2s2p\ ^3P$  by neglecting the difference between the radial integrals of the two transitions, and using the multiplet strength tables of Allen (1963). We shall adopt this value, scaled by  $(\Delta E_z / \Delta E_{\text{He}})^2$  for higher members of the isoelectronic sequence. We then compute the intensity for the  $1s2p\ ^1P - 2p^2\ ^1D$  line of Mg XI to be,

$$F(2\ ^1D - 1\ ^1P) = 2.34 \times 10^{-39} N_e N(i) \exp(-\epsilon/kT) / T^{3/2} \text{ photons/cm}^2\text{-sec} \quad (2)$$

at the earth. The flux in the Mg XII Lyman- $\alpha$  line may be estimated by Van Regemorter's (1962) approximate formula for allowed transitions,

$$F_{\text{Ly-}\alpha} = 4 \times 10^{-38} N_e N(i) \exp(-E_{\text{Ly-}\alpha}/kT) / T^{1/2} \text{ photons/cm}^2\text{-sec} \quad (3)$$

at the earth. The ratio  $F(2\ ^1D - 1\ ^1P) / F_{\text{Ly-}\alpha}$  varies from  $16 \times 10^{-3}$  at  $6 \times 10^6$  K to  $7.5 \times 10^{-3}$  at  $10^7$  K. This ratio compares well with the experimental ratio of  $5 \times 10^{-3}$  for the spectrum obtained at 1642 UT on March 20, 1969 shown in Figure 6. Shore has computed the total dielectronic recombination rate for hydrogen like ions up to O VIII. If we extrapolate his results to Mg XII, we may predict the emission rate for photons of wavelength close to Mg XII Lyman- $\alpha$  (due to stabilizing transitions of the type  $1s\ n\ell \rightarrow 2p\ n\ell$ ).

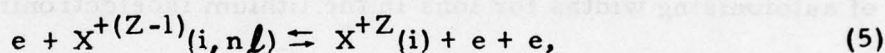
Using  $\alpha_o$  (as defined by Shore) =  $5 \times 10^{-2}$  we obtain



$$F_{\text{Ly-}\alpha}^D = 2.22 \times 10^{-38} N_e N(i) \exp(-E_{\text{Ly-}\alpha}/kT)/T^{3/2} \text{ photons/cm}^2\text{-sec} \quad (4)$$

at the earth. The ratio  $F_{\text{Ly-}\alpha}^D/F_{\text{Ly-}\alpha}$  varies from  $9 \times 10^{-2}$  at  $6 \times 10^6$  K to  $6 \times 10^{-2}$  at  $10^7$  K. Since  $\Gamma^{\text{auto}}(d)$  is not a strong function of  $Z$ , while  $\Gamma^{\text{rad}}(d)$  will increase roughly as  $Z^4$  and collisional excitation will decrease roughly as  $Z^2$ , dielectronic recombination should be a more efficient radiation process for the Lyman- $\alpha$  lines of silicon, sulphur, argon, calcium and iron, all of which have been observed in the corona.

Burgess and Summers (1969) have discussed the effect of electron density in decreasing the dielectronic recombination rate due to



where  $X^{+(Z-1)}(i, n\ell)$  represents a stabilized ion which has undergone dielectronic recombination, but has not had time to allow the recombined electron to decay to the lowest unoccupied level. It should be emphasized that this process, while decreasing the recombination rate, will not decrease the rate of radiation due to stabilizing transitions, which are in general dipole transitions with lifetimes of  $10^{-12}$  seconds or less. If the reaction described in equation (5) is not important recombination to a hydrogenic ion will result, because of transitions by the captured electron, in a photon belonging to the principal series of the helium like ion.

If the identification of the  $1s^2 2s^2 S - 1s 2s 2p^2 P$  line is correct, we would expect the decay of the  $1s 2p^2 D$  level to make a significant contribution to the observed  $1s^2 1S - 1s 2s^3 S$  line flux for Si XIII, and higher members of the helium isoelectronic sequence. The relative intensity of the  $1s^2 2s^2 S - 1s 2s 2p^2 P$  and  $1s^2 1S - 1s 2p^1 P$  lines is 0.07 for Ne, 0.16 for Si, and 0.21 for S. The decay of the  $1s 2p^2 S$  and  $1s 2s 2p^2 P$  levels results in lines which, at present, cannot be resolved from the  $1s^2 1S - 1s 2p^3 P$  line, and may contribute significantly to the observed flux for the highly charged ions of the helium isoelectronic sequence. Autoionizing states with configurations  $1s 2pn l$  with  $n \geq 3$  would appear to result in lines with wavelengths very close to that of the  $1s^2 1S - 1s 2p^1 P$  line. Unfortunately, there appear to be very few calculations of autoionizing widths for ions in the lithium isoelectronic sequence.

## V. CONCLUSIONS

We have observed coronal lines due to the decay of doubly excited states in the helium and lithium like ions of magnesium, silicon, and sulphur. With the exception of one weak line in Si XII, all of the lines are due to upper levels which are autoionizing. The one line observed which is not autoionizing is considerably weaker than an autoionizing line from an upper level with the same configuration, but a different term. The observed intensity of the  $1s2p^1P - 2p^2^1D$  line in Mg XI is consistent with the intensity expected for the formation of the upper level by dielectronic recombination.

The intensity of the  $1s^22s^2S - 1s2s2p^2P$  line relative to the  $1s^2^1S - 1s2p^1P$  line increases in intensity with increasing nuclear charge as would be expected if the upper level is formed by dielectronic recombination.

The most consistent explanation of the origin of the weak autoionizing lines which we have observed in helium like and lithium like ions is the process of dielectronic recombination in hydrogen like and helium like ions respectively.



#### ACKNOWLEDGMENTS

The authors would like to thank the group at the Naval Research Laboratory, especially J. F. Meekins and G. A. Doschek; and W. N. Neupert and M. Swartz of the Goddard Space Flight Center for allowing them to see their results in advance of publication. They would also like to thank D. C. Cartwright of their Laboratory for several illuminating discussions, and Dr. A. Gabriel for bringing several points to their attention in a critical reading of the manuscript and for bringing the paper by Gabriel, Jordan and Paget to their attention.

# REFERENCES

- Allen, C. W., 1963, Astrophysical Quantities (London, Athlone Press), § 25-27.
- Altick, P. L., and Moore, E. N., 1965, Phys. Rev. Letters, 15, 100.
- Austin, W. E., Purcell, J. D., Tousey, R., and Widing, K. C., 1966, Astrophys. J., 145, 373.
- Batstone, R. M., Evans, K., Parkinson, J. H., and Pounds, K. A., 1970, Further X-Ray Spectra of Solar Active Regions, to appear in Solar Physics.
- Burgess, A., 1964, Astrophys. J., 139, 776.
- Burgess, A., and Summers, H. P., 1969, Astrophys. J., 157, 1007.
- Burke, P. G., 1968, Advances in Atomic and Molecular Physics, 4, 173.
- Chan, Y.-M. C., and Stewart, A. L., 1967, Proc. Phys. Soc., 90, 619.
- Chapman, R. D., 1969, Astrophys. J., 156, 87.
- Compton, K. T. and Boyce, J. C., 1928, J. Franklin Inst., 205, 497.
- Cowan, R. D., 1968, J. Optical Soc. Amer., 58, 808.
- Edlén, B. and Tyrén, F., 1939, Nature, 143, 940.
- Edlén, B., 1947, Physica 13, 35.
- Fano, U., 1969, Atomic Physics, edited by B. Bederson, V. W. Cohen, and F. M. J. Pichanick (New York: Plenum Press), pp. 209.
- Feldman, U. and Cohen, L., 1969, Astrophys. J., 158, L169.
- Flemberg, H., 1942, Ark. Mat. Astr. Fys., 28A, 1.
- Gabriel, A. H., and Jordan, Carole, 1969, Nature, 221, 947.

- Gabriel, A.H., Jordan, Carole, and Paget, T.M., 1969, Sixth Int. Conf. on Physics of Electronic and Atomic Collisions, Abstracts of Papers. (Cambridge: MIT Press) pp. 558.
- Garcia, J.D., and Mack, J.E., 1965, Phys. Rev., 138, A987.
- Goldberg, L., 1966, Autoionization, ed. A. Temkin (Baltimore: Mono Book Corp.) pp. 1.
- Goldsmith, S., 1969, J. Phys. B., 2, 1075.
- Jordan, Carole, 1969, Mon. Not. R. Astron. Soc. 142, 499.
- Knox, H.O., and Rudge, M.R.H., 1969, J. Phys. B2, 521.
- Meekins, J.F., Kreplin, R.W., Chubb, T.A., and Friedman, H., 1968, Science, 162, 891.
- Meekins, J.F., Doschek, G.A., Friedman, H., Chubb, T.A., and Kreplin, R.W., 1970, Solar Physics, 13, 198.
- Moore, C.E., 1949, Atomic Energy Levels, NBS Circular 467, Vol. 1.
- Neupert, W.N., and Swartz, M., 1970a, Solar X-ray Spectra of Ions Up to Ni XXVII During Intense Flare Activity, preprint.
- Neupert, W.N., and Swartz, M., 1970b, Astrophys. J. Letters, 160, L189.
- Peacock, N.J., Speer, R.J., and Hobby, M.G., 1969, J. Phys. B., 2, 798.
- Perrott, R.H., and Stewart, A.L., 1968a, J. Phys. B., 1, 381.
- Perrott, R.H., and Stewart, A.L., 1968b, J. Phys. B., 1, 1226.
- Roth, N.V., and Elton, R.C., 1968, NRL Rep. 6638.



Sawyer, G.A., Jahoda, R.C., Ribe, F.L. and Stratton, T.F.,

1962, J. Quant. Spectrosc. Radiat. Transfer., 2, 467.

Shore, B.W., 1969, Astrophys. J., 158, 1205.

Van Regemorter, H., 1962, Astrophys. J., 136, 906.

Walker, A.B.C. Jr., and Rugge, H.R., 1970, Astron. Astrophys., 5, 4.

Wu, T.Y., 1944, Phys. Rev., 66, 291.

# V. RELATIVE INTENSITIES OF THE LYMAN LINES OF HYDROGEN-LIKE OXYGEN, MAGNESIUM, AND SILICON IN THE SOLAR CORONA\*

H. R. Rugge and A. B. C. Walker, Jr.

## ABSTRACT

Observations of the relative intensities of the Lyman lines of hydrogen-like O VIII, Mg XII, and Si XIV in the solar corona have been made by satellite-based x-ray crystal spectrometers and are reported here. A comparison between the experimentally observed values of the intensity ratio of the Lyman  $\alpha$  to the Lyman  $\beta$  line (Lyman ratio) has been made with the recent theoretical predictions of this ratio by Hutcheon and McWhirter for low density plasmas. Good agreement is found between the theory and observations for those times for which we have derived a valid coronal temperature model and applied it to the temperature-dependent theoretical ratio. Observations made at times of greater solar activity appear to be inconsistent with the theory.

\* This paper has also been published as TR-0074(9260-02)-5, The Aerospace Corporation, El Segundo, California (30 April 1974) and in Astronomy and Astrophysics **33**, 367-371 (1974).

# CONTENTS

ABSTRACT .....	93
I. INTRODUCTION .....	97
II. HUTCHEON AND McWHIRTER THEORY .....	99
Figure 1. The Lyman Ratio vs. Reduced Electron Temperature as Calculated by Hutcheon and McWhirter for Coronal Densities and a Maxwellian Plasma .....	101
III. LYMAN RATIO CALCULATION .....	103
IV. LYMAN INTENSITY OBSERVATIONS .....	105
Table 1. Lyman Ratio and Relative Intensities of the Lyman Lines in the Solar Corona (Photons) .....	106
V. DISCUSSION .....	109
REFERENCES .....	113



## I. INTRODUCTION

The relative intensities of spectral lines of hydrogen-like ions formed in a plasma of sufficiently low density reflect the magnitudes of the rate constants responsible for the population and depopulation of the individual excited states. In particular, for the hydrogen-like ions of carbon and heavier elements, densities in the solar corona are sufficiently low to allow the metastable  $2s^2S$  level to decay by two photon emission (Beigman and Vainshtein, 1967; Smith, 1969). As a result the relative intensities of the Lyman lines become independent of density and are only functions of temperature. We have recently reported the fluxes of a number of solar coronal emission lines derived from several spectra obtained under a variety of solar conditions (Walker, Rugge and Weiss 1974 a, b, hereafter referred to as papers I and II) in the wavelength range between 3 and 25 Å. These data were taken with crystal spectrometers flown onboard the satellites OV1-10 and OV1-17. The purpose of this paper is to make a detailed comparison between the ratio of the intensities of the Lyman  $\alpha$  and Lyman  $\beta$  lines (hereafter called the Lyman ratio) observed in these spectra for O VIII, Mg XII and Si XIV and the recent theoretical predictions of the temperature dependence of these ratios for a low density Maxwellian plasma made by Hutcheon and McWhirter (1973) using the latest atomic rate coefficient data. Thermal models of the corona were constructed for use in this comparison. These models, which take the form of differential emission measure functions, were constructed for conditions of relatively quiet solar activity using extensive data from two series of spectral scans. In addition, we also present the

observed Lyman ratio for several spectra taken near times of enhanced solar activity as well as relative intensities of some higher members of the Lyman series of lines in Mg XII and Si XIV.

## II. HUTCHEON AND McWHIRTER THEORY

Recently, Hutcheon and McWhirter (1973) have extended the earlier calculations of population densities and resonance line intensities of hydrogen-like ions of McWhirter and Hearn (1963) to apply to the low density conditions found in the solar corona. The analysis of Hutcheon and McWhirter includes four population and depopulation processes which operate at low densities and includes the separate treatment of the hydrogen-like 2s and 2p sublevels and the effect of cascades for levels up to principal quantum number 20. Cascade contributions for higher levels are treated by an asymptotic formula. The four low density processes included in the Hutcheon and McWhirter analysis are:

- (1) Electron excitation and de-excitation
- (2) Ionization and three-body recombination
- (3) Radiative decay (including two photon decay of  $2s^2S$ ).
- (4) Radiative recombination.

Hutcheon and McWhirter do not consider the population and depopulation of the doubly excited levels  $np\ n'l'$  in helium-like ions. Radiative decays of these levels can result in photons which are observationally indistinguishable from Lyman line photons in hydrogenic ions since

$$\lambda_{1s \rightarrow np} \cong \lambda_{1s\ n'l' \rightarrow np\ n'l'} \quad n' \geq n+2 \quad .$$



Walker and Rugge (1971) have discussed these transitions, and we have observed transitions from the  $2s2p$  and  $2p^2$  levels (Paper I), which are resolvable from Lyman  $\alpha$ , for magnesium and silicon. Shore (1969) points out that the rate coefficient for dielectronic recombinations into doubly excited levels, which accounts for substantially all of their population for equilibrium conditions (Gabriel and Paget, 1972), is proportional to the oscillator strength of the corresponding Lyman transition. Since for the allowed Lyman transitions the collisional excitation coefficient is also proportional to the oscillator strength (Van Regemorter, 1962) the Lyman ratios which result from dielectronic recombination and from direct collisional excitation should be equal. Since collisional excitation is the major population mechanism for the excited levels  $np^2P$  of hydrogen-like ions in the corona, the neglect of the decay of doubly excited levels by Hutcheon and McWhirter, which in any event contribute less than 1% of the observed line flux for O VIII and less than 10% for Si XIV (Walker, 1972) should not preclude the use of their results to predict Lyman line intensity ratios in the corona to acceptable accuracy.

The Lyman ratio calculated by Hutcheon and McWhirter is shown in figure 1 plotted vs. reduced electron temperature,  $\theta = T_e/Z^2$  where  $T_e$  is the electron temperature (in  $^{\circ}K$ ) and  $Z$  is the nuclear charge of the hydrogen-like ion.

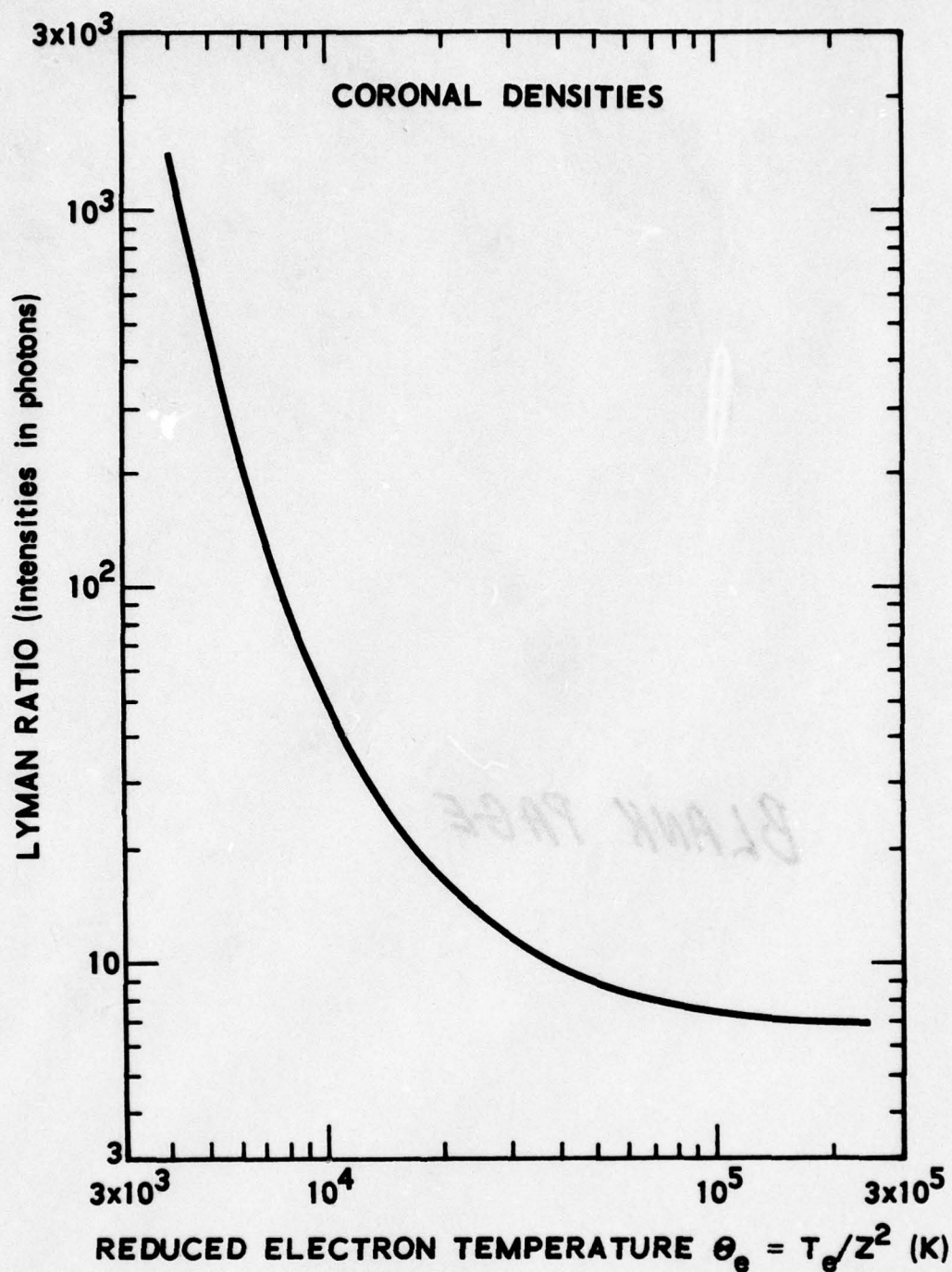


Figure 1. The Lyman Ratio vs. Reduced Electron Temperature as Calculated by Hutcheon and McWhirter for Coronal Densities and a Maxwellian Plasma. The reduced electron temperature is given by  $\Theta = T_e/Z^2$  where  $T_e$  is the true electron temperature and  $Z$  is the nuclear charge of the hydrogen-like ion.

### III. LYMAN RATIO CALCULATION

In order to make a comparison of the Lyman ratios calculated by Hutcheon and McWhirter with our observed ratios, the theoretical values, which are a function of temperature, must be integrated over the coronal temperature distribution (differential emission measure) which prevailed in the corona at the time of the observation. We may compute the proper theoretical ratio for element Z according to the formula (Paper I).

$$R_{Z\alpha\beta} = \frac{\int dT_e M(G_k, T_e) F_{Z\alpha}(T_e)}{\int dT_e M(G_k, T_e) F_{Z\beta}(T_e)} \quad (1)$$

where  $F_{Z\alpha}$  and  $F_{Z\beta}$  are the photon fluxes of Lyman  $\alpha$  and Lyman  $\beta$ , and  $M(G_k, T_e)$  is the differential emission measure of the corona at the electron temperature  $T_e$ , which is specified by the parameters  $G_k$  (see paper I). If we define  $R_{Z\alpha\beta}(T_e)$  as the Lyman ratio calculated by Hutcheon and McWhirter, the observed ratio may be calculated from the formula (1) as

$$R_{Z\alpha\beta} = \frac{\int dT_e M(G_k, T_e) F_{Z\alpha}(T_e)}{\int dT_e M(G_k, T_e) \times \left[ F_{Z\alpha}(T_e) / R_{Z\alpha\beta}(T_e) \right]} \quad (2)$$

We have carried out the integrals in equation 2 for two sets of observations; the first for 8 spectral scans of a KAP crystal obtained near 1730 UT on 4 January 1967 and the second for a spectral scan with an EDDT crystal obtained near 0604UT on 20 March 1969. For both



observations the differential emission measure takes the form (Papers I and II).

$$M(T_e) = C 10^{-T_2/T_1} \left[ 1 + 1.1513 (T_2 - T_0)/T_1 - 1.1513B (T_e - T_0)^2/T_1 (T_2 - T_0) \right] \quad 1.0 \times 10^6 \text{ K} \leq T_e \leq T_0 \quad (3a)$$

$$M(T_e) = C 10^{-T_2/T_1} \left[ 1 + 1.1513 (T_2 - T_0)/T_1 - 1.1513 (T_e - T_0)^2/T_1 (T_2 - T_0) \right] \quad T_0 \leq T_e \leq T_2 \quad (3b)$$

$$M(T_e) = C 10^{-T_e/T_1} \quad T_e \geq T_2 \quad (3c)$$

with  $T_0 = 2 \times 10^6 \text{ K}$  and  $T_2 = 3 \times 10^6 \text{ K}$  for both sets of observations.

The best fit for 4 January 1967 was found for  $T_1 = 4.0 \times 10^6 \text{ K}$ , and for 20 March 1969 (0604 UT) the best fit was obtained with  $T_1 = 3.5 \times 10^6 \text{ K}$ .

In carrying out the integral in equation 2, we have approximated the emission function for Lyman  $\alpha$  by assuming collisional excitation as the only process for populating the 2p state. Explicit calculations of Hutcheon and McWhirter for the Lyman  $\alpha$  line including all processes are not available. This approximation will introduce an error considerably smaller than that already existing in the theoretical calculation as a result of uncertainties in the atomic rate coefficients or in the observations themselves. The values obtained for R, calculated from the theory of Hutcheon and McWhirter and the evaluation of the integrals in equation 2, are presented for O VIII, Mg XII and Si XIV in Table 1 under the column labeled Predicted Ratio. The indicated uncertainties in the ratio ( $\pm 15\%$ ) are those estimated by Hutcheon and McWhirter to be due to the present uncertainties in the atomic rate coefficients used in the calculation.

#### IV. LYMAN INTENSITY OBSERVATIONS

The O VIII observations used in this note were obtained on 4 January 1967 from 8 consecutive scans of a KAP crystal spectrometer flown onboard the OV1-10 satellite (Paper II). The spectra were added to obtain very good counting statistics resulting in the relatively small uncertainty in the Lyman ratio displayed in Table 1. Appropriate corrections were made to the photon fluxes to take into account the measured spectrometer efficiency which is a function of wavelength.

The Mg XII and Si XIV observations were made on 20 March 1969 with an EDDT crystal spectrometer flown onboard the OV1-17 satellite (Paper I). A variety of solar activity conditions applied during the 4 (5 in the case of Mg XII) scans. The 0555UT and 0604UT spectra were taken during relatively quiet conditions as indicated by, for example, the Mg XII Lyman  $\alpha$  line fluxes, while considerably higher counting rates applied for the Lyman  $\alpha$  line at the other times listed in Table 1. The relative Lyman  $\alpha$  line strengths (in counts) are given in Table 1 in parentheses in the relative intensity columns. Two flares occurred at 1550UT and 16300UT on 20 March 1969, following the 1529UT scan and preceeding the 1642UT scan, thus probably accounting for the largest Lyman  $\alpha$  counting rates being observed in the 1642UT spectrum.

The counting rates were corrected for the measured spectrometer efficiencies at the appropriate wavelengths and, in addition, the fluxes of the Si XIV Lyman  $\beta$  line were corrected for blending with the Si XIII  $1^1S - 6^1P$  line by assuming the ratio of the Si XIII  $1^1S - 6^1P$  to  $1^1S - 5^1P$

Table 1

Lyman Ratio and Relative Intensities of the  
Lyman Lines in the Solar Corona (Photons)

O VIII 4 January 1967 1720-1752 UT (8 scans)

Predicted Lyman Ratio

1720-1752 UT

$10.8 \pm 1.6$

Observed Lyman Ratio

1720-1752 UT

$10.5 \pm 0.5$

Relative Intensities

1720-1752 UT

Ly  $\alpha$  1 (8000 counts - 8 scans)

Ly  $\beta$  0.095

Mg XII 20 March 1969

Predicted Lyman Ratio

0604 UT

$10.8 \pm 1.6$

Observed Lyman Ratio

0555 UT

0604 UT

1529 UT

1642 UT

1706 UT

$10.3 \pm 2.6$

$9.9 \pm 2.8$

$6.0 \pm 0.5$

$8.0 \pm 0.5$

$7.5 \pm 0.6$

Relative Intensities

	<u>0555 UT</u>	<u>0604 UT</u>	<u>1529 UT</u>	<u>1642 UT</u>	<u>1706 UT</u>
Ly $\alpha$	1(1100 counts)	1(700 counts)	1(4200 counts)	1(8000 counts)	1(5000 counts)
Ly $\beta$	.097	.10	.167	.125	.13
Ly $\gamma$	-	-	-	-	-
Ly $\delta$	-	~.05	~.02	~.02	~.03
Ly $\epsilon$	-	-	-	~.01	-



Table 1 (continued)

S XIV 20 March 1969

Predicted Lyman Ratio

Observed Lyman Ratio

0604UT

0604UT

1529UT

1642UT

1706UT

$10.2 \pm 1.5$

$7.2 \pm 5.5$

$6.7 \pm 2.0$

$3.9 \pm 0.6$

$7.2 \pm 2.6$

Relative Intensities

0604UT

1529UT

1642UT

1706UT

Ly  $\alpha$

1(50 counts)

1(370 counts)

1(750 counts)

1(250 counts)

Ly  $\beta$

.14

.15

.26

.14

Ly  $\gamma$

-

~.035

~.05

-

could be extrapolated from the respective ratios along the series of the  $1^1S - 5^1P$ ,  $1^1S - 4^1P$ , and  $1^1S - 3^1P$  lines. The total correction varied from 8% to 15% for the Si XIV Lyman  $\beta$  lines with an uncertainty smaller than that resulting from counting statistics for this line.

The ratios of the Lyman  $\alpha$ , Lyman  $\beta$ , Lyman  $\delta$  and Lyman  $\epsilon$  lines of Mg XII are also reported in Table 1. The uncertainties in these ratios vary from  $\approx 25$  to  $\approx 50\%$  as a result of counting statistics in the lines and the background (continuum and noise) which was subtracted. Unfortunately, the Lyman  $\gamma$  line of Mg XII is blended with the much stronger  $1^1S - 2^3S$  line of Si XIII and hence its flux cannot be observed. Although we also observed the Lyman  $\alpha$  lines of NeX, Al XIII, and S XV, the Lyman  $\beta$  lines of these ions were either blended with stronger lines, or too weak to observe and as a result the Lyman ratio for these lines is not being reported.

## V. DISCUSSION

Since a coronal differential emission measure was derived for only the spectra obtained on 4 January 1967 (O VIII) and the 0604UT spectrum obtained on 20 March 1969 (Mg XII, Si XIV), these are the only times for which a definitive comparison can be made between the observed Lyman ratios, as reported here, and the Lyman ratios obtained by an integration of the Lyman ratio predicted by Hutcheon and McWhirter through the temperature structure of the corona as characterized by the differential emission measure function which applied at the time of the observations. Table 1 shows that for these times the predicted and observed ratios are in good agreement, well within the uncertainties of the observations which, unfortunately, are non-negligible for the 0604UT Mg XII and Si XIV ratios as a result of the relatively low counting rates for these lines. Solar activity conditions for the 0555UT Mg XII scan were much more similar to the 0604UT scan than to scans taken at somewhat later times, as indicated by the total counts in the Mg XII Ly $\alpha$  lines (Table 1). The observed Lyman ratio at 0555UT is again in good agreement with the predicted value at 0604UT and essentially the same as the ratio measured at 0604UT, only 10 minutes later. However, for the three scans taken at 1529UT, 1642UT and 1706UT, the observed Lyman ratio falls systematically below the predicted value for both Mg XII and Si XIV and, at times, well outside the combined uncertainties of the predicted and observed ratios. The regions primarily producing the Mg XII and Si XIV lines were considerably more active than in the previous scans as indicated by the Lyman  $\alpha$  counts and, as mentioned above, flares occurred at about 1550UT and 16300UT. If the Hutcheon and



and McWhirter theory is correct, and we obtain good agreement with the theory for these periods in which we can confidently define the coronal model, then the disagreement obtained at the later times must be a consequence of the breakdown of some of the theoretical assumptions or the lack of inclusion of processes which play an important role only during more active solar times. It might be assumed, as is surely the case, that the emission measure differs considerably at these later times from that which obtained at 0604UT. This, however, cannot explain the large divergence between the theory and observations since the minimum value the theory ever attains (for a reduced temperature  $\Theta = T/Z^2 = 256 \times 10^6 \text{ }^\circ\text{K}$ , i.e.  $T \approx 50 \times 10^6 \text{ }^\circ\text{K}$  for Si XIV) for the Lyman ratio is  $R > 7$ , regardless of the dependence of the emission measure on temperature (see Fig. 1). Any "reasonable" emission measure function will yield even higher values for  $R$ . Both the ratios derived at 1529UT for Mg XII and for Si XIV at 1642UT clearly have a value less than this minimum theoretical value.

A possible error in the observational data which could give rise to a smaller ratio would be the blending of a line, which is excited only at high temperatures associated with solar activity, with the Lyman  $\beta$  line. However, we have searched the finding list of emission lines in the recent compilation of Kelly and Palumbo (1973), and can find no lines which are coincident with, or sufficiently close to, the wavelength of the Lyman  $\beta$  lines of Mg XII and Si XIV. At this time we cannot recommend a ready solution to this problem, but conclude that for relatively quiet solar times when we can construct an accurate coronal model, good agreement is found

between observed and predicted Lyman ratios for O VIII, Mg XII and Si XIV.

A number of authors (e.g. Beigman and Vainshtein, 1967; Jacobs, 1968) have suggested that the Lyman ratio observed for various hydrogen-like ions in the corona may be used to derive a coronal temperature. If we use figure 1 and the calculated Lyman ratios to obtain such a "coronal temperature",  $T_c$ , for the appropriate times we have:  $T_c \approx 2.1 \times 10^6$  °K for O VIII,  $T_c \approx 4.6 \times 10^6$  °K for Mg XII (0604UT) and  $T_c \approx 6.9 \times 10^6$  °K for Si XIV (also at 0604UT!) In fact the temperature corresponding to the peak of the emission functions (temperature at which  $M(G_k, T_e) F_{Z\alpha}(T_e)$  is a maximum) for the coronal emission measure of 4 January 1967, applying to O VIII, is  $T_e \approx 2.75 \times 10^6$  °K. For 0604UT, 20 March 1969 for Mg XII and Si XIV the respective peak emission function temperatures are  $T_e \approx 6.2 \times 10^6$  °K and  $10.5 \times 10^6$  °K. These results suggest that considerable caution must be exercised in interpreting Lyman ratios to obtain "coronal temperatures". The cause of this effect is the very rapid increase in the Lyman ratio at low temperatures as shown in figure 1. The convolution of these theoretical ratios with any reasonable emission function may predict coronal temperatures considerably lower than the temperature of most efficient excitation of a particular hydrogen-like ion.



REFERENCES

- Beigman, I. L. and Vainshtein, L. A. 1967, *Astronomichiskii Zhurnal* 44, 668 (English Trans. *Soviet Astronomy A. J.* 11, 531).
- Gabriel, A. H. and Paget, T. M. 1972, *Jour. Physics B* 5, 673.
- Hutcheon, R. J. and McWhirter, R. W. P. 1973, *Jour. Phys. B* 6, 2668.
- Jacobs, A. 1968, *Solar Phys.* 5, 359.
- Kelly, R. L. and Palumbo, L. J. 1973, "Atomic and Ionic Emission Lines below 2000 Å: Hydrogen through Krypton". Naval Research Laboratory Report No. 7599, U. S. Govt. Printing Office, Washington, D. C.
- McWhirter, R. W. P. and Hearn, A. G. 1963, *Proc. Phys. Soc.* 82, 641.
- Shore, B. 1969, *Astrophys. J.* 158, 1205.
- Smith, T. S. 1969, "Les Transitions Interdites dan Les Spectres, des Astres", *Les Congres et Colloques de L'Universite' de Liege*, Vol. 54 Univ. of Liege, Belgium, p. 243.
- Van Regemorter, H. 1962, *Astrophys. J.* 136, 906.
- Walker, A. B. C. 1972, *Space Sci. Rev.* 13, 672.



Walker, A. B. C. and Rugge, H. R. 1971, *Astrophys. J.* 164, 181.

Walker, A. B. C., Rugge, H. R., Weiss, K. 1974a, *Astrophys. J.*  
188, (Paper I)

Walker, A. B. C., Rugge, H. R., Weiss, K. 1974b, "Relative  
Coronal Abundances Derived from X-Ray Observations II:  
Nitrogen, Oxygen, Neon, Magnesium, and Iron", to be published  
in *Astrophys. J.* Aug. 15, 1974 (Paper II).

# VI. RELATIVE CORONAL ABUNDANCES DERIVED FROM X-RAY OBSERVATIONS, I: SODIUM, MAGNESIUM, ALUMINUM, SILICON, SULFUR, AND ARGON\*

A. B. C. Walker, Jr., H. R. Rugge, and Kay Weiss

## ABSTRACT

We have observed the coronal spectrum between 3.5 and 8.5 Å and several levels of coronal activity, and determined absolute fluxes for 79 lines and for the continuum. Identifications have been determined for the majority of the lines observed, and in particular for the resonance lines of Mg XI, Mg XII, Al XII, Al XIII, Si XIII, Si XIV, SXV and SXVI. The measured fluxes of these lines have been used to construct a model of the temperature dependence of the coronal emission measure between  $1.5$  and  $10 \times 10^6$  K. This model is used to determine the relative abundances of Mg, Al, Si, and S. The relative abundances of Ar and Na were also computed, using the observed intensities of weak lines of these two elements. The relative abundances found are ( $A_{\text{Si}}$  has been arbitrarily set equal to  $35 \times 10^{-6}$ ,  $A_{\text{Mg}} = 30 \times 10^{-6}$ ,  $A_{\text{Al}} = 2.5 \times 10^{-6}$ ,  $A_{\text{Si}} = 35 \times 10^{-6}$ ,  $A_{\text{S}} = 9 \times 10^{-6}$ ,  $A_{\text{Ar}} = 6 \times 10^{-6}$ , and  $A_{\text{Na}} = 1.7 \times 10^{-6}$ . These abundances are in good agreement with the results of previous analyses of the coronal XUV spectrum, and with photospheric abundances.

We have used the coronal model based on the line fluxes to calculate the expected continuum fluxes, and compared these calculated fluxes with the observed continuum fluxes. The agreement between calculated and observed continuum flux is good near  $\sim 8\text{Å}$ , however, the calculated spectrum falls off more rapidly than the observed spectrum below  $\sim 6\text{Å}$ .

\*This paper has also been published as TR-0074(9260-02)-2, The Aerospace Corporation, El Segundo, California (21 November 1973) and in The Astrophysical Journal **188**, 423-440 (1974).

AD-A050 483

AEROSPACE CORP EL SEGUNDO CALIF IVAN A GETTING LABS  
COMPILATION OF SCIENTIFIC RESULTS FROM THE SATELLITE OV1-17.(U)  
DEC 77 H R RUGGE

F/G 3/2

F04701-77-C-0078

UNCLASSIFIED

TR-0078(3960-01)-1

SAMSO-TR-77-216

NL

2 OF 4  
AD  
A050483





# CONTENTS

ABSTRACT .....	115
I. INTRODUCTION .....	121
II. EXPERIMENTAL METHOD .....	123
III. OBSERVED SPECTRA .....	125
IV. IDENTIFICATION OF LINES .....	133
V. THE OBSERVED X-RAY CONTINUUM .....	147
VI. FORMULATION OF THE LINE FLUX INTEGRAL EQUATION .....	151
VII. ANALYSIS OF THE OBSERVED LINE FLUXES .....	157
VIII. ANALYSIS OF THE OBSERVED CONTINUUM .....	163
IX. SUMMARY .....	167
REFERENCES .....	169

## FIGURES

1.	Efficiency of the EDDT Spectrometer . . . . .	124
2.	Coronal spectra recorded at 0602 UT and 1529 UT . . . . .	126
3.	Coronal spectrum recorded at 1642 UT, shortly after the class 1 B flare at 1630 UT . . . . .	127
4.	Coronal spectra recorded at 1706 UT . . . . .	128
5.	Counting rate in the proportional counter during the time the spectra shown in Figures 2-4 were recorded . . . . .	129
6.	Franhofer Institute map of the sun for 1969 March 20 . . . . .	130
7.	Spectrum recorded at 1543 UT on 1969 March 21 . . . . .	132
8.	Enlarged portion of the 1642 UT spectra showing the Mg XI $1s^2 \ ^1S$ - $1s3p \ ^1P$ and $^3P$ lines . . . . .	144
9.	Spectrum of the x-ray continuum observed at 0602 UT on 1969 March 20 . . . . .	148
10.	Spectrum of the continuum observed at 1529, 1642, and 1706 UT on 20 March 1973 . . . . .	149
11.	Coronal models based on the 0604 UT spectrum . . . . .	160

## TABLES

1.	Wavelengths of Lines Observed in EDDT Spectra . . . . .	134
2.	Finding List of Lines Observed . . . . .	141
3.	Comparison of Observed and Calculated Positions of Possible Iron Lines . . . . .	145
4.	Relative Abundances Derived from XUV Line Intensities . . . . .	159
5.	Comparison of Observed and Calculated Line Intensities . . . . .	162
6.	Fractional Contribution of Various Elements to the X-ray Continuum . . . . .	164
7.	Comparison of Relative Abundances . . . . .	167



## I. INTRODUCTION

The flux in the solar spectrum below 25 Å is highly variable. All of the emission lines observed in this spectral region have their maximum emission at temperatures in excess of  $1.5 - 1.8 \times 10^6$  °K, the temperature at which previous analyses of EUV line fluxes [Jordan (1966), Pottasch (1967), and Widing and Sandlin (1968)] have found a maximum of material in the corona. These lines originate in ions which have appreciable abundance primarily in active regions.

We have studied the solar spectrum below 25 Å with three uncollimated Bragg crystal spectrometers and a proportional counter on board the satellite OV1-17 (1969 - 025A), which was launched in March of 1969. In this paper we use observations obtained with the proportional counter and one of the three crystal spectrometers to report on the absolute flux in the solar spectrum below 8.5 Å during a period of high solar activity on 1969 March 20. We have used these fluxes to construct models of the structure and composition of the solar atmosphere.

In a series of pioneering papers, Pottasch (1967) made use of solar EUV line fluxes to construct a model of the solar atmosphere, and to determine elemental abundances. His analysis is based on a technique which averages over the emission function of ions which have a significant fractional abundance over a narrow temperature range. Pottasch's method must be modified for the high temperature region of the solar atmosphere since many of the important ions are helium-like and have a large fractional abundance over a broad temperature range, while the emission measure may be a rapidly varying function of temperature. In addition, Pottasch considered only line emission resulting from collisional excitation. Recently, it has been demonstrated [Walker and Rugge (1971), Walker (1972) and Gabriel (1972)] that dielectronic recombination can make substantial contributions to resonance line fluxes.

In analyzing x-ray line fluxes to construct a model of the coronal structure, we have included the line emission accompanying dielectronic

recombination, and explicitly include the temperature variation of the emission function for each line considered.

Although we have presented the fluxes for three levels of solar activity, we have analyzed only one set of line fluxes, which we believe were obtained during conditions of thermal equilibrium in the corona.

## II. EXPERIMENTAL METHOD

The OV1-17 crystal spectrometers were accurately pointed at the sun by a compact solar pointer [Chater and Howey (1967)]. We shall be concerned here with only one of the crystals used; EDDT ( $2d = 8.81\text{\AA}$ ). The spectrometer is driven by a synchronous motor and scans continuously through 360 deg. Two crystals (EDDT and LiF) are mounted back to back. X-rays diffracted from the crystals are recorded by a krypton filled proportional counter, with a  $5.8\text{ mg/cm}^2$  beryllium window. The events recorded are stored in scalers which are sampled every 0.11 sec, which corresponds to 1.67 arcmin of crystal travel. This number was erroneously reported as 1.9 arcmin in Walker and Rugge (1970). In-flight calibration of the detector is provided by an  $\text{Fe}^{55}$  source mounted at one end of the crystal holder. No change in the source induced counting rate was observed in flight, when compared to laboratory calibration. Events observed in the detector are recorded only if their energy corresponds to a preselected range, defined by a pulse height window. The energy analysis of the recorded events reduces background events and scattered light to a low level.

The spectrometers were calibrated in the laboratory, using a demountable Henke-type x-ray tube [Henke (1963)] to excite characteristic x-ray lines from a fluorescent target. The entire instrument was calibrated in flight configuration at seven wavelengths. The Mn  $K\alpha$  measurements were obtained by using an intense  $\text{Fe}^{55}$  radioactive source. A flow-proportional counter was used to determine the absolute flux in the calibrating beam. The efficiency of the EDDT spectrometer was also calculated using the measured efficiency of each component of the spectrometer according to the relation

$$E(\lambda) = P(\lambda) R_c(\lambda) \omega^{-1} E_d(\lambda) A_d = \epsilon(\lambda) P(\lambda)$$

where  $E(\lambda)$  is the energy recorded under the observed line,  $P(\lambda)$  is the incident power,  $R_c(\lambda)$  is the coefficient of reflection of the crystal,  $\omega$  is the angular velocity of the crystal,  $E_d(\lambda)$  is the detector efficiency, and  $A_d$  is the detector area. The directly measured and computed efficiencies for EDDT are shown in Figure 1, along with the efficiency curve which was used to obtain the absolute fluxes reported here.



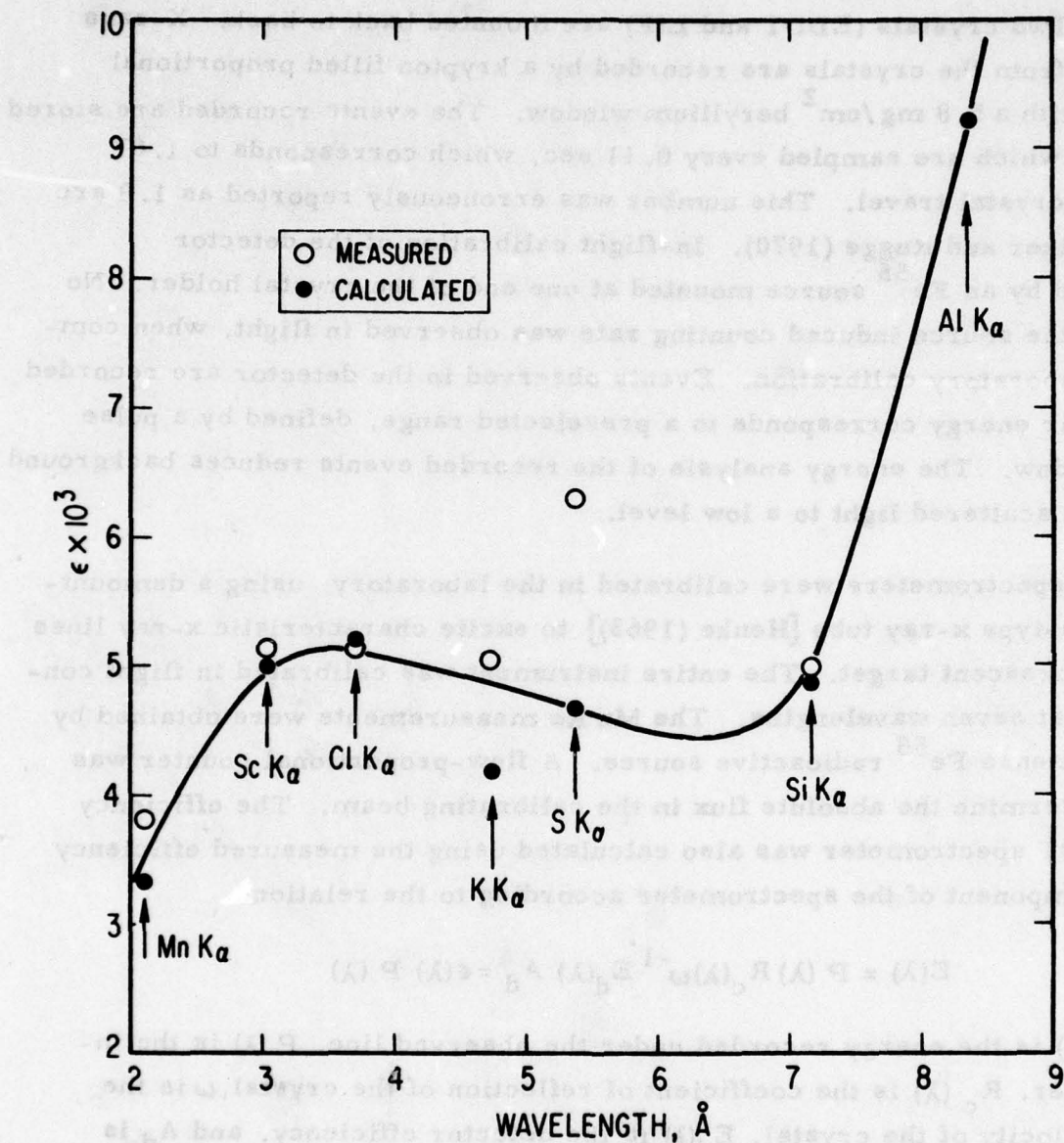


Figure 1. Efficiency of the EDDT Spectrometer.

### III. OBSERVED SPECTRA

We shall report here on EDDT spectra obtained at 0602 UT, 1529 UT, 1642 UT, and 1706 UT on 1969 March 20. The sun was highly active on that day. The daily 2800-MHz solar flux measured at Ottawa was 215 flux units, one of the highest levels recorded during that year. There were a number of subflares reported during the day starting at 0700 UT, including a class - B flare reported at 1450 UT, and class 1B flares reported at 1550 and 1630 UT (ESSA 1969). SID events were also reported at or near these two later times.

Spectra obtained with the EDDT spectrometer are shown in Figures 2, 3, and 4. There were no transient events reported near 0602 UT, so we may assume that the flux observed is associated with one or more of the active regions on the disk. The remaining spectra were obtained during or shortly after flares. Figure 5 shows the counting rate in two channels of the proportional counter, and clearly demonstrates the enhancement associated with the 1630 UT flare. Figure 6 shows the Fraunhofer Institute map for this date. All of the flares listed above occurred above or near region 994. This was also the most intense radio region at 9.1 and 21 cm. on that date (ESSA 1969).

Considerable information can be obtained by studying the profiles of the emission lines observed. For an uncollimated plane crystal spectrometer, the line profile is determined by the sampling rate, the natural width or rocking curve of the crystal, and the distribution of discrete sources across the solar disk in the direction of scan. Doppler widths are too narrow to be observed with the present spectrometer. The crystal rocking curve width is an increasing function of wavelength. We have not measured the natural width of the EDDT crystal used; however, we may still set an upper limit to the size of the region of enhanced emission. For the spectra obtained at 0602 UT and 1529 UT, with the exception of the Mg XII Lyman- $\alpha$  line (8.42A), the line profiles are approximately 5 arcmin wide. The Mg XII Lyman- $\alpha$  line is 15 arcmin wide. However, the Mg XII Lyman- $\alpha$  should have a profile similar to that of the Mg XII Lyman- $\beta$  line. The profile of the Lyman- $\beta$  line is 5 arcmin wide, strongly suggesting that the Lyman- $\alpha$  line width is instrumental.





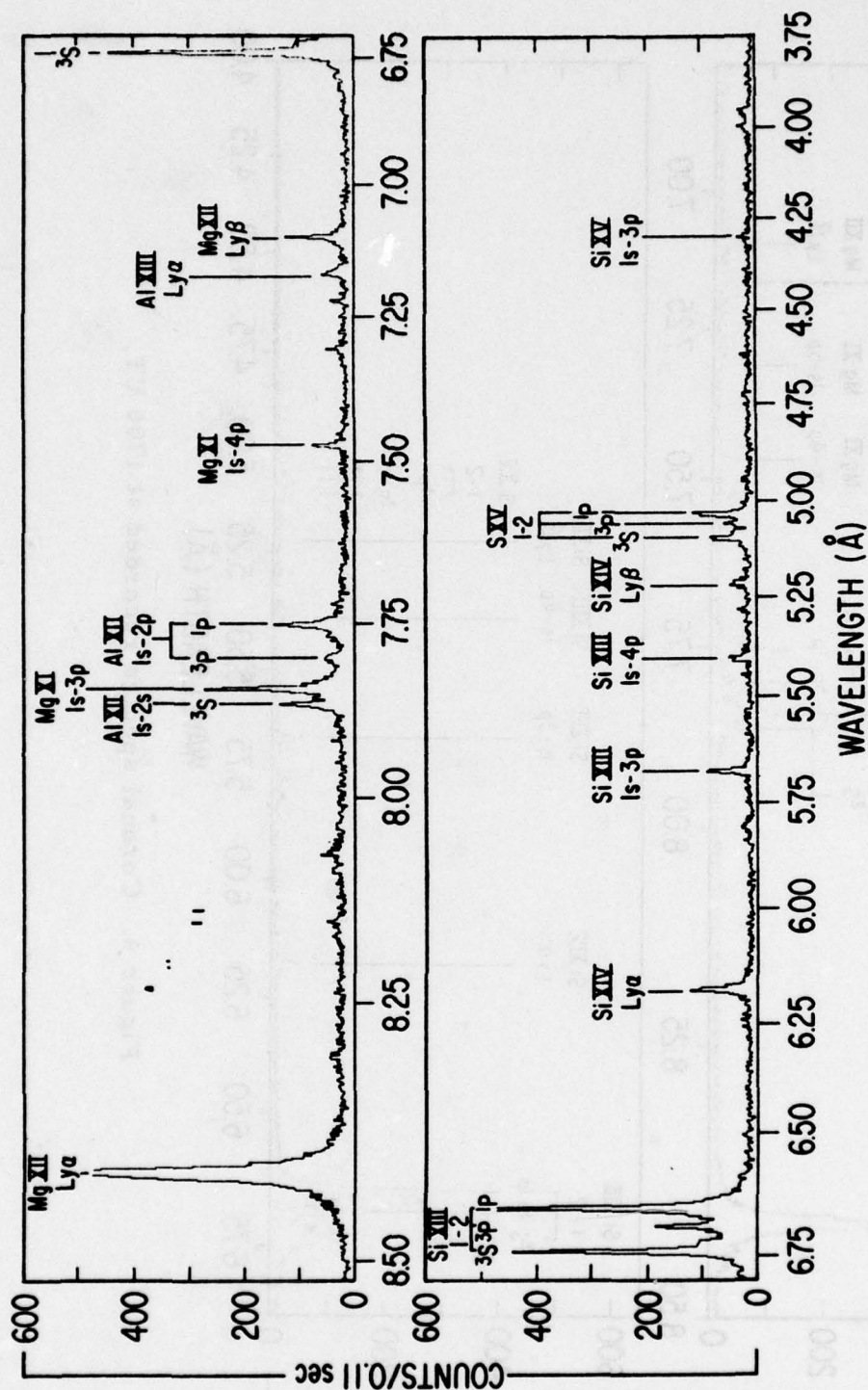


Figure 3. Coronal spectrum recorded at 1642 UT, shortly after the class 1 B flare at 1630 UT.

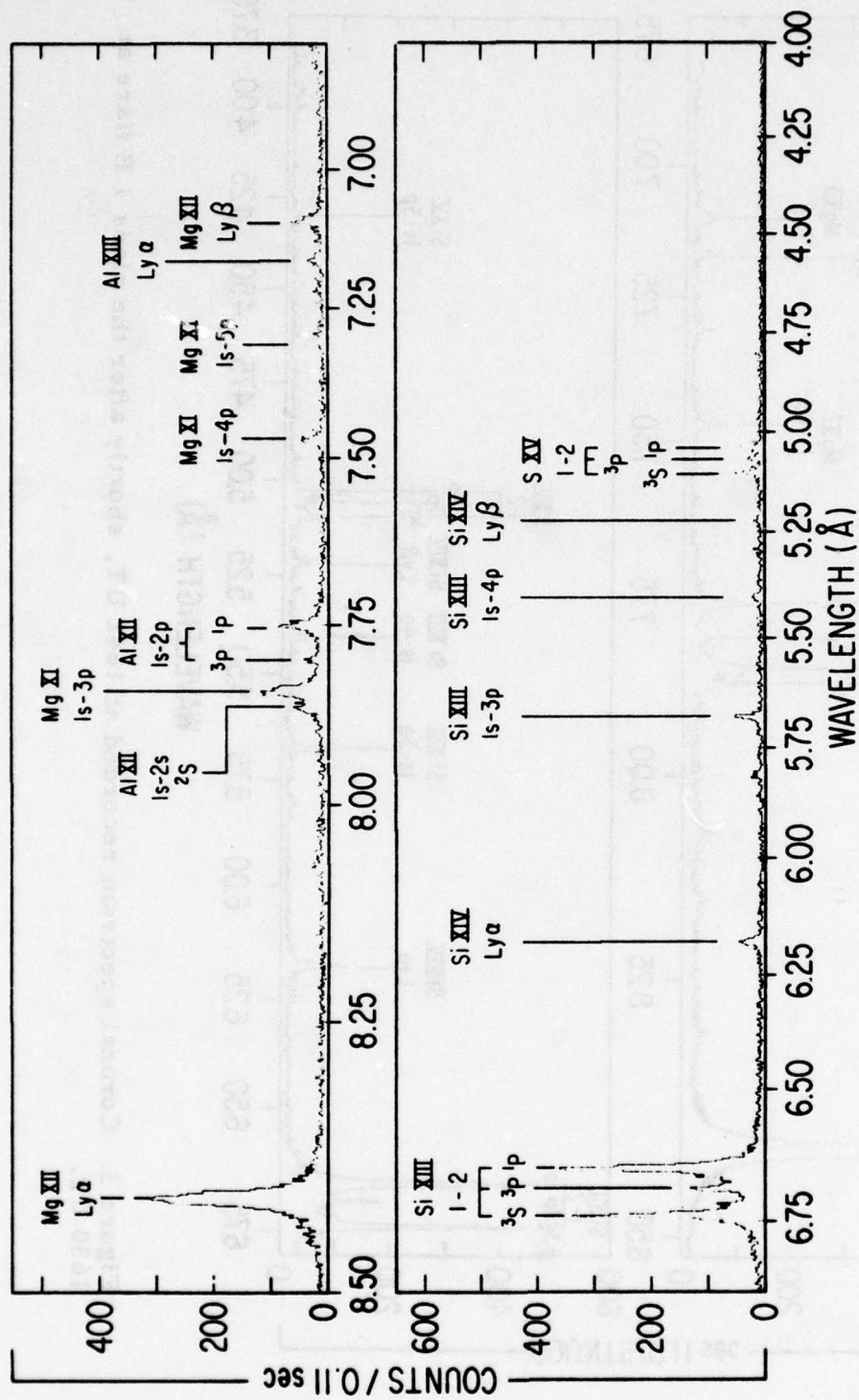


Figure 4. Coronal spectra recorded at 1706 UT.

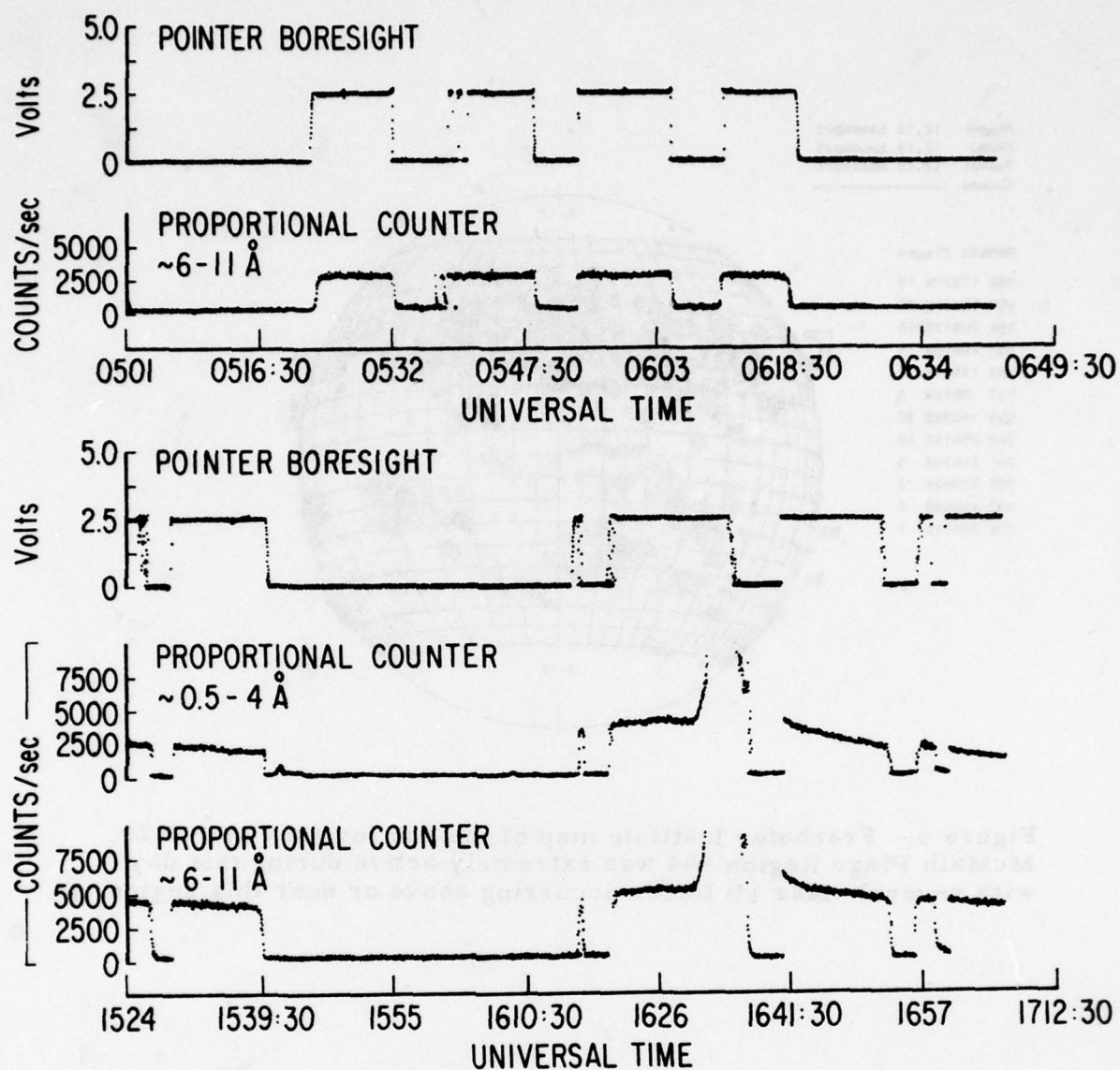


Figure 5. Counting rate in the proportional counter during the time the spectra shown in Figures 2-4 were recorded. The pointer boresight indicates the periods during which the experiment was sun pointed. The flare at 1630 UT caused counter saturation.



Plages 12.12 Anacapr1  
 Filam. 12.15 Anacapr1  
 Promin. 12.15 Anacapr1  
 Corona

**McMath Plages**

986 12S77W 13  
 988 15S40W 35  
 994 20W17E260  
 995 22W59W 15  
 996 17N41W 10  
 997 8S14W 3  
 999 16S34E 32  
 000 25S16E 18  
 001 30S38E 9  
 002 22S82W 2  
 003 11W56E 7  
 004 30N71W 7

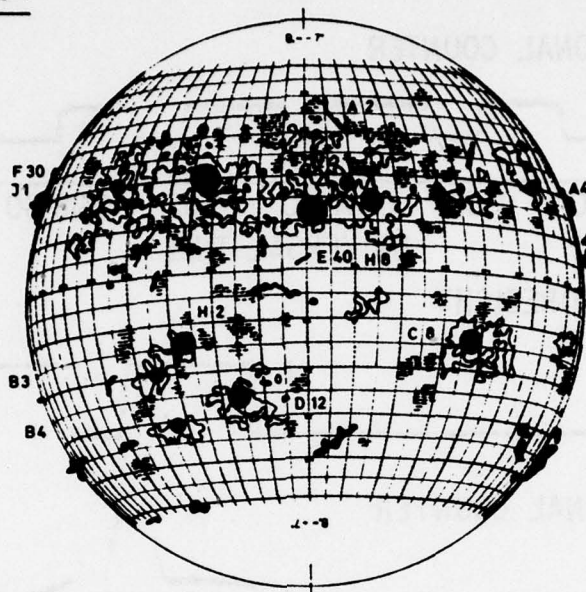
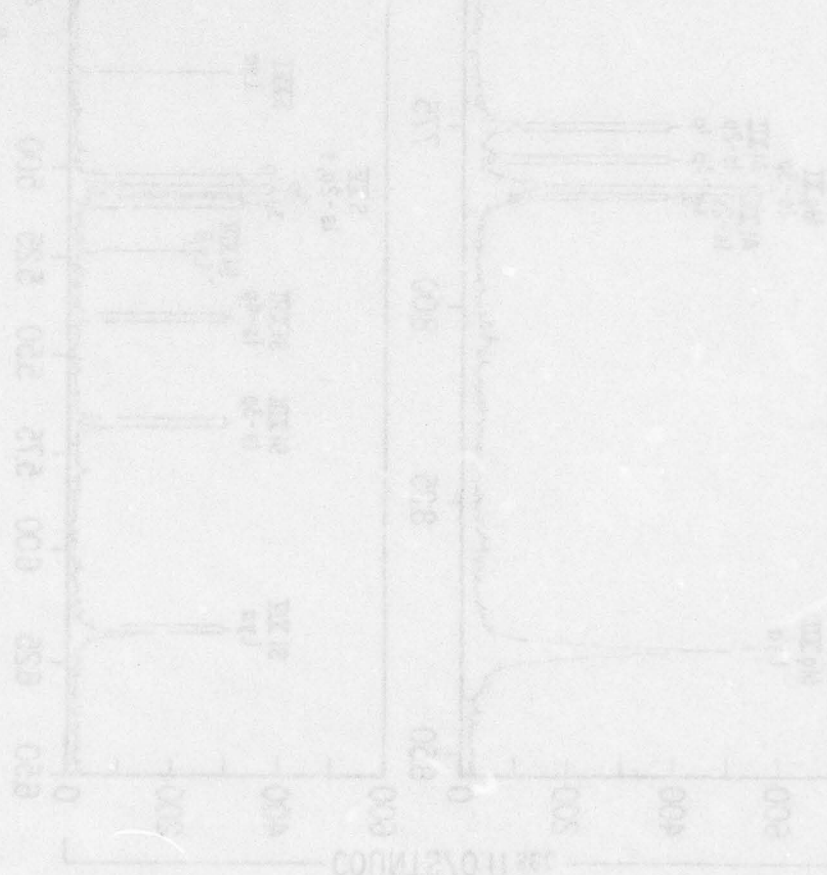


Figure 6. Franhofer Institute map of the sun for 1969 March 20. McMath Plage Region 994 was extremely active during this day with several class 1B flares occurring above or near this region.

The two flares (1550 and 1630 UT) which preceded the 1642 UT spectra were located at N20, E20 and N12, W8, respectively on the disk (ESSA 1969), approximately 5 arcmin apart as viewed from the earth. The line profiles in the 1642 UT spectrum appear slightly broader than those obtained at 1529 UT, suggesting that at least two regions contributed significantly to the observed flux.

If there are two or more regions of enhanced emission which are sufficiently well separated in a direction parallel to the direction of crystal scan, then the observed line profiles will show a distinct line corresponding to each of the emitting regions. Figure 7 shows a spectrum obtained at 1543 UT on March 21, which illustrates this situation. The interesting set of spectra obtained on March 21, also a day of very high solar activity, will be more fully discussed in a subsequent paper.



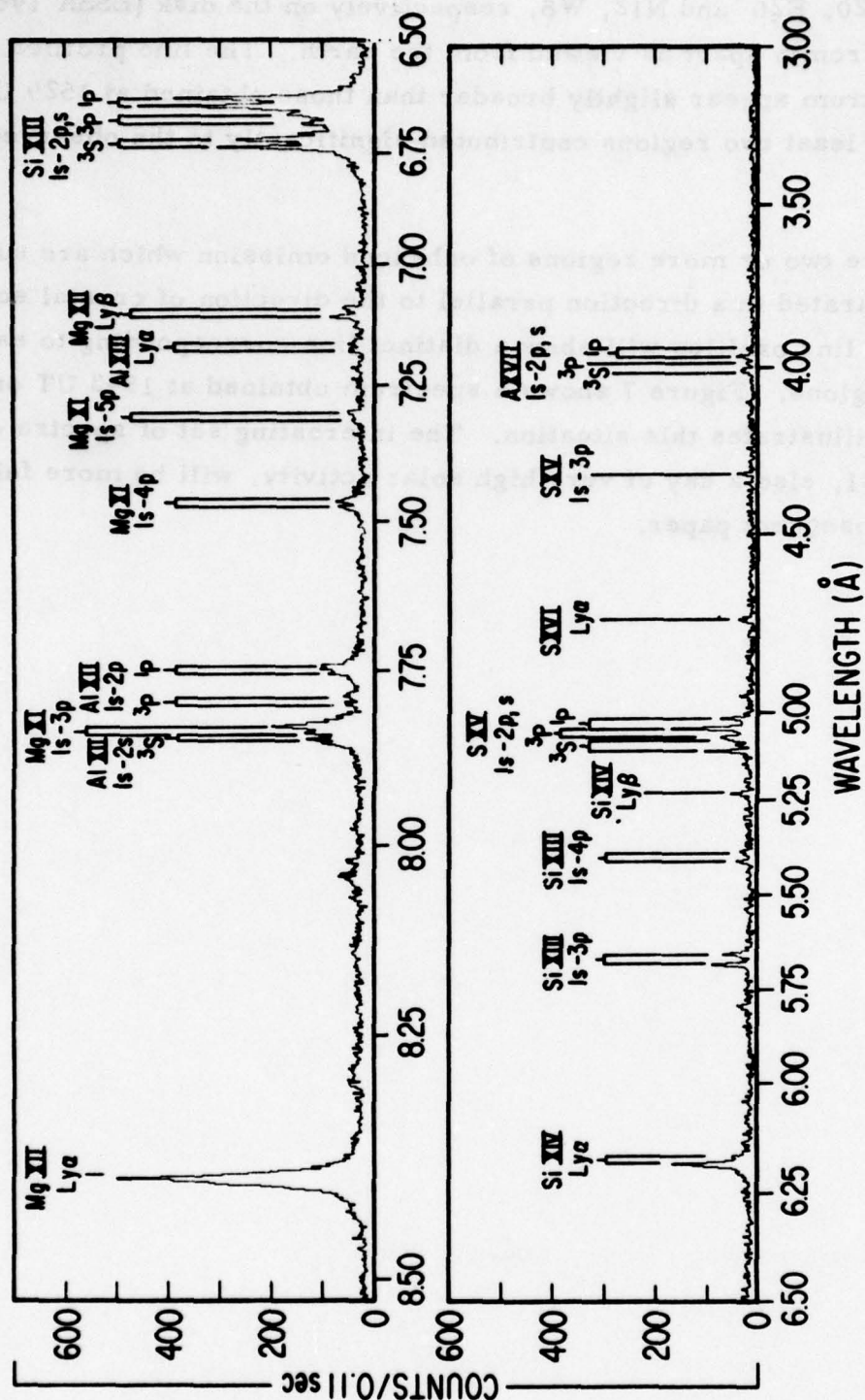


Figure 7. Spectrum recorded at 1543 UT on 1969 March 21. Two separate regions contributed strongly to the coronal flux. The region on the left was clearly hotter, showing stronger Si XIV and S XVI lines, although the Mg XI lines from both regions are equally intense.



#### IV. IDENTIFICATION OF LINES

Precise wavelengths from laboratory observations are not available for all of the lines observed by the EDDT spectrometer. The strongest emission lines observed are due to transitions in helium-like and hydrogen-like ions. As we shall see, forbidden lines are often emitted with intensities comparable to those of resonance lines because of the low collisional de-excitation rates in the corona. To obtain the wavelengths of lines originating in hydrogen-like spectra, we have used the calculations of Garcia and Mack (1965). For lines of the helium-like iso-electronic sequence, the Atomic Energy Level Tables of Moore (1949), and of Kelly (1968) tabulate wavelengths up to Al XII for allowed transitions, and to [O VII] for forbidden transitions. Vainshtein and Sofonava (1971) and Gabriel (1972) have calculated wavelengths for higher members of the helium isoelectronic sequence. For transitions not tabulated in the above references, we have extrapolated published values for lower members of the isoelectronic sequence. Details of these extrapolations are given in Walker and Rugge (1970):

Table 1 lists the wavelengths of lines observed in the EDDT spectra, gives the line identifications and predicted or laboratory-determined wavelengths, and the fluxes of each line in the spectra shown in Figure 2, 3, and 4. The extrapolated wavelengths are in good agreement with our measurements. The references given in Table 1 include recent observations of a number of helium-like and hydrogen-like lines in laboratory plasmas. A finding list for the lines observed is given in Table 2.

The wavelengths listed in Table 1 as observed were determined by using the Mg XII Lyman- $\alpha$  line at 8.421A as a standard. All other wavelengths were assigned using the position of this line, and the precisely known scanning rate of the spectrometer. The wavelength of the Mg XII line was confirmed to be correct to within the accuracy of the spectrometer calibration (.005A) using the geometry of the spectrometer and the precisely known wavelength of the Fe XVII 17.05A and O-VIII 18.96 A lines observed with the KAP spectrometer [Walker and Rugge (1970)] These observed wavelengths agree with our absolute laboratory wavelength calibration to within the .05A accuracy of that calibration.

Table 1  
Wavelengths of Lines Observed in EDDT Spectra

Observed Wavelength (Å)	Line Intensity ( $10^{-5}$ ergs $\text{cm}^{-2}$ $\text{sec}^{-1}$ )			Ion	Predicted Wavelength (Å)	Transition		Ref.
	0602 UT	1529 UT	1642 UT			Multiplet	J-J	
8.573	-	0.7	1.1	-	8.567			1
8.550	-	0.6	1.7	Mg XI	8.548	$1s^2p^1P - 2p^2^1D$	1-2	1
8.518	-	-	0.8	Mg XI	8.519	$1s^2s^3S - 2s2p^3P$		1
8.454	0.2	0.7	1.3	Na XI	8.459	$1s^2S - 3p^2P$	$11/2-1/2$ $11/2-3/2$	2
8.451	0.1	0.5	1.2					
8.443	0.4	0.2	0.7					
8.421*	17.4	102.8	190.8	Mg XII	8.421	$1s^2S - 2p^2P$	$11/2-1/2$ $11/2-3/2$	2
8.393 <sup>†</sup>	0.1	0.6	0.8	Fe XXIII	8.380	$1s^22s^1S - 1s^22s4p^3P$	0-1	
8.383*	0.3	0.2	0.6	Fe XXIV	8.378	$1s^22p^2P - 1s^24s^2S$	$3/2-1/2$	3
8.305*	-	1.0	2.9	Fe XXIII	8.307	$1s^22s^2^1S - 1s^22s4p^1P$	0-1	3
8.289*	-	0.5	0.8					
8.275	-	-	0.6	Fe XXIV	8.279	$1s^22p^2P - 1s^24s^2S$	$1/2-1/2$	3
8.238 <sup>†</sup>	-	-	0.5	Fe XXIV	8.225	$1s^22p^2P - 1s^24d^2D$	$1/2-3/2$	3
8.172*	-	0.3	1.7					
8.150*	-	0.9	0.6					
8.091*	0.3	0.7	2.8					
8.080*	0.3	1.1	0.9					
8.068*	2.3	3.4	4.2	Mg X	8.073	$1s^22p^2P - 1s2p3p^2D$		1

Table 1 (con't)

Observed Wavelength (Å)	Line Intensity ( $10^{-5}$ ergs $\text{cm}^{-2} \text{sec}^{-1}$ )				Ion	Predicted Wavelength (Å)	Transition		Ref.
	0602 UT	1529 UT	1642 UT	1706 UT			Multiplet	J-J	
8.034	0.6	1.0	1.6	0.8	Mg X	8.039	$1s^2 2s^2 S - 1s2s3p^2 P$		1
7.893	0.8	1.4	2.1	1.4					
7.873*	4.5	12.0	21.2	9.5	{ Al XI	7.878 7.875	$1s^2 2p^2 P - 1s2p^2 D$	$3/2-5/2$ $1/2-3/2$	4
7.864*	0.3	0.6	1.8	1.8	{ Al XII	7.871	$1s^2 1S - 1s2s^3 S$	0-1	
7.852*	11.0	37.2	44.4	29.9	Mg XI	7.863	$1s^2 1S - 1s3p^3 P$	0-1	1
7.830	2.0	6.0	5.8	4.4	{ Mg XI	7.850 7.848 7.846	$1s^2 1S - 1s3p^1 P$ $1s^2 2s^2 S - 1s2s2p^2 P$	0-1 $1/2-3/2$ $1/2-1/2$	1 4
7.807	1.8	9.3	8.2	5.8	{ Al XI	7.810 7.809	$1s^2 2s^2 S - 1s2s2p^2 P$	$1/2-1/2$ $1/2-3/2$	4
7.769	0.4	4.4	6.2	3.4	{ Al XII	7.807 7.804	$1s^2 1S - 1s2p^3 P$	0-1 0-2	4
7.751*	5.4	19.6	21.3	19.4	{ Al XI	7.802 7.799	$1s^2 2p^2 P - 1s2p^2 S$	$3/2-1/2$ $1/2-1/2$	4
7.734	0.2	1.7	3.9	1.9			$1s^2 3p^2 P - 1s2p3p^2 D$ $1s^2 3s^2 S - 1s2p3s^2 P$		1
7.724	0.4	2.2	2.1	1.1	Al XII	7.756	$1s^2 1S - 1s2p^1 P$	0-1	5



Table 1 (con't)

Observed Wavelength (Å)	Line Intensity ( $10^{-5}$ ergs $\text{cm}^{-2}$ $\text{sec}^{-1}$ )				Ion	Predicted Wavelength (Å)	Transition		Ref.
	0602 UT	1529 UT	1642 UT	1706 UT			Multiplet	J-J	
7.474*	2.0	7.0	10.2	7.7	Mg XI	7.473	$1s^2 1S - 1s4p^1P$	0-1	5
7.316*	1.0	2.9	5.7	4.0	Mg XI	7.310	$1s^2 1S - 1s5p^1P$	0-1	5
7.223	0.7	1.1	4.0	1.7	Mg XI	7.228	$1s^2 1S - 1s6p^1P$	0-1	6
7.177	0.2	1.0	3.6	1.5	Mg XI	7.180	$1s^2 1S - 1s7p^1P$	0-1	6
7.173*	0.8	5.1	7.6	4.4	Al XIII	7.173	$1s^2 S - 2p^2P$	$1/2-1/2$ $1/2-3/2$	2
7.156	0.2	0.7	2.6	1.4	Mg XI	7.153	$1s^2 1S - 1s8p^1P$	0-1	6
7.142	0.2	2.3	1.2	0.4					
7.128	-	0.1	2.0	1.0	Mg XI	7.129	$1s^2 1S - 1s9p^1P$	0-1	6
7.101*	2.0	20.3	27.6	17.1	Mg XII	7.106	$1s^2 S - 3p^2P$	$1/2-1/2$ $1/2-3/2$	2
6.805	1.3	1.7	2.7	3.3					
6.788*	0.9	3.3	6.6	3.6	Si XII	$\overline{6.788}$ $\overline{6.786}$	$1s^2 2s^2 S - 1s2s2p^4P$	$1/2-1/2$ $1/2-3/2$	4
6.772	0.4	2.7	2.1	1.9	Si XII	6.786	$1s^2 2p^2P - 1s2p^2P$	3/2-1/2	4
6.765	1.3	3.3	6.0	8.0					
6.739*	29.3	85.0	138.4	110.0	Si XII	$\overline{6.744}$ $\overline{6.741}$	$1s^2 2p^2P - 1s2p^2D$	$3/2-5/2$ $1/2-3/2$	4
					Si XIII	$\overline{6.739}$	$1s^2 1S - 1s2s^3S$	0-1	4
					Mg XII	6.738	$1s^2 S - 4p^2P$	1/2-1/2	2

Table 1 (con't)

Observed Wavelength (Å)	Line Intensity ( $10^{-5}$ ergs $\text{cm}^{-2} \text{sec}^{-1}$ )				Ion	Predicted Wavelength (Å)	Transition		Ref.
	0602 UT	1529 UT	1642 UT	1706 UT			Multiplet	J-J	
6.719	13.2	26.8	32.3	21.1	Si XII	6.720 6.718	$1s^2 2s^2 S - 1s2s2p^2 P$	$1/2-1/2$ $1/2-3/2$	4
6.688*	18.9	47.7	65.9	59.7	Si XII	6.690 6.689	$1s^2 2s^2 S - 1s2s2p^2 P$	$1/2-1/2$ $1/2-3/2$	4
						6.688 6.685	$1s^2 1S - 1s2p^3 P$	0-1 0-2	4
						6.682 6.678	$1s^2 2p^2 P - 1s2p^2 2S$	$3/2-1/2$ $1/2-1/2$	4
						6.647	$1s^2 1S - 1s2p^1 P$	0-1	4
6.649*	49.5	157.1	226.7	168.5	Al XII	6.646	$1s^2 1S - 1s3p^3 P$	0-1	1
						6.635	$1s^2 1S - 1s3p^1 P$	0-1	5
6.609	1.1	6.1	8.7	5.8	Mg XII	6.580	$1s^2 S - 5p^2 P$	$1/2-1/2$ $1/2-3/2$	2
6.588*	0.9	1.2	7.9	2.1			$1s^2 S - 6p^2 P$	$1/2-1/2$ $1/2-3/2$	2
6.503	-	-	2.5	-	Mg XII	6.497	$1s^2 S - 6p^2 P$	$1/2-1/2$ $1/2-3/2$	2
6.257†	-	-	1.4	-	Si XIII	6.263	$1s2p^1 P - 2p^2 1D$	1-2	1
6.236†	-	-	1.3	-	Si XIII	6.244	$1s2s^3 S - 2s2p^3 P$		1
6.213†	-	-	0.6	-	Si XIII	6.224	$1s2s^1 S - 2s2p^1 P$	0-1	1
6.200†	-	-	0.9	-	Si XIII	6.200	$1s2p^1 P - 2p^2 1S$	1-0	1
6.179*	3.1	25.5	47.7	15.1	Si XIV	6.182	$1s^2 S - 2p^2 P$	$1/2-1/2$ $1/2-3/2$	
5.842	0.4	0.6	2.3	0.8					

Table 1 (con't)

Observed Wavelength (Å)	Line Intensity ( $10^{-5}$ ergs $\text{cm}^{-2}$ $\text{sec}^{-1}$ )			Ion	Predicted Wavelength (Å)	Transition		Ref.
	0602 UT	1529 UT	1642 UT			Multiplet	J-J	
5.810*	1.6	4.3	6.2	4.3	Si XII	$1s^2 2p^2 P - 1s2p3p^2 D$		1
						$1s^2 2s^2 S - 1s2s3p^2 P$		
5.788	0.6	1.9	1.6	0.2				
5.680*	3.2	13.0	24.7	14.6	Si XIII	$1s^2 1S - 1s3p^3 P$	0-1	1
						$1s^2 1S - 1s3p^1 P$	0-1	
5.401*	0.9	4.6	12.8	4.9	Si XIII	$1s^2 1S - 1s4p^1 P$	0-1	6
5.282*		0.8	5.2	1.2	Si XIII	$1s^2 1S - 1s5p^1 P$	0-1	6
5.219*	0.4	3.9	16.6	2.7	Si XIII	$1s^2 1S - 1s6p^1 P$	0-1	6
					Si XIV	$1s^2 S - 3p^2 P$	$1/2-1/2$ $1/2-3/2$	2
5.136*†	-	0.6	0.8	0.7	S XIV	$1s^2 2s^2 S - 1s2s2p^4 P$	$1/2-1/2$ $1/2-3/2$ $3/2-1/2$	4
5.125†	-	0.2	0.6	0.3	S XIV	$1s^2 2p^2 P - 1s2p^2 4P$	$3/2-5/2$ $1/2-3/2$	4
5.105*	2.4	12.8	26.7	10.4	S XIV	$1s^2 2p^2 P - 1s2p^2 2D$	$1/2-3/2$ $1/2-1/2$	4
					S XV	$1s^2 1S - 1s2s^3 S$	0-1	4
5.088*	1.5	3.5	7.4	1.4	S XVI	$1s^2 2s^2 S - 1s2s2p^2 P$	$1/2-1/2$ $1/2-3/2$	4



Table 1 (con't)

Observed Wavelength (Å)	Line Intensity ( $10^{-5}$ ergs $\text{cm}^{-2} \text{sec}^{-1}$ )			Ion	Predicted Wavelength (Å)	Transition		Ref.
	0602 UT	1529 UT	1642 UT	1706 UT		Multiplet	J-J	
5.066*	2.5	9.8	10.6	6.5	{ S XIV 5.067 5.066	$1s^2 2s^2 S - 1s2s2p^2 P$	$1/2-1/2$ $1/2-3/2$	4
					{ S XV 5.066 5.063	$1s^2 1S - 1s2p^3 P$	0-2 0-1	4
					{ S XIV 5.062 5.058	$1s^2 2p^2 P - 1s2p^2 2S$	$3/2-1/2$ $1/2-1/2$	4
5.036*	4.9	19.7	43.0	12.7	S XV 5.038	$1s^2 1S - 1s2p^1 P$	0-1	4
4.968	-	0.5	2.1	0.4				
4.948*	0.4	1.1	3.0	0.2	Si XIV 4.947	$1s^2 S - 4p^2 P$	$1/2-1/2$ $1/2-3/2$	2
4.734*	0.1	1.5	1.7	0.8	S XVI 4.729	$1s^2 S - 2p^2 P$	$1/2-1/2$ $1/2-3/2$	2
4.303*	0.7	3.2	5.8	1.7	S XV 4.304 4.299	$1s^2 1S - 1s3p^3 P$ $1s^2 1S - 1s3p^1 P$	0-1 0-1	6
3.989	0.7	4.3	8.5	1.5	{ Ar XVI 3.995 3.991	$1s^2 2p^2 P - 1s2p^2 2D$	$1/2-3/2$ $1/2-1/2$	1
					{ Ar XVII 3.993	$1s^2 1S - 1s2s^3 S$	0-1	4
					{ Ar XVI 3.983 3.981	$1s^2 2s^2 S - 1s2s2p^2 P$	$1/2-1/2$ $1/2-3/2$	4
3.969	1.0	1.8	2.9	0.8	{ Ar XVI 3.969 3.968	$1s^2 2s^2 S - 1s2s2p^2 P$	$1/2-1/2$ $1/2-3/2$	4
					{ Ar XVII 3.969 3.965	$1s^2 1S - 1s2p^3 P$	0-2 0-1	4
					{ Ar XVI 3.966 3.962	$1s^2 2p^2 P - 1s2p^2 2S$	$3/2-1/2$ $1/2-1/2$	4
3.950	0.9	2.8	6.4	2.5	Ar XVII 3.948	$1s^2 1S - 1s2p^1 P$	0-1	4

Table 1 (con't)

\* Observed by Doschek (1972)

† Integrated flux less than 20 counts for all spectra.

Underlined transitions are expected to be the strongest transition in the blend.

References For Table 1

1. Walker, A. B. C. Jr. and Rugge, H. R. 1971, *Astrophys J.* 164, 181.
2. Garcia, J. D. and Mack, J. E., 1965, *J. Opt. Soc. Am.* 55, 654.
3. Doschek, G. A., Meekins, J. F., and Cowan, R. D., 1972, *Astrophys. J.* 177, 261.
4. Gabriel, A. H., 1972 a, *Mon. Not. Roy. Astr. Soc.* 160, 99.
5. Flemberg, H., 1942, *Ark. Mat. Astr. Fys.* 28A, 1.
6. Walker, A. B. C. Jr., 1972, *Unpublished Wave Numbers Extrapolations.*

**Table 2**  
**Finding List of Lines Observed.**  
**Wavelengths in angstroms**

Na XI

8.454  $1s^2 S - 3p^2 P$

Mg X

8.068  $\uparrow 1s^2 2p^2 P - 1s2p3p^2 D$

8.034  $\uparrow 1s^2 2s^2 S - 1s2s3p^2 P$

Mg XI

8.550  $\uparrow 1s2s^3 S - 2s2p^3 P$

8.518  $\uparrow 1s2p^1 P - 2p^2^1 D$

7.684  $1s^2^1 S - 1s3p^3 P$

7.852  $1s^2^1 S - 1s3p^1 P$

7.474  $1s^2^1 S - 1s4p^1 P$

7.316  $1s^2^1 S - 1s5p^1 P$

7.233  $1s^2^1 S - 1s6p^1 P$

7.177  $1s^2^1 S - 1s7p^1 P$

7.156  $1s^2^1 S - 1s8p^1 P$

7.128  $1s^2^1 S - 1s9p^1 P$

Mg XII

8.421  $1s^2 S - 2p^2 P$

7.101  $1s^2 S - 3p^2 P$

6.739\*  $1s^2 S - 4p^2 P$

6.588  $1s^2 S - 5p^2 P$

6.503  $1s^2 S - 6p^2 P$

Al XI

7.873\* $\uparrow 1s^2 2p^2 P - 1s2p^2^2 D$

7.852\* $\uparrow 1s^2 2p^2 S - 1s2s2p^2 P$

7.807\* $\uparrow 1s^2 2s^2 S - 1s2s2p^2 P$

$\left\{ \begin{array}{l} 1s^2 2p^2 P - 1s2p^2^2 S \\ 1s^2 3p^2 P - 1s2p3p^2 D \\ 1s^2 3s^2 S - 1s2p3s^2 P \end{array} \right.$

7.769  $\left\{ \begin{array}{l} 1s^2 3p^2 P - 1s2p3p^2 D \\ 1s^2 3s^2 S - 1s2p3s^2 P \end{array} \right.$

$\left\{ \begin{array}{l} 1s^2 3p^2 P - 1s2p3p^2 D \\ 1s^2 3s^2 S - 1s2p3s^2 P \end{array} \right.$

Al XII

7.873  $1s^2^1 S - 1s2s^3 S$

7.807  $1s^2^1 S - 1s2p^3 P$

7.751  $1s^2^1 S - 1s2p^1 P$

6.649\*  $\left\{ \begin{array}{l} 1s^2^1 S - 1s3p^3 P \\ 1s^2^1 S - 1s3p^1 P \end{array} \right.$

$\left\{ \begin{array}{l} 1s^2^1 S - 1s3p^3 P \\ 1s^2^1 S - 1s3p^1 P \end{array} \right.$

Al XIII

7.173  $1s^2 S - 2p^2 P$

Si XII

$\left\{ \begin{array}{l} 1s^2 2s^2 S - 1s2s2p^4 P \\ 1s^2 2p^2 P - 1s2p^2^4 P \\ 1s^2 2p^2 P - 1s2p^2^2 D \end{array} \right.$

6.788  $\left\{ \begin{array}{l} 1s^2 2p^2 P - 1s2p^2^4 P \\ 1s^2 2p^2 P - 1s2p^2^2 D \end{array} \right.$

6.739\* $\uparrow 1s^2 2p^2 P - 1s2p^2^2 D$

6.719  $\uparrow 1s^2 2s^2 S - 1s2s2p^2 P$

6.688\* $\uparrow 1s^2 2s^2 S - 1s2s2p^2 P$

$\left\{ \begin{array}{l} 1s^2 2p^2 P - 1s2p^2^2 S \\ 1s^2 2p^2 P - 1s2p3p^2 D \end{array} \right.$

5.810  $\uparrow 1s^2 2s^2 S - 1s2s3p^2 P$

$\left\{ \begin{array}{l} 1s^2 2p^2 P - 1s2p3p^2 D \\ 1s^2 2s^2 S - 1s2s3p^2 P \end{array} \right.$

Si XIII

6.739  $1s^2^1 S - 1s2s^3 S$

6.688  $1s^2^1 S - 1s2p^3 P$

6.649  $1s^2^1 S - 1s2p^1 P$

6.257  $\uparrow 1s2p^1 P - 2p^2^1 D$

6.236  $\uparrow 1s2s^3 S - 2s2p^3 P$

6.213  $\uparrow 1s2s^1 S - 2s2p^1 P$

6.200  $\uparrow 1s2p^1 P - 2p^2^1 S$

$\left\{ \begin{array}{l} 1s^2^1 S - 1s3p^3 P \\ 1s^2^1 S - 1s3p^1 P \end{array} \right.$

5.680  $\left\{ \begin{array}{l} 1s^2^1 S - 1s3p^3 P \\ 1s^2^1 S - 1s3p^1 P \end{array} \right.$

5.401  $1s^2^1 S - 1s4p^1 P$

5.282  $1s^2^1 S - 1s5p^1 P$

5.219\*  $1s^2^1 S - 1s6p^1 P$

Si XIV

6.179  $1s^2 S - 2p^2 P$

5.219  $1s^2 S - 3p^2 P$

4.948  $1s^2 S - 4p^2 P$



Table 2 (con't)

S XIV

5.136	$\left\{ \begin{array}{l} 1s^2 2s^2 S - 1s2s2p^4 P \\ 1s^2 2p^2 P - 1s2p^2 4P \end{array} \right.$
5.125 †	$1s^2 2p^2 P - 1s2p^2 4P$
5.105*†	$1s^2 2p^2 P - 1s2p^2 2D$
5.088 †	$1s^2 2s^2 S - 1s2s2p^2 P$
5.066*†	$\left\{ \begin{array}{l} 1s^2 2s^2 S - 1s2s2p^2 P \\ 1s^2 2p^2 P - 1s2p^2 2S \end{array} \right.$

Possible Weak Lines

5.271
5.705
5.692
5.118
5.009
4.322

S XV

5.105	$1s^2 1S - 1s2s^3 S$
5.066	$1s^2 1S - 1s2p^3 P$
5.036	$1s^2 1S - 1s2p^1 P$
4.303	$\left\{ \begin{array}{l} 1s^2 1S - 1s3p^3 P \\ 1s^2 1S - 1s3p^1 P \end{array} \right.$

Unidentified Lines

8.573
8.448
8.443
8.289
8.172
8.150
8.091
8.080
7.893
7.830
7.734
7.724
7.142
6.805
6.772
6.765
6.609
5.842
5.788
4.968

S XVI

4.734	$1s^2 S - 2p^2 P$
-------	-------------------

Ar XVI

3.989*†	$\left\{ \begin{array}{l} 1s^2 2p^2 P - 1s2p^2 2D \\ 1s^2 2s^2 S - 1s2s2p^2 P \end{array} \right.$
3.969*†	$\left\{ \begin{array}{l} 1s^2 2s^2 S - 1s2s2p^2 P \\ 1s^2 2p^2 P - 1s2p^2 2S \end{array} \right.$

Ar XVII

3.989	$1s^2 1S - 1s2s^3 S$
3.969	$1s^2 1S - 1s2p^3 P$
3.950	$1s^2 1S - 1s2p^1 P$

Fe XXIII

8.393	$1s^2 2s^2 1S - 1s^2 2s4p^3 P$
8.305	$1s^2 2s^2 1S - 1s^2 2s4p^1 P$

Fe XXIV

8.383	$1s^2 2p^2 P - 1s^2 4s^2 S$
8.275	$1s^2 2p^2 P - 1s^2 4s^2 S$
8.238	$1s^2 2p^2 P - 1s^2 4d^2 D$

† Autoionizing Line

\* Blended with a stronger line

There are a number of small features in the EDDT spectra which do not correspond to the expected position of emission lines of elements known to be abundant in the corona. There is the danger, in these cases, of being subjective in deciding which of these features are emission lines and which are fluctuations in the continuum. We have listed any "fluctuation" more than three standard deviations, as a line. We have not given fluxes for those "lines" for which the line flux in at least one spectrum does not exceed at least 20 counts, however, all lines are listed in Table 2.

In two previous papers [Walker and Rugge (1970, 1971),] we have identified a number of weak lines as due to the decay of autoionizing levels in helium-like and lithium-like ions; and pointed out the strong evidence to support the thesis that the strongest satellite lines are due to stabilizing transitions following dielectronic recombination. Gabriel and Paget (1972) have recently presented compelling evidence for the dielectronic origin of these satellites in thermal equilibrium by observations of the lines of O VII and O VI and of N VI and N V in a laboratory plasma. A complete discussion of these line identifications and the isoelectronic sequence wavelength extrapolations on which they were originally based, is given in Walker and Rugge (1971). Gabriel (1972) has reviewed other observations of autoionizing lines in the corona.

Figure 8 shows an enlargement of the spectrum near the Mg XI  $1s^2\ ^1S - 1s3p\ ^1P$  line. Note that the [Mg XI]  $1s^2\ ^1S - 1s3p\ ^3P$  line is resolved from the  $^1S - ^1P$  line. This line is of interest because it must compete with a fully allowed transition,  $1s2s\ ^3S - 1s3p\ ^3P$ .

We also observe between  $\sim 8.00\text{ \AA}$  and  $8.40\text{ \AA}$ , a number of weak lines which are generally in good agreement with the calculated positions of transitions of the type  $2l - 4l'$  in Fe XXIII and Fe XXIV. However, questions remain concerning the identification of some lines due to wavelength coincidences and disagreement on the position of the  $2s\ ^2S - 4p\ ^2P$  transition between the calculations of Chapman (1969) and of Cowan [Doschek et al. (1972)]. The calculations of Cowan, which included spin orbit effects, should be more accurate. In Table 3, we have compared the calculations of Chapman and Cowan, and the observations of Doschek et al and the present observations. One of the lines observed in our spectra is shown in Figure 8.

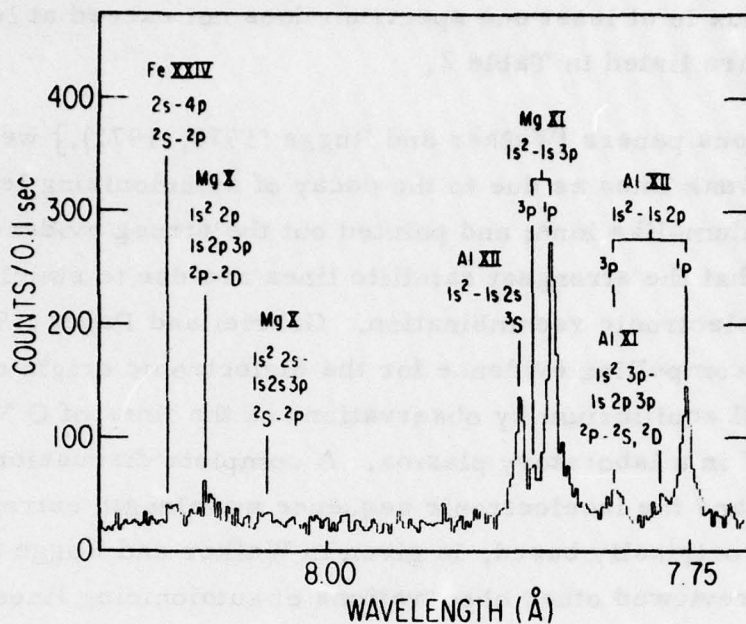


Figure 8. Enlarged portion of the 1642 UT spectra showing the Mg XI  $1s^2 1S - 1s3p 1P$  and  $3P$  lines.



Table 3  
Comparison of Observed and Calculated Positions of Possible Iron Lines

Ion	Transition	j-j	Cowan	Doschek et al	Chapman	This Paper
Fe XXIII	$1s^2 2s^2 1s - 1s^2 2s 4p^3 P$	0-1	8.380		8.449	8.393
Fe XXIV	$1s^2 2p^2 2P - 1s^2 4s^2 S$	$3/2 - 1/2$	8.378	8.378	8.378	8.383
Fe XXIV	$1s^2 2p^2 2P - 1s^2 4d^2 D$	$3/2 - 3/2$	8.314	8.317	8.330	
Fe XXIV	$1s^2 2p^2 2P - 1s^2 4d^2 D$	$3/2 - 5/2$	8.311			8.308
Fe XXIV	$1s^2 2p^2 2P - 1s^2 4d^2 D$	$3/2 - 5/2$	8.311	8.307		
Fe XXIII	$1s^2 2s^2 1s - 1s^2 2s 4p^1 P$	0-1	8.307			
Fe XXIV	$1s^2 2p^2 2P - 1s^2 4s^2 S$	$1/2 - 1/2$	8.279	8.290		$\left\{ \begin{array}{l} 8.289 \\ 8.275 \end{array} \right\}$
Fe XXIV	$1s^2 2p^2 2P - 1s^2 4d^2 D$	$1/2 - 3/2$	8.225	8.233		8.238
Fe XXIV	$1s^2 2s^2 S - 1s^2 4p^2 P$	$1/2 - 1/2$	7.989	7.990	8.093	8.092
Fe XXIV	$1s^2 2s^2 S - 1s^2 4p^2 P$	$1/2 - 3/2$	7.979			



## V. THE OBSERVED X-RAY CONTINUUM

The x-ray continuum, which is weak compared to the emission lines at longer wavelengths, is more important at shorter wavelengths. The continuum is due to thermal bremsstrahlung, radiative recombination and, at longer wavelengths, two photon decay of metastable  $^2S$  and  $^1S$  states. The intensity of the continuum observed during the scans on which the line intensities recorded in Table 1 were measured is shown in Figures 9 and 10. The theoretical curves which are compared with the 0602 UT continuum in Figure 9 will be discussed in Section VIII. Detector background (which amounts to less than a few percent of the observed continuum flux) has been subtracted from the flux shown in Figures 9 and 10. We do not believe that scattered radiation contributed significantly to the continuum because of the rejection of events outside of the wavelength of the spectrometer by pulse height analysis of the proportional counter detector. We believe that we have properly subtracted the wings of the emission lines from the continuum. However, there are weak lines which are unresolvable from fluxuations in the continuum, and they may make significant contributions to the flux that is attributed to the continuum.



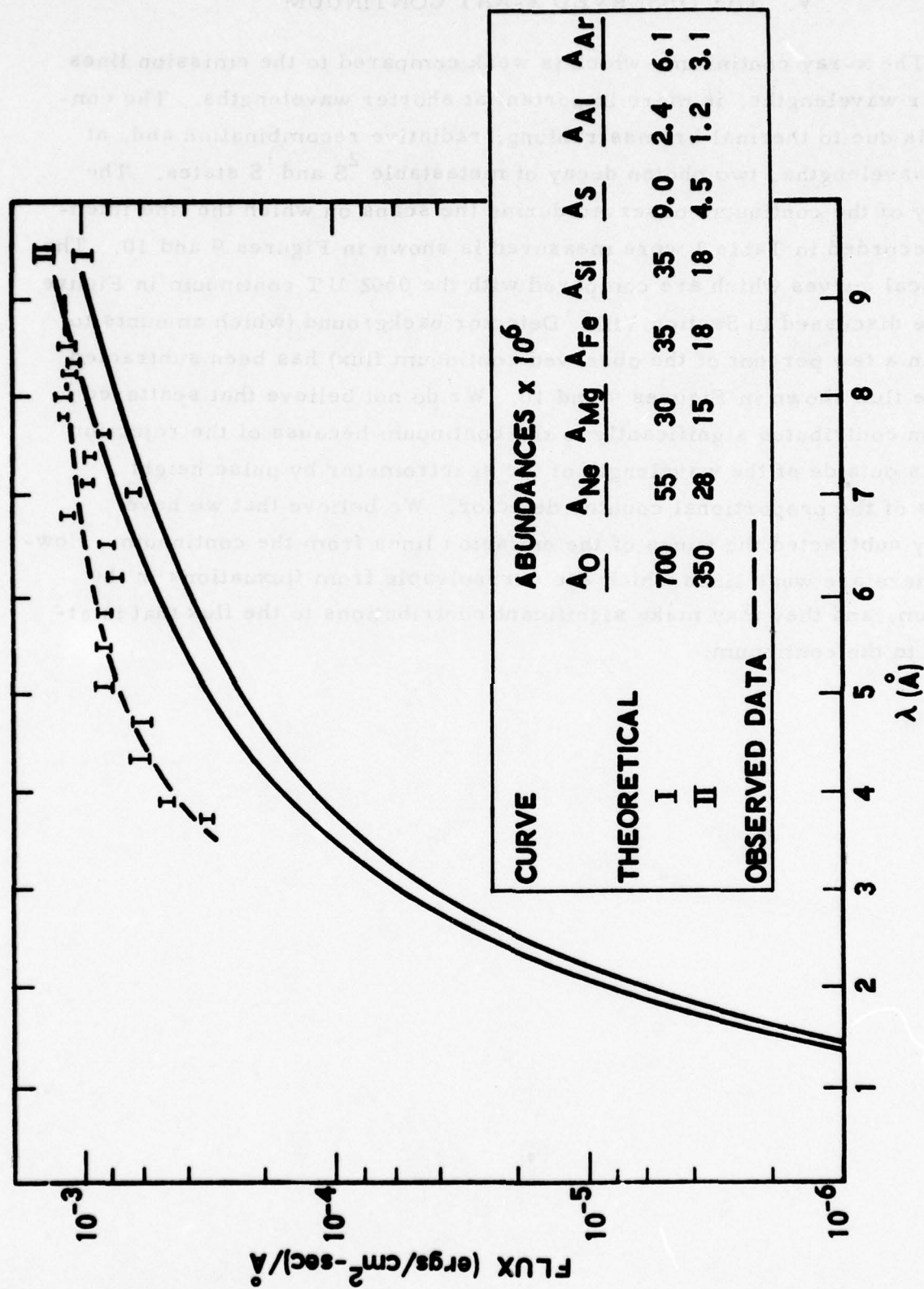


Figure 9. Spectrum of the x-ray continuum observed at 0602 UT on 1969 March 20. The theoretical curves are based on Model II in Figure 11.

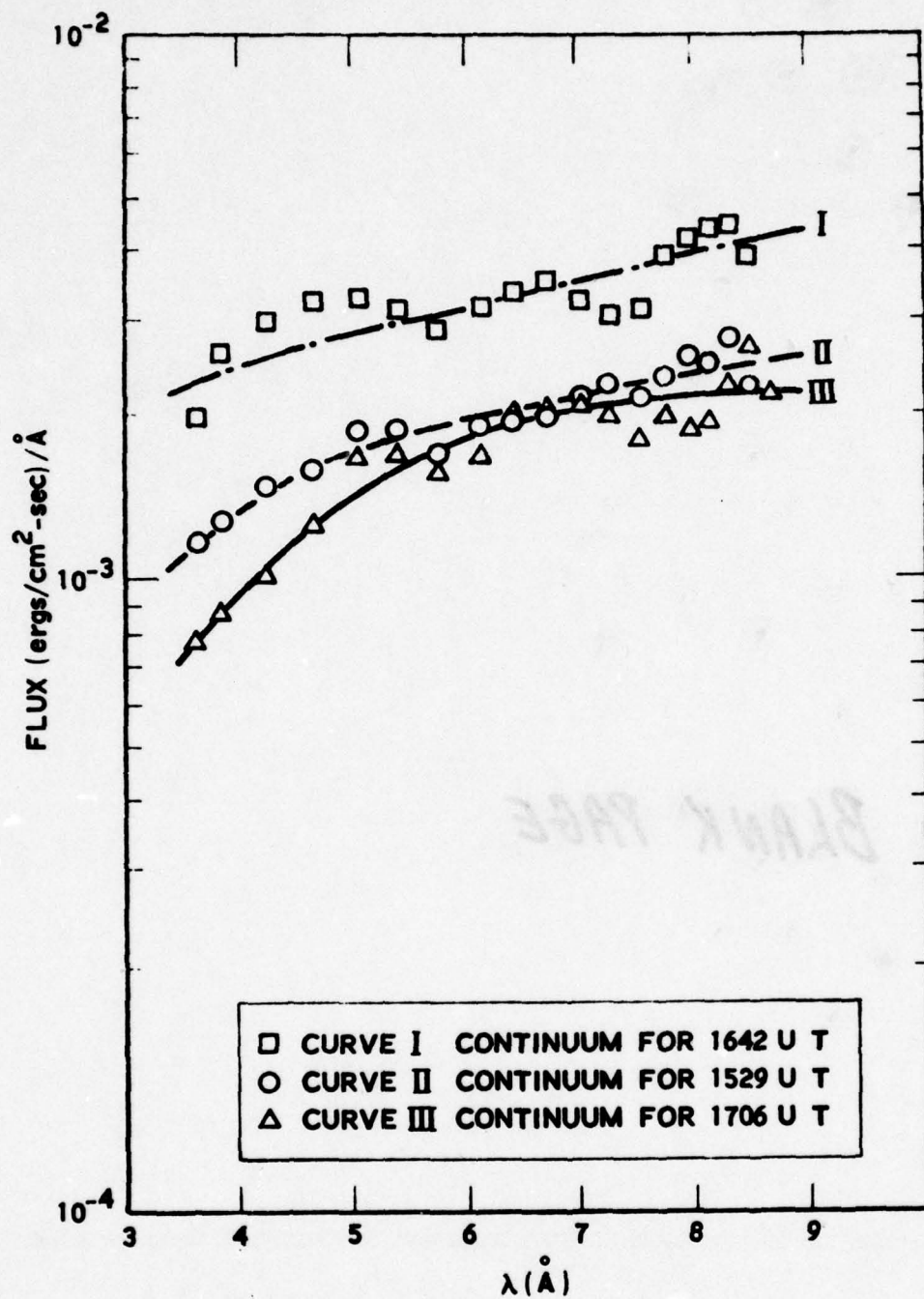


Figure 10. Spectrum of the continuum observed at 1529, 1642, and 1706 UT on 20 March 1973.

## VI. FORMULATION OF THE LINE FLUX INTEGRAL EQUATION

A number of authors have analyzed coronal permitted XUV line intensities to determine coronal structure and abundances. Noyes (1971) and Walker (1972) have reviewed these analyses, and the data on which they are based.

Jefferies et al (1972 a) have developed a general method for the analysis of line emission from an optically thin gas, and applied this method to coronal forbidden line intensities [Jefferies et al (1972 b, c)], and Gabriel and Jordan (1972) have reviewed the calculation of line intensities in low density plasmas. It would appear to be worthwhile to briefly review the formulation of the emission integral for permitted XUV coronal lines, using the formalism developed by Jefferies et al and by Gabriel and Jordan, in order to make explicit the limitations of the observational data, and the assumptions necessary in order to draw significant conclusions about coronal structure and abundances.

The intensity observed in an emission line (with upper level  $i$  and lower level  $j$ ) in ionization stage  $z$  of element  $Z$  is given by

$$I_{Zzij} = \iiint E_{Zzij} [T_e(x_\nu), n_e(x_\nu)] dx_1 dx_2 dx_3. \quad (1)$$

$$\nu = 1, 2, 3$$

The integral is over the coronal volume unresolved by the spectroscopic observation.

Ideally, the observation should limit the field of view normal to the line of sight to an (at least apparently) homogeneous structure, so that the variation of temperature,  $T_e(x_\nu)$ , and density  $n_e(x_\nu)$ , and hence the dependence of the emission function, is limited to the variable along the line of sight,  $x_3$ .

$$E_{Zzij}(x_3) = E_{Zzij} [T_e(x_3), n_e(x_3)]. \quad (2)$$

Unfortunately, the XUV observations which have sufficient spectral purity to permit detailed analysis do not, in general, have good spatial resolution on the disk, so we must retain the functional dependence of  $T_e$  and  $N_e$  on  $x_1$  and  $x_2$ . We have also assumed that the spectral resolution is sufficient to resolve an individual component of a line multiplet. In practice it may be necessary to sum over several individual lines.



The emission function for a particular line may be written

$$E_{Zzij} = \frac{hc}{\lambda_{ij}} A^r_{ij} \left[ n_{zi}(T_e, n_e) + \sum_{n'l' > n} n_{(z-1) in 'l'}(T_e, n_e) \right], \quad (3)$$

where  $A^r_{ij}$  is the transition probability for transition  $ij$ ,  $n_{zi}$  is the population of the excited level  $i$  in the ion whose charge is  $z$ , and  $n_{(z-1) in 'l'}$  is the population of the doubly excited level in the ion whose charge is  $(z-1)$ , with the same configuration as the level  $i$ , but with an additional electron in the level  $n'l'$ . As a number of authors have pointed out [see for example Walker, (1972) and Gabriel and Jordan (1972)], if  $n'l'$  is sufficiently large (in practice  $n \geq 4$ ) the transitions in  $'l' \rightarrow jn'l'$  cannot be resolved from the transition  $i \rightarrow j$ , and therefore effectively increases the flux in the line  $i \rightarrow j$ . For  $n \leq 3$ , the transition in  $'l' \rightarrow jn'l'$  can be resolved as a satellite line from  $i \rightarrow j$ , and in that case the emission is given by

$$E_{Zzij} = \frac{hc}{\lambda_{ij}} A^r_{ijn'l'} \left[ n_{(z-1) in 'l'}(T_e, n_e) \right] \quad (4)$$

where we have no longer made the assumption  $A^r_{ij} \approx A^r_{ijn'l'}$ .

For singly excited levels collisional excitation from the ground level strongly dominates the population of the levels in most cases of interest, and for allowed transitions collisional de-excitation may be neglected compared to radiative de-excitation.

In those cases we can express the level populations as

$$n_{zi} = \frac{n_e n_{zg}(T_e) \alpha^{ex}_{gi}(T_e)}{\Gamma_i^r} \quad (5)$$

where  $\Gamma_i^r$  is the total radiative width of the state  $i$  [ $\Gamma_i^r = \sum_k A^r_{ik}$ ] and  $\alpha^{ex}_{gi}(T_e)$  is the collisional excitation rate from the ground state.<sup>k</sup>

We may express the ground state density,  $n_{zg}$ , in terms of the relative population of the ionization stage of interest,  $a_z$ , the relative abundance of the element,  $A_z$ , and the number of hydrogen atoms per electron,  $a_H$ . This latter quantity is approximately constant since the hydrogen and helium in the corona are completely ionized.

$$n_{zg} = (n_{zg}/n_Z)(n_Z/n_H)(n_H/n_e)n_e = a_Z A_Z a_H n_e$$

We shall also have occasion to use the fractional population of an excited state

$$n_{zi} = (n_{zi}/n_Z)(n_Z/n_H)(n_H/n_e)n_e = f_{zi} A_Z a_H n_e$$

The emission function can be written as

$$E_{Zzij}^{\text{ex}} = \frac{hc}{\lambda_{ij}} \frac{A_{ij}^r n_e^2 a_H A_Z a_Z(T_e) \alpha_{gi}^{\text{ex}}(T_e)}{\Gamma_i^r} \quad (6)$$

Equation 6 can, in fact, be used for all of the lines which we must include in our calculations. The ionization equilibrium,  $a_Z$ , has been computed for thermal plasmas by Jordan (1969, 1970) and Landini and Fossi (1972), and is, to a good approximation, independent of density.

For the doubly excited satellite levels, dielectronic recombination is the dominant production process in thermal equilibrium.

$$E_{Zzij}^{\text{d}} = \frac{hc}{\lambda_{ij}} A_{ij}^r n_e^2 a_H A_Z a_Z(T_e) \sum_{n'l' > nl} \frac{\alpha_{gin'l'}^{\text{di}}(T_e)}{\Gamma_{in'l'}^r + \Gamma_{in'l'}^a} \quad (7)$$

where  $\alpha_{gin'l'}^{\text{di}}$  is the dielectronic recombination rate for the formation of the state in  $l'$  in ionization stage  $(z-1)$  from the ground state of ionization stage  $z$ , and  $\Gamma_{in'l'}^a$  is the autoionizing width of the state. The same equation without the summation is the emission function of an individual satellite line.

Walker (1972) has discussed the calculation of the rate constants in equations 5-7.

The flux observed by our spectroheliograph can be expressed as

$$F_{ZZ} = \epsilon(\lambda_{ij}) \iiint dS dx_3 a_H A_Z n_e^2(x_\nu) a_Z [T_e(x_\nu)] \left\{ J_{Zzij}^{\text{ex}} [T_e(x_\nu)] + J_{Zzij}^{\text{di}} [T_e(x_\nu)] \right\} \quad (8)$$

where  $\epsilon(\lambda_{ij})$ , the spectrometer efficiency includes the factor  $(1/4\pi R^2)$ , where  $R$  is the astronomical unit, and the functions  $J^{\text{ex}}$  and  $J^{\text{di}}$  are defined by equations 5 and 6 and include the dependence of the excitation function on atomic rate constants.

We have separated the integrals over the area  $S(x_1, x_2)$  which is unresolved by the telescope, and along the line of sight,  $x_3$ . Following Jefferies et al., we introduce the distribution function for the coronal plasma,  $\mu[T_e(x_\nu), n_e(x_\nu)]$  which describes the density and temperature of the plasma.

$$dN(T_e, n_e, x_1, x_2) = N_e \mu(T_e, n_e, x_1, x_2) dn_e dT_e.$$

The function  $\mu$  represents the fraction ( $dN$ ) of the total number of electrons in a unit column ( $N_e$ ) which are in neighborhoods where temperature and density are given by  $T_e$  and  $n_e$ . We may also introduce the partial distributions functions  $\phi(T_e)$  and  $\psi(T_e)$

$$\phi(T_e) = \int \mu(T_e, n_e) dn_e,$$

and

$$\psi(n_e) = \int \mu(T_e, n_e) dT_e$$

In principle, we would like to determine the function  $\mu$ , which characterizes the gas completely (we have ignored the possibility of mass motion of the gas for this discussion). We can express the flux observed by the instrument in terms of the distribution function  $\mu$  since

$$N_e = \int n_e(x_3) dx_3 = N_e \iint \mu(T_e, n_e) dT_e dn_e,$$

as

$$F_{Zzij} = \epsilon(\lambda_{ij}) a_H^A Z \iint dS N_e \iint dn_e dT_e \mu(T_e, n_e) a_z(T_e) J(T_e) n_e, \quad (9)$$

where

$$J(T_e) = J^{\text{ex}}(T_e) + J^{\text{di}}(T_e).$$



Equation 9 is an integral equation, with the kernel  $A_Z a_z(T_e) J(T_e)$  which we can calculate, and the value  $F$ , which we can measure. In order to develop a set of techniques to determine  $\mu(T_e, n_e)$ , let us assume that there is a functional relationship between temperature and density, i. e., :

$$n_e = n_e(T_e)$$

We may then write equation 9 as

$$F_{Zz_{ij}} = \epsilon(\lambda_{ij}) a_H A_Z \iint dS n_e \int dT_e n_e(T_e) \phi(T_e) a_z(T_e) J(T_e) \quad 10)$$

The integral equation for  $F_{Zz_{ij}}$  defined by equation 10 can, in principle, be solved to determine the temperature distribution of the emission measure; provided that observations including a sufficient number of lines with differing temperature dependence are available. In the next section we shall describe the techniques which we will use to solve this integral equation.

## VII. ANALYSIS OF THE OBSERVED LINE FLUXES

The traditional technique used to solve the line intensity integral in the form of equation 10 depends on the properties of the ionization stage population function,  $a_z(T_e)$ , which for many ions has a delta function-like dependence on temperature. This technique, which was originally used by Pottasch, allows the inversion of the integral equation. For the hydrogen- and helium-like ions which are observed below 25 Å, this simplification is not possible. We shall instead select a model of the coronal structure, with variable parameters, which will allow us to compute the line intensity integral numerically or analytically, and by varying the parameters, find a best fit to the observed line fluxes. This technique has been used in somewhat modified form by Batstone et al. (1970) and by Chambre (1971). In an earlier review, one of the authors (Walker, 1972) has described the technique we shall use, and has presented an analysis of observations obtained with the x-ray spectrometer on the OV1-10 satellite.

Let us express the emission measure per unit area as a function of a set of parameters  $G_k$ ,

$$N_e n_e(T_e) \phi(T_e) = M(G_k, T_e).$$

We may then calculate the flux in an emission line from an area  $S$  on the solar disk,

$$F_{Zzij}(G_k, A_Z, S) = \epsilon(\lambda_{ij}) a_H A_Z K(G_k, S) \quad (11)$$

with

$$K_{Zzij}(G_k, S) = \iint dS \int dT_e M(G_k, T_e) J(T_e) a_z(T_e) \quad (12)$$

In order to find the set of  $G_k$ 's which provide the best fit to the observational data we minimize the error function  $[X]^2$

$$[X]^2(G_k, A_Z, S) = \sum_{Z, z, ij} \frac{[F_{Zzij}(G_k, A_Z, S) - F_{Zzij}]^2}{[\Delta F_{Zzij}]^2}$$

where  $F_{Zij}$  and  $\Delta F_{Zij}$  are the experimental fluxes and their estimated errors.

Note that the abundances, or some subset of them, may be regarded as parameters.

As a trial function, we have selected the same functional form which Chambre (1971) found provided a good fit to the observations which he analyzed.

The functional form for the emission measure is given by

$$M(T) = C 10^{-T_2/T_1} \left[ 1 + 1.1513(T_2 - T_0)/T_1 \right. \\ \left. - 1.1513B(T - T_0)^2/T_1(T_2 - T_0) \right] \\ 1.0 \times 10^6 \text{ K} < T < T_0$$

$$M(T) = C 10^{-T_2/T_1} \left[ 1 + 1.1513(T_2 - T_0)/T_1 \right. \\ \left. - 1.1513(T - T_0)^2/T_1(T_2 - T_0) \right] \\ T_0 < T < T_2$$

$$M(T) = C 10^{-T/T_1}$$

$$T > T_2$$

where the parameter B is selected to make  $M(1 \times 10^6)/S(T_0) = 0.4$ . The temperature  $T_0$  is the most probable coronal temperature, and the condition on B is selected to make the function  $M(T)$  agree with the model of Pottasch below the most probable temperature  $T_0$ , where the observations to be analyzed here are insensitive to the detailed shape of the model.

The procedure adopted to determine the parameters  $T_0$ ,  $T_1$ ,  $T_2$ , and C was as follows. Relative abundances were assumed for Mg, Al, Si, and S, based on the recommended abundances given by Withbroe, and setting the absolute silicon abundance arbitrarily equal to  $35 \times 10^{-6}$ . The values



of  $T_0$  and  $T_2$  were set equal to the sets of values  $T_0 = 2 \times 10^6$  K,  $T_2 = 3 \times 10^6$  K,  $T_0 = 1.5 \times 10^6$  K,  $T_2 = 2.5 \times 10^6$  K, and  $T_0 = 2.5 \times 10^6$  K,  $T_2 = 3.5 \times 10^6$  K. The value of  $\chi^2$  was then calculated for values of  $T_1 = 2 \times 10^6$  K through  $T_1 = 8 \times 10^6$  in increments of  $0.5 \times 10^6$  K. All sets of values for  $T_0$  and  $T_2$  gave acceptable fits, however the set  $T_0 = 2 \times 10^6$  K,  $T_2 = 3 \times 10^6$  K gave the best fits and only those results will be reported here. We have analyzed line fluxes from Mg, Al, Si, and S ions observed for the 0602 UT spectra tabulated in Table 1.

The minimum  $\chi^2$  was found for  $T_1 = 3.5 \times 10^6$  K and the resultant coronal model is presented in curve III of Figure 11. The fit to the observations was further improved from a  $\chi^2$  value of  $\sim 10$  to the value of 2.6 reported in Figure 11 by varying the values of  $A_{Al}$ ,  $A_{Si}$ , and  $A_S$ . The abundances of argon and sodium were computed by comparing the observed and calculated fluxes of the Ar XVII resonance line, and of the Na XI Lyman  $\beta$  line, viz

$$A_Z = F_Z / \left[ \epsilon(\lambda) (hc/\lambda) a_H K (G_k, S) \right]$$

The abundances found are given in Table 4

Table 4

Relative Abundances Derived from XUV Line Intensities

<u>Element</u>	<u>Na</u>	<u>Mg</u>	<u>Al</u>	<u>Si</u> *	<u>S</u>	<u>Ar</u>
Abundance ( $\times 10^6$ )	1.7	30	2.5	35	9	6

The model atmosphere structure found for the corona may not be unique. In our earliest application of this technique, we showed that small changes in the parameter  $T_1$  from  $3.5 \times 10^6$  K to 4 or  $4.5 \times 10^6$  K, with no change in the relative abundances, resulted in minor changes in the value of  $\chi^2$ . This result suggests that the values of the relative abundances are better determined than the precise shape of the emission function. We have found a similar result for the present set of observations. We have investigated the effect of variations in the shape of the emission function by imposing a high temperature cutoff, while maintaining the values of  $T_0$ ,  $T_2$ , and  $A_Z$ .

\*Silicon abundance assumed equal to  $35 \times 10^{-6}$

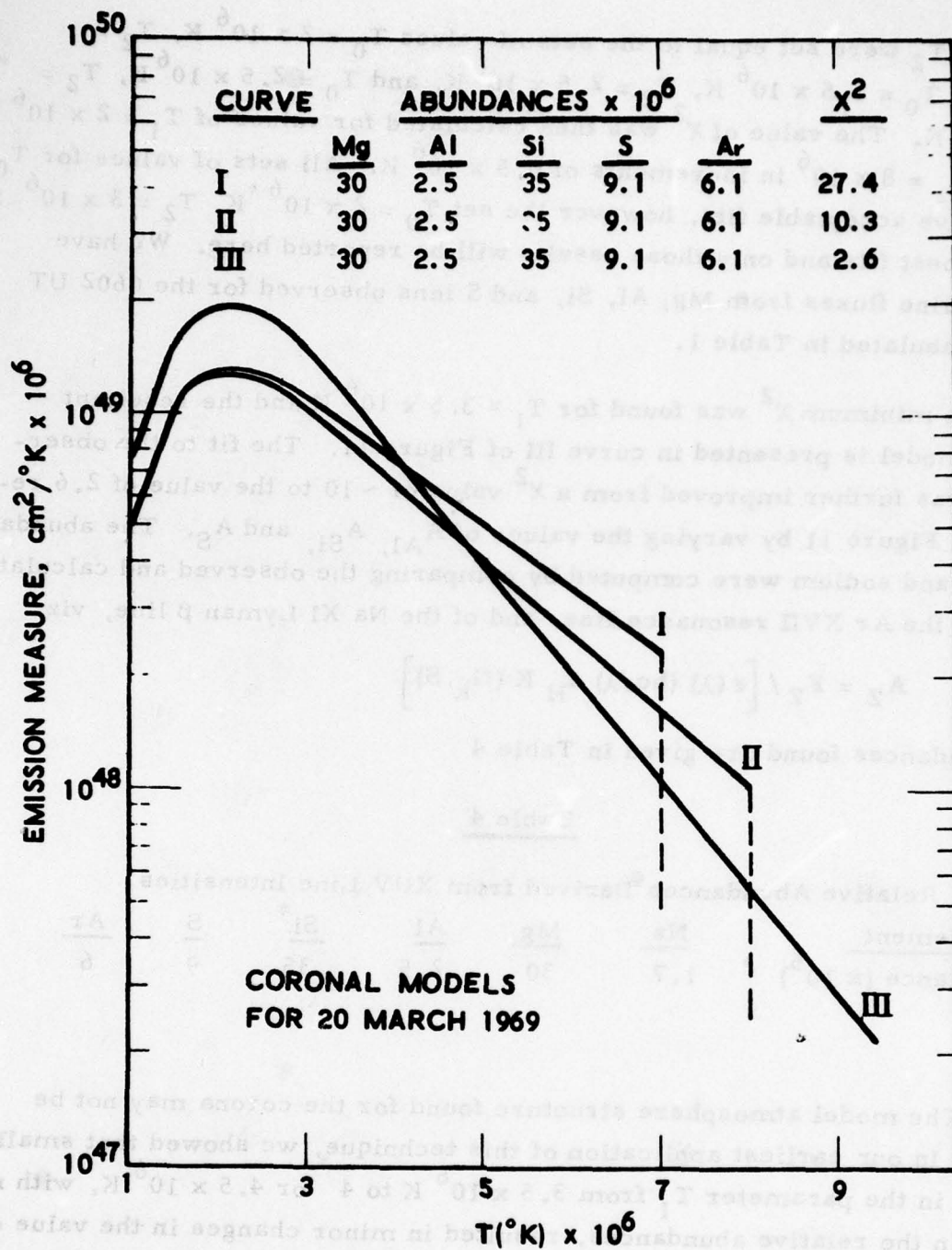


Figure 11. Coronal models based on the 0604 UT spectrum. The curves I, II and III fall off as  $\exp_{10}(-T/T_1)$ , where  $T_1$  is  $6 \times 10^6$  K,  $5 \times 10^6$  K, and  $3.5 \times 10^6$  K respectively.

Curves I and II in Figure 11 demonstrate the values of  $T_1$  which result in the best fit to the observations. The fits obtained with cutoffs at  $7 \times 10^6$  K and  $8 \times 10^6$  K give  $T_1 = 5 \times 10^6$  K and  $6 \times 10^6$  K respectively, but result in considerably larger values of  $\chi^2$ . This result suggests that some material as hot as  $\sim 9 - 10 \times 10^6$  K is necessary to explain the coronal spectrum even in the absence of non-equilibrium conditions. Table 5 compares the observed fluxes, and the fluxes computed with the models in Figure 11, and demonstrates the excellent fit to the observations provided by the models.

Wavelength (Å)	Observed Flux (10 <sup>-16</sup> W m <sup>-2</sup> nm <sup>-1</sup> )	Model I Flux (10 <sup>-16</sup> W m <sup>-2</sup> nm <sup>-1</sup> )	Model II Flux (10 <sup>-16</sup> W m <sup>-2</sup> nm <sup>-1</sup> )	Ratio (I/Obs)	Ratio (II/Obs)
3000	0.00	0.00	0.00	0.00	0.00
3500	0.00	0.00	0.00	0.00	0.00
4000	0.00	0.00	0.00	0.00	0.00
4500	0.00	0.00	0.00	0.00	0.00
5000	0.00	0.00	0.00	0.00	0.00
5500	0.00	0.00	0.00	0.00	0.00
6000	0.00	0.00	0.00	0.00	0.00
6500	0.00	0.00	0.00	0.00	0.00
7000	0.00	0.00	0.00	0.00	0.00
7500	0.00	0.00	0.00	0.00	0.00
8000	0.00	0.00	0.00	0.00	0.00
8500	0.00	0.00	0.00	0.00	0.00
9000	0.00	0.00	0.00	0.00	0.00
9500	0.00	0.00	0.00	0.00	0.00
10000	0.00	0.00	0.00	0.00	0.00
10500	0.00	0.00	0.00	0.00	0.00
11000	0.00	0.00	0.00	0.00	0.00
11500	0.00	0.00	0.00	0.00	0.00
12000	0.00	0.00	0.00	0.00	0.00
12500	0.00	0.00	0.00	0.00	0.00
13000	0.00	0.00	0.00	0.00	0.00
13500	0.00	0.00	0.00	0.00	0.00
14000	0.00	0.00	0.00	0.00	0.00
14500	0.00	0.00	0.00	0.00	0.00
15000	0.00	0.00	0.00	0.00	0.00
15500	0.00	0.00	0.00	0.00	0.00
16000	0.00	0.00	0.00	0.00	0.00
16500	0.00	0.00	0.00	0.00	0.00
17000	0.00	0.00	0.00	0.00	0.00
17500	0.00	0.00	0.00	0.00	0.00
18000	0.00	0.00	0.00	0.00	0.00
18500	0.00	0.00	0.00	0.00	0.00
19000	0.00	0.00	0.00	0.00	0.00
19500	0.00	0.00	0.00	0.00	0.00
20000	0.00	0.00	0.00	0.00	0.00

Comparison of Observed and Computed Flux Intensities  
Table 5



Table 5  
Comparison of Observed and Calculated Line Intensities

Wavelength	Ion	Transition	Line Intensity ( $10^{-5}$ ergs $\text{cm}^{-2} \text{sec}^{-1}$ )			
			Observed Flux	Error	Model I	Model II
7.85	Mg XI	$1s^2 1s - 1s3p \ ^1P$	11.0	0.62	12.0	10.7
8.42	Mg XII	$1s^2 S - 2p \ ^2P$	17.4	0.66	16.7	18.0
7.756	Al XII	$1s^2 1s - 1s2p \ ^1P$	5.4	0.45	5.7	5.4
7.173	Al XIII	$1s^2 S - 2p \ ^2P$	0.8	0.21	0.4	0.5
6.647	Si XIII	$1s^2 1s - 1s2p \ ^1P$	49.5	1.81	50.3	49.6
6.182	Si XIV	$1s^2 S - 2p \ ^2P$	3.1	0.47	1.3	2.0
5.038	S XV	$1s^2 1s - 1s2p \ ^1P$	5.0	0.64	4.0	4.3
4.729	S XVI	$1s^2 S - 2p \ ^2P$	0.11	0.10	0.01	0.02
3.95	Ar XVII	$1s^2 1s - 1s2p \ ^1P$	1.0	0.31	-	-
						10.8
						17.5
						5.4
						0.6
						49.2
						3.6
						5.0
						0.08
						-

## VIII. ANALYSIS OF THE OBSERVED CONTINUUM

The relative abundances we derived in the previous section were arbitrarily normalized to absolute abundances by assuming that  $A_{Si} = 35 \times 10^{-6}$ .

Two techniques have been used to determine absolute abundances based on XUV observations (Withbroe, 1971). One technique is based on the determination of absolute electron densities by radio observations (Pottasch 1963, 1967, and Dupree and Goldberg 1967), and the second is based on coronal white - light continuum measurements of the K - corona (Withbroe, 1970). There is a third technique which has been proposed by Walker (1972) and which uses x-ray observations entirely. Consider the x-ray continuum at a wavelength  $\lambda$ . There are three radiation processes which contribute substantially to the x-ray continuum, bremsstrahlung, radiative recombination, and two photon decay. Culhane (1969) has discussed the calculation of the emission function for bremsstrahlung and radiative recombination, and Walker (1972) has discussed the calculation of the emission function for two photon decay. We may write the emission functions for these processes in the form

$$\left. \begin{array}{l} E^{\text{rad}} \\ E^b \\ E^{2\gamma} \end{array} \right\} = a_H n_e^2(T_e) \sum_Z \sum_z A_Z a_z(T_e) \left\{ \begin{array}{l} J^{\text{rad}}_{Zz}(T, \lambda) \\ J^b_{Zz}(T, \lambda) \\ J^{2\gamma}_{Zz}(T, \lambda) \end{array} \right.$$

The intensity observed at the earth in the continuum may be expressed as

$$F(\lambda) = \epsilon(\lambda) a_H \sum_Z A_Z \iint dS \int dT_e M(G_k, T_e) \sum_z a_z(T_e) \times \quad (13)$$

$$\left\{ J^{\text{rad}}_{Zz}(T, \lambda) + J^b_{Zz}(T, \lambda) + J^{2\gamma}_{Zz}(T, \lambda) \right\}$$

In Table 6, we have tabulated the fractional part of the continuum intensity which is due to each element for bremsstrahlung and radiative recombination separately, and for the entire continuum. Note that the importance of  $A_H$  ( $A_H \equiv 1$ ) becomes substantial for higher temperatures where bremsstrahlung dominates the continuum. For those wavelengths where high temperature

Table 6  
Fractional Contribution of Various Elements to the X-Ray Continuum

Element	$\lambda = 3 \text{ \AA}$			$\lambda = 10 \text{ \AA}$			$\lambda = 20 \text{ \AA}^*$		
	Brems	Recomb	Total	Brems	Recomb	Total	Brems	Recomb	Total
H	.60	.006	.054	.65	.011	.100	.67	.091	.271
He	.25	.011	.030	.24	.021	.051	.24	.164	.135
C	.02	.046	.044	.015	.057	.051	.014	.33	.100
N	.007	.031	.028	.005	.035	.030	.005	.01	.003
O	.07	.723	.671	.05	.763	.665	.044	.09	.390
Ne	.007	.086	.079	.005	.065	.057	.004	.013	.004
Mg	.01	.034	.031	.005	.001	.002	.004	.025	.009
Si	.015	.031	.030	.007	.014	.013	.006	.096	.030
S	.005	.008	.008	.002	.009	.009	.002	.059	.017
Fe	.015	.013	.013	.01	.018	.017	.008	.119	.037

Element	$\lambda = 3 \text{ \AA}$			$\lambda = 10 \text{ \AA}^{**}$			$\lambda = 20 \text{ \AA}^{**}$		
	Brems	Recomb	Total	Brems	Recomb	Total	Brems	Recomb	Total
H	.66	.013	.32	.69	.043	.48	.705	.105	.577
He	.22	.025	.12	.22	.074	.168	.215	.170	.193
C	.016	.031	.024	.013	.065	.016	.012	.112	.024
N	.007	.014	.007	.004	.028	.007	.004	.005	.004
O	.065	.282	.178	.043	.505	.153	.038	.088	.041
Ne	.007	.087	.047	.004	.012	.006	.003	.019	.005
Mg	.008	.144	.079	.005	.011	.031	.005	.022	.032
Si	.010	.236	.125	.007	.022	.055	.006	.041	.060
S	.003	.030	.016	.002	.010	.004	.002	.019	.004
Fe	.012	.117	.066	.008	.232	.062	.007	.416	.057

\* Two photon decay accounts for ~35% of the total continuum flux.

\*\* Two photon decay accounts for ~7% of the total continuum flux.



material dominates the continuum, the line to continuum ratio becomes sensitive to absolute abundances; providing, in principle, a technique to determine absolute abundances.

One procedure by which the comparison of line and continuum fluxes may be accomplished is to compute the continuum using equation 13, with the emission measure function found from the analysis of the line fluxes and presented by curve III of Figure 11. The theoretical and experimental continuum fluxes are compared for two sets of abundances in Figure 9. The abundances of hydrogen ( $A_H = 1$ ), helium ( $A_{He} = .07$ ) carbon ( $A_C = 400 \times 10^{-6}$ ) and nitrogen ( $A_N = 80 \times 10^{-6}$ ) were the same for both calculations. The effect of renormalizing the abundances of oxygen, neon, magnesium, aluminum, silicon, sulfur, argon and iron is to shift the overall level of the continuum, without substantially changing the spectral shape. The derivation of the oxygen, neon, and iron abundances in Figure 9 is discussed in the subsequent paper [Walker et al. (1973)].

Unfortunately, the shapes of the theoretical and experimental curves are not in good agreement, and no definitive conclusions can be drawn from Figure 9 regarding absolute abundances. We believe that there are two principle causes for the disagreement between the experimental and theoretical continuum curves in Figure 9.

- 1) There may be unresolved lines which have not been subtracted from the continuum.
- 2) There may be a high energy tail of material which contributes to the short wavelength continuum, but which does not substantially alter the flux in the cooler lines used in constructing the emission measure model.

In order to carry out the technique proposed here for the calculation of absolute abundances, we must obtain observations of the x-ray continuum with greater sensitivity, and of the line spectrum over a broader wavelength (and therefore temperature) range.

# IX. SUMMARY

The coronal x-ray spectrum provides two advantages in the study of coronal abundances.

- 1) The lines are optically thin, and the analysis of line intensities is not dependent on a knowledge of the detailed structure of the emitting regions.
- 2) The lines are emitted by simple ions, primarily hydrogen-like and helium-like, and therefore, the theoretical atomic rate coefficients which must be used in the analysis should be more accurately known.

We have used observations of the resonance lines of Mg XI, Mg XII, Al XII, Al XIII, Si XIII, Si XIV, SXV and SXVI to construct a model of the temperature distribution of the coronal emission measure and to determine the relative abundances of that group of elements. The resonance line of Ar XVII was used to calculate the abundance of argon relative to the other elements, and the Lyman  $\beta$  line of Na XI was used to compute the sodium abundance. The abundances found are compared with the relative abundances suggested by Withbroe based on XUV and forbidden line observations, and photospheric abundances (as tabulated by Withbroe) in Table 7.

Table 7  
Comparison of Relative Abundances

Element		Na	Mg	Al	Si	S	Ar
Abundance ( $\times 10^6$ )	This paper	1.7	30	2.5	35*	9	6
	Withbroe (1971)	2.3	35	2.3	35*	11	4.5
	Photospheric	1.7	35	2.5	35	16	-

\*The coronal abundances are normalized to  $A_{Si} = 35 \times 10^{-6}$

With the normalization of the silicon abundance, the sodium, magnesium, and aluminum abundances are in good agreement. The coronal sulfur abundances appears to be somewhat lower than the photospheric value, however the difference is not significant, and most probably does not represent a physical difference between the corona and the photosphere.

We have analyzed the intensity in the x-ray continuum, and described a technique which should, in principle, allow absolute abundances to be determined from x-ray observations alone, by the comparison of line and continuum intensities. In attempting to apply this technique to the present observations, we found that the shape of the continuum predicted by the model based on the line fluxes did not agree with that of the observed continuum, although the absolute fluxes did agree between  $\sim 6$  and  $\sim 8.5$  Å.

We have also presented identifications and absolute line and continuum fluxes for the coronal spectrum below 8.5 Å for several levels of coronal activity. We believe that these fluxes are accurate to  $\pm 10\%$ , or better, because of the inclusion of an inflight calibration system for the detection system.

The authors would like to acknowledge the assistance of Mrs. M. Wray and Dr. H. Hilton in the calculation of the coronal line emission functions.



- 1972 b, *ibid*, 317.  
1972 c, *ibid*, 327.

- Moore, C. D.: 1952, Atomic Energy Levels Vol. I. NBS Circular 467.
- Noyes, R.: 1971, Ann. Rev. Astron. Astrophys. 2, 209.
- Pottasch, S. R.: 1967, Bull. Astron. Inst Neth 19, 113.
- Vainshtein, L. A. and Seifronova, U. I. 1971: Astron. Zh. 47, 223  
(English Transl. 1971, Soviet Astron. - AJ 15, 275).
- Walker, A. B. C. Jr.: 1972, Space Sci. Rev. 13, 672.
- Walker, A. B. C. Jr. and Rugge, H. R.: 1970, Astron. Astrophys. 5, 4.
- Walker, A. B. C. Jr. and Rugge, H. R.: 1971, Astrophys. J. 164, 181.
- Widing, K. G. and Sandlin, G. D. 1965, Astrophys. J. 152, 545.
- Withbroe, G. L.: 1970, Solar Phys. 11, 42.
- Withbroe, G. L.: 1971 in The Menzel Symposium on Solar Physics, Atomic Spectra, and Gaseous Nebulae, Ed. K. B. Gebbie, NBS Special Publication 353, p. 127.

# VII. RELATIVE CORONAL ABUNDANCES DERIVED FROM X-RAY OBSERVATIONS, III: THE EFFECT OF CASCADES ON THE RELATIVE INTENSITY OF Fe XVII LINE FLUXES, AND A REVISED IRON ABUNDANCE\*

A. B. C. Walker, Jr., H. R. Rugge, and Kay Weiss

## ABSTRACT

Observations of the helium-like resonance lines of N, O, Ne, Na, Mg, Al, Si, S, and Ar below 25 Å, made from the U.S. Air Force satellites OV1-10 and OV1-17, have previously been used to construct coronal models and to determine the relative abundances of these elements. Lines of Fe XVII are also prominent in the coronal spectrum below 25 Å. The intensities of the lines of the 2p-3d transitions near 15 Å have also been used in conjunction with these coronal models, and the assumption that the excited states are populated only by collisional excitation from the ground state ("coronal excitation"), to determine the Fe abundance. We have observed eight lines of Fe XVII which originated from the  $2p^5 3s$ ,  $2p^5 3d$  and  $2s2p^6 3d$  configurations in the coronal spectrum between 13 and 18 Å. Many of the upper levels are populated by cascade so that the assumption of "coronal excitation" is not a valid one for most of these lines. Recent theoretical work on the spectrum of Fe XVII has taken account of the statistical equilibrium of the first 36 excited states in computing the intensities of the observed lines. Although the theoretical atomic rate constants for Fe XVII (especially the collisional excitation rates) cannot be as accurately calculated as those of the simpler ions, the relative intensities of the 2p-3d Fe

---

\* This paper has also been published as TR-0075(9260-02)-1, The Aerospace Corporation, El Segundo, California (1 October 1974) and in The Astrophysical Journal **194**, 471-482 (1974).



XVII lines observed in the corona are now in good agreement with theoretical predictions. The measured flux in the lines from the  $2s^2 2p^5 3s$  levels, which are populated in part by cascade from the  $2p^6 3l$  ( $l = 1, 2, 3$ ) levels, have been used to obtain the excitation rate coefficients for the  $2s 2p^6 3l^3 L$  levels, since the theoretical rate coefficients for these excitations are less accurately known than those for the  $2p-3l$  transitions. Using this more complete theoretical model, and higher resolution observations which allow a number of line blends to be resolved, we have revised our earlier calculation of the coronal abundance of Fe. We find an iron abundance relative to hydrogen of  $26 \times 10^{-6}$ , which is in excellent agreement with the photospheric iron abundance.

## CONTENTS

ABSTRACT .....	171
I. INTRODUCTION .....	175
II. OBSERVATIONS .....	179
III. FORMULATION OF THE LINE FLUX INTEGRAL EQUATION .....	189
IV. DETERMINATION OF ATOMIC RATE CONSTANTS .....	199
V. CALCULATION OF THE REVISED IRON ABUNDANCE .....	205
VI. SUMMARY .....	207
ACKNOWLEDGMENTS .....	211
REFERENCES .....	213

## TABLES

1.	Fe XVII Lines Observed in the Coronal Spectrum . . . . .	182
2.	Lines Observed Near the Fe XVII 2p-3s and 2p-3d Transitions for the 20 March 1969 Spectra . . . . .	185
3.	Comparison of Experimental and Theoretical Line Intensities . . . . .	193
4.	Threshold Collision Strengths for Fe XVII . . . . .	202
5.	Calculated Ratios of Fe XVII Line Intensities (Ratios are given in photons at $4 \times 10^6$ °K) . . . . .	204
6.	Comparison of Relative Abundances . . . . .	209

## FIGURES

1.	Portion of the spectrum recorded by the KAP spectrometer on OV1-17 for 20 March 1969, showing the Fe XVII $2s^2 2p^6 \ ^1S - 2s^2 2p^6 3p \ ^1P$ and $^3P$ lines . . . . .	180
2.	Portion of the spectrum recorded by the KAP spectrometer on OV1-17 for 20 March 1969, showing the Fe XVII $2s^2 2p^6 \ ^1S - 2s^2 2p^6 53d$ $\ ^1P, \ ^3D, \text{ and } ^3P, \text{ and } 2s^2 2p^6 \ ^1S_0 - 2s^2 2p^6 53s \ ^1P_1,$ $\ ^3P_1 \text{ and } ^3P_2$ lines . . . . .	181
3.	Level diagram for Fe XVII, showing the principal decay paths for the first 36 excited levels . . . . .	192



## I. INTRODUCTION

The pioneering work of Pottasch (1967 and the references cited therein) in analyzing EUV and soft X-ray spectra provided a detailed temperature structure for the quiet corona, and a technique to determine relative coronal abundances. Pottasch was able to include lines from a sufficient number of ionization stages of iron and of silicon (and consequently a broad temperature range for each element) to define a temperature structure for each element. The results of this analysis forced an increase of an order of magnitude in the coronal abundance ratio  $A_{\text{Fe}}/A_{\text{Si}}$  compared to the then currently accepted photospheric value. More recently, the relative abundance of iron in the solar wind has been measured directly (Bame, et al., 1970; Holtzer and Axford, 1970; Lange and Scheib, 1970). These results strongly support the revised iron abundances.

The redetermination of Fe I and Fe II oscillator strengths has led to the revision of the photospheric iron abundance (Gartz et al., 1969a) so that it is consistent with coronal determinations of the Fe/Si ratio (Jordan and Pottasch, 1968) and with results from meteorites (Gartz et al., 1969b) and the solar wind (Bame et al., 1970). Withbroe (1971) and Pagel (1974) have recently reviewed solar abundance determinations by a number of techniques, and in particular the studies of the abundance of iron using permitted EUV lines, which are excited primarily in the transition region.

In the present paper we study the abundance of iron in the hottest stable coronal configurations, the coronal condensations.

In two previous papers (Walker, Rugge, and Weiss, 1974a, b, hereafter referred to as papers I and II) we have used observations of lines of the helium- and hydrogen-like ions of nitrogen, oxygen, neon, sodium, magnesium, aluminum, silicon, sulphur, and argon, which are prominent in the spectrum of the quiet corona between 4 and 25 Å, to construct a coronal model, and to determine the relative abundance of these elements. The atomic rate constants required for the analysis are relatively well known for these simple ions [Walker (1972), Gabriel and Jordan (1972)], and the assumption of coronal excitation conditions (i. e., excited states are populated entirely by collisional excitation from the ground state) should not result in a significant error.

The lines of the neon-like ion Fe XVII are also observed in the spectrum of the quiet corona, and we have used the fluxes in these lines, and the model based on the hydrogenic and helium-like lines fluxes, to compute the relative coronal abundance of iron (paper II). However, the excited configurations of neon-like ions are complex, and a number of parent levels of strong lines are populated chiefly by cascade from higher levels. In the present paper we reexamine the coronal abundance of iron, using an improved theoretical model of the excitation of Fe XVII lines which includes the effects of cascades among 36 levels. We also use

higher resolution spectral observations, which allow a number of lines which were blended with the Fe XVII lines in the spectra used in paper II to be resolved in the present analysis. We also discuss the agreement between the theoretical model of the excitation of the Fe XVII spectrum, and the observed coronal line fluxes, and derive values for the excitation rate coefficients from the ground level to the  $2s2p^63(s, p, d)$  levels. The presently available theoretical excitation rate coefficients for these transitions are less reliable than those for the  $2p-3(s, p, d)$  transitions.



## II. OBSERVATIONS

In paper II we used the spectra obtained with the KAP crystal spectrometer on the OV1-10 satellite to determine the flux in the Fe XVII lines used for the abundance analysis. We believe the calibration of the OV1-10 spectra to be highly reliable; however, the resolution of the OV1-10 spectra is not sufficient to clearly resolve a number of the Fe XVII multiplets, or to resolve the question of the importance of possible line blends which might affect the accuracy of the observed line fluxes. In Figures 1 and 2 we show the Fe XVII lines observed in the higher resolution spectra obtained with the KAP crystal spectrometer on the OV1-17 satellite. The full spectra for this time period are shown in the paper by Walker and Rugge (1970). The spectra shown in Figures 1 and 2 were obtained at the same time as the EDDT spectra between 3.5 and 8.5 Å which were analyzed in detail in paper I. The iron lines observed in the spectra of Figures 1 and 2, and in the spectra analyzed in paper II are listed in Table 1. The fluxes given in Table 1 have been corrected for line blends, as described below.

The calibration of the OV1-10 spectrometer was discussed in paper II. It was necessary to renormalize the calibration of the OV1-17 KAP spectrometer, since the inflight calibration data indicated a decrease in detector efficiency by a factor of 2 at a wavelength of  $\sim 2\text{Å}$ . Unfortunately it was not possible to provide an inflight calibration system at wavelengths

within the range of the KAP spectrometer itself. We used the model constructed with the OV1-17 EDDT crystal spectrometer observations in paper I to calculate the Ne IX and O VIII resonance line fluxes, and determined a corrected KAP spectrometer calibration curve by comparing these calculated fluxes with the observed line intensities.

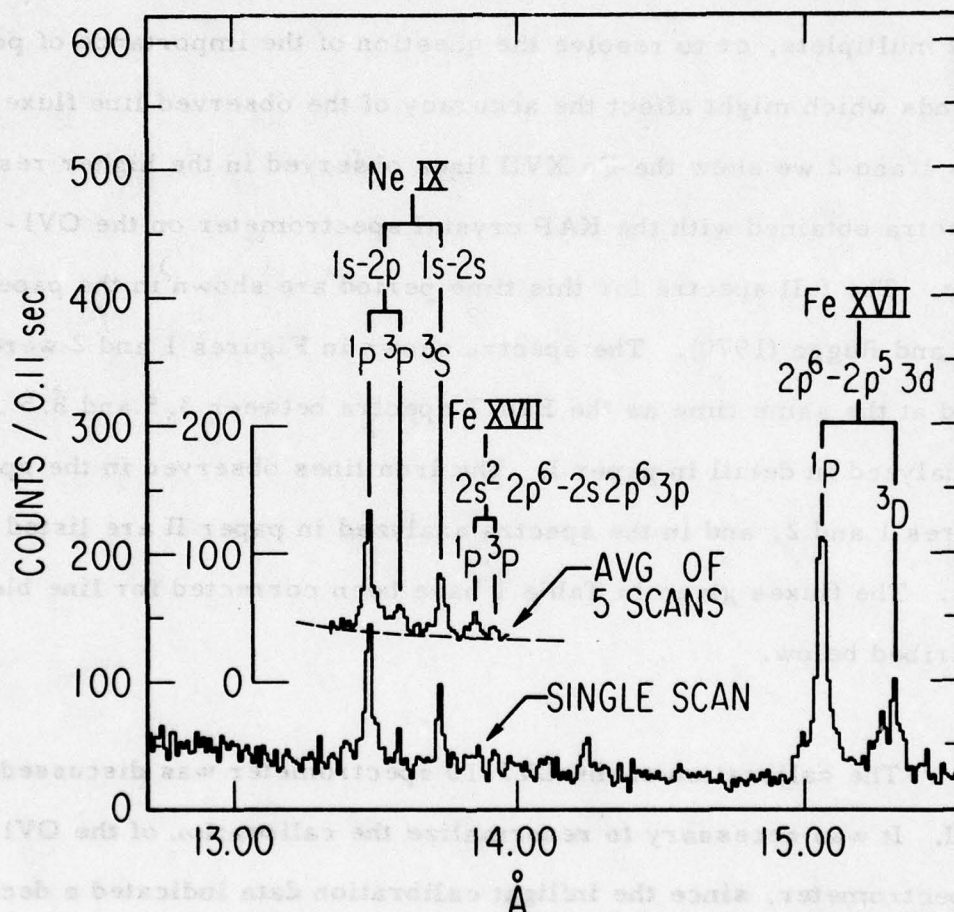


Fig. 1. Portion of the spectrum recorded by the KAP spectrometer on OV1-17 for 20 March 1969, showing the Fe XVII  $2s^2 2p^6$   $1S - 2s2p^6 3p$   $1P$  and  $3P$  lines.

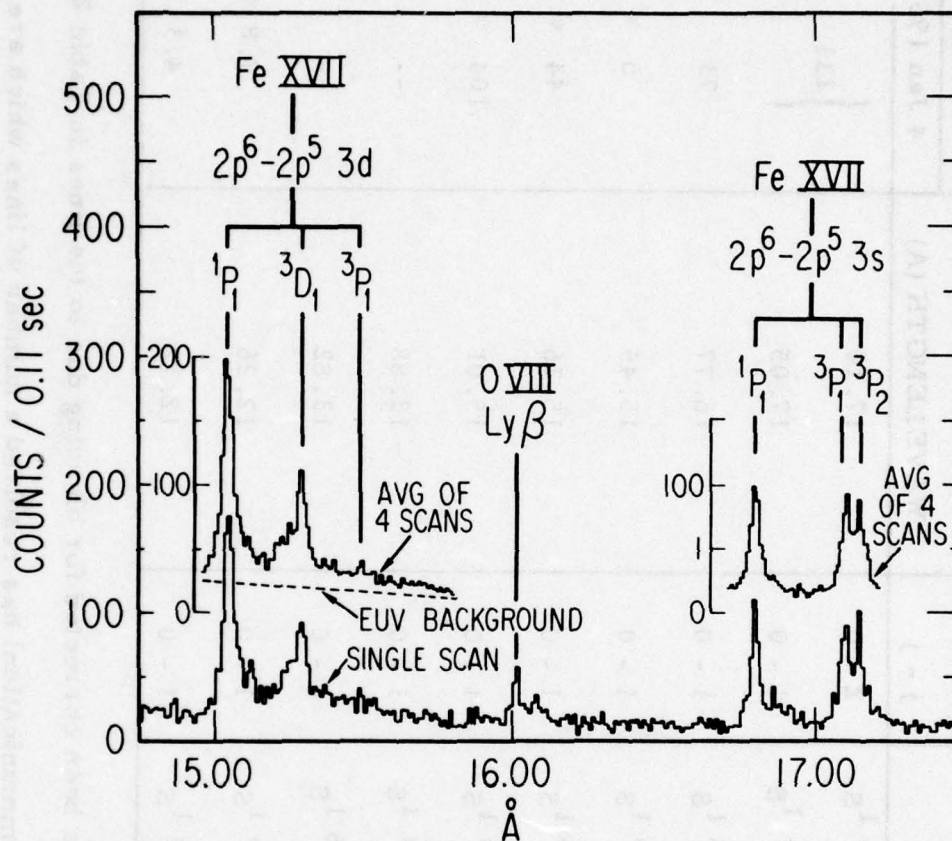


Fig. 2. Portion of the spectrum recorded by the KAP spectrometer on OV1-17 for 20 March 1969, showing the Fe XVII  $2s^2 2p^6 1s - 2s^2 2p^5 3d$   $1P$ ,  $3D$ , and  $3P$ , and  $2s^2 2p^6 1s_0 - 2s^2 2p^5 3s$   $1P_1$ ,  $3P_1$  and  $3P_2$  lines.



Table 1. Fe XVII Lines Observed in the Coronal Spectrum

j - j	WAVELENGTH (Å)	Flux ( $10^{-5}$ ergs/cm <sup>2</sup> -sec)	
		4 Jan 1967	20 Mar 1969
$2s^2 2p^5 3s^3 P - 2s^2 2p^6 1S$	17.10	131	458
$3s^3 P - 2s^2 2p^6 1S$	17.05		492
$3s^1 P - 2s^2 2p^6 1S$	16.77	73	442
$3d^3 P - 2s^2 2p^6 1S$	15.45	5 *	56
$3d^3 D - 2s^2 2p^6 1S$	15.26	44 *	342
$3d^1 P - 2s^2 2p^6 1S$	15.01	104 *	610
$2s^2 2p^6 3p^3 P - 2s^2 2p^6 1S$	13.88	--	18
$3p^1 P - 2s^2 2p^6 1S$	13.82	--	43
$2s^2 2p^5 4d^3 D - 2s^2 2p^6 1S$	12.26	7.8 **	--
$4d^1 P - 2s^2 2p^6 1S$	12.12	4.3	--

\* These line fluxes have been corrected for blending due to the lines in Table 2.

\*\* Parkinson (private communication) has resolved a number of lines which are blended with the Fe XVII  $2^1S - 4^3D$  line in the OV1-10 spectra. The absolute flux given in this table should, therefore, be treated with caution.

The strongest lines of Fe XVII are observed from the  $2s^2 2p^5 3d$  and  $2s^2 2p^5 3s$  configurations, with the two groups of multiplets being roughly equal in intensity. Pottasch (1966) pointed out that the small excitation cross-section for the  $2s^2 2p^5 3s$  configuration was inconsistent with the assumption that this state is populated by direct excitation from the ground state; and he suggested that cascade from  $2s^2 2p^5 3p$  was the main mode of populating the  $2s^2 2p^5 3s$  configuration. Calculations by Bely and Bely (1967) confirmed the importance of excitation to  $2s^2 2p^5 3p$ ; however, they did not consider the problem of the relative intensities of all of the observable lines in detail. Beigman and Urnov (1969) used cross-sections calculated in L-S coupling to calculate the relative intensities of the  $2s^2 2p^5 3s$  multiplet group and of the individual lines of the  $2s^2 2p^5 3d$  multiplet. Their results were in general agreement with observation. They also pointed out that the  $2s^2 2p^5 3p$  level was itself populated to a considerable degree by cascade from the  $2s 2p^6 3p$  levels. Loulergue and Nussbaumer (1973) have recently calculated the relative intensities of each of the lines observed in the corona from the  $2s^2 2p^5 3d$ ,  $2s 2p^6 3p$  configurations including cascades among 36 levels. In the present paper we compare these calculated line intensities and intensities calculated with a revised set of collisional excitation rates, with observations of the coronal spectrum made from the OV1-10 and OV1-17 satellites. The higher resolution OV1-17 observations, which have not been reported in detail previously, are of particular interest because they allow the intensities of the  $^1S_0 - ^3P_1$  (17.051Å) and forbidden  $^1S_0 - ^3P_2$  (17.10Å) transitions of the  $2s^2 2p^5 3s$  configuration to be determined separately.

The identification of the Fe XVII lines is discussed by Parkinson (1973), who has observed these lines in a high resolution spectrum obtained with a rocket-borne spectrometer. The  $2p^6\ ^1S_0 - 2p^53s\ ^3P_2$  line at  $17.10\ \text{\AA}$ , which is clearly resolved from the  $^1S_0 - ^3P_1$  line in the spectrum of Figure 2 and in the spectrum published by Parkinson, is of interest since it illustrates the importance of forbidden (in this case quadrupole) transitions in the low density corona. The higher resolution OV1-17 spectra allow us to resolve a number of lines which were blended with the Fe XVII 2p-3d multiplet in the OV1-10 spectra. In Table 2, we list the lines observed near the 2p-3d and 2p-3s multiplets in the spectra shown in figures 1 and 2. Parkinson has observed unidentified lines at  $\sim 15.06$  (this line is only partially resolved from the Fe XVII resonance line at  $15.012\ \text{\AA}$ ),  $15.10$ ,  $15.15$ ,  $15.21$ ,  $15.35$ ,  $15.43-15.53$ ,  $15.56$ , and  $15.66\ \text{\AA}$  near the 2p-3d multiplet, and lines at  $16.83$ ,  $17.12$ , and  $17.15\ \text{\AA}$ , near the 2p-3s multiplet. The wavelengths of the weak lines observed in our spectra and by Parkinson are in reasonably good agreement. Parkinson suggests that these lines may be satellite lines due to transitions of the form  $2p^6nl - 2p^53d(s)nd$  ( $n \geq 3$ ) in Fe XVI. We assess the potential importance of line blends due to these satellite lines in the next section.

In Table 2, we have compiled a list of lines which could be blended with the Fe XVII lines, using the compilation of Kelly and Palumbo (1973), and the recent work on the fluorine (Fe XVIII) and oxygen (Fe XIX) isoelectronic sequences by Swartz et al (1971), Neupert et al (1973),



Table 2. Lines Observed Near the Fe XVII 2p-3s and 2p-3d Transitions for the 20 March 1969 Spectra

Observed Wavelength	Predicted Wavelength	Ion	Transitions	j-j
(Å)	(Å)			
17.10	17.10	Fe XVII	$2s^2 2p^6 1S-2s^2 2p^5 3s^3 P$	0-2
	17.09	Cr XVI	$2s^2 2p^5 2P-2s^2 2p^4 3d^2 D$	1/2-3/2
17.06	17.051	Fe XVII	$2s^2 2p^6 1S-2s^2 2p^5 3s^3 P$	0-1
16.92				
16.90				
16.83				
16.77	16.775	Fe XVII	$2s^2 2p^6 1S-2s^2 2p^5 3s^1 P$	0-1
.....	.....	.....	.....	.....
-	15.623	Fe XVIII	$2s^2 2p^5 2P-2s^2 2p^4 (1D) 3s^2 D$	3/2-5/2
-	15.598	Fe XIX	$2s^2 2p^4 1S-2s^2 2p^3 3s^3 P$	0-1
-	15.567	Fe XVIII	$2s^2 2p^5 2P-2s^2 2p^4 3s^2 D$	3/2-3/2
15.54				
15.51				
15.49	15.491	Fe XVIII	$2s^2 2p^5 2P-2s^2 2p^4 3s^2 S$	1/2-1/2
15.45	15.452	Fe XVII	$2s^2 2p^6 1S-2s^2 2p^5 3d^3 P$	0-1
	15.452	Fe XIX	$2s^2 2p^4 1S-2s^2 2p^3 3s^1 P$	0-1
-	15.413	Fe XIX	$2s^2 2p^4 1D-2s^2 2p^3 3s^3 P$	2-1
15.36	15.361*	Fe XIX	$2s^2 2p^4 3P-2s^2 2p^3 3s^3 P$	0-1
15.33	15.341*	Fe XIX	$2s^2 2p^4 1D-2s^2 2p^3 3s^1 P$	2-1
-	15.306	Fe XIX	$2s^2 2p^4 1D-2s^2 2p^3 3s^3 P$	2-1
-	15.288	Fe XIX	$2s^2 2p^4 3P-2s^2 2p^3 3s^1 P$	1-1
	15.261	Fe XVII	$2s^2 2p^6 1S-2s^2 2p^5 3d^3 D$	0-1
15.26	15.258	Fe XVIII	$2s^2 2p^5 2P-2s^2 2p^4 (1S) 3s^2 S$	3/2-1/2
-	15.237	Fe XIX	$2s^2 2p^4 3P-2s^2 2p^3 3s^3 P$	0-1
15.21				
15.19				
-	15.176	O VIII	$1s^2 S - 4p^2 P$	1/2-3/2
-	15.173	Fe XIX	$2s^2 2p^4 3P-2s^2 2p^3 3s^3 S$	1-1
-	15.158	Fe XIX	$2s^2 2p^4 1D-2s^2 2p^3 3s^1 P$	2-1
15.13	15.132*	Fe XIX	$2s^2 2p^4 3P-2s^2 2p^3 3s^3 S$	0-1
-	15.110	Fe XIX	$2s^2 2p^4 3P-2s^2 2p^3 3s^1 P$	0-1
15.08	15.083*	Fe XIX	$2s^2 2p^4 3P-2s^2 2p^3 3s^1 P$	2-1
-	15.069	Fe XIX	$2s^2 2p^4 3P-2s^2 2p^3 3s^3 P$	2-2
15.01	15.012	Fe XVII	$2s^2 2p^6 1S-2s^2 2p^5 3d^1 P$	0-1
	14.971	Fe XIX	$2s^2 2p^4 3P-2s^2 2p^3 3s^3 S$	2-1
-	14.927	Fe XIX	$2s^2 2p^4 3P-2s^2 2p^3 3s^1 P$	2-1

\* These Fe XIX lines are coincident in wavelength with the observed lines; however, transitions in doubly excited states of Fe XVI may be partly responsible for the observed line flux.

Feldman et al (1973), Fawcett et al (1974), and Doschek et al (1974). The most serious potential blends are due to Fe XVIII and Fe XIX lines. Lines of less abundant elements such as Cr will be too weak to cause significant blending. The blends which may be important are Fe XIX  $2^3P_2 - 3^3S_1$  for the line at 15.012 Å. Fe XIX  $2^3P_0 - 3^3P_1$  and Fe XVIII  $2^2P_{3/2} - 3^2S_{1/2}$  for the line at 15.261 Å, and Fe XIX  $2^1S_0 - 3^3S_1$  for the line at 15.45 Å. Unfortunately, it is difficult to calculate the flux in 2p - 3s transitions in Fe XVIII, and Fe XIX accurately, since collision strengths are not available for these ions, and cascades from  $2p^43p$  and  $2p^33p$  levels are probably important in populating the  $2p^33s$  levels. However we may assess the strength of a blended line if we can observe the flux in a line from the same upper level, and if we know the relevant oscillator strengths. In the case of Fe XVIII  $3^2S_{1/2}$ , we observe the transition  $2^2P_{1/2} - 3^2S_{1/2}$  at 15.49 Å. We may obtain the oscillator strengths by interpolation from the results of Cohen et al. (1968) who calculated the gf values for these transitions in Mn XVII and Co XIX. We find that the flux in the Fe XVIII  $2^2P_{3/2} - 3^2S_{1/2}$  line at 15.258 Å is ~ 25% of that in the weak  $2^2P_{1/2} - 3^2S_{1/2}$  line at 15.491 Å. The correction to Fe XVII  $2^1S - 3^3D$  is less than 2%. For the Fe XIX lines at 14.971 Å ( $2^3P_2 - 3^3S_1$ ) and at 15.453 Å ( $2^1S_0 - 3^1P_1$ ), we may use the comparable transitions at 15.173 Å ( $2^3P_1 - 2^3S_1$ ) and at 15.341 Å ( $2^1D_2 - 3^1P_1$ ) respectively. We observe no significant line at 15.173 Å, and so assume that the line at 14.971 Å is weak. We do observe a line at 15.33 Å. However, if we assume that the transition probabilities

are proportional to the statistical weights, the  $2^1S - 3^1P$  line at  $15.452\text{\AA}$  is too weak to cause significant blending. For the  $2^3P_0 - 3^3P_1$  transition at  $15.237\text{\AA}$ , there is no comparable transition which can be resolved in our spectra; however, the weakness of other Fe XIX lines suggests that this blend is unimportant as well.

In paper II, we assumed, for the 4 January 1967 spectra, that all of the flux observed between  $15.0$  and  $15.5\text{\AA}$ , with the exception of an appropriate correction for the X-ray continuum, was due to the 3 Fe XVII  $2s-3d$  transitions. Using the higher resolution OV1-17 observations, we may now correct the OV1-10 observations for 4 January 1967 for the weak lines which are listed in Table 2. The corrected fluxes are given in Table 1. The correction is 26% for  $15.012\text{\AA}$ , 12% for  $15.261\text{\AA}$ , and 50% for  $15.452\text{\AA}$ .



### III. FORMULATION OF THE LINE FLUX INTEGRAL EQUATION

The intensity of the lines emitted from an optically thin medium such as the corona is given by the volume integral of an emission function  $E_{ij} [T_e(x_v), n_e(x_v)]$  which is a function of the local temperature and density of the medium. The emission function  $E_{ij}$  may be expressed as (Paper I)

$$1) \quad E_{ij} = \frac{hc}{\lambda} A^r_{ij} \left\{ n_{z,i} [T_e(x_v), n_e(x_v)] + \sum_{n'l' > n_c l_c} n_{z-1,i'} [T_e(x_v), n_e(x_v)] \right\}$$

where  $n_{z,i}$  is the population of the excited level  $i$  in ionization stage  $z$ , and  $n_{z-1,i'}$  is the population of the doubly excited state with the same configuration as  $i$ , but with an additional electron, with the quantum numbers  $n'l'$ ; and the summation is carried out over those states for which  $n'l'$  is sufficiently large that the wavelength of the emitted photon in  $n'l' \rightarrow jn'I'$  is unresolvable from that for transition  $i \rightarrow j$ . The singly excited levels are populated chiefly by collisional excitation, and the doubly excited levels are populated chiefly by dielectronic recombination. For those cases where  $n'l'$  is small, the resulting satellite lines may be resolved from the parent line and their flux must be calculated separately. The line flux resulting from the decay of doubly excited levels is generally only a few percent of the observed resonance line flux, and has not been included in most previous analyses.

The population of the excited states  $n_{z,i}$  can be calculated from the equations of statistical equilibrium (see, for example, Gabriel and Jordon 1972).

In the case of Fe XVII, we must include the effects of cascades, by solving the equations

$$2) \quad \frac{dn_{z,i}}{dt} = n_e n_{z,g} \alpha_{gi}^{\text{ex}} + \sum_{k>i} n_{z,k} A_{ki}^r - n_{z,i} \sum_{k<i} A_{ik}^r$$

where  $n_{z,g}$  is the population of the ground level,  $\alpha_{gi}^{\text{ex}}$  is the excitation rate from the ground level into the excited level  $i$ , and  $A_{ik}^r$  is the radiative decay rate from state  $i$  to state  $k$ . If we order the states according to energy,  $i=1$  referring to the lowest lying excited state, and  $i=N$  to the highest excited state, the emission function which results from collisional processes can be written in terms of the equilibrium solution to equation 2) as

$$E_{ij}^{\text{ex}}(T_e, n_e) = \frac{hc}{\lambda_{ij}} A_{ij}^r n_{zi}$$

$$3) \quad = \frac{hc}{\lambda_{ij}} A_{ij}^r n_e n_{z,g} \frac{\sum_{k=i}^N \alpha_{gk}^{\text{ex}} \left| \Gamma_{m\delta_{mp}} - A_{mp}^r \right|}{\prod_{k=i}^N \Gamma_k}$$

where  $m = i+1, \dots, N$ ;  $p = i, \dots, k-1, \dots, N$  (i.e.,  $p \neq k$ ) and  $A^r_{mp} \equiv 0$  for  $p \geq m$ . We have defined the total radiative width of the state  $k$ ,

$\Gamma_k = \sum_{l=1}^r A^r_{kl}$ . The symbol  $\delta_{mp}$  refers to the Kronecker delta

$[\delta_{mp} = 1, m=p, \delta_{mp} = 0, m \neq p]$ .

Loulergue and Nussbaumer (1973) have calculated the emission functions for the lines listed in Table 1, taking into account cascades from the first 36 excited levels. A level diagram showing the principal radiative decay paths for these levels is shown in Figure 3. The levels which decay to the ground state are shown in bold type in Figure 3.

From equation 3 it is obvious that the population of each excited state, and consequently the intensity of all transitions, is proportional to the electron density,  $n_e$ , to the ground state population of the ion,  $n_{z,g}$ , and to the weighted sum of a set of collisional excitation rates from the ground state,  $\alpha^{ex}_{gk}$ . Therefore, as Loulergue and Nussbaumer point out, the relative intensity of the observed Fe XVII lines will not be sensitive to electron density, and will be only slightly dependent on electron temperature [owing to the slightly differing temperature dependence of the  $\alpha^{ex}_{gk}$  whose major temperature dependence will go as  $\exp(-hc/\lambda_{gk} kT)$ ].

The intensities calculated by Loulergue and Nussbaumer are compared with the relative fluxes observed on OV1-10 and OV1-17, and by Parkinson (1973) in Table 3.



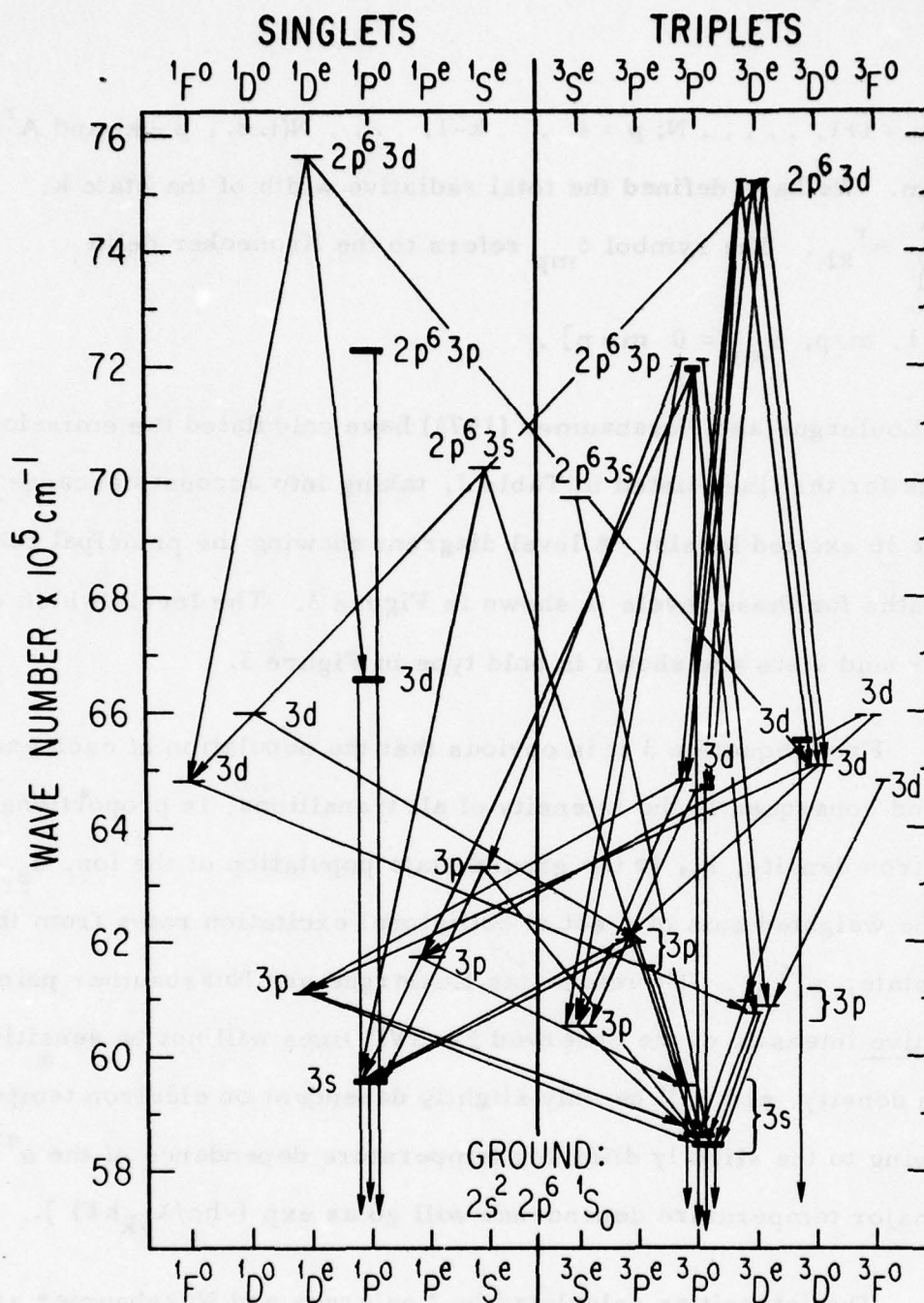


Fig. 3. Level diagram for Fe XVII, showing the principal decay paths for the first 36 excited levels. (Those levels with transitions to the ground level are shown in bold type.)

Table 3. Comparison of Experimental and Theoretical Line Intensities

TRANSITION	THEORY			EXPERIMENT		
	(A)	(B)	(C)	4 Jan 1967(C)	20 Mar 1969(C)	30 Nov 1971(D)
3s - 2p	17.10	0.23	0.74	.59	1.25	0.64
3s - 2p	17.05	0.58	0.97	.91	0.80	0.82
3s - 2p	16.77	0.38	0.54	.51	0.70	0.58
3d - 2p	15.45	0.008	0.08	.09	0.05	0.11
3d - 2p	15.26	0.33	0.37	.37	0.43	0.50
3d - 2p	15.01	1.00	1.00	1.00	1.00	1.00
3p - 2s	13.88	0.002	.10	.03	--	0.04*
3p - 2s	13.82	0.15	.15	.07	--	0.07
4d - 2p	12.26	--	--	--	0.07	--
4d - 2p	12.12	--	--	0.04	--	--

(A) Loulergue and Nussbaumer (T=5.5x10<sup>6</sup>)  
 (B) Loulergue and Nussbaumer (T=5.5x10<sup>6</sup>)  
 (C) Walker, Rugge, and Weiss (T=4.0x10<sup>6</sup>)  
 (D) Parkinson

$$\left[ \begin{matrix} \Omega \\ 2s^2 2p^6 1S - 2s 2p^6 3L \end{matrix} \right] \equiv 0$$

triplet cross sections=singlet cross section x statistical weights

\* The ratios for Parkinson spectra are taken from Loulergue and Nussbaumer. Examination of Parkinson spectra by the present authors suggests .04 is closer to Parkinson's measured ratio than the value of .05 quoted by Loulergue and Nussbaumer.

In the next section, we discuss the problem of selecting the best set of atomic rate constants for the solution of equation 3, and present a calculation of the relative intensities of the Fe XVII lines based on somewhat different assumptions regarding the  $2s^2 2p^6 - 2s 2p^6 3s$ ,  $3p$ , and  $3d$  excitation rate coefficients than those made by Louergue and Nussbaumer.

In equation 1, we included the flux resulting from decay of the doubly excited states in the sodium-like ion Fe XVI. The statistical equilibrium equation for these states must include dielectronic recombination and collisional excitation as mechanisms for the population of excited states,

$$4) \quad \frac{dn_{z-1, i'}}{dt} = n_e n_{z-1, g} \alpha_{gi'}^{ex} + n_e n_{z, g} \bar{\alpha}_{gi'}^{di} + \sum_{k' > i'} n_{z-1, k'} A_{k'i'}^r - n_{z-1, i'} \left[ \sum_{k' < i'} A_{i'k'}^r + \sum_j A_{i'j\epsilon}^a \right],$$

$\bar{\alpha}_{gi'}^{di}$  is the total rate for the capture of an electron into the doubly excited state  $i'$ ,  $A_{i'j\epsilon}^a$  is the rate for the inverse process in which a doubly excited state autoionizes emitting an electron of energy  $\epsilon$ , and the other symbols have the same meaning as before. For lithium-like and helium-like ions collisional excitation of doubly excited states and cascades from other doubly excited states are negligible, and we may write the population of doubly excited states quite simply (Gabriel, 1972). However, in the case of sodium-like ions cascades from doubly excited states such as  $2s2p^6 3s3p$  to  $2s^2 2p^5 3s3p$  may well be important; and the Fe XVI ion



has an appreciable population at sufficiently high temperatures that inner shell excitations such as  $2s^2 2p^6 3s \rightarrow 2s^2 2p^5 3s n l$  will be quite important [Goldberg et al. (1965), Bely (1967)] .

However, if we use spectra of sufficiently high resolution so that transitions resulting from levels with  $n = 3$  can be resolved, inner shell excitations can then contribute only to the flux in the Fe XVII 2p - 3s lines [Resolvable satellite lines to these lines have been reported previously by Rugge and Walker (1968) and by Parkinson (1973)] . Unresolvable satellites to the 2p - 3d resonance line ( $^1S - ^1P$ ) will be due entirely to dielectronic recombination, and the term containing  $\alpha_{gi}^{ex}$  in equation 4 may be neglected for this transition. Cascades of the type  $2s^2 2p^5 n'(p, f) n l \rightarrow 2s^2 2p^5 3d n l$ , and  $2s 2p^6 3d n l \rightarrow 2s^2 2p^5 3d n l$  can contribute to the emission of unresolvable satellites to the 2p-3d lines. However, since dielectronic recombination rates are proportional to oscillator strengths, rates for the 2s-2p transition (where  $\Delta n = 0$ ) will be small, while the small intensity of the singly excited 2p - 4d transitions [ $\sim 10\%$  of the 2p - 3d resonance line (from Table 4)] suggests that these higher excitations will not be significant. The population of doubly excited levels due to cascades should, therefore, be small. The population of the doubly excited levels,  $(z-1, i')$  may then be expressed as

$$n_{z-1, i'} = n_e n_{Z, g} \frac{\alpha_{gi'}^{di}}{(\Gamma_{i'}^r + \Gamma_{i'}^a)} = n_e n_{Z-1, g} \frac{\alpha_{gi'}^{di}}{A_{i'g}^r}$$

where (Shore, 1969)

$$\alpha_{gi'}^{di} = \frac{1}{2} \left[ \frac{2\pi\hbar^2}{mkT_e} \right]^{3/2} \frac{g_i}{g_g} A_{gi'}^a \exp(-hc/\lambda_{gi,kT_e}) .$$

The  $g$ 's are statistical weights. Burgess (1965) and Shore (1969) have discussed the sum of the dielectronic recombination rates,  $\alpha_{gi'}^{di}$ , for the states  $i'$  (i.e., in  $l'$ ) over large values of  $n' l'$ . This sum is the quantity required in the evaluation of equation 1. Tucker and Koren (1971) have developed a simple expression which approximates Shore's results. Tucker and Koren find that the ratio of flux due to dielectronic recombinations, and that due to collisional excitation may be written

$$E^{di}/E^{ex} \approx 40(Z+1)^3 / T_e .$$

For the Fe XVII 2p-3d resonance line this results in a 4% enhancement at  $\sim 5 \times 10^6$  °K. We shall assume that dielectronic contributions to the non-resonance transitions ( $^1S$ - $^3P$ ) and ( $^1S$ - $^3D$ ) are negligible.

Using the formalism developed in paper I, we may write the flux in the Fe XVII 2p-3d multiplet, which was used in paper II to derive the iron abundance, as

$$F_{2p-3d} = \sum_{ij} \epsilon(\lambda_{ij}) a_H A_{Fe} \iint dS n_e(T_e) \phi(T_e) \times$$

5)

$$a_{Fe XVII}(T_e) \times [J_{ij}^{ex}(T_e) + J_{ij}^{di}(T_e)]$$

where we may write the excitation functions  $J_{ij}^{ex}$  as

$$6) \quad J_{ij}^{ex} = \frac{hc}{\lambda_{ij}} A_{ij}^r \frac{\sum_{k=i}^N \alpha_{gk}^{ex} |\Gamma_m \delta_{mp} - A_{mp}^r|}{\prod_{k=i}^N \Gamma_k^r},$$

and the function  $J_{ij}^{di}$  as

$$J_{ij}^{di} = \frac{hc}{\lambda_{ij}} \alpha_{ij}^{ex} \frac{1.95 \times 10^{-5}}{T_e} \frac{A_{ij}^r}{\Gamma_i^r}$$

The sum over  $ij$  extends over the  $^1S_0 - ^1P_1$ ,  $^1S_1 - ^3D_1$ , and  $^1S_0 - ^3P_1$  transitions for  $J^{ex}$ , and over  $^1S_0 - ^1P_1$ , only for  $J^{di}$ . The quantity  $N_e n_e(T_e) \phi(T_e)$  is the emission measure of the corona as a function of temperature,  $a_{Fe XVII}(T_e)$  is the fractional population of iron ions in the Fe XVII state,  $A_{Fe}$  the abundance of iron,  $a_H$  the number of electrons per hydrogen ion, and  $\epsilon(\lambda_{ij})$  the spectrometer efficiency function [ $\epsilon(\lambda_{ij})$  also includes the geometrical factor  $1/4\pi(A.U.)^2$ ]. The integral over the area unresolved by the spectrometer,  $S$ , is extended over the entire disk for the OV1-10 and OV1-17 observations.



#### IV. DETERMINATION OF ATOMIC RATE CONSTANTS

Loulergue (1971) has calculated the energies for all levels in Table 2, and the radiative decay rates for all electric dipole transitions. Garstang (1966, 1969) has calculated the decay rates for those levels which have magnetic dipole or quadrupole decays of importance. Bely and Bely (1967) have calculated collision strengths for excitations to the  $2s^2 2p^5 3s$ ,  $2s^2 2p^5 3p$ , and  $2s^2 2p^5 3d$  configurations in intermediate coupling, for those levels which have strong excitation cross-sections. For the excitations to the  $2s2p^6 3s$ ,  $2s2p^6 3p$ , and  $2s2p^6 3d$  singlet levels, Bely and Bely have extrapolated lithium-like cross-sections, viz.

$$Q(2s^2 2p^6 \rightarrow 2s2p^6 nl) = Q(2s^2 \rightarrow 2snl)$$

and

$$Q(2s^2 \rightarrow 2snl) = 2Q(2s \rightarrow nl) .$$

However, Bely and Bely do not calculate or estimate cross-sections for excitations to the  $2s2p^6 3s$ ,  $2s2p^6 3p$ , or  $2s2p^6 3d$  triplet levels.

Beigman and Vainshtein (1968) do calculate cross-sections for both the  $2s2p^6 3l$  singlet and triplet levels; however, they do not include configuration interaction in their calculations. According to Bely and Bely, configuration interaction will be important for these levels.

Flower (1971) has calculated excitation cross-sections in L-S coupling for a number of levels for which Bely and Bely do not present results. Loulergue and Nussbaumer have used the cross-sections of Bely

and Bely where available, and the results of Flower for other levels.

For the excitations to the  $2s2p^6 3s$ ,  $2s2p^6 3p$ , and  $2s2p^6 3d$  triplet levels, Loulergue and Nussbaumer assumed that the triplet cross-sections are equal to the singlet cross-sections multiplied by the ratio of statistical weights.

We have chosen to use the cross-sections for beryllium-like ions to obtain cross-sections for the  $2s2p^6 3s$ , and  $2s2p^6 3d$  singlet excitations, using the relation

$$Q(2s^2 2p^6 \ ^1S \rightarrow 2s2p^6 \ 3\ell \ ^1L) = Q(2s^2 \ ^1S \rightarrow 2s3\ell \ ^1L)$$

We have used the observed relative fluxes of the  $2s^2 2p^6 \ ^1S - 2s2p^6 3p \ ^1P$  and  $^3P$  transitions to derive the collisional excitation rates into their respective upper levels. We believe this approach is justified because the upper levels of these lines are not appreciably populated by cascade, and should satisfy the coronal excitation condition, with the result that the line fluxes are directly proportional to the respective excitation coefficients and the branching ratios. Finally, we have used the relative fluxes in the  $2s^2 2p^5 3s \ ^1P$  and  $^3P$  transitions to derive the collisional excitation rates into the  $2s2p^6 3s \ ^3S$  and  $2s2p^6 3d \ ^3D$  levels. Since the  $2s^2 2p^5 3s$  levels are populated by cascade from a large number of levels, the values of the  $^3S$  and  $^3D$  cross-sections derived depends on the accuracy of the theoretical cross sections for these other levels, as well as on the accuracy of the experimental line intensity ratios.

Gabriel and Jordan (1972) have reviewed the published cross-section data for beryllium-like ions. Theoretical calculations for the cross-sections of interest have been carried out by Eissner (1972), and experimental measurements have been made by Johnson and Kunze (1971) and Tondello and McWhirter (1971). We have used the Ne VII excitation rates calculated by Eissner and extrapolated to higher Z using the Z dependence of the lithium-like 2s-3 $\ell$  excitations calculated by Bely (1966), to obtain values of  $\Omega$  for Fe XVII. The collision strengths which we have adopted are presented in Table 4. The calculated Fe XVII line intensities which we derive, using the collision strength given in Table 4 and the same set of radiative transition rates as Louergue and Nussbaumer, are compared with the experimental results in Table 3. The ratios tabulated are calculated for  $4.0 \times 10^6$  °K. We have chosen this temperature since it is the temperature of most efficient excitation for Fe XVII lines for the coronal temperature structure derived for 20 March 1969 in paper II. Both sets of theoretical calculations are in reasonably good agreement with the observations, and it is difficult to argue that the experimental data favors either set of calculated fluxes. In Table 5, we have tabulated the quantity  $J_{ij}^{\text{ex}}(T_e) / [\alpha_{gi}^{\text{ex}}(hc/\lambda_{ij})(A_{ij}^r/\Gamma_i)]$ , which is the ratio of line fluxes which would be calculated including cascades, to those which would be calculated without including cascades. The results in Table 3 include the effects of dielectronic recombination, while those in Table 5 do not.



Table 4. Threshold Collision Strengths for Fe XVII

Configuration	Level	Collision Strength ( $\times 10^3$ )	Ref.
$2s2p^63d$	$^1D_2$	65.2 (73)*	Bely & Bely
	$^3D_1$	-- (100)**	
	$^3D_2$	--	
	$^3D_3$	--	
$2s2p^63p$	$^1P_1$	22.4 (10.1)**	Bely & Bely
	$^3P_2$	--	
	$^3P_0$	--	
	$^3P_1$	-- (6.5)**	
$2s2p^63s$	$^1S_0$	32.4 (30.1)*	Bely & Bely
	$^3S_1$	-- (45)**	
$2s^22p^53d$	$^1P_1$	147	Bely & Bely
	$^1D_2$	2.9	Flower
	$^3F_3$	--	
	$^3F_2$	19.8	Flower
	$^3D_1$	47.3	Bely & Bely
	$^3D_3$	--	

\* Collision strengths extrapolated from the Beryllium-like collision strengths calculated by Eissner.

\*\* Collision strengths derived from observed coronal line ratios in this paper.

Table 4. Threshold Collision Strengths for Fe XVII (Continued)

Configuration	Level	Collision Strength ( $\times 10^3$ )	Ref.
$2s^2 2p^6 3d$	$^3D_2$	--	Flower
	$^3P_2$	17	
	$^3F_4$	--	
	$^1F_3$	4.1	Flower
	$^3P_1$	1.2	Bely & Bely
	$^3P_0$	3.8	Flower
$2s^2 2p^5 3p$	$^1S_0$	64	Bely & Bely
	$^3P_2$	0.6	Bely & Bely
	$^3P_1$	4.7	Flower
	$^1P_1$	1.6	Flower
	$^3P_0$	3.4	Bely & Bely
	$^1D_2$	0.5	Bely & Bely
	$^3D_1$	11.6	Flower
	$^3D_3$	--	
	$^3D_2$	0.4	Bely & Bely
	$^3S_1$	4.7	Flower
	$^1P_1$	1.45	Bely & Bely
	$^3P_0$	--	
	$^3P_1$	1.67	Bely & Bely
	$^3P_2$	--	
$2s^2 2p^5 3s$			

**Table 5. Calculated Ratios of Fe XVII Line Intensities**  
 (Ratios are given in photons at  $4 \times 10^6$  K)

Line	Cascades Included	Cascades Not Included
17.10A	.62	0
17.05	.96	.017
16.77	.54	.013
15.45	.10	.014
15.26	.39	.33
15.01	1.05	1.00
13.88	.03	.03
13.82	.07	.07



## V. CALCULATION OF THE REVISED IRON ABUNDANCE

In paper II, we calculated the abundance of iron using equation 5, and the coronal emission measure model developed from an analysis of O VII, O VIII, Ne IX, Ne X, and Mg IX line fluxes. In the present paper we follow the same procedure, using the OVI-10 Fe XVII 2p-3d multiplet line fluxes, and the improved Fe XVII line excitation functions derived from section 4. We have also corrected the observed OVI-10 fluxes for the blending caused by the unidentified satellite lines observed in the higher resolution OVI-17 spectra, and listed in Table 2. As discussed in Section 2, this correction was accomplished by multiplying the OVI-10 fluxes by the ratio of the flux observed in the 2p-3d multiplet to the total line flux observed between 15 and 15.5 Å for the OVI-17 spectra. We believe this procedure is justified since the analysis carried out in papers I and II found that the coronal temperature structure derived from the two sets of observations were the same, so that the relative Fe XVII line intensities and Fe XVI satellite line intensities should be the same for both spectra. The corrected OVI-10 2p-3d multiplet fluxes are given in Table 1. Using the corrected flux, and using the improved Fe XVII line excitation functions, we find the revised iron abundance to be  $A_{\text{Fe}} = 26 \times 10^{-6}$ . This abundance assumes a silicon abundance normalized to  $A_{\text{Si}} = 35 \times 10^{-6}$ , as discussed in papers I and II. This revised iron abundance agrees more closely with the value of  $25 \times 10^{-6}$ , found in recent photospheric analyses [Withbroe (1971), Smith and Whaling (1973)], than the value of  $40 \times 10^{-6}$  which was found in paper II.

## VI. SUMMARY

We have calculated the relative intensity of eight Fe XVII lines observed in the coronal spectrum between 13 and 18A, and find that these theoretical intensity ratios are in reasonably good agreement with observations. Using the improved line emission functions calculated from this analysis, we have used the Fe XVII  $2p^6 1S-2p^5 3d 1P$ ,  $3D$ , and  $3P$  line fluxes, and a coronal model derived from the analysis of O VII, O VIII, Ne IX, Ne X, and Mg XI line fluxes to compute the abundance of iron in the corona. We find  $A_{Fe} = 26 \times 10^{-6}$ , which is in good agreement with the photospheric iron abundance [Smith and Whaling (1973)], and with the coronal iron abundance determined from the analysis of XUV fluxes (Dupree, 1971). The coronal abundances found in papers I and II, and in the present paper are summarized in Table 6, and compared with transition region and photospheric abundances.

We have also compared the results of papers I and II, and the present paper with the recent compilation by Cameron (1974) of solar system abundances in Table 6. In general, the agreement is good; however, there is a significant difference for the neon abundance. Cameron's neon abundance is obtained from cosmic ray observations. Since the neon lines used in our analysis were quite strong, and were excited near the mid-range of temperatures in our model (paper II) we believe our neon results to be

quite reliable, and the difference may, therefore, be significant. In the case of the sulfur and argon abundances, the lines analyzed were near the high temperature end of our model (paper I), and are thought to be somewhat less reliable than the other abundances. Consequently, we do not regard the difference between our results and Cameron's computation to be significant for these elements.



Table 6. Comparison of Relative Abundances

Element	<u>Active Region</u> Walker, et al.	<u>Abundance (<math>\times 10^6</math>)</u> <u>Transition Region</u>		<u>Photospheric</u> Withbroe	<u>Solar System</u> Cameron
		Withbroe	Dupree		
N	90	89	150	115	117
O	700	450	595	676	676
Ne	54	28	27	-	108
Na	1.7	2.3	1.9	1.7	1.9
Mg	30	35	30	35	33
Al	2.5	2.3	3.5	2.5	2.7
Si	35*	35*	35*	35	31.6
S	9	11	20	16	16
Ar	6	4.5	-	-	3.7
Fe	26	35	20	25 <sup>†</sup>	26

† In a recent analysis, Smith and Whaling (1973) find a value of  $25 \times 10^{-6}$  for the iron abundance, in agreement with the earlier result of Withbroe.

\* The coronal abundance values have been normalized relative to the silicon abundance, which was assumed to be  $35 \times 10^{-6}$ .

# ACKNOWLEDGMENTS

We should like to thank Drs. Loulergue and Nussbaumer for allowing us to see their results in advance of publication, and for several useful comments and suggestions during the course of our investigation. We would like to thank Dr. Loulergue for sending the results of some of her unpublished calculations, and Dr. Parkinson for communicating his results to us in advance of publication. We are grateful to Dr. Eissner for sending us the results of his theoretical calculations of beryllium-like excitation

We would also like to thank Dr. H. H. Hilton and Mrs. M. Wray for their help in the theoretical calculations, and Dr. D. Cartwright for a helpful discussion on the problems associated with extrapolating the beryllium-like cross-sections. We are grateful to Mrs. A. Keys and Mrs. J. Chafe for typing the manuscript.

# REFERENCES

- Bame, S. J., Asbridge, J. R., Hundhausen, A. J., and Montgomery, M. P., 1970, J. Geophys. Res. 75, 6360.
- Bely, O., 1966 Ann. d' Astrophys. 29, 683; 1967 ibid 30, 953.
- Bely, O., and Bely, F., 1967, Solar Phys. 2, 285.
- Cameron, A. G. W. 1974, Space Sci. Rev. 15, 121.
- Chapman, R. D. and Shadmi, Y., 1973, J. Opt. Soc. Am. 63, 1440
- Cohen, L. Feldman, U. and Kastner, S. O., 1968, J. Opt. Soc. Am. 58, 331.
- Doschek, G. A., Feldman, U., and Cohen, L. 1973, J. Opt. Soc. Am. 63, 1463
- Dupree, A. K., 1972, Astrophys. J. 178, 527.
- Eissner, W., 1972, Unpublished results quoted by Gabriel and Jordan (1972), and private communication.
- Fawcett, B. C., Cowan, R. D. and Hayes, R. W. 1974, Ap. J. 187, 377.
- Feldman, U., Doschek, G. A. Cowan, R. D., and Choen, L. 1973, J. Opt. Soc. Am. 63, 1445.
- Flower, D. R., 1971, J. Phys. B 4, 697.
- Gabriel, A. H., 1972, M.N.R.A.S. 160, 99.



- Gabriel, A. H., and Jordan, Carole, 1972, Case Studies in Atomic Collision Physics II Ed: E. W. McDaniel and M. R. C. McDowell (North Holland Pub. Co., Amsterdam) p. 211.
- Garstang, R. H., 1966, Publ. Astron. Soc. Pacific 78, 399.
- Garstang, R. H., 1969, Publ. Astron. Soc. Pacific 81, 488.
- Gartz, T., Holweger, H., Kock, M., Richter, J., Boschek, B., Holweger, H., and Unsold, A., 1969a, Nature, 222, 1254.
- Gartz, T., Holweger, H., Kock, M., and Richter, J., 1969b, Astron. & Astrophys. 2, 446.
- Goldberg, L., Dupree, A. K., and Allen, J. W., 1965, Ann. d' Astrophys. 28, 589.
- Holtzer, T. E., and Axford, W. J., 1970, J. Geophys. Res. 75, 6354.
- Johnson, W. D., and Kunze, H. J., 1971, Phys. Rev. A 4, 962.
- Jordan, C., and Pottasch, S. R., 1968, Solar Phys. 4, 104.
- Jordan, C., 1970, M.N.R.A.S. 149, 1.
- Kelly, R. L., and Palumbo, L. J. 1973, Atomic and Ionic Emission Lines Below 2000 Angstroms, Hydrogen through Krypton, NRL Report 7699, U. S. Government Printing Office, Washington, D.C.
- Lange, J., and Scherb, F., 1970, J. Geophys. Res. 75, 6350.
- Loulergue, M., 1971, Astron. & Astrophys. 15, 216.
- Loulergue, M., 1973, Private communication.

Loulergue, M., and Nussbaumer, H., 1973, *Astron. & Astrophys.* 24, 209.

Neupert, W. N., Swartz, M., and Kastner, S. O., 1973, *Solar Phys.* 31, 171.

Nussbaumer, H., 1969, *M.N.R.A.S.* 145, 141.

Pagel, B. E. J. 1974, *Space Sci. Rev.* 15, 1.

Parkinson, J. H., 1973, *Astron. & Astrophys.* 24, 215.

Pottasch, S. R., 1966, *Bull., Astron. Inst. Neth.* 18, 237.

Pottasch, S. R., 1967, *Bull., Astron. Inst. Neth.* 19, 113.

Rugge, H. R. and Walker, A. B. C., Jr., 1968, in [A. P. Mitra,  
L. G. Jacchia and W. S. Neuman (eds.)] *Space Res.* 8, North  
Holland Pub. Co. (Amsterdam) p. 439.

Shore, B., 1969 *Astrophys. J.* 158, 1205.

Smith, P. L. and Whaling, W., 1973, *Astrophys. J.* 183, 313.

Tondello, G., and McWhirter, R. W. P., 1971, *J. Phys. B* 4, 715.

Walker, A. B. C., Jr. 1972, *Space Sci. Rev.* 13, 672.

Walker, A. B. C., Jr., and Rugge, H. R., 1970, *Astron. & Astrophys.* 5, 4.

Walker, A. B. C., Jr., Rugge, H. R., and Weiss, Kay, 1974a,  
Astrophys. J. 188, 423, (Paper I).

1974b, Coronal Abundances Derived from X-ray Observations  
II: Nitrogen, Oxygen, Neon, Magnesium, and Iron, to be published  
in the Astrophysical Journal (August 15) (Paper II).

Withbroe, G. L., 1971 in The Menzel Symposium on Solar Physics,  
Atomic Spectra, and Gaseous Nebulae, (Ed. K. B. Gebbie) NBS  
Special Publication 353 (U. S. Govt. Printing Office, Washington)  
p. 127.



# VIII. THE RELATIVE ABUNDANCE OF NEON AND MAGNESIUM IN THE SOLAR CORONA\*

H. R. Rugge and A. B. C. Walker

## ABSTRACT

A technique is proposed for determining the relative solar coronal abundance of neon and magnesium. The relative abundance is calculated directly from the relative intensity of the resonance lines of Ne X (12.134 Å) and Mg XI (9.169 Å) without the need for the development of a detailed model of the thermal structure of the corona. Relatively low resolution Bragg crystal spectrometer results from the OV1-10 satellite are used to determine a coronal neon to magnesium relative abundance of  $1.47 \pm 0.38$ .

---

\* This paper has also been published as TR-0076(6960-01)-1, The Aerospace Corporation, El Segundo, California (8 October 1975) and in The Astrophysical Journal (Letters) **203**, L139-143 (1976).

## CONTENTS

ABSTRACT .....	217
I. INTRODUCTION .....	221
II. THEORY .....	223
III. SATELLITE OBSERVATIONS .....	227
(a) Intensity of the Magnesium Resonance Line .....	228
(b) Intensity of the NeX Resonance Line .....	229
(c) Calculation of the Relative Ne/Mg Relative Intensities .....	230
IV. DISCUSSION .....	233
REFERENCES .....	235

## FIGURES

1. The Intensities of the NeX and MgXI resonance lines (left hand scale) and the ratio of the NeX to the MgXI resonance line intensities (right hand side) plotted versus temperature .....	224
2. The measured energy ratio of the NeX resonance line to the MgXI resonance line plotted against the average Mg intensity per scan (in counts) .....	231

## I. INTRODUCTION

Solar abundances determined from the analysis of chromospheric line intensities are subject to uncertainties owing to the particular atmospheric models and the values of the atomic rate constants used. In addition, they are incomplete since the chromospheric spectrum contains no lines from the important noble gasses. Published compilations of solar system abundances are frequently strongly weighted by meteoric data for the nonvolatile elements (Urey, 1972; Cameron, 1974). Recent determinations of solar abundances using other techniques such as the analysis of permitted coronal lines (Pottasch, 1967; Walker, 1975), the solar wind (Bame, Ashbridge, Hundhausen, and Montgomery, 1970) and solar cosmic rays (Bertsch, Fichtel and Reames, 1972; Crawford, Price, Cartwright and Sullivan, 1975) have confirmed the general abundance models derived from chromospheric and meteoric studies, but have raised questions about the abundances of specific elements, in particular neon, argon and oxygen.

In the present paper, we develop a technique which allows the relative abundance of neon and magnesium to be calculated directly from the relative intensity of the resonance lines of Ne X (12.134 Å) and Mg XI (9.169 Å) without the development of a detailed model of the thermal structure of the corona. The intensity ratio of these lines is not sensitive to temperature over the temperature range where these active region lines are efficiently excited. The close proximity of the two lines in wavelength minimizes the error introduced by uncertainties in spectrometer calibration curves.



The presently available data, obtained on the OV1-10 satellite, are only of moderate spectral resolution, so that it is necessary to correct the neon and magnesium line intensities for a number of line blends in order to carry out the analysis. However, even with these limitations, the present analysis has allowed us to establish the Ne/Mg abundance ratio to  $\pm 30\%$ . The Ne/Mg abundance ratios recently quoted in the literature have varied by a factor of 4. While the abundance of magnesium relative to silicon (which has been used as a standard by the workers studying meteoric abundances) is subject to some uncertainty, the variation in the most recently published work is relatively small, so that the improved Ne/Mg ratio derived in the present paper can be converted to an absolute neon abundance reasonably unambiguously.

## II. THEORY

The measured relative flux of the Ne X and Mg XI resonance lines can be written (Walker, Rugge and Weiss, 1974a),

$$R = \frac{F(\text{Ne})}{F(\text{Mg})} = \frac{\lambda_{\text{Mg}}}{\lambda_{\text{Ne}}} \frac{\epsilon(\lambda_{\text{Ne}})}{\epsilon(\lambda_{\text{Mg}})} \frac{A_{\text{Ne}}}{A_{\text{Mg}}} \frac{\int dT_e M(G_k, T_e) a_{\text{NeX}}(T_e) J_{\text{NeX } 1s^2-1s2p}(T_e)}{\int dT_e M(G_k, T_e) a_{\text{MgXI}}(T_e) J_{\text{MgXI } 1s^2-1s2p}(T_e)} \quad (1)$$

where  $F$  is in units of  $\text{ergs cm}^{-2} \text{sec}^{-1}$ .

The coronal emission measure function,  $M(G_k, T_e)$  is assumed to depend on a set of parameters  $G_k$ ,  $\epsilon(\lambda)$  is the spectrometer efficiency at the wavelength  $\lambda$ ,  $A_Z$  is the abundance of element  $Z$  with respect to hydrogen, and  $a_{Zz}(T_e)$  is the fractional population of ion  $z$  of element  $Z$ . The function  $J(T_e)$  depends only on atomic rate constants and is, to first order, simply equal to the collisional excitation rate. We have calculated the emission functions,  $a_{Zz}(T_e) J_{Zz}(T_e)$  (Walker, 1972; Walker and McKenzie, 1975) including all relevant collisional and radiative and dielectronic recombination processes and cascades up to levels with  $n = 6$ . Earlier calculations of these emission functions carried out by Tucker and Koren (1971) agree with our latest calculations to within  $\approx 10\%$  when normalized to the same abundances. For the simple, highly charged ions of interest here, the theoretical excitation rates, often a serious source of error in this type of analysis, should be accurate to  $\pm 20\%$  or better.

The results of our calculations are presented in figure 1, from which it can be seen that the ratio  $I_{\text{Ne}}/I_{\text{Mg}}$  is approximately independent of temperature for  $3 \times 10^6 \text{ }^\circ\text{K} \leq T \leq 9.5 \times 10^6 \text{ }^\circ\text{K}$ . The emission functions for the Ne X and Mg XI resonance lines have their maxima well within the temperature range where the ratio remains approximately constant.

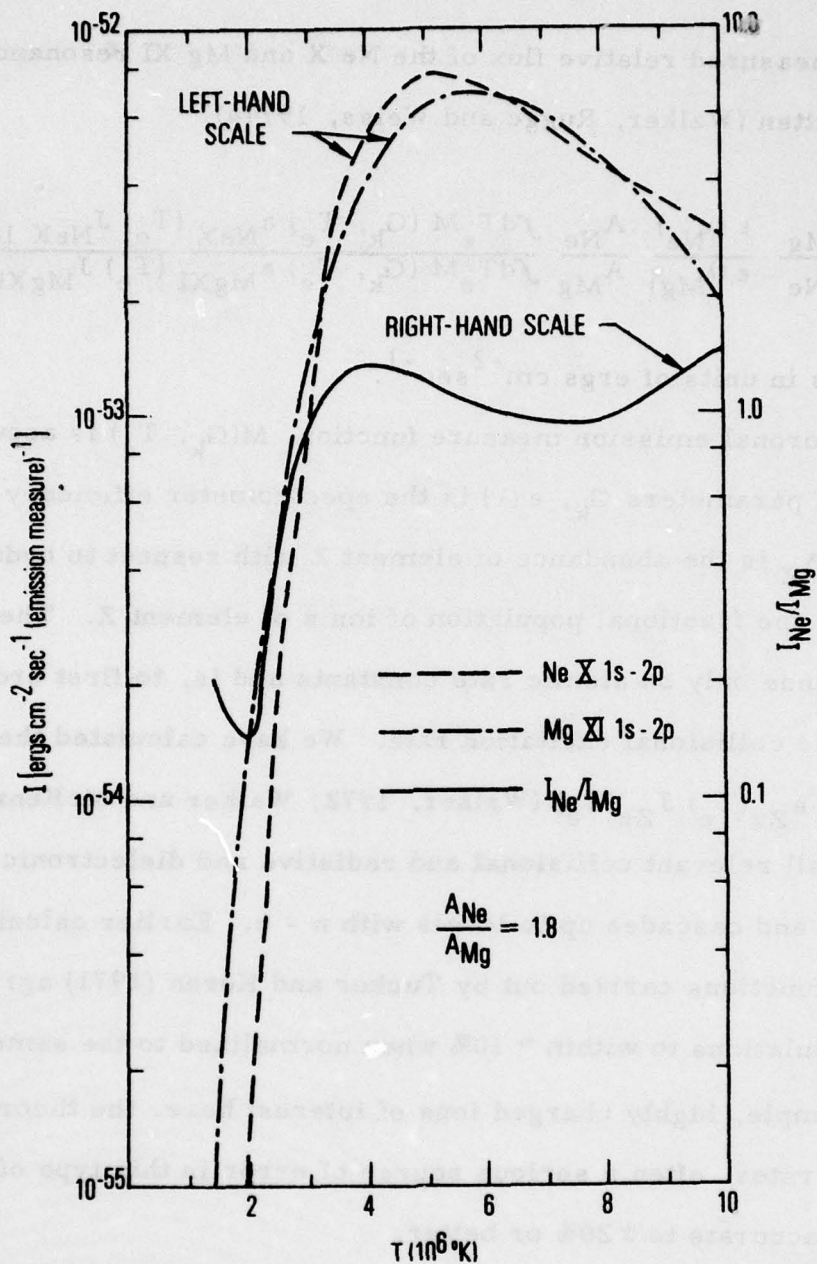


Figure 1. The intensities of the NeX and MgXI resonance lines (left hand scale) and the ratio of the NeX to the MgXI resonance line intensities (right hand side) plotted versus temperature. The calculations are carried out for an assumed neon to magnesium relative abundance of 1.8.



AD-A050 483

AEROSPACE CORP EL SEGUNDO CALIF IVAN A GETTING LABS F/G 3/2  
COMPILATION OF SCIENTIFIC RESULTS FROM THE SATELLITE OV1-17.(U)  
DEC 77 H R RUGGE F04701-77-C-0078

UNCLASSIFIED

TR-0078(3960-01)-1

SAMSO-TR-77-216

NL

3 OF 4  
AD  
A050483



Thus, relative abundances calculated from the observed line intensity ratios, using equation 1, will depend only weakly on the shape assumed for the emission measure function.

For the lines under consideration here, the relatively complicated active region emission measure function found by Walker, Rugge and Weiss (1974a, b) reduces to the form proposed by Chambe (1971) and used by Batstone, et al. (1970) and Acton, et al. (1972) to characterize active regions;

$$M(T) = C 10^{-T/T_1} \quad (2)$$

Walker, Rugge and Weiss found  $T_1 = 3.5 \times 10^6$  °K and  $T_1 = 4.0 \times 10^6$  °K, Batstone, et al. found  $T_1 \sim 7 \times 10^6$  °K and Acton, et al., using lower energy lines, found  $T_1 \sim 3.2 \times 10^6$  °K for a large active region of the type most commonly observed by the OV1-10 satellite. We have evaluated equation 1 using the differential emission measure functional form given in equation 2 for a number of values of  $T_1$ . For  $2.0 \times 10^6$  °K  $\leq T_1 \leq \infty$ , evaluation of the integrals in equation 1 above  $1 \times 10^6$  °K yields a value of R which varies by only  $\pm 5\%$ . For  $T_1 = 1.5 \times 10^6$  °K, a maximum variation of 10% from the  $T = \infty$  value is found with a relatively rapid fall off in R below  $T_1 = 1.5 \times 10^6$  °K. In the region which best characterizes the OV1-10 active regions,  $3 \times 10^6$  °K  $\leq T_1 \leq 10 \times 10^6$  °K, the variation in R derived from equations 1 and 2 is but a few percent.

### III. SATELLITE OBSERVATIONS

The accuracy of the technique described in Section II is improved if a reasonably large body of observations can be used to establish the intensity ratio of the Ne X and Mg XI resonance lines, since the effects of variations in the emission measure function will be averaged out. The largest body of well calibrated observations with sufficient resolution appears to be the observations obtained with the KAP Bragg crystal spectrometer on board the OV1-10 satellite [Rugge and Walker, 1968, Walker and Rugge, 1969]. The calibration of the OV1-10 spectrometer and the procedure used to correct the observations for scattered light and to subtract the x-ray continuum and background from lines is described in detail by Walker, Rugge, and Weiss (1974b). Unfortunately, direct application of the technique described in Section II is not possible because of the relatively low spectral resolution of the OV1-10 spectrometer, which was limited by the lack of spatial collimation and the available telemetry rate. The low resolution of the spectrometer results in the blending of closely spaced lines, and, when several strong localized sources are visible on the solar disk, in confusion due to the overlapping of the spectra from each source. Because of this latter difficulty, only scans in which the solar x-ray spectrum was dominated by a single active region were used in the analysis. As a result of this weeding process 14 orbits of data, obtained between December 1966 and April 1967, were selected for analysis.

#### (a) Intensity of the Magnesium Resonance Line

The Mg XI resonance line at  $9.169 \text{ \AA}$  is not clearly resolved from the intercombination line  $1s^2 1S - 1s2s^3P$ , and from the close dielectronic



satellite lines (Walker and Rugge, 1971) in the OV1-10 spectra. Parkinson (1972, 1974) has recently obtained a highly resolved solar spectrum of this wavelength region. Gabriel (1972) and Bhalla, Gabriel, and Presnyakov (1974) have considerably improved the theoretical understanding of the temperature dependence of the intensities of the satellite lines, and Gabriel and Jordan (1972, 1973) have developed the theory of the relative intensities of the intercombination and forbidden ( $1s^2\ ^1S - 1s2s\ ^3S$ ) lines at 9.232 Å and 9.315 Å respectively.

We have chosen to integrate the total number of counts above background between 9.165 and 9.320 Å, thereby including the intensities of the resonance, intercombination, and forbidden lines of Mg XI, as well as all of the nearby satellite lines of Mg X. This total intensity is then corrected to yield the resonance line intensity in the following way. Parkinson's (1972) Mg XI spectrum is used to determine the relative contribution of the Mg XI lines in the wavelength interval directly. His measurements of the intensity of these He-like lines is in good agreement with recent theory (Gabriel, 1972; Bhalla, Gabriel and Presnyakov, 1974) and other observations of He-like lines [Rugge and Walker, 1970, 1971; Acton, et al., 1971, 1972; Parkinson, 1971]. The relative intensities of all the satellite lines in the wavelength interval for the OV1-10 data are calculated from the relative intensities of these lines observed by Parkinson, corrected for a temperature difference using the Bhalla, et al. theory. The somewhat lower effective temperatures obtained from the OV1-10 data compared to the Parkinson data ( $3.2 \times 10^6$  °K to  $4.0 \times 10^6$  °K, respectively) raise the satellite line fractional contribution in our spectra compared to that obtained by Parkinson. The Mg XI resonance line intensity is obtained by dividing the total line intensity in the 9.165 to

9.32 Å interval by a factor of 3.2. The uncertainty in this factor results primarily from the calculation of the temperature correction to the Mg X satellite line relative intensities. It is estimated to be  $\sim \pm 15\%$ .

(b) Intensity of the Ne X Resonance Line

The two strongest lines closest to the Ne X resonance line at 12.134 Å are the neon-like Fe XVII lines at 12.12 Å ( $1s^2 2s^2 2p^6 {}^1S - 1s^2 2s^2 2p^5 4d {}^1P_1$ ) and at 12.26 Å ( $1s^2 2s^2 2p^6 {}^1S - 1s^2 2s^2 2p^5 4d {}^3D_1$ ). The 12.26 Å line can be separated from the Ne X resonance line for most of the OV1-10 spectra, but the 12.12 Å line cannot. To obtain the intensity of the 12.12 Å Fe XVII line, we have chosen to establish the value of the (presumed) constant ratio between the 12.12 Å and 12.26 Å Fe XVII lines and the much stronger and easily resolved lines of Fe XVII at 15.01 Å ( $1s^2 2s^2 2p^6 {}^1S - 1s^2 2s^2 2p^5 3d {}^1P_1$ ) and at 16.77 Å ( $1s^2 2s^2 2p^6 {}^1S - 1s^2 2s^2 2p^5 3s {}^1P_1$ ).

To obtain these ratios we have analyzed several orbits of higher resolution KAP crystal spectrometer data, obtained with the OV1-17 satellite (Walker and Rugge, 1970; Walker, Rugge and Weiss, 1974c), and the high resolution rocket spectrum obtained by Parkinson (1974). The 12.26 Å line of Fe XVII is easily separated from the blended line formed by the Ne X resonance line (12.134 Å) and the Fe XVII 12.12 Å line in the OV1-17 spectra. Parkinson (1974) has observed the relative intensities of the Fe XVII 12.12 Å line to the 12.26 Å line to be 1.2. Froese (1967) has calculated this ratio to be 1.1 and, very recently, Loulergue and Nussbaumer (1975) have calculated a ratio of 1.2. We have used a value of 1.2 for the ratio in our analysis. Thus, we calculate the line intensity of the 12.12 Å Fe XVII line, which must be subtracted from the blended lines at 12.13 Å to obtain the Ne X resonance line intensity, using measured ratios between this line and other strong and easily resolved Fe XVII lines also measured with the OV1-10 spectrometer.

The major uncertainty in this correction, which is substantial, results from the inaccuracy in the determination of the Fe XVII ratios. The total uncertainty in correctly assessing the intensity of the NeX resonance line after subtracting the 12.12 Å line is estimated to be ~ 25%.

(c) Calculation of the Relative Ne/Mg Relative Intensities

The ratios of the Ne X resonance line intensity (in  $\text{ergs cm}^{-2} \text{sec}^{-1}$ ) to the Mg XI resonance line intensity (in the same units),  $R$ , obtained from the data are shown in Figure 2, plotted against the relative intensity (in counts) of the Mg lines near 9.2 Å. As can be seen from the figure, there is little, if any, correlation between the ratio  $R$  and the total 9.2 Å intensity. This should be the case if the ratio is, as expected, essentially temperature independent for the observations used. The scatter in the data is consistent with a constant ratio having the uncertainties discussed earlier. If we assume the ratio is, in fact, constant, we may average the data and obtain a ratio of the Ne X resonance line intensity to that of the Mg XI resonance line of  $0.90 \pm 0.24$ . Using the result of equation 1, this leads directly to a relative solar coronal neon to magnesium abundance of  $1.47 \pm 0.38$ .



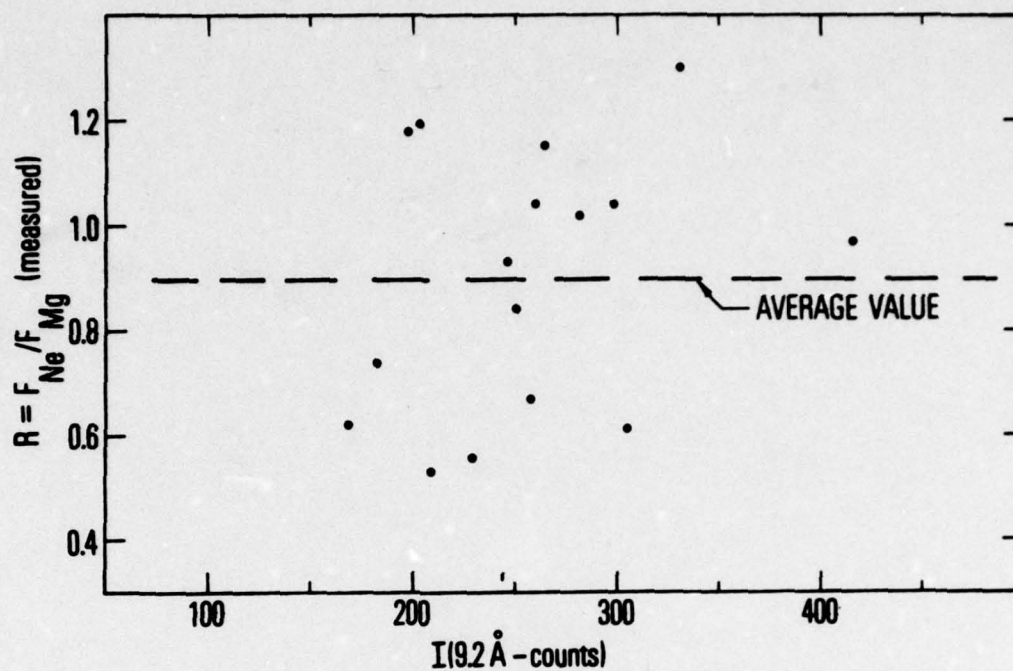


Figure 2. The measured energy ratio of the NeX resonance line to the MgXI resonance line plotted against the average Mg intensity per scan (in counts). Each data point represents the average of several scans; the majority represent the average of a full orbit of data

#### IV. DISCUSSION

The technique described in this paper has been applied to relatively low resolution x-ray data obtained on the OV1-10 satellite. The relative solar coronal neon to magnesium abundance has been found to be  $1.47 \pm 0.38$ . This compares with a value recently obtained by the authors, using a less direct technique, of 1.8 [Walker, Rugge and Weiss, 1974a, b]. Other recent solar results have ranged from a Ne/Mg ratio of  $\sim 0.6$  obtained from the analysis of the Li-like lines in the solar XUV spectrum [Flower and Nussbaumer, 1975],  $\sim 0.8$  obtained from solar cosmic ray measurements [Crawford, et al., 1975],  $\sim 0.9$  [Withbroe, 1971; Dupree, 1972] and 1.75 [Malinovsky and Heroux (1972)] obtained from coronal XUV measurements, to a ratio of  $\sim 2.9$  [Bertsch, et al., 1972] obtained from other solar cosmic ray measurements.

Since, as mentioned above, most recent measurements of the Mg abundance have been found to be between  $30$  and  $35 \times 10^{-6}$  relative to H, we may use this value and the Ne/Mg ratio obtained in this paper to derive a Ne abundance relative H of  $\sim 47 \times 10^{-6}$ .

We would like to again emphasize the basic simplicity of the technique described in this paper when it is applied to high resolution solar crystal spectrometer data easily obtainable with presently flown instrumentation. The ultimate accuracy of the Ne/Mg results obtained are limited only by the uncertainties in resonance line calculations and the slight variations in the resonance line intensity ratios with active region temperature.

# REFERENCES

- Acton, L. W., Catura, R. C., Meyerott, A. J., and Culhane, J. L.  
1971, Nature Phys. Sci., 233, 75.
- Acton, L. W., Catura, R. C., Meyerott, A. J., Wolfson, C. J. and  
Culhane, J. L. 1972, Solar Phys., 26, 183.
- Bame, S. J., Asbridge, J. R. Hundhausen, A. J. and Montgomery,  
M. P. 1970, J. Geophys. Res., 75, 6370.
- Batstone, R. M., Evans, K., Parkinson, J. H. and Pounds, K. A.  
1970, Solar Phys., 13, 389.
- Bertsch, D. L., Fichtel, C. E., and Reames, D. V. 1972, Ap. J.,  
171, 169.
- Bhalla, C. P., Gabriel, A.H., and Presnyakov, L. P. 1975, to be  
published in Mon. Not. R. Astr. Soc.
- Cameron, A. G. W. 1974, Space Sci. Rev., 15, 121.
- Champe, G. 1971, Astron. Astrophys., 12, 210.
- Crawford, H. J., Price, P. B., Cartwright, B. G., and Sullivan, J. D.  
1975, Ap. J., 195, 213.
- Dupree, A. K. 1972, Ap. J., 178, 527.
- Flower, D. R. and Nussbaumer, H. 1975, Astron. Astrophys., 39, 295.
- Froese, C. 1967, Bull. Astron. Inst. Neth., 19, 86.
- Gabriel, A.H. 1972, Mon. Not. R. Astr. Soc., 160, 99.
- Gabriel, A. H. and Jordan, Carole 1972, Case Studies in Atom. Collision  
Physics II Ed. W. W. McDaniel and M. R. C. McDowell, North  
Holland Publishing Co., Amsterdam, p. 211.
- Gabriel, A. H. and Jordan, Carole 1973, Ap. J. 186, 327.



- Loulergue, M. and Nussbaumer, H. 1975, preprint, to be submitted to Astronomy and Astrophys.
- Malinovsky, M. and Heroux, L. 1973, Ap. J., 181, 1009.
- Mewe, R. 1972, Solar Phys., 22, 459.
- Parkinson, J. H. 1971, Nature Phys. Sci., 233, 44.
- Parkinson, J. H. 1972, Nature Phys. Sci., 236, 68.
- Parkinson, J. H. 1974, Proceedings of the IAU Symposium No. 68, Buenos Aires, Ed. S. R. Kane, to be published.
- Pottasch, S. R. 1967, Bull. Astron. Soc. Neth. 19, 113.
- Rugge, H. R. and Walker, Jr., A. B. C. 1968, Space Research VIII, ed. A. P. Mitra, No. Holland Publ. Co., Amsterdam, p. 439.
- Rugge, H. R. and Walker, Jr., A. B. C. 1970, Solar Phys., 15, 372.
- Rugge, H. R. and Walker, Jr., A. B. C. 1971, Solar Phys., 18, 244.
- Tucker, W. H., and Koren, M. 1971, Ap. J., 168, 283.
- Urey, H. C. 1972, Ann. of the New York Acad. of Sci., 194, 35.
- Walker, Jr., A. B. C. 1972, Space Sci. Rev., 13, 672.
- Walker, A. B. C. 1975, Proceedings of the IAU Symposium No. 68, Buenos Aires, Ed. S. R. Kane, to be published.
- Walker, Jr., A. B. C. and McKenzie, D. L. 1975, private communication.
- Walker, Jr., A. B. C. and Rugge, H. R. 1969, Solar Flares and Space Research, eds. C. deJager and Z. Svestka, North Holland Publ. Co., Amsterdam, p. 102.
- Walker, Jr., A. B. C. and Rugge, H. R. 1970, Astron. Astrophys., 5, 4.
- Walker, Jr., A. B. C. and Rugge, H. R. 1971, Ap. J. 164, 181.
- Walker, Jr., A. B. C. Rugge, H. R. and Weiss, K. S. 1974a, Ap. J., 188, 423.

Walker, Jr., A. B. C., Rugge, H. R. and Weiss, K. S. 1974b, Ap. J.,  
192, 169.

Walker, Jr., A. B. C., Rugge, H. R. and Weiss, K. S. 1974c, Ap. J.,  
194, 471.

Withbroe, G. L. 1971, NBS Special Pub., No. 353, p. 127.

BLANK PAGE

# IX. OBSERVATION AND ANALYSIS OF Fe XVIII SOLAR X-RAY EMISSION\*

H. R. Rugge and A. B. C. Walker, Jr.

## ABSTRACT

X-ray spectra from the solar corona, obtained with a crystal spectrometer on the OV1-17 satellite, are used to analyze Fe XVIII emission lines between  $\sim 14$  and  $\sim 16 \text{ \AA}$ . The first comprehensive and accurate determinations of the coronal Fe XVIII wavelengths and relative intensities are made for the 2p-3d and 2p-3s transitions. Eighteen emission lines or line blends of Fe XVIII were observed and analyzed, including all X-ray lines previously observed in hot laboratory plasmas in this wavelength region. The measured OV1-17 wavelengths are in excellent agreement with the best laboratory measurements. The relative intensities for the Fe XVIII lines are used to deduce relative effective collision strengths for a number of transitions. The potential effects of cascades, to the  $2s^2 2p^4 3d$ , 3p and 3s levels of Fe XVIII, on the interpretation of these relative collision strengths are discussed in detail. Calculations of the relative collision strengths using the modified Bethe approximation are compared to the OV1-17 deduced values. All 2p-3s values are observed to be substantially larger than predicted, probably indicating the important role played by cascades in populating the 3s levels. Agreement between the 2p-3s values is better, but not very good. Several explanations are offered for this discrepancy. Finally, the measured energy flux emitted in the X-ray region by the corona in the form of Fe XVII and Fe XVIII emission lines is compared for a variety of coronal conditions using the OV1-17 spectra. This comparison shows that

\* This paper has also been published as TR-0077(2960-01)-1, The Aerospace Corporation, El Segundo, California (1 September 1977) and in The Astrophysical Journal **219** (1978).



accurate estimates of X-ray emission from hot astrophysical plasmas in the 14 to 16 Å wavelength range must include contributions from Fe XVIII.

## CONTENTS

ABSTRACT .....	239
I. INTRODUCTION .....	243
II. THE OV1-17 SATELLITE X-RAY DATA .....	245
III. DETERMINATION OF THE WAVELENGTHS OF THE Fe XVIII X-RAY EMISSION LINES .....	247
IV. Fe XVIII RELATIVE INTENSITIES AND RELATIVE EFFECTIVE COLLISION STRENGTHS .....	257
a. Fe XVIII Relative Intensities .....	257
b. Past Theoretical Calculations .....	258
c. Effective Collision Strength Definition .....	259
d. Interpretation of Effective Collision Strength for Fe XVIII .....	263
e. Modified Bethe Approximation .....	265
f. Results of the Relative Effective Collision Strengths .....	266
g. Potential Problems with Line Blends .....	271
h. Comparison with a Previous Analysis of Fe XVIII .....	274
V. Fe XVIII AND Fe XVII RELATIVE X-RAY INTENSITIES .....	277
VI. SUMMARY AND DISCUSSION .....	281
ACKNOWLEDGMENTS .....	285
REFERENCES .....	287

## FIGURES

1.	Sum of four spectral scans recorded by the KAP spectrometer on the OV1-17 satellite for 1969 March 21 . . . . .	249
2.	Sum of three spectral scans recorded by the KAP spectrometer on the OV1-17 satellite for 1969 March 21 . . . . .	250
3.	Energy level diagram for Fe XVIII showing those levels which give rise to observable X-radiation by decay to the ground state levels . . . . .	254

## TABLES

1.	Fe XVIII 2p-3d Wavelengths and Intensity Ratios . . . . .	252
2.	Fe XVIII 2p-3s Wavelengths and Intensity Ratios . . . . .	253
3.	Fe XVIII 2p-3d Effective Collision Strength Ratios . . . . .	268
4.	Fe XVIII 2p-3s Effective Collision Strength Ratios . . . . .	269
5.	Comparison of Fe XVIII and Fe XVII Intensities. . . . .	279



## I. INTRODUCTION

The soft X-ray spectrum of the solar corona is dominated by the emission lines of high stages of ionization of iron during flares. In large flares, the density of lines from the 2p-3d and 2p-3s transitions in the ions Fe XVII through Fe XXIV has made it difficult to identify individual transitions in presently available flare X-ray spectra (Doschek, 1975). In addition to flare spectra, the X-ray spectra of hot active regions also display bright emission lines from the 2p-3d and 2p-3s transitions in Fe XVII and Fe XVIII. Detailed observations (Neupert, Swartz, and Kastner 1973, Walker, Rugge, and Weiss 1974a, Parkinson 1975, Hutcheon, Pye, and Evans 1976) and analyses (Louergue and Nussbaumer 1973, 1975, Walker, Rugge, and Weiss 1974a) of Fe XVII X-radiation from active regions have been carried out. However, no comprehensive and accurate observations of similar radiation from Fe XVIII are yet available. In the present paper we analyze a number of high resolution solar X-ray spectra taken from the OV1-17 satellite, including several taken after a moderate (class 1B) flare, in which we have been able to identify all of the principal Fe XVIII 2p-3d and 2p-3s transitions previously seen only in laboratory plasmas. The line identifications have been carried out using recent analyses of high resolution spark-excited laboratory X-ray spectra of Fe XVIII and have resulted in the clarification of the identity of several lines previously observed in the spectra of flares and hot active regions.

Theoretical models of the excitation of the spectrum of neon-like Fe XVII (Louergue and Nussbaumer 1973, 1975) have resulted in good agreement between the predicted and observed relative intensities of the

2p-3d and 2p-3s transition arrays. Unfortunately, theoretical collision strengths for the more complicated fluorine-like isoelectronic sequence have not yet been calculated and, consequently, it has not been possible to calculate the relative intensities of the principal lines of the 2p-3d and 2p-3s transition arrays for Fe XVIII. Neither has it been possible to properly include the spectra of this ion in theoretical models of X-ray emitting astrophysical plasmas. In the present paper we present the first comprehensive and accurate evaluation of the relative intensities of all of the important 2p-3d and 2p-3s transitions in Fe XVIII under coronal conditions and use these intensities to calculate the relative effective collision strengths for these Fe XVIII transitions. In addition, we compare the relative contribution of Fe XVII and Fe XVIII X-ray intensities from the solar corona for a variety of plasma conditions.

Section II of this paper briefly describes the satellite experiment and the X-ray data. Section III discusses the observation of the Fe XVIII spectra, the Fe XVIII 2p-3d and 2p-3s wavelengths measured by the OV1-17 instrument and a comparison of these wavelengths with laboratory measurements of hot plasmas. Section IV concerns itself with the relative intensities of the strongest Fe XVIII lines and the determination of the relative effective collision strengths for these transitions. Section V briefly assesses the importance of Fe XVIII X-ray intensities compared to those of Fe XVII, the source of the strongest coronal X-ray lines from active regions. Finally, Section VI presents a summary of the paper and its principal conclusions.

## II. THE OV1-17 SATELLITE X-RAY DATA

The data presented in this paper were obtained with an uncollimated Bragg crystal spectrometer experiment flown on the OV1-17 satellite which has been previously described (Walker and Rugge 1970). The experiment consisted of a solar pointer containing 3 scanning Bragg crystal spectrometers (KAP, EDDT, LiF crystals) which covered the 1.5 to 25 Å wavelength interval. The Fe XVIII results described in this paper were obtained with the KAP (potassium acid phthalate) crystal and a photoelectric detector. The spectral resolution of the measurements is limited by the inherent line width attributable to the KAP crystal, if larger than 1.67 arc min., or by the on-board data sampling time (determined by the satellite telemetry) which corresponds to 1.67 arc min. of travel by the crystal.

The data presented in this paper were obtained on 1969 March 20 and 21, with much of the data used for detailed quantitative analysis having been taken about 70 minutes after a class 1B flare which occurred on March 21 at ~1330 UT. As a result, the majority of the Fe XVIII and other "hot" coronal X-ray lines originated from a small region on the solar disk. Consequently, the potential problem of artificially broadened spectral lines as a result of multiple strong sources, often encountered with full disk measurements of the sun using crystal spectrometers, is minimized for these data and the inherent instrumental spectral resolution is attained. This condition allows improved assignment of wavelengths for emission lines.



A total of eight spectra obtained under varying conditions of the solar coronal plasma were used in the evaluation of relative line intensities of Fe XVIII and in the comparison of Fe XVIII to Fe XVII line emission. Four of these eight spectral scans were taken consecutively, each scan requiring 4 minutes, after the class 1B flare.

### III. DETERMINATION OF THE WAVELENGTHS OF THE Fe XVIII

#### X-RAY EMISSION LINES

A number of experimenters have previously reported the observation of Fe XVIII emission lines from the solar corona (e.g., Evans, Pounds, and Culhane 1967, Neupert et al. 1967, Rugge and Walker 1968, Doschek, Meekins, and Cowan 1973, Walker, Rugge, and Weiss 1974b, Parkinson 1975, and Hutcheon, Pye, and Evans 1976.) Most of these reported spectra have been of relatively low resolution, with the exception of those of Parkinson (1975) and Hutcheon, Pye, and Evans (1976), both of which had excellent spectral resolution. Only Parkinson (1975) has attempted an analysis of the Fe XVIII lines to date. Unfortunately his Fe XVIII measurements suffer from low counting rates. However, he does present wavelength measurements for six Fe XVIII lines. Most of these wavelengths agree well with the best laboratory measurements (Feldman et al. 1973) of these lines.

We have used X-ray spectra of the Fe XVIII lines taken  $\sim 70$  minutes after a class 1B flare on 1969 March 21 to determine the wavelengths of a number of the strongest lines or line blends of Fe XVIII which occur between  $\sim 14$  to  $\sim 16\text{\AA}$ . Over this wavelength region our spectral resolution was  $\sim 0.01\text{\AA}$ , determined primarily by the OV1-17 satellite telemetry sampling rate.

The absolute wavelengths of the Fe XVIII lines were obtained by using the well-determined wavelengths of the Ne IX 1s-2p resonance line ( $13.447\text{\AA}$ ), the Fe XVII 2p-3d  $^1P_1$  ( $15.012\text{\AA}$ ) and 2p-3s  $^1P_1$  ( $16.769\text{\AA}$ ) lines and the constant and well-measured scanning rate of the potassium acid

phthalate Bragg crystal ( $0.2500 \text{ deg s}^{-1}$ ). A total of eighteen Fe XVIII lines or line blends were observed with sufficient intensity to be unequivocally assigned a wavelength. The wavelengths were determined from a single spectral scan. Either the scan taken at 1442 UT or at 1446 UT on March 21 ( $\sim 70$  minutes after a class 1B flare) was used for the wavelength assignment of the great majority of the lines.

Figure 1 presents the sum of four spectral scans taken between  $\sim 13.5$  and  $\sim 15.0 \text{ \AA}$ . The four scans, taken between 1442 and 1458 UT on 1969 March 21, were added to better show some of the weaker lines. However, the addition slightly degrades the resolution available in a single spectral scan and, in addition, does not indicate the appropriate intensities of the Fe XVIII lines relative to the other strong lines as they appeared at 1442 UT, the time of the greatest emission of Fe XVIII radiation from the previously flaring region. The expected positions of the sixteen  $2p-3d$  Fe XVIII lines, as well as those of several strong lines of other ions, are indicated in Figure 1. Four of the Fe XVIII multiplets indicated in Figure 1 are not resolved into individual lines by our spectrometer.

Figure 2 presents similar data for the wavelength region from  $\sim 15$  to  $\sim 17 \text{ \AA}$ . In this figure three spectral scans have been added; those from 1446 to 1458 UT on March 21. The expected positions of twelve Fe XVIII lines are shown, with the dashed lines indicating those blended with stronger lines of other ions. No attempt at wavelength determination was made for these blended lines. Strong lines from other ions are also indicated in Figure 2.



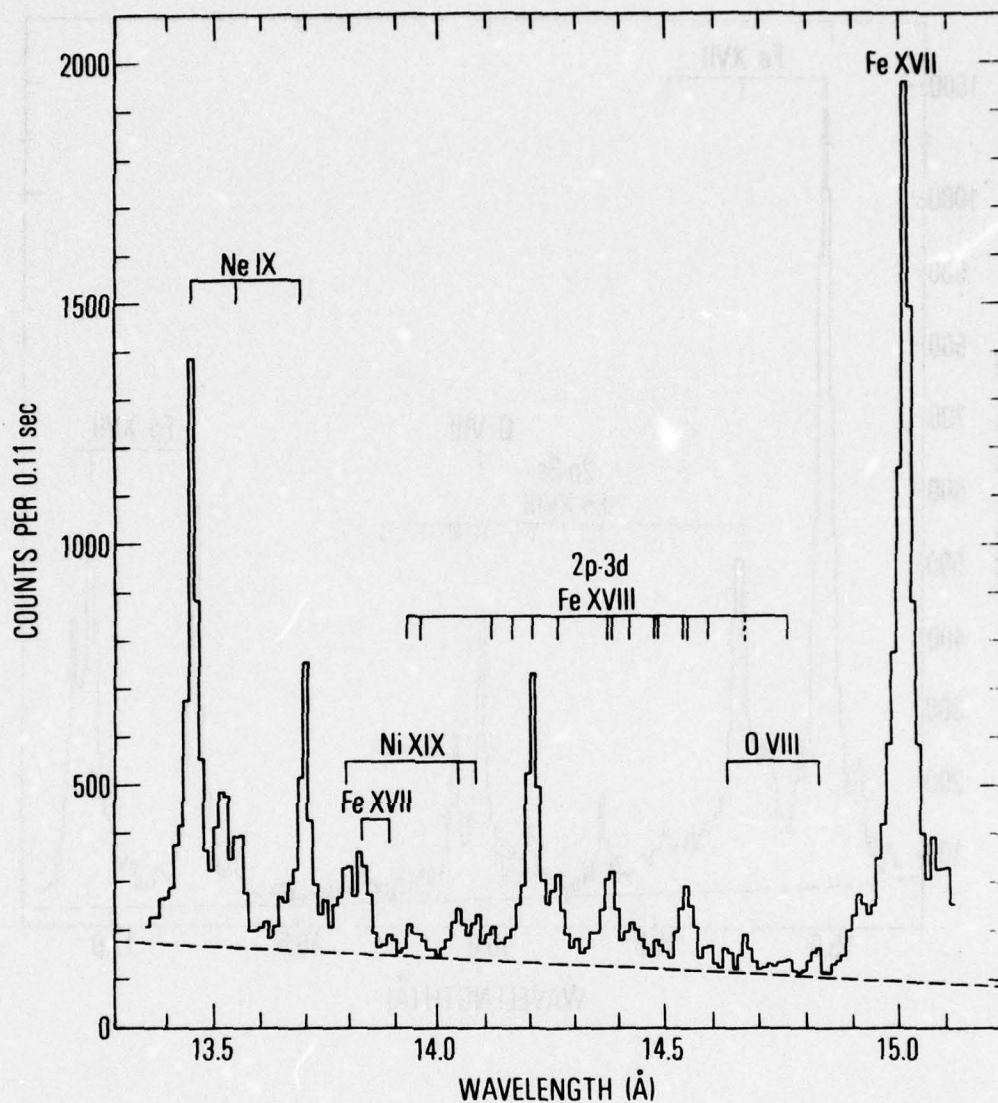


FIG. 1 - Sum of four spectral scans recorded by the KAP spectrometer on the OV1-17 satellite for 1969 March 21. The predicted positions of the Fe XVIII 2p-3d transitions are indicated.

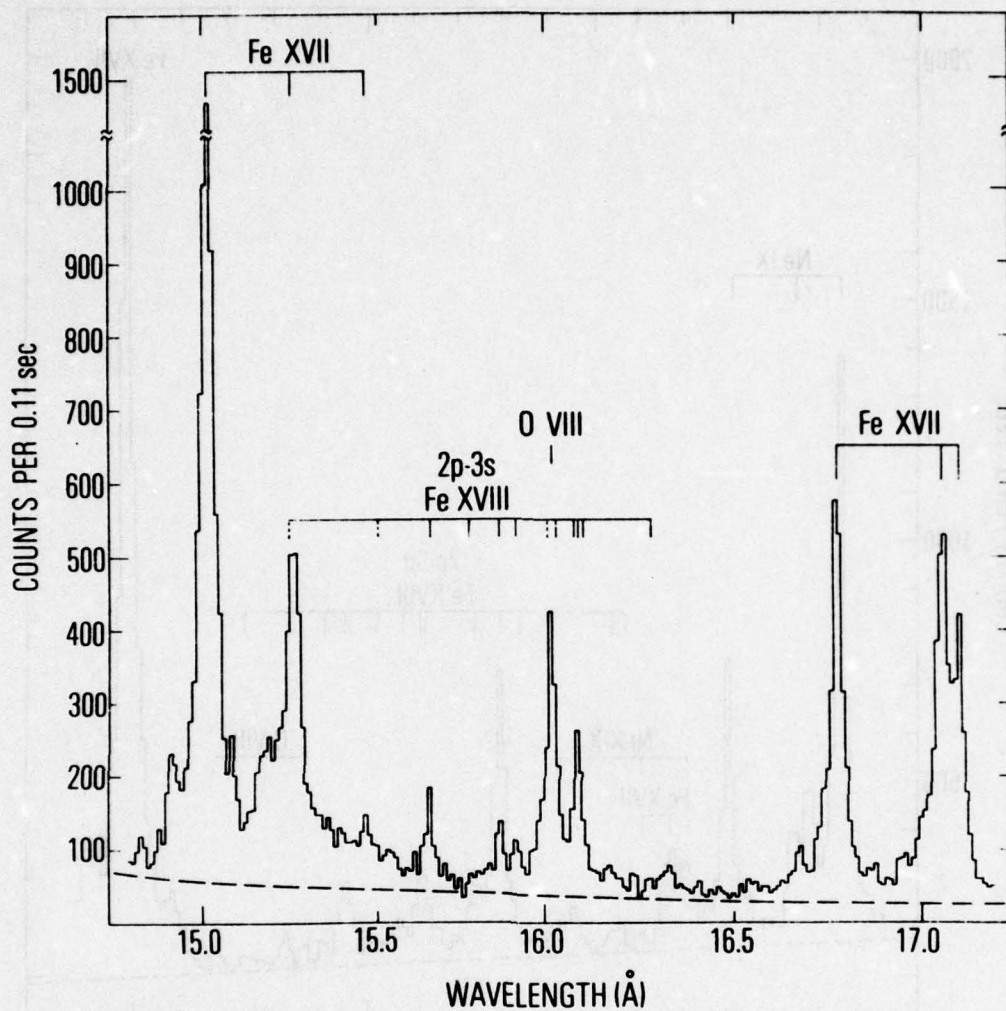


FIG. 2 - Sum of three spectral scans recorded by the KAP spectrometer on the OV1-17 satellite for 1969 March 21. The predicted positions of the Fe XVIII 2p-3s transitions are indicated. The dashed lines indicate blends with stronger lines of other ions.

The wavelengths of the Fe XVIII lines determined by our spectrometer are presented in Table 1 (2p-3d transitions) and in Table 2 (2p-3s transitions). The wavelengths are presented to 3 significant figures after the decimal. The uncertainty in wavelength for the stronger lines is estimated to be  $\pm 0.005 \text{ \AA}$ . The other information presented in the tables is discussed below in § IV.

The most definitive work to date on the wavelengths of the emission lines of Fe XVIII in the 10-20 $\text{\AA}$  region comes from the laboratory work of Feldman et al. (1973) who have considered the fluorine isoelectronic sequence in great detail. Earlier work on identification of Fe XVIII lines in laboratory plasmas was carried out, e.g., by Fawcett, Gabriel, and Saunders (1967), Cohen, Feldman, and Kastner (1968), Connerade, Peacock, and Speer (1970), Cohen and Feldman (1970), and Swartz et al. (1971). Some of these investigators have questioned a number of identifications made by others listed here, including some of Fe XVIII. At present, the paper of Feldman et al. (1973) seems to have resolved many of these past difficulties.

We have used the wavelength data of Feldman et al. (1973) for the 3s and 3d states which decay radiatively to the ground state term of Fe XVIII ( $1s^2 2s^2 2p^5 {}^2P_{1/2,3/2}$ ), and constructed the energy level diagram shown as Figure 3. It should be noted that not all possible upper level states are shown; but, for the most part, only those which gave rise to observable X-radiation. It should also be noted that although no 3p states are shown they do exist, lying in energy between 3s and the 3d states. However, since they cannot have an allowed transition to the  $2p^5$  ground



TABLE 1  
Fe XVIII 2p-3d Wavelengths and Intensity Ratios

OV1-17 Wavelength (Å)	Feldman et al. (1973) Wavelength (Å)	Transition	OV1-17 Intensity Ratio (Photons) $I(\lambda)/I(14.2\text{Å})$
13.943	$\left\{ \begin{array}{l} 13.919 \\ 13.954 \end{array} \right\}$	$\left\{ \begin{array}{l} 2P_{3/2} - 1^1S13d \ 2D_{3/2} \\ 2P_{3/2} - 1^1S13d \ 2D_{5/2} \end{array} \right\}$	$0.20 \pm 0.02$
14.118	14.121	$2P_{1/2} - 1^1S13d \ 2D_{3/2}$	$0.08 \pm 0.02$
14.151	14.150	$2P_{3/2} - 1^1D13d \ 2D_{3/2}$	$0.10 \pm 0.04$
14.200	14.200	$2P_{3/2} - 1^1D13d \ 2D_{5/2}$	$1.00 \pm 0.025$
14.254	14.255	$2P_{3/2} - 1^1D13d \ 2S_{1/2}$	$0.36 \pm 0.02$
14.368	$\left\{ \begin{array}{l} 14.361 \\ 14.373 \end{array} \right\}$	$\left\{ \begin{array}{l} 2P_{1/2} - 1^1D13d \ 2D_{3/2} \\ 2P_{1/2} - 1^3P13d \ 2D_{5/2} \end{array} \right\}$	$0.43 \pm 0.02$
14.422	$\left\{ \begin{array}{l} 14.419 \\ 14.419 \end{array} \right\}$	$\left\{ \begin{array}{l} 2P_{1/2} - 1^1D13d \ 2P_{3/2} \\ 2P_{3/2} - 1^3P13d \ 2F_{5/2} \end{array} \right\}$	$0.25 \pm 0.015$
14.474	$\left\{ \begin{array}{l} 14.467 \\ 14.485 \end{array} \right\}$	$\left\{ \begin{array}{l} 2P_{1/2} - 1^1D13d \ 2S_{1/2} \\ 2P_{3/2} - 1^3P13d \ 4P_{5/2} \end{array} \right\}$	$0.11 \pm 0.01$
14.541	$\left\{ \begin{array}{l} 14.536 \\ 14.551 \end{array} \right\}$	$\left\{ \begin{array}{l} 2P_{3/2} - 1^3P13d \ 4F_{5/2} \\ 2P_{3/2} - 1^3P13d \ 4P_{3/2} \end{array} \right\}$	$0.40 \pm 0.02$
14.589	14.581	$2P_{3/2} - 1^3P13d \ 4P_{1/2}$	$0.13 \pm 0.015$
14.660	14.666	$2P_{1/2} - 1^3P13d \ 2D_{3/2}$	$0.16 \pm 0.015$
14.761	14.772	$2P_{1/2} - 1^3P13d \ 4P_{3/2}$	$0.12 \pm 0.02$

TABLE 2  
Fe XVIII 2p-3s Wavelengths and Intensity Ratios

OV1-17 Wavelength (Å)	Feldman et al. (1973) Wavelength (Å)	Transition	OV1-17 Intensity Ratio (Photons) $I(\lambda)/I(14.2\text{Å})$
Blended	15.258	$2P_{3/2} - (1S)3s\ 2S_{1/2}$	—
Blended	15.491	$2P_{1/2} - (1S)3s\ 2S_{1/2}$	—
15.622	15.623	$2P_{3/2} - (1D)3s\ 2D_{5/2}$	$0.47 \pm 0.03$
15.763	15.764	$2P_{3/2} - (3P)3s\ 2P_{1/2}$	$0.12 \pm 0.03$
15.830	15.826	$2P_{3/2} - (3P)3s\ 2P_{3/2}$	$0.34 \pm 0.04$
15.866	15.869	$2P_{1/2} - (1D)3s\ 2D_{3/2}$	$0.30 \pm 0.04$
Blended	{ 16.003	$2P_{3/2} - (3P)3s\ 4P_{3/2}$	—
	{ 16.024	$2P_{1/2} - (3P)3s\ 2P_{1/2}$	
16.078	{ 16.073	$2P_{3/2} - (3P)3s\ 4P_{5/2}$	$1.15 \pm 0.05$
	{ 16.087	$2P_{1/2} - (3P)3s\ 2P_{3/2}$	
	{ 16.109	$2P_{1/2} - (3P)3s\ 4P_{1/2}$	
16.277	16.270	$2P_{1/2} - (3P)3s\ 4P_{3/2}$	$0.14 \pm 0.03$

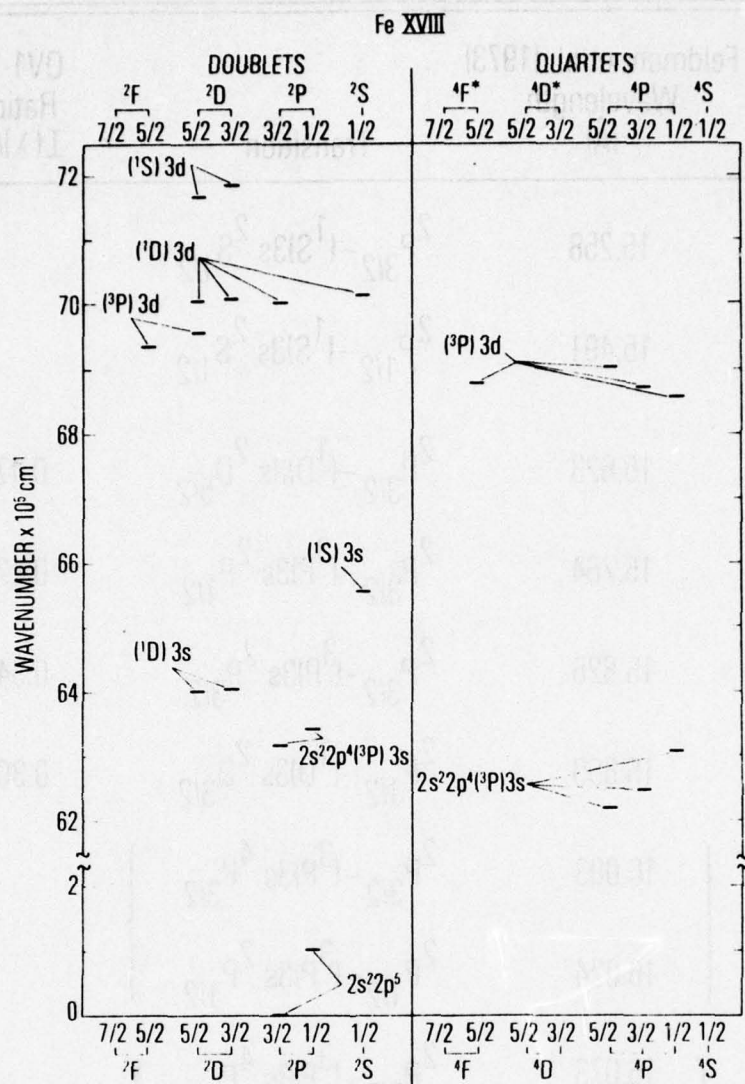


FIG. 3 - Energy level diagram for Fe XVIII showing those levels which give rise to observable X-radiation by decay to the ground state levels. The asterisks on the quartet states indicate that not all possible levels of this configuration are displayed because radiation from the undisplaced states has not been observed.



state levels of Fe XVIII, they instead populate the 3s levels by decaying to those states. The importance of this effect upon calculated line intensities will be discussed in § IV.

All of the Fe XVIII X-ray lines or line blends observed by Feldman et al. (1973) have been seen in the OV1-17 spectra, although several are sufficiently close in wavelength that they cannot be resolved from each other or, in a few cases, from blends with other strong lines. However, the majority of these multiple lines are obviously broader, in the OV1-17 spectra, than single emission lines. Tables 1 and 2 list the wavelengths measured by Feldman et al. (1973) for the 2p-3d and 2p-3s transitions, respectively. Also shown are the lower and upper levels assigned by Feldman et al. for each transition. In the Tables the lower level of the ground state term is given as either  $^2P_{3/2}$  or  $^2P_{1/2}$  to indicate, respectively, the  $1s^2 2s^2 2p^5 \ ^2P_{3/2}$  or  $1s^2 2s^2 2p^5 \ ^2P_{1/2}$  levels. The upper levels are abbreviated by, for example, listing the  $14.200\text{\AA}$  upper level  $1s^2 2s^2 2p^4 (^1D)3d \ ^2D_{5/2}$  as  $(^1D)3d \ ^2D_{5/2}$ ; the core electrons always being  $1s^2 2s^2 2p^4$ . A similar convention is used in Table 2 for the 2p-3s transitions.

The agreement between the Fe XVIII wavelengths measured by our spectrometer on the OV1-17 satellite and those measured by Feldman et al. (1973) in a laboratory plasma are excellent even for the weaker lines and well within the uncertainties of measurement for both experiments. This agreement, as well as the behavior of the lines measured during a variety of solar conditions, convinces us that all of the lines observed do indeed belong to the Fe XVIII ion.

One of the lines observed by the OV1-17 spectrometer and listed as a line of Fe XVIII in Table 1 at  $14.660\text{\AA}$  was not observed by Feldman et al. (1973) in the laboratory. However, the close correspondence of the measured wavelength to that calculated for the Fe XVIII transition and its behavior with solar activity leads us to believe it is an Fe XVIII line as indicated in Table 1.

#### IV. Fe XVIII RELATIVE INTENSITIES AND RELATIVE EFFECTIVE COLLISION STRENGTHS

This section discusses the relative intensities of the Fe XVIII lines (or line blends) measured by the OV1-17 satellite spectrometer and the relationship of those measured intensities to effective collision strengths for the appropriate transitions. The deduced effective collision strengths are compared to the only available calculations which make use of the Bethe approximation and the results of such a comparison are presented and discussed. Potential problems arising from line blends are also discussed in this section, as is a comparison with previously obtained results.

##### a) Fe XVIII Relative Intensities

The measured Fe XVIII photon intensities relative to the photon intensity of the Fe XVIII line at  $14.200\text{\AA}$ , the strongest Fe XVIII line observed, are presented in Table 1 (2p-3d transitions) and in Table 2 (2p-3s transitions). These ratios and their uncertainties were determined as follows: For each spectral scan in which a given line was visible, its relative intensity was determined by correcting the counts in each line by the wavelength dependent efficiency of the spectrometer. (This is a relatively small correction since all the lines lie between  $\sim 14$  and  $16\text{\AA}$ .) The uncertainty attributable to each line was that associated with the counting statistics of that line and its background subtraction. A weighted average of the relative intensity for each line was then obtained using all



of the spectral scans (a maximum of eight) in which that line was clearly discernable. All but the weakest lines appeared in most of the eight available spectral scans. Five of the eighteen Fe XVIII lines observed had intensities (after background subtraction) represented by more than 1000 counts, four had intensities represented by less than 200 counts; the remaining lines had intensities represented by between 200 and 1000 counts. For the four lines with the lowest number of counts (14.118 Å, 14.151 Å, 15.763 Å and 16.277 Å), the uncertainties owing to decisions concerning background subtraction and limits of spectral integration are probably greater than those shown, which result from counting statistics only.

#### b) Past Theoretical Calculations

The primary mechanism for populating excited levels in Fe XVIII, which lead to the radiative transitions of interest in this paper, is collisional excitation. Thus, to calculate the Fe XVIII X-ray intensities collision strengths are required, as are oscillator strengths to calculate radiative branching ratios from excited states. While detailed calculations of the collision strengths required to calculate the collisional excitation rates in neon-like Fe XVII have been carried out (Loulergue and Nussbaumer 1973, 1975), the more difficult fluorine-like Fe XVIII calculations have not yet been attempted. For the case of Fe XVII Loulergue and Nussbaumer (1973) first used a 36 level scheme to describe the statistical equilibrium equations including terms up to  $n = 3$ . A similar calculation for Fe XVIII, i.e., including all  $n = 3$  levels, would necessitate a

calculation with 92 levels. Loulergue and Nussbaumer (1975) have recently carried their Fe XVII calculations further to include  $n = 4$  levels, adding another 89 levels. However, they included only a total of 51 Fe XVII levels in their line intensity calculations and found only relatively minor changes from the results of the 36 level (up to  $n = 3$  only) calculations. Until at least a complete calculation up to and including the  $n = 3$  levels is completed, a detailed comparison between measured and calculated Fe XVIII X-ray line intensities cannot be meaningfully carried out.

Tucker and Koren (1971) have estimated the "summed" collision strengths for the  $2p-3d$  and  $2p-3s$  transitions in Fe XVIII. These estimates were obtained by scaling the collision strengths for boron-like ions. In turn, the boron-like collision strengths were obtained by using calculations of Bely and Petrini (1970) for the excitation of  $2p-nl$  transitions in lithium-like ions. Inasmuch as the Fe XVIII wavelengths and correct designations of a number of levels were not well known at the time of the work of Tucker and Koren (1971) and because only an order of magnitude accuracy can be expected, these calculations do not serve as an effective check on any experimentally obtained results.

Kato (1976) has also carried out an estimate of the "summed" collision strength for Fe XVIII using similar techniques. His "summed" collision strength differs from that of Tucker and Koren (1971) by a factor of 20.

#### c) Effective Collision Strength Definition

The basic theory of collisional excitation and subsequent radiation of coronal ions has been put forth, for example, by Van Regemorter (1962).

Using this theory it can be shown that the energy flux at the earth,  $E$  (ergs  $\text{cm}^{-2} \text{s}^{-1}$ ), for a given transition between states  $j$  and  $i$  may be written as: (see, e.g., Walker 1972)

$$E \approx 3.05 \times 10^{-33} E_{ij} \frac{\bar{Q}_{ij}}{\omega_i} B_{ji} a_H A_Z \int G(T) M(T) dT \quad (1)$$

where  $E_{ij}$  is the energy difference between the upper ( $j$ ) level and the lower ( $i$ ) level (ergs),  $\bar{Q}_{ij}$  is the temperature-averaged collision strength,  $\omega_i = 2J_i + 1$  is the statistical weight of the lower state,  $a_H$  is the number of hydrogen ions per electron in the plasma,  $A_Z$  is the elemental abundance relative to hydrogen and

$$G(T) = T^{-1/2} \exp\left(-\frac{E_{ij}}{kT}\right) a_{ZZ}(T) \quad (2)$$

where  $T$  is the electron temperature,  $k$  is the Boltzmann constant and  $a_{ZZ}(T)$  is the fraction of the element  $Z$  in ionization stage  $z$  ( $z = 18$  for Fe XVIII) determined from ionization equilibrium considerations.  $M(T)$  is the differential emission measure given by

$$\int M(T) dT = \int n_e^2 dV \quad (3)$$

where  $n_e$  is the electron density ( $\text{cm}^{-3}$ ). The branching ratio,  $B_{ji}$ , must be included if excitation from the ground level  $i$  to the upper level  $j$  can result not only in a decay back to level  $i$  but also to another level lying below the upper ( $j$ ) level.



$\bar{\Omega}$ , the temperature-averaged collision strength is defined by

$$\bar{\Omega} = \int_0^{\infty} \Omega(E) \exp\left(-\frac{E}{kT}\right) d\left(\frac{E}{kT}\right) . \quad (4)$$

$\Omega(E)$  is related to the cross section for collisional excitation from state  $i$ ,  $\sigma(E)$ , by

$$\sigma(E) = \frac{\pi \hbar^2}{2mE} \cdot \frac{\Omega(E)}{\omega_i} , \quad (5)$$

where  $m$  is the electron mass,  $E$  the energy of the incident electron and the other symbols have their usual meaning. Since  $\Omega$  is usually only weakly dependent on energy near threshold (see, e.g., Walker 1972) the approximation is often made that  $\bar{\Omega} \approx \Omega$  evaluated at threshold.

It should be noted that the collision strength defined by eqns. (1), (4) and (5) is the usual definition, but differs from that used by Tucker and Koren (1971) in that they include the statistical weight of the initial state,  $\omega_i$ , in their definition of the collision strength.

The effective collision strength,  $\Omega_{\text{eff}}$ , can be defined as

$$\Omega_{\text{eff}} = \bar{\Omega} \cdot B_{ji} . \quad (6)$$

Thus, when a radiative transition from level  $j$  to  $i$  results only from level  $j$  being filled by collisional excitation from level  $i$  (the so-called coronal excitation condition), the effective collision strength may be deduced from the line intensity by use of equations (1) through (6).

The relative effective collision strength for two lines from the same ion may be obtained in terms of the measured intensities of the relevant transitions (1 and 2) of interest from equations (1) and (6) as

$$\frac{\Omega_{\text{eff}}^{(1)}}{\Omega_{\text{eff}}^{(2)}} \approx \frac{\omega_1 E_1 \lambda_1}{\omega_2 E_2 \lambda_2} \quad (7)$$

where we have assumed the integral  $\int G(T)M(T)dT$  is identical for both transitions. The  $\omega$ s are the statistical weights of the lower levels of the transitions and the  $\lambda$ s the wavelengths of the relevant transitions. In fact, since  $G(T)$  contains a term involving the energy of the transition (see eq. 2) this approximation is only valid when comparing transitions with similar wavelengths as is the case for the Fe XVIII transitions of interest here. The same ratio can also be obtained in terms of the measured photon intensity,  $I$ , ratio as

$$\frac{\Omega_{\text{eff}}^{(1)}}{\Omega_{\text{eff}}^{(2)}} \approx \frac{\omega_1 I_1}{\omega_2 I_2} \quad (8)$$

For the purpose of this paper we use equation (8) as the definition of the relative effective collision strength. Thus, we may use the measured Fe XVIII photon intensities relative to the 14.200Å Fe XVIII transition given in Tables 1 and 2 to calculate directly the Fe XVIII effective collision strengths relative to the effective collision strength for the 14.200Å transition.

#### d) Interpretation of Effective Collision Strength for Fe XVIII

The interpretation of the effective collision strength for an ion as complex as Fe XVIII is not as simple as for an ion in which the coronal excitation condition applies rigorously. There are two primary reasons for the departure from this straightforward interpretation; (1) cascades (very probably) play an important role in populating a number of important levels of Fe XVIII, and (2) Fe XVIII has two ground state levels ( $^2P_{3/2}$  and  $^2P_{1/2}$  - see Fig. 3) both of which can serve as the lower level in radiative transitions, but only one of which effectively serves as the lower level for collisional excitation ( $^2P_{3/2}$ ). Thus, while the operative definition of the relative effective collision strength (Equation 8) in terms of the observed radiation from a given transition will yield the appropriate relative intensity ratio for a hot, optically thin astrophysical or laboratory plasma, it will not necessarily provide accurate results if the relative collision strengths are used for collisional excitation calculations. The lack of accuracy, for various transitions, will vary directly with the importance of the two conditions given above relative to that of the coronal excitation condition.

Although no calculations have been performed to date, it is anticipated that cascades will play a significant role in populating a number of important levels in Fe XVIII. This conclusion is reached by analogy with the situation for Fe XVII where detailed calculation have been performed theoretically and a comparison has been made with experimental results (Loulergue and Nussbaumer, 1975). In Fe XVII the strongest effect of cascades is on the 3s states. For this ion only a few percent of the



population of the 3s levels arises from collisional excitation directly from the ground state. The majority of the 3s level population arises from cascades from 3p levels, many of which are populated, in turn, by cascade from the 3d levels. A similar set of 3p levels exist in Fe XVIII. States in which a 2s electron, rather than a 2p electron, is excited can also lead to cascades to the  $2p^4 3d$ , 3p and 3s levels in Fe XVIII. In view of these results for Fe XVII, it seems reasonable that these same mechanisms may operate for Fe XVIII to some degree. To the extent that they do operate, the usefulness of the relative effective collision strengths, inferred from radiative intensities, for collisional excitation calculations is diminished. It is anticipated, by analogy with Fe XVII, that the effect will be greatest for the 3s states. Some evidence for that view is presented in § IV f. The cascade effect may also affect the 3p states, but its importance cannot be properly assessed at this time.

Another difficulty for Fe XVIII is the presence of two ground state levels, the  $1s^2 2s^2 2p^5 \ ^2P_{3/2}$  and  $\ ^2P_{1/2}$  (see Fig. 3). Radiative transitions from upper levels to both ground state levels occur (see Tables 1 and 2) and thus equation (8) may be used to infer an effective collision strength (relative to the  $14.2\text{\AA}$  transition effective collision strength) for a transition having a ground state level  $\ ^2P_{1/2}$ . However, the excitation which gave rise to this transition in all probability did not arise from this ground state level but rather from the  $\ ^2P_{3/2}$  ground state level. This may be easily demonstrated by approximating the situation by assuming the two ground levels form a two-level ion and calculating the relative populations of the two levels. The necessary collision strength may be accurately extrapolated from data presented by Blaha (1969) and the magnetic dipole

transition probability for the transition obtained, e.g., from Petrosian (1970) or Kastner (1976). If a temperature of  $\sim 5 \times 10^6$  K is assumed (the variation with T goes only as  $T^{-1/2}$ ), the electron density must exceed  $10^{12} \text{ cm}^{-3}$  before even one percent of the ground state ions populate the  $^2P_{1/2}$  level. Thus the effective collision strength ratios for transitions involving the  $^2P_{1/2}$  ground level have meaning only for calculating radiative intensity ratios, and not for collisional excitation from that  $^2P_{1/2}$  state.

#### e) Modified Bethe Approximation

Although no detailed calculations on the collisional excitation of Fe XVIII have been carried out an approximation, which is often used, relates the collision strength to the oscillator strength. This is the Bethe approximation modified by use of the averaged Gaunt factor,  $\bar{g}$ , as introduced by Seaton (1962) and Van Regemorter (1962). This approximation is only valid for allowed transitions and at high energies, where the short-range interaction between the perturbing electron and the atomic electron may be neglected. Although this modified Bethe approximation has been extensively used in astrophysics, straightforward application of the  $\bar{g}$  empirical formula may give considerable error for cross section determinations (Bely and Van Regemorter 1970).

The approximation may be written as

$$\Omega_{\text{eff}} \approx \frac{8\pi}{\sqrt{3}} \omega_{if} \bar{g}_{ij} \frac{\lambda_{ij}}{hc} I_H B_{ji}, \quad (9)$$

where  $\bar{g}_{ij}$  is the averaged Gaunt factor,  $\lambda_{ij}$  is the wavelength of the transition,  $h$  and  $c$  have their usual meaning,  $f_{ij}$  is the oscillator strength,  $I_H$  is the Rydberg and the other parameters have been defined earlier in this paper. Evaluating the constants one obtains,

$$\Omega_{\text{eff}} \approx 0.0159 \omega_i f_{ij} \bar{g}_{ij} \lambda_{ij} B_{ji} \quad (10)$$

where  $\lambda_{ij}$  is in Å. Therefore the ratio of effective collision strengths for two transitions 1 and 2 is

$$\frac{\Omega_{\text{eff}}^{(1)}}{\Omega_{\text{eff}}^{(2)}} \approx \frac{\omega_1 f_1 \lambda_1 B_1}{\omega_2 f_2 \lambda_2 B_2} \quad (11)$$

It is assumed the averaged Gaunt factors are equal for the two transitions. This assumption, often made, must be used since no calculations of the Gaunt factor exist for Fe XVIII. Mewe (1972) has presented interpolation formulae for the averaged Gaunt factors for several isoelectronic sequences, but not that of Fe. In any case he treats only excitation to atomic levels without taking into account their multiplet structure.

Thus, relative effective collision strengths may be approximated by use of equation (11) if the oscillator strengths for the transitions of interest are known.

#### f) Results for the Relative Effective Collision Strengths

The effective collision strengths for the Fe XVIII transitions measured by the OV1-17 spectrometer relative to the effective collision



strength for the strong Fe XVIII line at  $14.2\text{\AA}$  may be obtained directly by using equation (8) and the listed intensity ratios of the transitions given in Tables 1 and 2. The results are given in Tables 3 and 4 for the 2p-3d and 2p-3s transitions, respectively. The values with the asterisks are those line blends for which the collision strengths had to be weighted because of an admixture of the two ground state levels in the blend. This is discussed in the next sub-section.

We have attempted to compare these experimentally obtained results with calculations based on the modified Bethe approximation by using equation (11). In order to carry out this calculation the oscillator strengths and branching ratios, which can be derived from the oscillator strengths, are required. Dr. R. D. Cowan has previously calculated the (unpublished) required oscillator strengths for Fe XVIII using Hartree-Fock wave functions in a manner similar to his earlier calculations (Cowan 1967, 1968) for use in the paper by Feldman et al. (1973). Dr. Feldman has kindly made these calculations available to us. Using Cowan's oscillator strengths and the transition designations of Feldman et al. (1973) we have calculated the relative collision strengths for both the 2p-3d and 2p-3s transitions. The results are shown in the last column of Table 3 and 4, respectively.

Examination of Table 4 shows that all values of the collision strength ratios calculated by the Bethe approximation are substantially below their measured values. We believe this is strong evidence to indicate that the role of cascades from the 3p levels to the 3s levels is as important in Fe XVIII as in Fe XVII. If this is indeed the case a meaningful comparison between the two sets of values cannot be made.

TABLE 3  
Fe XVIII 2p-3d Effective Collision Strength Ratios

OV1-17 Wavelength (Å)	Feldman et al. (1973) Wavelength (Å)	Transition	OV1-17 $\Omega_{\text{eff.}} (\lambda/\Omega_{\text{eff.}} (14.2\text{Å}))$	Calculated <sup>†</sup> $\Omega_{\text{eff.}} (\lambda/\Omega_{\text{eff.}} (14.2\text{Å}))$
13.943	13.919	$2P_{3/2} - (1S)3d\ 2D_{3/2}$	0.20	0.06
	13.954	$2P_{3/2} - (1S)3d\ 2D_{5/2}$		
14.118	14.121	$2P_{1/2} - (1S)3d\ 2D_{3/2}$	0.04	0.45
14.151	14.150	$2P_{3/2} - (1D)3d\ 2D_{3/2}$	0.10	0.03
14.200	14.200	$2P_{3/2} - (1D)3d\ 2D_{5/2}$	1.00	1.00
14.254	14.255	$2P_{3/2} - (1D)3d\ 2S_{1/2}$	0.36	0.21
14.368	14.361	$2P_{1/2} - (1D)3d\ 2D_{3/2}$	0.22	0.73
	14.373	$2P_{1/2} - (3P)3d\ 2D_{5/2}$		
14.422	14.419	$2P_{1/2} - (1D)3d\ 2P_{3/2}$	0.20*	0.04
	14.419	$2P_{3/2} - (3P)3d\ 2F_{5/2}$		
14.474	14.467	$2P_{1/2} - (1D)3d\ 2S_{1/2}$	0.06*	0.01
	14.485	$2P_{3/2} - (3P)3d\ 4P_{5/2}$		
14.541	14.536	$2P_{3/2} - (3P)3d\ 4F_{5/2}$	0.40	0.38
	14.551	$2P_{3/2} - (3P)3d\ 4P_{3/2}$		
14.589	14.581	$2P_{3/2} - (3P)3d\ 4P_{1/2}$	0.13	0.05
14.660	14.666	$2P_{1/2} - (3P)3d\ 2D_{3/2}$	0.08	—
14.761	14.772	$2P_{1/2} - (3P)3d\ 4P_{3/2}$	0.06	< 0.01

\* Blend with mixed ground level

† Bethe Approximation

TABLE 4  
Fe XVIII 2p-3s Effective Collision Strength Ratios

OV1-17 Wavelength (Å)	Feldman et al. (1973) Wavelength (Å)	Transition	OV1-17 $\Omega_{\text{eff.}}(\lambda)/\Omega_{\text{eff.}}(14.2\text{Å})$	Calculated <sup>†</sup> $\Omega_{\text{eff.}}(\lambda)/\Omega_{\text{eff.}}(14.2\text{Å})$
Blended	15.258	$2p_{3/2} - (1s)3s\ 2s_{1/2}$	—	< 0.01
Blended	15.491	$2p_{1/2} - (1s)3s\ 2s_{1/2}$	—	0.01
15.622	15.623	$2p_{3/2} - (1d)3s\ 2d_{5/2}$	0.47	0.06
15.763	15.764	$2p_{3/2} - (3p)3s\ 2p_{1/2}$	0.12	0.01
15.830	15.826	$2p_{3/2} - (3p)3s\ 2p_{3/2}$	0.34	0.02
15.866	15.869	$2p_{1/2} - (1d)3s\ 2d_{3/2}$	0.15	0.05
Blended	{ 16.003	$2p_{3/2} - (3p)3s\ 4p_{3/2}$	—	0.08
	{ 16.024	$2p_{1/2} - (3p)3s\ 2p_{1/2}$		
16.078	{ 16.073	$2p_{3/2} - (3p)3s\ 4p_{5/2}$	1.14*	< 0.01
	{ 16.087	$2p_{1/2} - (3p)3s\ 2p_{3/2}$		
	{ 16.109	$2p_{1/2} - (3p)3s\ 4p_{1/2}$		
16.277	16.270	$2p_{1/2} - (3p)3s\ 4p_{3/2}$	0.07	< 0.01

\*Blend with mixed ground level

† Bethe Approximation



For the 2p-3d transitions (Table 3), even for the stronger lines, the agreement is generally not too good with differences between the Bethe-approximation calculation and the measured ratios being up to a factor of three. For some of the weaker lines the difference is even larger. The worst case is for our weak 14.118 $\text{\AA}$  line where the measured ratio is  $\sim 10$  times smaller than the theoretical prediction. For this case, as has been done for all the other lines if possible, we have checked other available data for the relative line strengths and find general agreement with our measured values as opposed to the Bethe-approximation calculations.

We have used the visually estimated (from film) Fe XVIII relative line strengths as qualitatively presented by Feldman et al. (1973) to discern strong from weak lines in their plasma, the conditions of which may have differed considerably from those in the solar corona at the time of our measurements. Qualitatively our results agree with theirs. Hutcheon, Pye and Evans (1976) have published a high resolution X-ray spectrum of the corona, also taken about 1 hour after a small flare. Unfortunately they have only provided the intensity ratios of a number of Fe XVII lines. Their spectra are quite similar to ours for the time period from 1442 to 1458 UT on 1969 March 21. Therefore, we have used their spectra as shown, and also information provided in their paper concerning the efficiency of their Bragg spectrometer, to make estimates of the relative intensities of those Fe XVIII 2p-3d lines we could easily observe in their spectra. The semi-quantitative results we obtain are in excellent agreement with our relative intensities for the 2p-3d transitions. We therefore conclude this is further evidence that our measured line intensities, on which the experimental

relative effective collision strengths are based, are correct and any disagreements with calculations based on the modified Bethe approximation result from one or more of three potential difficulties.

The first possible reason for the disagreement between calculated and measured 2p-3d relative collision strengths may be the influence of cascades on the 3d levels. Although the effect should be smaller than on the 2p-3s transitions of Fe XVIII, Table 4 dramatically illustrates the effects of cascades for 2p-3s transitions. Until detailed calculations are performed, the influence of cascades on the 3d levels of Fe XVIII cannot be properly assessed.

The second and third potential reasons for the discrepancy between the measured and calculated values in Table 3 have to do with the modified Bethe approximation. As mentioned earlier, the approximation is only valid at "high" incident electron energies, where short-range forces can be neglected. The temperature in the coronal plasma may not be high enough to make this approximation valid. Additionally, it was necessary to assume that the  $\bar{g}$ s were equal for all transitions. Variations of  $\bar{g}$  from its usual assumed value of  $\sim 0.2$  of a factor of two or three are observed (see, e.g., Mewe 1972) and may also account for some of the discrepancies in Table 3.

#### g) Potential Problems with Line Blends

The possibilities of blended lines add a further degree of complication to the analysis of the already complex Fe XVIII analysis. A first, and relatively minor, problem was mentioned in the last sub-section. In Tables 3 and 4, three line blends ( $14.422\text{\AA}$ ,  $14.474\text{\AA}$ ,  $16.078\text{\AA}$ ) have admixtures of

the two ground state levels ( $^2P_{3/2}$ ,  $^2P_{1/2}$ ) as their lower level. Therefore, the application of equation (8) is not straightforward since a value must be assigned for the statistical weight of the lower level of the transition. For these three cases we have weighted the contribution to each blend by the value the theory, based on the Bethe approximation, would give to each. This approximation may be somewhat valid for the 2p-3d transitions, but should not be expected to be as good for the 2p-3s transitions because of the cascading effects from the 3p levels, discussed above, which it is not possible to take into account properly in this procedure. However, the maximum error introduced by this uncertainty is a factor of 2, the ratio of the statistical weights of the two ground state levels.

A potentially more important problem occurs because of the possibility of other Fe XVIII transitions lying sufficiently close in wavelength to observed Fe XVIII lines to form unresolved blends. Feldman et al. (1973) discuss this possibility in their work on the fluorine isoelectronic sequence. They find that this difficulty may exist for three Fe XVIII excited levels which have the  $2p^4(^1D) 3d$  configuration; the three potential pairs of "blended" levels are the ( $^2D_{5/2}$ ,  $^2P_{3/2}$ ); ( $^2D_{3/2}$ ,  $^2P_{1/2}$ ); and ( $^2S_{1/2}$ ,  $^2F_{5/2}$ ) where the first level of each pair is the designation used by Feldman et al. (1973) in our Tables 1 and 3. The theoretical wavelength calculations of Feldman et al. (1973) cannot distinguish between the possibility of a single level or two levels. Their laboratory observations cannot distinguish between these possibilities in the fluorine isoelectronic sequence beyond about S VIII for the first two pairs of levels and beyond about Sc XIII for the third pair of levels. For lower members of the isoelectronic sequence both levels give rise to individual observable lines.



The effect of including the three additional Fe XVIII levels gives rise to the possibility of five blended lines, those at 14.200Å and 14.419Å for the first pair of levels, those at 14.150Å and 14.361Å for the second pair of levels, and that at 14.255Å for the third pair of levels. (We have used Feldman et al.'s (1973) wavelengths.) The possibility of blends with the line at 14.419Å have already been included in Tables 1 and 3 (and in the calculation of relative collision strength in Table 3). The line arising from the  $(^1D)3d\ ^2P_{3/2}$  level at 14.419Å contributes slightly less than 1/2 of the calculated relative collision strength (which is too low by a factor of 5) of the line we observe at 14.422Å. Thus its existence or nonexistence cannot reconcile this particular calculation with the observation. The first possible blend listed above is the most important ( $^2D_{5/2},\ ^2P_{3/2}$ ) since we have used the  $^2D_{5/2}$  line at 14.200Å to normalize all other collision strengths. The presence of the  $^2P_{3/2}$  transition, with an intensity given by the Bethe approximation and Cowan's oscillator strength, has the effect of increasing the collision strength for the 14.200Å line by about 50%. If this were the only "blended" transition, it would uniformly decrease all of the other 2p-3d and 2p-3s relative collision strengths by a factor of 1.5. While obviously changing the results of a comparison of the Bethe calculation and observations, it would not result in overall better agreement between them.

Furthermore, there is no reason to expect only one "blended" level will be significantly populated without the other possible "blended" levels being populated. We have therefore carried out a calculation assuming all levels that may exist will be populated according to Bethe approximation. Again, the net result is the same. Although individual lines change the ratios of the calculated to observed relative collision strengths, the overall

agreement is not improved by these procedures. Therefore, we believe, even with the inclusion of other potential Fe XVIII levels which could give rise to additional "blended" lines, the agreement between the calculated relative collision strengths using Cowan's oscillator strengths and the modified Bethe approximation, and the observed collision strengths is not improved. Presumably the discrepancy results for the reasons given in the last sub-section. At the present time we endorse Feldman et al.'s (1973) designations for the various transitions, which are based on a study of the entire isoelectronic sequence, until evidence that the other potential "blended"  $2p^4 ({}^1D) 3d$  levels are of importance is produced.

#### h) Comparison with a Previous Analysis of Fe XVIII

Before leaving the subject of collision strengths it should be pointed out that Parkinson (1975) has analyzed six Fe XVIII lines observed in his high resolution X-ray spectra taken from a rocket. His strongest Fe XVIII line ( $14.2\text{\AA}$ ) had but 60 counts, his weakest 12, and the four remaining lines 24 counts each, after background subtraction. Consequently, the accuracy of the line intensities and the collision strengths derived by Parkinson are limited by the relatively poor statistics. Parkinson (1975) uses equations essentially similar to our equations (1) and (10) to evaluate the oscillator strength for his observed transitions; however, he neglects the branching ratio,  $B_{ji}$ , in his formulation. (He also adopts Tucker and Koren's (1971) nonstandard usage of the definition of the collision strength incorporating the statistical weight factor.) In Parkinson's (1975) Table X he presents his inferred oscillator strengths for Fe XVIII which are all a factor of  $\sim 100$  smaller than would be estimated from the analogy with Fe XVII as well as

from Cowan's calculations (which were not available to Parkinson). Therefore we have redone his Fe XVIII calculation using only information presented in his paper for abundances, ionization equilibria, differential emission measure and line intensities. With this information we have attempted to rederive his values of the Fe XVIII oscillator strengths. We find values almost exactly a factor of 100 higher than those given by Parkinson. In order to check our calculation, we performed a similar calculation, again using only Parkinson's data and assumptions, for his 15.01 Å line of Fe XVII and obtained a result that agreed with his to within  $\leq 20\%$ . Therefore, we assume an error in arithmetic by a factor of 100 was made by Parkinson, and to obtain values properly reflecting his analysis both the deduced values of his oscillator strengths and collision strengths for Fe XVIII (only) should be multiplied by a factor of 100. Taking into account the limitations in statistical accuracy of Parkinson's intensity ratios for the six Fe XVIII lines he observed, these ratios are in agreement with ours listed in Tables 1 and 2.



## V. Fe XVIII AND Fe XVII RELATIVE X-RAY INTENSITIES

Fe XVII X-radiation between  $\sim 13.5$  and  $17.5\text{\AA}$  represents the largest energy flux emanating from the solar corona for any ion in this wavelength range. This wavelength range is important because many solar X-ray measurements, some with relatively poor spectral resolution, have obtained data in this spectra region. For example, both the S-054 (Krieger 1976) and S-056 (McKenzie, private communication) X-ray telescopes flown on Skylab had at least one filter position in which one or more of the Fe XVII X-ray lines accounted (by calculation) for  $\geq 20\%$  of the energy deposited on their film recording the solar image in X-rays at coronal temperatures often found in active regions. Fortunately, with recent theoretical (Loulergue and Nussbaumer 1975) and experimental (Walker, Rugge, and Weiss 1974a, Parkinson 1975, Hutcheon, Pye, and Evans 1976) work a proper assessment of the amount of energy emitted by the Fe XVII ion can be made for essentially any optically thin astrophysical plasma. As has been stated earlier in this paper, this is not the situation in any sense for Fe XVIII. No detailed theoretical work has been carried out to date on Fe XVIII fluxes and this paper is the first experimental work to present a relatively accurate and detailed examination of Fe XVIII X-radiation from the corona. For this reason we will compare the relative energy flux of the total Fe XVII and Fe XVIII X-ray emission from the solar corona. Relatively little X-ray flux is emitted by either ion outside the 13 to  $17.5\text{\AA}$  region, compared to the energy emitted within this wavelength region.

We have used eight spectral scans, taken over the two day period 1969 March 20 and 21, to obtain the energy ratio of the Fe XVIII flux relative to both the strongest Fe XVII transition at  $15.01\text{\AA}$  ( $2p-3d^1P_1$ ) and to the total Fe XVII flux in the 13 to  $17.5\text{\AA}$  wavelength interval. These data, along with other related data, are presented in Table 5. A variety of solar conditions prevailed during the individual scans as can be seen from intensity of the Fe XVIII line at  $14.2\text{\AA}$  (in counts) and the Fe XVIII ( $14.2\text{\AA}$ ) to Fe XVII ( $15.01\text{\AA}$ ) energy flux ratios. As has been mentioned before, the four consecutive spectra taken beginning about 1442 UT on 1969 March 21 followed a class 1B flare which occurred  $\sim 1330$  UT. Thus, the change in the "spectral hardness" of the spectra can be determined as a function of time after the flare from the data presented in the table.

As can be seen from the fourth and fifth columns of Table 5, a non-negligible amount of X-radiation may originate from Fe XVIII ions, especially during and after flares as well as from "hot" active regions. Thus, an accurate estimate of Fe XVIII X-radiation produced by hot, optically thin astrophysical plasmas is essential to precise calculations of energy loss and spectral output of such plasmas as well as to the interpretation of broad-band or low resolution X-ray pictures of the sun.

TABLE 5  
Comparison of Fe XVIII and Fe XVII Intensities

Date (1969)	Fe <u>XVIII</u> (14.2Å) Intensity (Counts)	E (14.2Å) E (15.01Å)	E (Fe <u>XVIII</u> ) E (15.01Å)	E (Fe <u>XVIII</u> ) E (Fe <u>XVII</u> )
20 March				
0528 U.T.	44	0.04	0.23	0.06
0615 U.T.	131	0.09	0.56	0.15
21 March				
0419 U.T.	342	0.14	0.82	0.22
0423 U.T.	365	0.13	0.77	0.20
1442 U.T.	612	0.24	1.4	0.38
1446 U.T.	639	0.21	1.2	0.32
1450 U.T.	546	0.17	1.0	0.26
1454 U.T.	307	0.15	0.90	0.23



## VI. SUMMARY AND DISCUSSION

In this paper we have presented the first accurate and comprehensive measurements of the wavelengths and relative intensities of the strongest X-ray lines of Fe XVIII emitted by the solar corona. The Fe XVIII data were obtained from eight relatively high resolution X-ray spectra of the sun taken from a Bragg crystal spectrometer flown on the OV1-17 satellite on 1969 March 20 and 21. We have definitely identified eighteen Fe XVIII coronal lines or line blends and compared their wavelengths with the best available values obtained from measurements of hot laboratory plasmas. The agreement between the solar and laboratory wavelengths is excellent. We have used the measured Fe XVIII relative intensities to deduce the relative effective collisions strengths for this ion and essentially all of the higher  $z$  members of the fluorine isoelectronic sequence since  $z^2\Omega \approx \text{constant}$  for the higher  $z$  values along an isoelectronic sequence. The use of these deduced relative collision strengths in collisional excitation calculations was mentioned and the potential complicating effects of cascade processes were discussed in detail.

The OV1-17 deduced relative collision strengths were compared to calculations of the same quantities using the modified Bethe approximation. In all cases the 2p-3s calculated collision strength ratios were significantly smaller than the values obtained from the OV1-17 satellite Fe XVIII line intensity measurements. We concluded this was evidence for the existence of strong cascading effects from the 3p to the 3s levels in Fe XVIII. While agreement between the Bethe approximation calculations

and the OV1-17 relative collision strengths was better for the 2p-3d transitions than for the 2p-3s, it was not nearly as good as the accuracy we believe is inherent in Cowan's calculated oscillator strengths. Reasons for this discrepancy were presented as were potential complications to the analysis from line blends. It was concluded that potential line blending could not remove the discrepancy between the calculated values and the values deduced from the OV1-17 X-ray spectra.

All eight X-ray spectra were used to compare the X-ray energy flux of the corona in Fe XVIII to that in Fe XVII for a variety of solar conditions. It was concluded that Fe XVIII X-radiation is non-negligible compared to that of Fe XVII, especially from hot active regions and, presumably, from flares.

In the work presented in this paper we have used only relative intensities rather than absolute intensities for the Fe XVIII emission lines. There are several important reasons for this. First, the relative efficiency of the OV1-17 KAP crystal spectrometer, over a short wavelength region, is substantially better known than the absolute efficiency. However, we believe we know the absolute efficiency to within a factor of two. Second, in order to derive absolute Fe XVIII line intensities the differential emission measure function,  $M(T)$  (eqn. (3)), must be derived. Craig and Brown (1976) have shown that the problem of determining differential emission measure is ill-conditioned and may not lead to unique solutions.

The third problem, for Fe ions in general, is with the  $G(T)$  function or, more precisely, with the ionization equilibrium part of its calculations, i.e.,  $a_{ZZ}$  (see eq. 2). Until very recently Jordan's (1969, 1970) calculations

of  $a_{ZZ}(T)$  have been almost universally used in coronal calculations. Recently, however, Jacobs et al. (1977) have included additional autoionization terms in a detailed ionization equilibrium calculation which have the major effect of shifting the peak of the ionization equilibrium curves as calculated by Jordan (1969, 1970) toward lower temperatures by  $\sim 1.5 \times 10^{60}$  K for Fe XVIII. Until it becomes clear which, if either, of the two calculations are correct for Fe ions, it appears to be a thankless task to attempt a proper evaluation of the absolute intensities of our Fe XVIII (or Fe XVII) line intensities. This statement probably applies equally well to other recent and future Fe ion line measurements in the X-ray region.

In any case, we believe the most valuable contribution experimental measurements can make to the understanding of Fe XVIII line emission from the solar corona are the relative intensities of these lines, given in Tables 1 and 2. It was precisely these observed intensity ratios, for Fe XVII, that led to a reassessment of the theory (Pottasch 1966) and the subsequent theoretical understanding of that complex ion (Loulergue and Nussbaumer 1975). A similar understanding of Fe XVIII awaits the difficult and tedious calculation of the collision strengths similar to that performed by Loulergue and Nussbaumer (1973) for Fe XVII.



#### ACKNOWLEDGMENTS

We should like especially to thank Dr U. Feldman for several very helpful discussions concerning the fluorine isoelectronic sequence spectra and for making available Dr. R. D. Cowan's oscillator strength and wavelength calculations for Fe XVIII. In addition, one of us (HRR) would like to thank Dr. Cowan for an extended discussion on the accuracy of the oscillator strength calculations and the validity of the modified Bethe approximation. Dr. D. L. McKenzie carefully read the manuscript and made a number of useful suggestions. We are grateful to Joanne Kari for typing the manuscript.

# REFERENCES

- Bely, O., and Petrini, D. 1970, Astr. and Ap., 6, 318.
- Bely, O., and Van Regemorter, H. 1970, Ann. Rev. Astr. and Ap., 8, 329.
- Blaha, M. 1969, Astr. and Ap., 1, 42.
- Cohen, L. and Feldman, U. 1970 Ap. J., 160, L105.
- Cohen, L., Feldman, U., and Kastner, S. O. 1968, J. Opt. Soc. Am., 58, 331.
- Connerade, J. P., Peacock, N. J., and Speer, R. J. 1970, Solar Phys., 14, 159.
- Cowan, R. D. 1967, Phys. Rev., 163, 54.
- Cowan, R. D. 1968, J. Opt. Soc. Am. 58, 808.
- Craig, I.J.D., and Brown, J.C. 1976, Astr. and Ap., 49, 239.
- Doschek, G. A. 1975, Solar Gamma-, X-, EUV-Radiation, Proceedings of IAU Symposium No. 68, Buenos Aires, ed. Sharad R. Kane (Dordrecht: Reidel), p. 165.

Doschek, G. A., Meekins, J. F., and Cowan, R. D. 1973, Solar Phys., 29, 125.

Evans, K. D., Pounds, K. A., and Culhane, J. L. 1967, Nature, 214, 41.

Fawcett, B. C., Gabriel, A.H., and Saunders, P.A.H. 1967, Proc. Phys. Soc., London, 90, 863.

Feldman, U., Doschek, G. A., Cowan, R. D., and Cohen, L. 1973, J. Opt. Soc. Am., 63, 1445.

Hutcheon, R.J., Pye, J. P., and Evans, K. D. 1976, Mon. Not. Roy. Astr. Soc., 175, 489.

Jacobs, V. L., Davis, J., Kepple, P. C., and Blaha, M. 1977, Ap.J., 211, 605.

Jordan, C. 1969, Mon. Not. Roy. Astr. Soc., 142, 199.

Jordan, C. 1970, Mon. Not. Roy. Astr. Soc., 148, 17.

Kastner, S. O. 1976, Solar Phys., 46, 179.

Kato, T. 1976, Ap. J. Suppl., 30, 397.

Krieger, A. S. 1976, Bull. Am. Astr. Soc., 8, 376. Talk given at the Solar Physics Division Meeting of the 148th Am. Astr. Soc. Meeting, Haverford, PA, 14 June.

Loulergue, M., and Nussbaumer, H. 1973, Astr. and Ap., 24, 209.

Loulergue, M., and Nussbaumer, H. 1975, Astr. and Ap., 45, 125.

Mewe, R. 1972, Astr. and Ap., 20, 215.



Neupert, W. M., Gates, W., Swartz, M., and Young, R., 1967, Ap. J., 149,  
L79.

Neupert, W. N., Swartz, M., and Kastner, S. O. 1973, Solar Phys., 31, 171.

Parkinson, J. H. 1975, Solar Phys., 42, 183.

Petrosian, V. 1970, Ap. J., 159, 833.

Pottasch, S. 1966, Bull. Astr. Inst. Neth., 18, 443.

Rugge, H. R., and Walker, A.B.C., Jr. 1969, in Space Res., 8, ed. A. P.

Mitra, L. G. Jacchia, and W. S. Newmann (Amsterdam: North Holland)  
p. 102.

Swartz M., Kastner, S. O., Rothe, E., and Neupert, W. 1971, J. Phys.  
B., 4, 1747.

Seaton, M. 1962, in Atomic and Molecular Processes, ed. D. R. Bates  
(New York: Academic) p. 374.

Tucker, W. H., and Koren, M. 1971, Ap. J., 168, 283.

Van Regemorter, H. 1962, Ap. J. 136, 906.

Walker, A.B.C., Jr. 1972, Space Sci. Rev., 13, 672.

Walker, A.B.C., Jr., and Rugge, H. R. 1970, Astr. and Ap., 5, 4.

Walker, A.B.C. Jr., Rugge, H. R., and Weiss, K. 1974a, Ap. J., 194, 471.

Walker, A.B.C., Jr., Rugge, H. R., and Weiss, K. 1974b, Ap. J., 192, 169.

X. POLAR CAP MEASUREMENTS OF SOLAR-FLARE  
PROTONS WITH ENERGIES DOWN TO 12.4 keV\*

P. F. Mizera, J. F. Fennell, and J. B. Blake

ABSTRACT

Solar protons with energies down to 12.4 keV were measured over the polar caps by instruments aboard the OV1-17 satellite. The observations were made following the 21 March 1969 solar-particle event. The polar-cap differential fluxes measured by OV1-17 and Injun-5 from 0.012 MeV to 1.1 MeV are well represented by a single power law. Over a 22 hour period the spectral index changed from 1.7 to 1.9. Temporal and spatial comparisons were made with data from the Explorer-35 and Injun-5 spacecraft. Good agreement is found at energies ( $> 300$  keV) where a comparison can be made.

---

\* This paper has also been published as TR-0073(3260-20)-5, The Aerospace Corporation, El Segundo, California (1 October 1972) and in the Journal of Geophysical Research 77, 4845-4850.



## CONTENTS

ABSTRACT .....	291
INTRODUCTION .....	295
SATELLITE AND INSTRUMENTATION .....	297
RESULTS .....	301
DISCUSSION .....	309
ACKNOWLEDGMENTS .....	311
REFERENCES .....	313

## TABLES

1. Description of Particle Instruments on the OV1-17 Satellite .....	298
2. A Comparison of Interplanetary and Polar Proton Fluxes ( $E > 0.3$ MeV) Taken by Explorer-35 and OV1-17 During the 21 March Solar Flare .....	302

## FIGURES

1. Count-rate profiles vs invariant latitude for protons over the South Pole on 22 March and 23 March 1969 .....	303
2. Differential spectrum on 0.0124 MeV to 1.1 MeV solar protons on 22 March 1969 .....	305
3. Solar protons spectrum on 23 March 1969 .....	306

## INTRODUCTION

An important aspect of solar cosmic ray research has been the use of solar particles as a test probe of the configuration of the magnetosphere and, in particular, to examine the access of such particles to low altitudes over the polar caps. This work has been reviewed by Paulikas et al., (1970), Lanzerotti, (1972) and Burrows, (1972).

These reviews have discussed the differences in the general behavior of electrons and protons. Proton fluxes commonly show latitudinal structure; electron fluxes usually do not. Quasi-trapped solar electrons generally have much lower intensities than the polar-plateau intensities whereas protons ( $\approx 10$  MeV) show similar fluxes in both regions. Time delays to the polar caps are strongly dependent on the particle species and are not well understood. However, these comparisons of solar particles have been for protons with  $E \geq 300$  keV and electrons with  $E \leq 2$  MeV. The magnetic rigidity for protons at these energies are much larger than electrons while the electrons have velocities substantially higher than the protons. These large differences must contribute to the variance in the observations of particle access and polar-cap structure.

In this report polar-cap observations from the OV1-17 satellite of solar protons with energies down to 12.4 keV are presented. We believe this to be the lowest energy at which solar protons have been observed over the polar cap. From higher-energy measurements from OV1-17, it was possible to compare proton intensities over the pole with interplanetary measurements made by Explorer-35. These comparisons with interplanetary protons ( $E > 300$  keV) and the internal consistency of polar data ( $0.012 \text{ MeV} < E \leq 1.1 \text{ MeV}$ ) argue for the solar origin of the particle fluxes.

## SATELLITE AND INSTRUMENTATION

The OV1-17 (1969-025A) satellite was launched from the Western Test Range at 0747 UT on 18 March 1969. The orbit was near-circular, with an apogee of 468 km and a perigee of 398 km. The inclination was  $99^{\circ}$ , with the orbital plane initially near the noon-midnight meridian. It was intended that the OV1-17 be gravity-gradient stabilized; however, the satellite was tumbling slowly during the 21 March 1969 solar-particle event. On-board magnetometers and sun sensors supplied aspect data and thus particle pitch angle.

The instruments used to obtain the data discussed in this report included a cylindrical electrostatic analyzer (PESA) and an array of geiger tubes and semi-conductor detectors (URCHIN). The PESA measured protons in twelve contiguous, differential energy channels. The URCHIN contained three Geiger-Mueller tubes (GM) and five semi-conductors (SD) mounted in an orthogonal array. The main function of the URCHIN instrument was the measurement of 10 keV to 600 keV electrons in the outer radiation zone and auroral regions. However, when electron intensities were low, the URCHIN provided proton fluxes from 200 keV to 700 keV.

The mounting of the PESA and URCHIN on the satellite was such that the look direction of the PESA was centered upon the nominal zenith; while the URCHIN look directions were centered upon the nominal zenith, nadir and the normal to the orbital plane. Table 1 lists instrument parameters relevant to this report. A more complete description of the instrumental parameters for both Explorer-35 and Injun-5 can be found in Van Allen et al. (1971).

A brief discussion of the pertinent data reduction procedures follows:

### a) PESA

The largest source of uncertainty in the PESA analysis arises from the low count-rates during this event and a low relatively constant

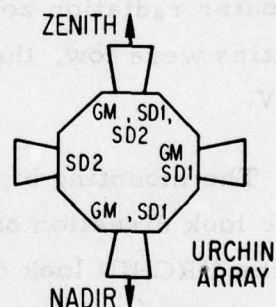


**Table 1. Description of Particle Instruments on the OV1-17 Satellite<sup>a</sup>**

<u>INSTRUMENT</u>	<u>SENSOR</u>	<u>PARTICLE ENERGY</u>	<u>FIELD OF VIEW</u>	<u>GEOMETRIC FACTOR</u>
PESA		12.4 < E <sub>p</sub> < 185 keV 12 CHANNELS	7° x 9° (FWHM)	0.0047 cm <sup>2</sup> - ster $\frac{\Delta E}{E}^*$
URCHIN	GM	E <sub>p</sub> > 235 keV E <sub>e</sub> > 10 keV	10° HALF ANGLE	0.0047 cm <sup>2</sup> - ster
	SD1 - 1	E <sub>p</sub> > 212 keV E <sub>e</sub> > 100 keV	10° HALF ANGLE	0.047 cm <sup>2</sup> - ster
	- 2	E <sub>p</sub> > 310 keV E <sub>e</sub> > 200 keV		
	SD2 - 1	E <sub>p</sub> > 425 keV E <sub>e</sub> > 300 keV	10° HALF ANGLE	0.047 cm <sup>2</sup> - ster
	- 2	E <sub>p</sub> > 675 keV E <sub>e</sub> > 600 keV		

$$* \frac{dJ}{dE} (E_0) = \text{COUNT RATE} (0.0047 \cdot E_0)^{-1}$$

$$\text{Where } \frac{\Delta E}{E} = 26 \% \text{ (FWHM)}$$



<sup>a</sup>PESA measures 12.4 to 185 keV protons in 12-contiguous differential channels every 32 seconds. URCHIN contains an array of geiger tubes (GM) and semi-conductor detectors (SD) schematically shown in lower right corner. GM, SD1 and SD2 thresholds are listed for both electrons and protons. SD1 and SD2 switches from high to low energy thresholds every 4 seconds.

background. The background was largest when the spacecraft was illuminated by the sun and approached 30% of the total count-rate in the highest energy channels. Average background rates for each channel were determined by examining the polar-cap data before the onset of the 21 March 1969 event and appropriate subtractions were made on the PESA measurements presented here.

b) URCHIN

Differential proton fluxes from 200 keV to 700 keV were obtained by fitting a power-law function to the four integral channels at 212 keV, 310 keV, 425 keV and 675 keV. Individual outputs were averaged over 16-second intervals and then summed over the same time intervals as the PESA data. In all cases, the resulting power-law fit was within one standard deviation of each data point. The final absolute values were obtained by evaluating the function at 250 keV and 500 keV. As an additional check, the highest and lowest energy channels were used to obtain a differential intensity which was in excellent agreement with the power-law fit.

The absence of significant electron contamination was determined by examining the known polar-cap electron fluxes measured during this event aboard the OV1-19 satellite (A. L. Vampola, private communication) and computing the URCHIN response to such fluxes.

## RESULTS

A direct comparison was made of the polar-cap intensities measured by OV1-17 with the interplanetary intensities observed by Explorer-35 for proton energies above 300 keV and is given in Table 2. At the time of the 21 March 1969 solar particle event, Explorer-35 was located well outside the magnetosphere in the noon-dusk sector. The data from Explorer-35 are a 30-minute average over all pitch angles. The OV1-17 data are averaged over pitch angles outside the loss cone for invariant latitudes greater than  $78^\circ$ . It is not the purpose of this table to make quantitative comparisons, but only to show the similarity between interplanetary and low-altitude measurements in the energy range where a comparison can be made.

Interplanetary protons were first observed above threshold by Explorer-35 on 21 March at 0800 UT. The flux was increasing approximately 40%/hour at 1500 UT when the first OV1-17 polar-cap data were acquired. The comparison of the South Polar flux measured at 1530 UT with the North Polar flux at 1500 UT showed an increase commensurate with the interplanetary observations of Explorer-35. On 22 March the interplanetary intensity decreased by  $\approx 25\%$  during the two hour period centered on the OV1-17 polar traverse. On 23 March the variation was less than 15%.

Polar profiles of proton count-rates vs. invariant latitude are shown in Figure 1. Intensities are plotted for protons from 12 keV to  $> 700$  keV. The top two profiles are for the differential proton channels (PESA) centered at 12.4 keV and 90 keV and represent 2-second averages taken every 32 seconds. Representative statistical errors are indicated. The next two profiles are 16-second averages of the proton channels greater than 212 keV and 675 keV (SD1 and SD2). The bottom curve gives the proton intensity above 235 keV (GM). Note that the GM counting rate is approximately 10% of that of SD1 ( $E > 212$  keV) as would be expected based upon the relative geometric factors (Table 1). The abrupt rise in the GM rate



**Table 2. A Comparison of Interplanetary and Polar Proton Fluxes  
( $E > 0.3$  MeV) Taken by Explorer-35 and OV1-17  
During the 21 March Solar Flare<sup>a</sup>**

<u>EXPLORER - 35</u>			<u>OV1 - 17</u>		
$E_{\text{protons}} > 0.3 \text{ MeV}$					
<u>DATE</u>	<u>U.T.</u>	<u>FLUX</u>	<u>U.T.</u>	<u>FLUX</u>	<u>POLE</u>
21 MARCH	08:00	$\approx 3.8$	—	—	—
21 MARCH	15:00	76	15:00	84	NORTH
21 MARCH	16:00	104	15:30	170	SOUTH
22 MARCH	06:00	408	05:45	640	SOUTH
23 MARCH	03:00	1710	03:30	1280	SOUTH

<sup>a</sup>Integral fluxes ( $\text{cm}^2 \text{ster-sec}^{-1}$ ) from Explorer-35 are 30-minute averages over all pitch angles. Those from OV1-17 are averaged over the polar cap ( $\Lambda > 78^\circ$ ) for pitch angles outside the loss cone.

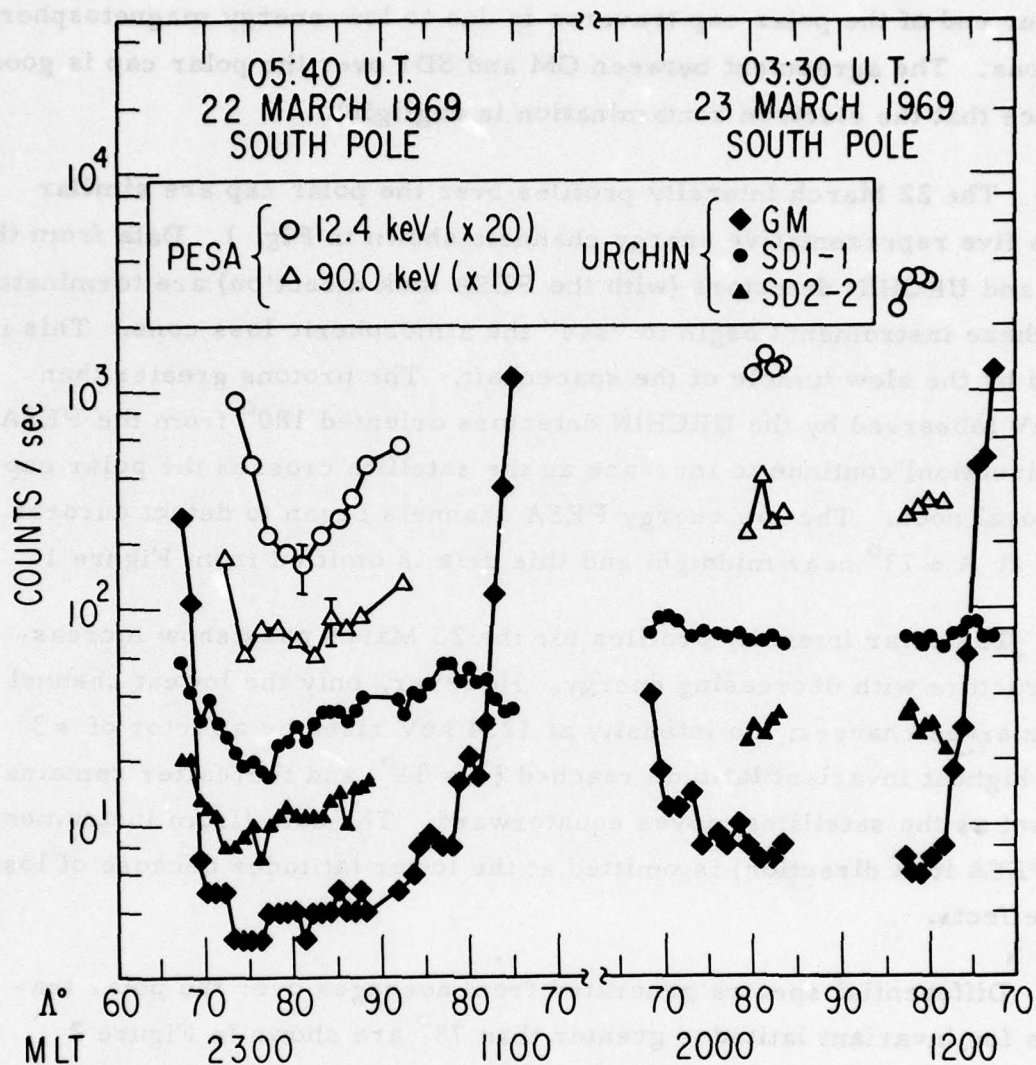


Fig. 1 . Count- rate profiles vs invariant latitude for protons over the South Pole on 22 March and 23 March 1969. Open symbols represent 2-second averages at 12.4 keV and 90 keV multiplied by 20 and 10, respectively. Solid symbols are for 16-second averages of SD1-1, SD2-2, and GM ( $E > 212$ ,  $E > 675$ , and  $E > 235$  keV). Electrons ( $E > 10$  keV) are present when  $GM > 0.1$  SD1. Representative statistical error bars are indicated. Universal time and magnetic local time are also given.

at either end of the polar cap traverse is due to low-energy magnetospheric electrons: The agreement between GM and SD1 over the polar cap is good evidence that the electron contamination is negligible.

The 22 March intensity profiles over the polar cap are similar for the five representative energy channels shown in Fig. 1. Data from the PESA and URCHIN detectors (with the PESA look direction) are terminated when these instruments begin to "see" the atmospheric loss cone. This is caused by the slow tumble of the spacecraft. The protons greater than 200 keV (observed by the URCHIN detectors oriented  $180^\circ$  from the PESA look direction) continue to increase as the satellite crosses the polar cap near local noon. The low energy PESA channels began to detect auroral fluxes at  $\Lambda \approx 73^\circ$  near midnight and this data is omitted from Figure 1.

The polar intensity profiles for the 23 March pass show increasing structure with decreasing energy. However, only the lowest channel show marked changes; the intensity at 12.4 keV rises by a factor of  $\approx 3$  at the highest invariant latitude reached ( $\Lambda \approx 84^\circ$ ) and thereafter remains constant as the satellites moves equatorward. The data (from instruments with PESA look direction) is omitted at the lower latitudes because of loss cone-effects.

Differential spectra generated from averages over the polar traverses for invariant latitudes greater than  $78^\circ$  are shown in Figure 2 (22 March) and Figure 3 (23 March). The solid triangles are the PESA measurements from 12.4 keV to 185 keV. The solid circles at 250 keV and 500 keV are data from four URCHIN integral channels obtained in the manner described in the previous section. Injun-5 data are shown as open circles at 0.39 MeV, 0.54 MeV, 0.72 MeV, and 1.1 MeV. The Injun-5 data also were taken over the South Pole and within a few hours of the OV1-17 measurements. The error bars represent counting statistics and include background subtraction for the PESA data. The points represent



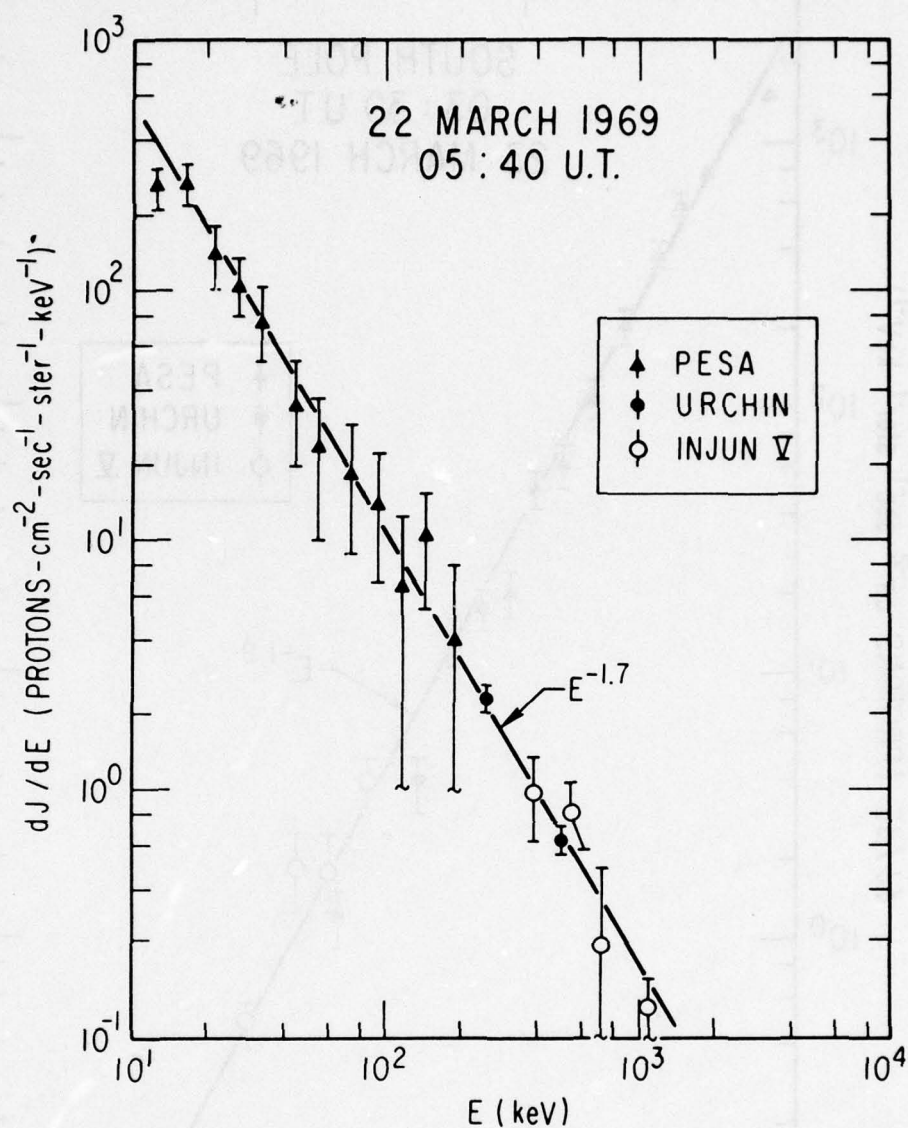


Fig. 2. Differential spectrum of 0.0124 MeV to 1.1 MeV solar protons on 22 March 1969. The solid triangles (PESA) and solid circles (URCHIN) are polar cap averages ( $\Lambda > 78^\circ$ ); the open circles are Injun-5 averages ( $\Lambda > 75^\circ$ ) taken 4 hours before OV1-17 measurements. The solid line is a weighted least squares fit (of the form  $dJ/dE = AE^{-m}$ ) to all points. No relative normalization has been made between the three data sets.

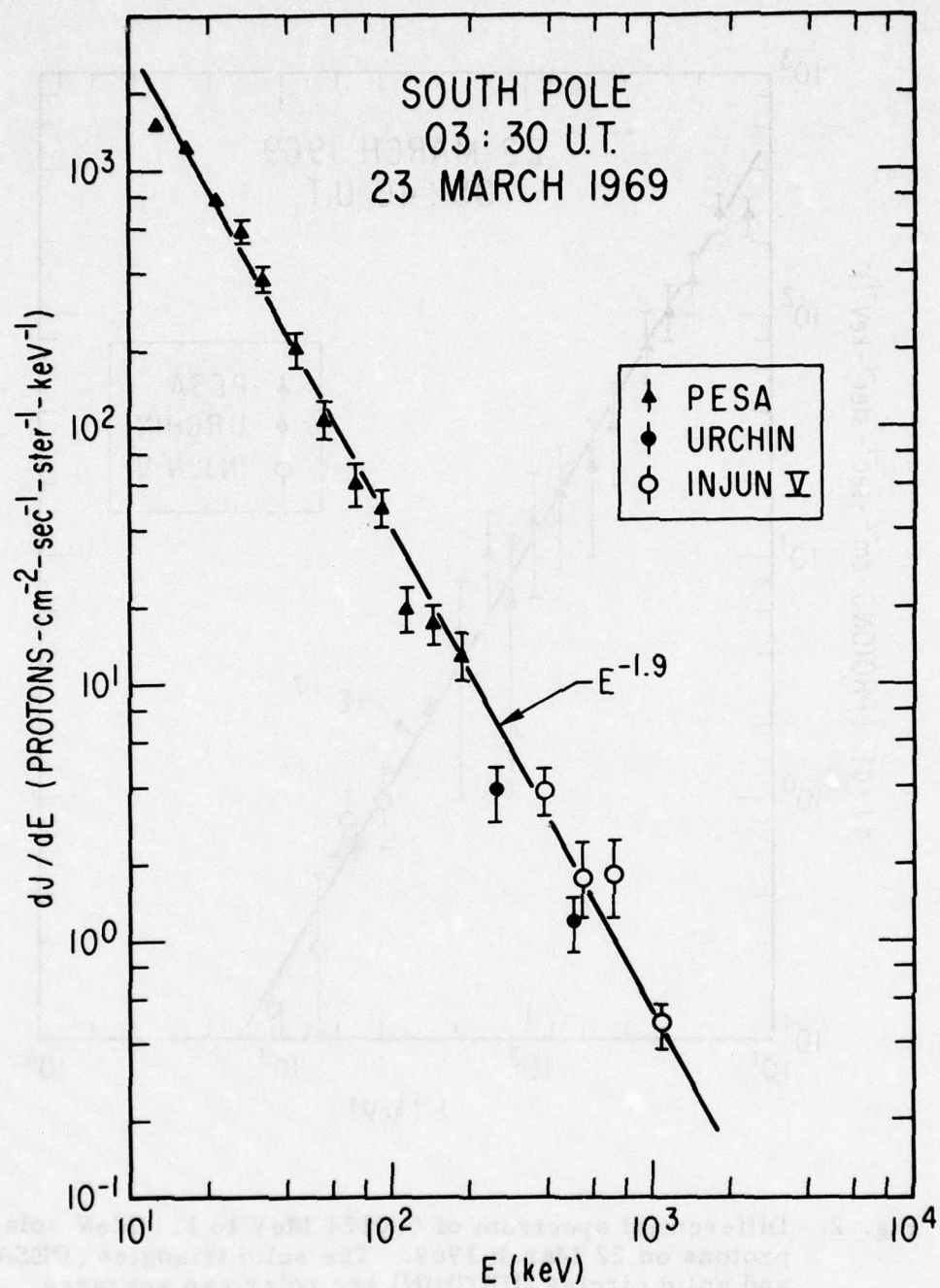


Fig. 3. Solar proton spectrum on 23 March 1969. The format is the same as in Fig. 2.

absolute fluxes. No relative normalization has been made between the three data sets. A single power-law function is seen to represent both spectra over two orders of magnitude in energy.



## DISCUSSION

The evidence that solar protons down to 12 keV have access to the polar caps is presented summarily. a) The polar profiles are very similar at all energies (12 keV to 700 keV). However, the 23 March profiles show some increased structure at lower energies. b) The slopes of the differential spectra obtained on 22 and 23 March are virtually the same. The ratio of the  $E \geq 478$  keV proton intensity to the  $E \geq 320$  keV proton intensity observed on both days by Explorer-35 also indicates a similar spectral dependence. c) The least-squares fit to the differential spectra produces a factor of three increase for the observed proton flux over the polar cap between 0540 UT on 22 March and 0330 UT on 23 March. This agrees well with the increase seen by Explorer-35 in the  $E \geq 320$  keV interplanetary proton intensity for the same time period.

The only interplanetary observations of protons above solar wind energy and below a few hundred keV were reported by Frank (1970). He observed fluxes of  $\approx 20$  keV protons during two solar particle events, but no detailed correlation of the low energy fluxes with the energetic particles ( $E \geq 1$  MeV) was seen. As Frank points out, one would expect differences in the relative intensities as a function of time over such a large energy range. It is clear that the correlation observed in the OV1-17 data between low and high energies is somewhat fortuitous and would not be the case in general. Indeed, a low energy enhancement on 23 March produces a softer spectrum than had been observed on the previous day. This behavior is not unexpected; for example, 1 MeV and 10 MeV protons show many detailed differences during an event in spite of a general temporal correlation.

The increase of 12 keV protons on 23 March at  $\Lambda \approx 84^\circ$ , which is not observed at the higher energies, occurs well above the trapping boundary as defined by the low energy electrons ( $\Lambda \approx 76^\circ$ ). It seems most probable that this soft-proton enhancement encountered by OV1-17 is not of magnetospheric origin and occurs on field lines accessible to

solar protons. However, lacking interplanetary intensities at these energies, it is impossible to be certain of the origin of this enhancement.

Solar protons of a few tens of keV would provide a useful way for studying anisotropic access to the magnetosphere. The interplanetary proton anisotropies appears to be larger and last longer at the lowest energies currently observed (Engelman et al., 1971; Haskell and Hynds, 1971; Van Allen et al., 1971). Low-energy events are also observed to occur more frequently, with higher intensities, with more structure, and with longer duration than those at higher energies (Singer, 1970; Armstrong et al., 1970; Ogilvie and Arens, 1971). A lowering of the energy threshold to  $\approx 10$  keV would be expected to continue these trends.

Comparison of low-energy solar protons with interplanetary measurements will provide useful probes in determining whether or not these particles (with their smaller gyroradii) have direct entry through the magnetotail to the polar caps. The rigidity for a 12 keV proton is the same as that for a 4.3 MeV electron, and solar electrons with energies a factor of 10 lower have been observed to populate the polar caps with negligible time delays.

We have presented evidence for the presence of solar protons down to 12 keV over the polar caps following the 21 March 1969 solar flare. Further elucidation of the behavior of these low-energy protons and their frequency of occurrence requires long-term measurements and, in particular, correlation of interplanetary and polar-cap intensities.

## ACKNOWLEDGMENTS

The authors would like to thank Dr. J. R. Stevens for his efforts in the design and calibration of the PESA instrument and Dr. J. A. Van Allen for providing the Explorer-35 and Injun-5 data.

BLANK PAGE



# REFERENCES

- Armstrong, T. P., S. M. Krimigis, and R. W. Behannon, Proton fluxes at 300 keV associated with propagating interplanetary shock waves, J. Geophys. Res., 75, 5980, (1970).
- Burrows, J. R., A review of the magnetospheric characteristics of solar flare particles, COSPAR Symposium on November 1969 Solar Particle Event, to be published.
- Engelmann, J., R. J. Hynds, G. Morfill, F. Axisa, A. Bewick, A. C. Durney, and L. Koch, Penetration of solar protons over the polar cap during the February 25, 1969 event, J. Geophys. Res., 76, 4245, (1971).
- Frank, L. A., On the presence of low-energy protons ( $5 \leq E \leq 50$  keV) in the interplanetary medium, J. Geophys. Res., 75, 707, (1970).
- Haskell, G. P., and R. J. Hynds, Mechanisms for the injection of protons into the magnetosphere, Earth's Particle and Fields, ed. by B. M. McCormac, to be published, D. Reidel, Dordrecht, Holland, (1972).
- Lanzerotti, L. J., Solar energetic particles and the configuration of the magnetosphere, Rev. of Geophys., 10, 379 (1972).
- Ogilview, K. W., and J. F. Arens, Acceleration of protons by interplanetary shocks, J. Geophys. Res., 76, 13 (1971).

Paulikas, G. A., J. B. Blake, and A. L. Vampola, Solar particle observations over the polar caps, Particle and Fields in the Magnetosphere, ed. by B. M. McCormac, D. Reidel, Dordrecht, Holland, (1970).

Singer, S., and M. D. Montgomery, Detailed directional and temporal properties of solar energetic particles associated with propagating interplanetary shock waves, J. Geophys. Res., **76**, 6628 (1971).

Van Allen, J. A., J. F. Fennell, and N. F. Ness, Asymmetric access of energetic solar protons to the earth's North and South polar caps, J. Geophys. Res., **76**, 4262 (1971).

# XI. OBSERVATIONS OF RING-CURRENT PROTONS AT LOW ALTITUDES\*

P. F. Mizera and J. B. Blake

## ABSTRACT

Variable intensities of geomagnetically trapped protons with energies between 12.4 keV to 500 keV were observed during times encompassing the magnetic storms on 20 March and 24 March 1969. These proton fluxes were measured for  $1.0 < L < 1.1$  near the magnetic equator, at local midnight with solid-state detectors and an electrostatic analyzer on the low-altitude satellite OV1-17. Marked increases of proton intensities at energies below 100 keV occurred during this magnetically disturbed period. In contrast, proton intensities with  $E > 200$  keV were observed to be a relatively stable and permanent feature of this region of the near-earth magnetosphere. The altitude range for these measurements was 400 to 470 kilometers, a region where the atmospheric density is such that charge-exchange lifetimes are comparable with the bounce period and short relative to the longitudinal drift period. The OV1-17 observations of proton intensities with  $E > 200$  keV are in substantial agreement with similar measurements taken with the AZUR satellite and reported recently by Moritz (Zeitschrift für Geophysik, in press 1972). Further, the lower energy proton intensities, measured with OV1-17 instrumentation, support Moritz's suggestion that the source of these low-altitude protons is the ring current.

\*This paper has also been published as TR-0073(3260-20)-8, The Aerospace Corporation, El Segundo, California (12 January 1973) and in the Journal of Geophysical Research 78, 1058-1062 (1973).



# CONTENTS

ABSTRACT .....	315
INTRODUCTION .....	319
SATELLITE AND INSTRUMENTATION .....	321
RESULTS .....	323
DISCUSSION .....	329
ACKNOWLEDGMENTS .....	333
REFERENCES .....	335

# FIGURES

1. Low-Altitude Protons with Energy Greater Than 212 keV .....	322
2. Equatorial Proton Count-Rates as a Function of Energy for 19-22 March 1969 .....	325
3. Equatorial Proton Count-Rates on 19 March, Showing Quiescent Intensities, and on 25 March, Showing Post-Storm Intensities .....	326
4. Differential Energy Spectrum of the Low-Altitude Equatorial Protons Measured on 25 March 1969 by OV1-17 .....	328

## INTRODUCTION

Observations are presented and discussed in this paper of short-lived proton fluxes with energies between 12.4 keV and 500 keV. These measurements were made near the geomagnetic equator at altitudes between 400 km and 470 km during March and April 1969. The atmospheric density in this region of space is such that the protons have lifetimes comparable with the bounce period and short compared to the longitudinal drift period; therefore, a continuous strong source is required to maintain this transiently-trapped population. The present work shows that the low-altitude protons with energies near 40 keV exhibit greater variability than those at higher energies and are correlated with the growth of the ring current during magnetic storms. Maximum intensity variations up to a factor of 12.5 were observed at low energies; while during the same time period protons with energies greater than 200 keV showed variations of less than a factor of 3.

Observations of protons with energies between 250 keV and 1.5 MeV and in the same region of the magnetosphere have been reported recently by Moritz (1972) and Hovestadt et al. (1972) from instruments aboard the German research satellite AZUR. Their measurements showed a rather constant proton intensity at low altitudes near the magnetic equator. Moritz (1972) has suggested that the source of these fluxes is the outer-zone proton population. Briefly, a charge-exchange interaction of an outer-zone proton with the exospheric hydrogen results in a fast neutral. At low altitude this neutral is stripped and the resulting proton is trapped until a third atmospheric interaction

removes it. The measurements reported here support this hypothesis of Moritz.

Intense equatorial fluxes with energies less than 10 keV, observed at altitudes below 800 km, have been reported by Heikkila (1971). There is speculation that these low-energy measurements may shed light on previously reported intense fluxes of low-energy particles at low altitudes (See references in Heikkila (1971)). The question naturally arises as to a possible correlation between these low-energy proton observations and those at higher energies reported by the AZUR experimenters. The measurements reported here bridge the energy gap between 10 keV and 250 keV and indicate that the fluxes observed by Heikkila (1971) are much too intense to be directly related with the OV1-17 and AZUR observations.



## SATELLITE AND INSTRUMENTATION

A brief description of the particle instrumentation and satellite parameters follows; a more detailed description can be found in Mizera et al. (1972).

The instruments were flown aboard the OV1-17 (1969-025A) satellite. This spacecraft was injected into an orbit with a perigee of 398 km, an apogee of 468 km and an inclination of 99 degrees. During the time period covered by this paper the intended gravity-gradient stabilization was not achieved and aspect information was obtained from a three-axis magnetometer and a solar aspect sensor.

Proton fluxes from 12.4 keV to 185 keV were measured in 12 contiguous intervals by a cylindrical electrostatic analyzer (PESA). The PESA had a geometric factor of  $4.7 \times 10^{-3} E_0 \text{ cm}^2\text{-ster}$  where  $E_0$  is the central energy of a particular channel; e.g., for the 12.4 keV channel, 1 count/sec indicated a differential flux of 17.1 protons/cm<sup>2</sup>-ster-sec-keV.

Protons of higher energies were measured by an array of solid-state detectors (URCHIN) which provided four integral thresholds of 212 keV, 310 keV, 425 keV, and 675 keV along three mutually perpendicular axes. Each detector had a geometric factor of  $4.7 \times 10^{-2} \text{ cm}^2\text{-ster}$  and a 20 degree conical field of view.

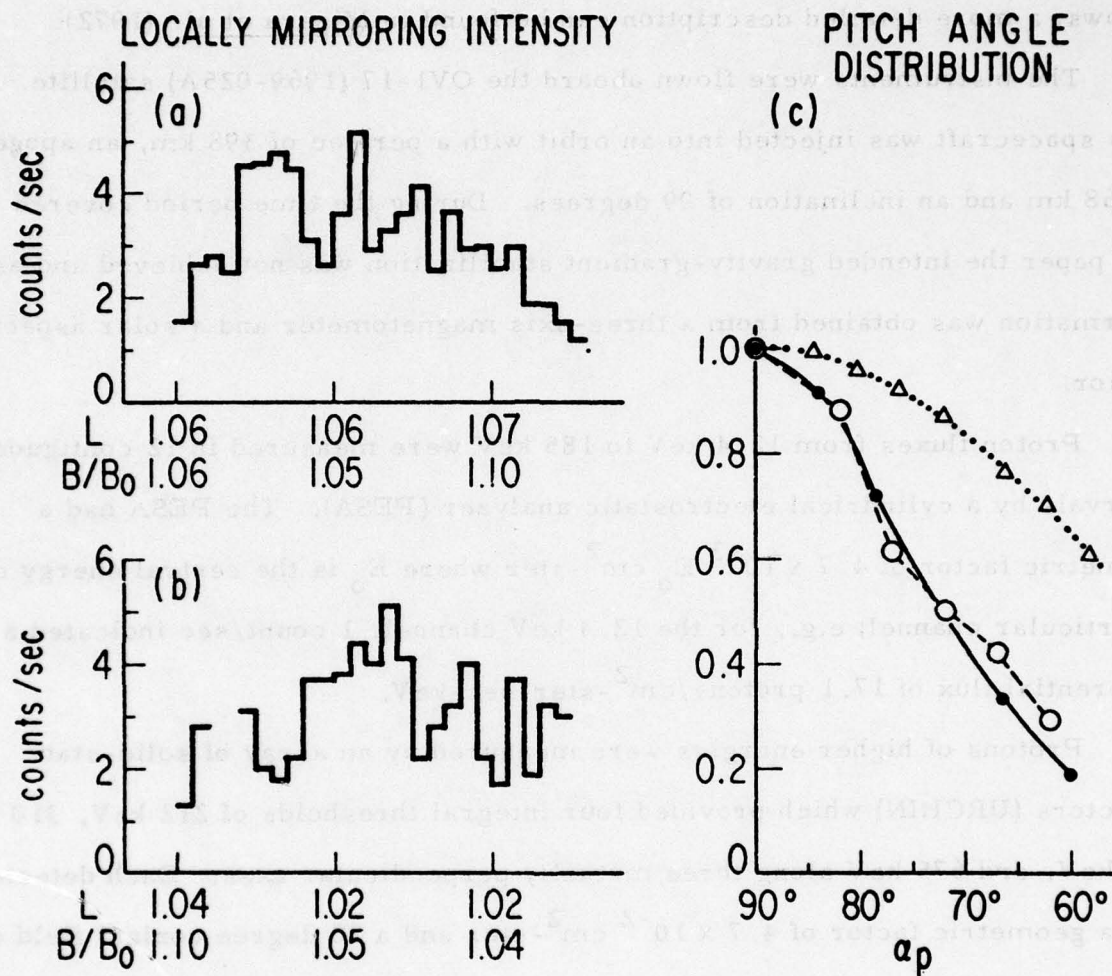


Fig. 1. Low-Altitude Protons with Energy Greater Than 212 keV.

## RESULTS

The data presentation is divided chronologically into two intervals during 1969, the period covering the 20 and 24 March magnetic storms and that of the 28 April magnetic storm. The earlier measurements were obtained when both the low-energy (PESA) and medium-energy (URCHIN) instruments were operational. At this time the satellite had a random tumble which prevented a detailed study of the proton intensity as a function of a pitch-angle. Pitch-angle measurements taken near 28 April were obtained when the satellite was spinning along one axis; however, only the URCHIN was still operational.

Two equatorial, low-altitude passes near local midnight are presented in Fig. 1a and 1b and show four-second count-rate averages of mirroring protons with energies greater than 212 keV. The former data were taken on 26 April, the latter on 28 April. The peak intensity of these protons was located near the magnetic equator and remained relatively constant before, during and after the 28 April storm. The absolute intensities were essentially the same as the intensities greater than 250 keV measured by Moritz (1972) some seven months subsequent to the OV1-17 observations.

The open circles in Fig. 1c show the pitch-angle distribution for protons with energies greater than 212 keV measured at the equator and averaged over the time period from 26 April to 30 April 1969. The solid curve is the pitch-angle distribution predicted by Moritz using the geometry of the outer-zone low-energy proton population as the source. The open triangles show the pitch-angle distribution that would result from an isotropic source distribution and particle lifetime inversely proportional to the atmospheric density at the mirror points.



Figure 2 shows a time history of low-altitude protons from the 12.4 keV - 185 keV differential channels and the 212 keV and 310 keV integral channels from 19 March to 22 March 1969. These measurements are for locally mirroring particles, near the magnetic equator, at local midnight and covering times before, during and after the 20 March storm. The sudden commencement occurred around 2000 UT on 19 March and the main phase began near 0300 UT on 20 March when a maximum magnetic field depression of 87 $\gamma$  was recorded. The first histogram (shown at the bottom of Fig. 2) displays the quiescent profile prior to this magnetic storm. Count-rates of the PESA were at or near background and represent an upper limit on the proton intensities in the energy interval of 12.4 keV to 185 keV. The second histogram of data, taken 2 hours after main phase, shows that enhancements occurred at low energies. The peak count-rates moved to higher energies during the storm recovery up to a maximum energy near 55 keV. There was no statistically significant increase of higher energy protons throughout this entire time period.

A more dramatic example of enhanced low-energy fluxes at low altitudes occurred following the large magnetic storm of 24 March 1969 when the  $D_{st}$  index reached -274  $\gamma$  in an eight-hour time period. Figure 3 shows measurements taken at 1400 UT on 25 March near local midnight, approximately 36 hours after main phase. Increased count-rates were seen in all energy channels relative to the quiescent values of 19 March, also shown in Fig. 3. The largest enhancements (up to a factor of 12.5) were observed for protons with energies between 32 keV and 90 keV. Higher energy protons, with energies greater than 212 keV and 310 keV, showed intensity increases of less than a factor of 3.

CHANNEL ENERGY (keV)

1	12.4
2	16.2
3	21.0
4	27.2
5	33.0
6	42.5
7	55.0
8	71.6
9	93.0
10	115
11	141
12	185
14	>212
15	>310

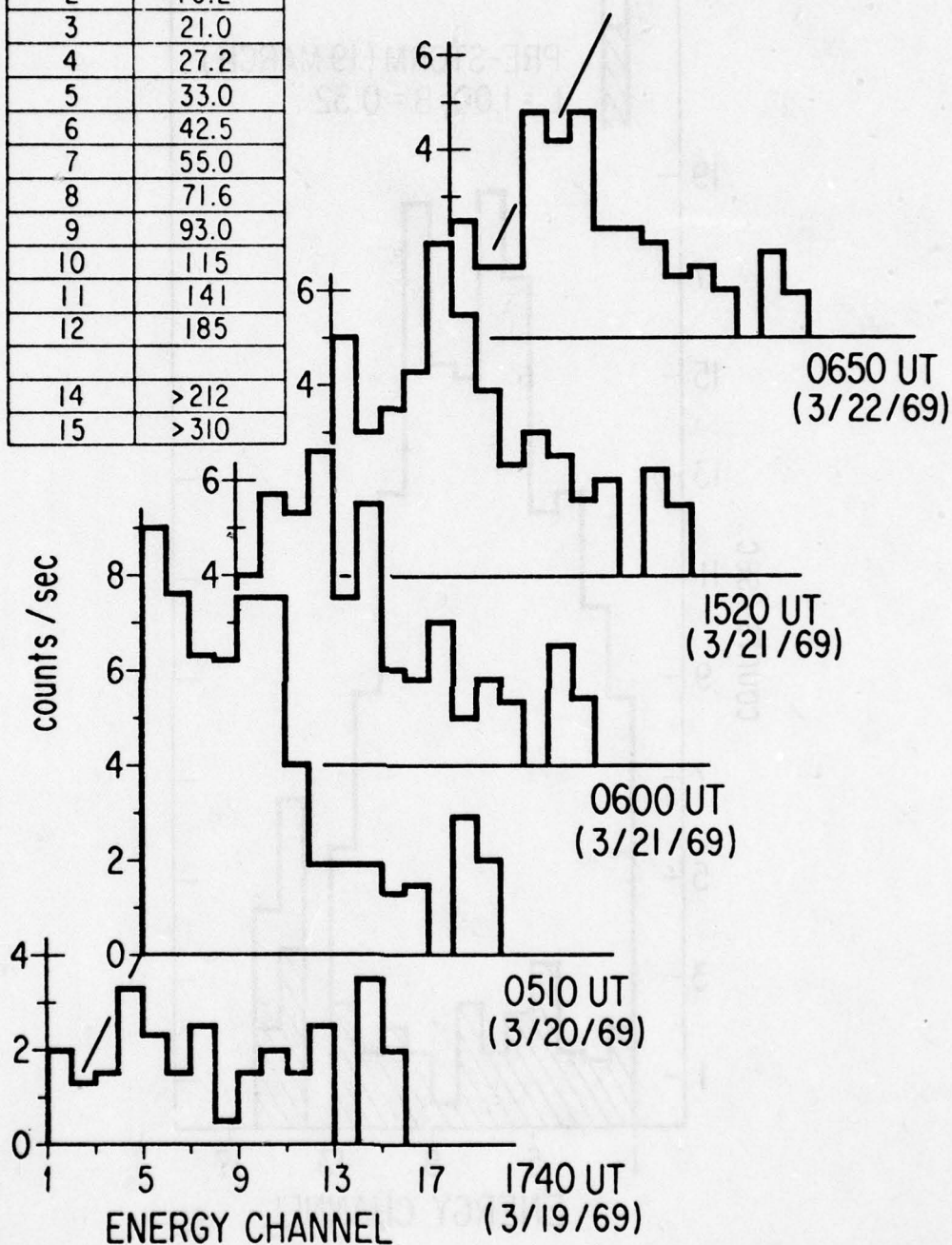


Fig. 2. Equatorial Proton Count-Rates as a Function of Energy for 19-22 March 1969.

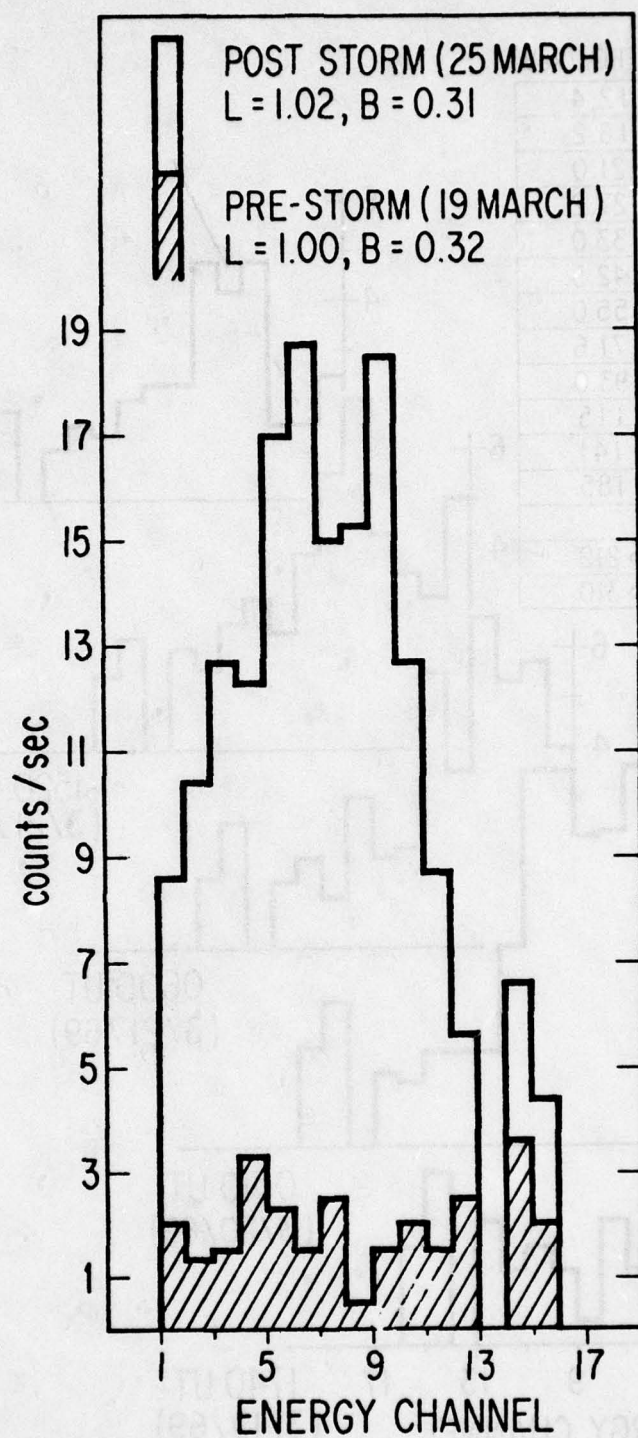


Fig. 3. Equatorial Proton Count-Rates on 19 March, Showing Quiescent Intensities, and on 25 March, Showing Post-Storm Intensities.



The differential spectrum of protons from 12.4 keV to 500 keV (calculated from the measurements taken on 25 March) is shown in Fig. 4. The dashed line through the points is drawn to guide the eye. Included in this data are two points near 350 keV and 700 keV taken from Moritz (1972) and were obtained on 11 March 1970 following a magnetic storm of magnitude similar to the 24 March 1969 event.



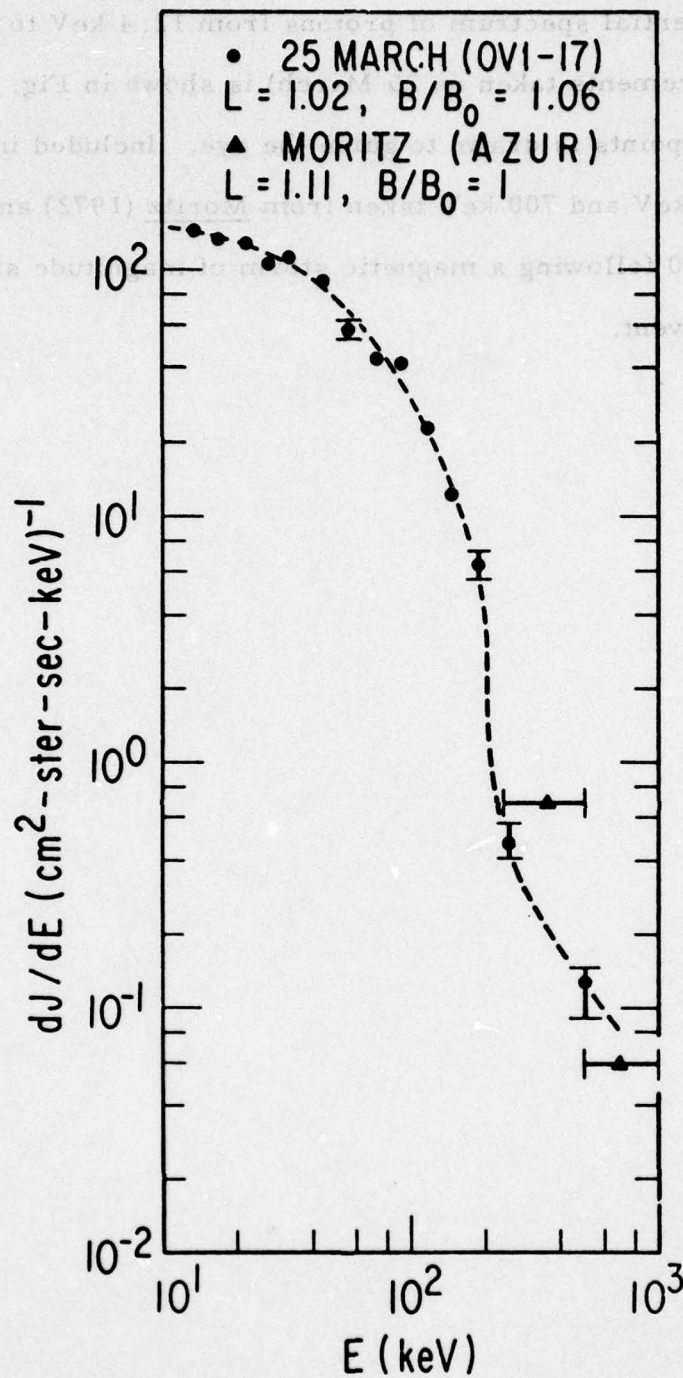


Fig. 4. Differential Energy Spectrum of the Low-Altitude Equatorial Protons Measured on 25 March 1969 by OV1-17.

## DISCUSSION

The observations reported in this paper of 200 keV protons with intensities approaching  $100/\text{cm}^2\text{-ster-sec}$  confirm the results of Moritz (1972) and Hovestadt et al. (1972). The OV1-17 data were taken at relatively quiet times at altitudes between 400 km and 470 km near the magnetic equator. These fluxes were observed to have anisotropic pitch-angle distributions peaked at  $90^\circ$  and are well represented by the calculations of Moritz (shown in Fig. 1c) which use an empirical model of the outer-zone proton population as the source. Also shown in Fig. 1c is a calculated pitch-angle distribution which results from a low-altitude isotropic source distribution and by assuming a loss rate proportional to the atmospheric density at the mirror point. The resulting flat pitch-angle distribution is due to the small changes in atmospheric density as a function of equatorial pitch angle in this region of the magnetosphere. Thus the observed pitch-angle distribution results primarily from the geometry of the high-altitude source.

The extension of the theory of Moritz (1972) to lower energy protons leads to the prediction that the low-altitude protons should reflect the spatial and temporal behavior of the ring current. For example, the lifetime against charge exchange of 200 keV protons near 410 km is short compared with the gradient drift period:  $\tau_q \approx 1.3 \text{ sec}$ ;  $\tau_D / \tau_q > 10^4$ . An atomic oxygen density of  $1.2 \times 10^8/\text{cm}^3$  was taken from CIRA (1965) for moderate solar activity at 2200 LMT; a charge-exchange cross-section of  $10^{-17} \text{ cm}^2$  was taken from Allison (1958). The gradient drift period (in minutes) at the equator is given by  $\frac{44}{LE}$ , with E in MeV and L in units of Earth radii, (Hess, 1968). For the case of 40 keV protons, the difference between the charge-exchange lifetime and this gradient drift period is even greater:  $\tau_q \approx 0.1 \text{ sec}$ .  $\tau_D / \tau_q > 6 \times 10^5$ .



At high altitudes, ion-cyclotron instabilities appear to be the major loss mechanism for the storm-time ring current (Cornwall et al., 1971); therefore the temporal evolution of the low-altitude protons cannot be predicted solely by charge-exchange considerations. Nevertheless, variability of the low-altitude proton fluxes must be the direct result of the ring-current temporal variations whatever their cause since the near-earth proton fluxes must track the source with essentially zero time delay. In particular, the changes in the ring current known to occur during magnetic storms should be seen at the low altitudes. The time profiles in Fig. 2 show that this variability exists particularly at energies near the peak of the ring current. The ion-cyclotron instability phenomenon, generated by the enhanced ring-current, drives the equatorial proton pitch-angle distributions towards isotropy (Cornwall et al., 1971) and therefore, the geometry of this source differs from the quiet-time outer-zone proton population. Definitive pitch-angle measurements at ring-current energies are not available from the OV1-17 instrument, but a flatter distribution than that measured (Fig. 1c) is predicted and verified by limited pitch-angle measurements obtained while the spacecraft was randomly tumbling.

It is impossible to give a quantitative description of the low-altitude proton intensities without a detailed knowledge of the storm-time ring current. Since the charge-exchange cross-sections are strongly energy dependent and are not simple functions of energy over the range of interest (12 keV to 500 keV), the energy spectrum of the energetic neutrals generated in the outer zone would not be simply related to the parent proton spectrum. Furthermore, the peak intensity of the storm-time ring current will occur, in general, at different

altitudes than that of the quiet-time outer-zone protons. The production rate of energetic neutrals is directly proportional to the local ambient hydrogen density which decreases radially as the 4th or 5th power of an Earth's radius near  $L=3$  (Meier, 1970). In spite of these complexities; based on the quantitative analysis delineated by Moritz (1972), one would predict that the low-altitude spectrum should peak near the energy region where the maximum intensity of the ring current occurs. This behavior is observed in the data shown in Fig. 3 and in Fig. 4.

The magnitude of the ring current intensity required to provide the enhanced fluxes observed at low altitudes following the 24 March storm can be estimated qualitatively using the transformation given by Moritz (1972). This involves calculating the probability of neutralizing protons near the peak of the ring current and stripping the resulting energetic hydrogen atoms near the point of observation. The low-altitude flux of  $95/\text{cm}^2\text{-ster-sec-keV}$  at 40 keV measured on 25 March requires a ring-current differential flux of  $10^6$  to  $10^7/\text{cm}^2\text{-ster-sec-keV}$ . It is assumed that the peak of the energetic neutral source was located near or slightly outside of the plasmapause [the latter was near  $L = 3.5$  at midnight during the time of interest, C. R. Chappell, private communication]. The following relevant parameters were used:

$$\rho(\text{H}) = 2 \times 10^2 \text{ H/cm}^3 \text{ (Meier, 1970), } \sigma_{10}(\text{H}) = 1.4 \times 10^{-16} \text{ cm}^2, \sigma_{10}(\text{O}) = 1.87 \times 10^{-16} \text{ cm}^2 \text{ and } \sigma_{01}(\text{O}) = 2.01 \times 10^{-16} \text{ cm}^2 \text{ (Allison, 1968).}$$

Taking into consideration the assumptions implicit in this calculation, the result is in reasonable agreement with ring-current observations of Frank (1970).

If the energy input to the upper atmosphere (by the double charge-exchange process) is to compete with solar or auroral energy inputs, extremely large outer-zone fluxes would be required. An estimate of this intensity needed to provide a low-altitude energy flux of  $1 \text{ erg/cm}^2 \text{-ster-sec}$  is obtained from data presented here. The maximum energy flux greater than 10 keV was approximately  $10^{-4} \text{ ergs/cm}^2 \text{-ster-sec}$  between 20 March to 25 March. Increasing this flux by a factor of  $10^4$  would require ring-current fluxes approaching  $10^{10}/\text{cm}^2 \text{-ster-sec}$  near 40 keV. Thus, the low-altitude equatorial observations (presented here) suggest that high-altitude proton fluxes cannot provide an energy input to the atmosphere comparable to that from solar or auroral phenomena.



# O

## ACKNOWLEDGMENTS

The authors wish to thank Given Boyd and Elaine Platz for their assistance in the data reduction and analysis.

BLANK PAGE

# REFERENCES

- Allison, S. K., Experimental Results on Charge-Changing Collisions of Hydrogen and Helium Atoms and Ions at Kinetic Energies above 0.2 keV, Rev. Mod. Phys., 30, 1137, 1958.
- Cornwall, J. M., F. V. Coroniti, and R. M. Thorne, Unified Theory of SAR Arc Formation at the Plasmopause, J. Geophys. Res., 76, 4428, 1971.
- Frank, L. A., Direct Detection of Asymmetric Increases of Extraterrestrial 'Ring Current' Proton Intensities in the Outer Radiation Zone, J. Geophys. Res., 75, 1263, 1970.
- Heikkila, W. J., Soft Particle Fluxes near the Equator, J. Geophys. Res., 76, 1076, 1971.
- Hess, W. H., The Radiation Belt and Magnetosphere, Blaisdell Publishing Co., Waltham, Mass., 1968.
- Hovestadt, D., B. Hausler, and M. Scholer, Observation of Energetic Particles at Very Low Altitudes Near the Geomagnetic Equator, Phy. Rev. Letters, 28, 1340, 1972.
- Meier, R. R., Observations of Lyman -  $\alpha$  and the Atomic Hydrogen Distribution in the Thermosphere and Exosphere, Space Res. X, 572 1970.
- Mizera, P. F., J. F. Fennell, and J. B. Blake, Polar Cap Measurements of Solar-Flare Protons with Energies Down to 12.4 keV, J. Geophys. Res. 77, 4845, 1972.
- Moritz, J., Energetic Protons at Low Equatorial Altitudes: A Newly Discovered Radiation Belt Phenomenon and its Explanation. To be published in Zeitschrift für Geophysik, 1972. Also, Energetic Protons at Low L-values of the Equatorial Magnetosphere, Fifteenth Plenary Meeting COSPAR, Madrid, May 1972; and postdeadline paper EOS. Trans. AGU, 53, 730, 1972.

## XII. OBSERVATIONS OF PRECIPITATING PROTONS WITH RING-CURRENT ENERGIES\*

P. F. Mizera

### ABSTRACT

Precipitating protons with energies characteristic of the storm-time ring current were measured during all phases of magnetic activity near the low-altitude trapping boundary at midnight. The objective of this study was to examine the energy dependence of the precipitating fluxes as a function of latitude (or  $L$  shell) and relative to the plasmapause and the low-energy isotropic electron enhancements which are associated with the outer-zone boundary. The low-energy measurements, taken by the OV1-17 satellite, covered the time period from 19 March-3 April 1969. Data, provided by the OV1-19 spacecraft during the same time period, were used to extend the measurements to higher energies and to examine pitch-angle distributions. Protons from 12.4 keV to 500 keV were observed to precipitate outside of the plasmapause. The higher energy fluxes peaked equatorward of the low-energy maximum intensities. Statistically, the 55-keV proton boundary tracks the midnight plasmapause with an average poleward displacement of 0.8  $L$ . From these and other related observations, we conclude that ring-current protons are in strong pitch-angle diffusion on closed field lines between the midnight plasmasphere and the electron

\* This paper has also been published as TR-0074(4260-20)-7, The Aerospace Corporation, El Segundo, California (23 December 1973) and in the Journal of Geophysical Research 79, 581-588 (1974).



trapping boundary. These precipitating fluxes are probably responsible for H arcs which are found at the low-latitude termination of the visual auroral forms during magnetic storms. In addition, we estimate that less than 1% of the total ring-current energy is lost by direct particle precipitation.

AD-A050 483

AEROSPACE CORP EL SEGUNDO CALIF IVAN A GETTING LABS F/G 3/2  
COMPILATION OF SCIENTIFIC RESULTS FROM THE SATELLITE OV1-17.(U)  
DEC 77 H R RUGGE F04701-77-C-0078

UNCLASSIFIED

TR-0078(3960-01)-1

SAMSO-TR-77-216

NL

4 OF 4

AD  
A050483



## CONTENTS

ABSTRACT .....	337
INTRODUCTION .....	341
SATELLITES AND INSTRUMENTS .....	343
PRESENTATION AND DISCUSSION OF OBSERVATIONS .....	345
Profiles .....	345
Pitch-Angle Distributions .....	350
Differential Energy Spectra .....	352
Conjugate Observations .....	355
SUMMARY AND DISCUSSION .....	357
ACKNOWLEDGMENTS .....	365
REFERENCES .....	367



## FIGURES

1.	Count rate profiles vs L of 21-keV, 55-keV and 145-keV precipitating protons for a quiet time on 28 March 1969 . . . . .	346
2.	Similar observations as shown in Fig. 1 but taken approximately 4 hours into main phase of a moderate magnetic storm on 3 April 1969 . . . . .	348
3.	Similar observations as the previous 2 figures with the exception that 92-keV electron fluxes from OV1-19 are used to illustrate the trapping boundary . . . . .	349
4.	92-keV electrons and 282-keV protons, measured by OV1-19 on 20 March 1969, illustrate the pitch-angle dependence near the trapping boundary . . . . .	351
5.	Flux vs time plots at all pitch angles for 282-keV, 436-keV and 567-keV protons . . . . .	353
6.	The solid curves are differential spectra of precipitating protons taken on 20 March 1969 . . . . .	354
7.	Count rate profiles of $E > 10$ -keV (solid curves) and $E > 100$ -keV (solid-dashed curves) electrons taken in opposite hemispheres on 3 April 1969 . . . . .	356
8.	All of the 55-keV precipitating proton observations from OV1-17 taken during 19 March to 3 April 1969 . . . . .	359
9.	The critical energy threshold for ion-cyclotron instabilities is shown for a moderately disturbed time ( <u>Thorne and Kennel, 1971</u> ) . . . . .	363

## INTRODUCTION

The midnight morphology of precipitating protons with energies characteristic of the ring current is presented for a series of magnetic disturbances which occurred between 19 March-3 April 1969. Most observations of this type have been for low energies (i. e. ,  $E < 20$  keV) and grouped under the generic term of auroral precipitation. In a survey of high-latitude particle precipitation, Paulikas (1971) has pointed out that comprehensive observations of precipitating protons have been rather limited, especially for energies greater than 10-50 keV. Some proton observations have recently been presented by Burch (1973) for  $E < 23$  keV and by Amundsen et al. (1972) for  $E > 100$  keV.

Large spatial and temporal variations occur in the outer-zone proton population during magnetic storms giving rise to the asymmetric ring current (Frank, 1970; Smith and Hoffman, 1973). Recently, higher energy proton observations suggest that outer-zone trapped fluxes are almost continually in weak pitch-angle diffusion (Berg and Soraas, 1972). However, 40-keV precipitating protons were found by Cornwall et al. (1971a) with isotropic angular distributions in this same region which suggests strong pitch-angle diffusion. Amundsen et al. (1972) reported proton angular distributions that change from anisotropic to isotropic at the poleward termination of the fluxes near midnight.

The earthward termination of the proton ring current is near the evening plasmapause (Russell and Thorne, 1970; Frank, 1971). This is where ion-cyclotron instabilities should result in pitch-angle scattering of ring-current protons (Cornwall et al., 1970; Williams et al., 1973). Cornwall et al. (1971b) have argued that intense ion-cyclotron waves could be generated at the plasmapause from the enhanced ring-current population resulting in

pitch-angle diffusion. The electromagnetic waves serve as the intermediary for the energy transferred from the ring-current protons to the ionospheric electrons. These in turn could excite the atomic oxygen 6300Å line which dominates SAR arc spectra. A good correlation has been shown between the location of SAR arcs and the local plasmopause (Cole, 1970; Chappell et al., 1971). In addition, Cole (1965) has pointed out that SAR arcs would be a feasible sink for the storm ring-current energy and the plasmopause has been shown to be at the earthward edge of the ring current (Russell and Thorne, 1970; Williams et al., 1973).

Pcl micropulsations, attributed to proton ion-cyclotron waves, have been shown to occur inside the plasmopause (Mullen and Heacock, 1972). Eather and Carovillano (1971) invoke this same wave-particle instability to explain the proton aurora at higher latitudes. In a later presentation, Cornwall et al. (1971a) suggested that observations of isotropic 40-keV and 80-keV precipitating protons were the result of such pitch-angle scattering occurring just inside the plasmopause.

The equatorial morphology of the ring current has been discussed in relation to the plasmopause, plasmasheet and the electron trapping boundary (Frank, 1971). The low-latitude trapping boundary has also been used in numerous studies of electron precipitation (Fritz, 1970; Koons et al., 1972; Brown and Stone, 1972). Using similar boundaries as familiar reference points, the spatial and temporal characteristics of precipitating protons with ring-current energies are examined near local midnight.



## SATELLITES AND INSTRUMENTS

Measurements were taken with instruments on the OV1-17 and OV1-19 satellites (1969-025A, -025C). Both spacecraft were launched at 0747 UT on 18 March 1969 into polar orbits in the noon-midnight meridian. OV1-17 was placed in a nearly circular orbit with an apogee of 468 km and a perigee of 398 km. The OV1-19 had an apogee of 5796 km and a perigee of 471 km. During the time interval from 19 March-3 April, the OV1-17 spacecraft had a random tumbling motion while the OV1-19 spacecraft was spin stabilized at 8.4 rpm.

Most of the data presented were obtained from an electrostatic analyzer (PESA) which measured protons from 12.4 keV to 185 keV in 12 contiguous steps and an array (URCHIN) of thin-window geiger tubes and solid-state detectors flown on the OV1-17 satellite. A more detailed description of the instrumentation including geometric factors can be found in Mizera et al. (1972).

Normally the URCHIN measured electrons from  $E > 10$  keV to  $E > 600$  keV in three orthogonal directions. Because the geiger tube threshold for protons was higher than the lowest energy solid-state channel, it was possible to discriminate protons from  $E > 212$  keV to  $E > 675$  keV when electron fluxes were low.

The OV1-19 instruments included a differential electron channel at 92 keV (Vampola, 1971) and proton channels at 282 keV, 436 keV and 567 keV (Stevens et al., 1970). These measurements were used to complement the OV1-17 data.

## PRESENTATION AND DISCUSSION OF OBSERVATIONS

Qualitative features of precipitating protons with energies between 12.4 to 500 keV are shown for a variety of magnetic storm conditions covering times from 19 March-3 April 1969. The fluxes were found near local midnight at low altitudes on L shells between the plasmopause and the low-latitude termination of the auroral zones, just inside the outer zone electron trapping boundary.

### Profiles

A quiet-time profile of precipitating protons taken on 28 March 1969 is shown in Fig. 1. The morphology is illustrated at the top by averaged count rates of precipitating 21-keV, 55-keV and 145-keV protons and the location of the maximum intensity of precipitating protons with  $E > 212$  keV. The high-latitude boundary of the outer zone is illustrated by locally mirroring ( $e_{\perp}$ ) and precipitating ( $e_{\parallel}$ ) electrons with  $E > 10$  keV. The trapping boundary has been discussed in detail by Fritz (1970) who used the ratio of precipitating to mirroring electrons with  $E > 40$  keV. The 40-keV boundary was also compared to electrons with  $E > 10$  keV by Fritz and Gurnett (1965). The spectrum softened as the 40-keV boundary was crossed from low latitudes. Figure 1 and subsequent examples show the location of electrons with  $E > 100$  keV in order to illustrate where the precipitating spectrum softens. For the sake of completeness, the standard 40-keV boundary is estimated between  $L = 7.0$  and  $7.2$  in Fig. 1.

The midnight plasmopause is shown near  $L = 5.5$ . This estimate is based on the empirical method of Chappell (1972) and is discussed in more detail in the following section. Observationally, the maximum intensity of 21-keV precipitating protons is found just inside the low-altitude electron trapping boundary. The maxima of higher energy protons are found on



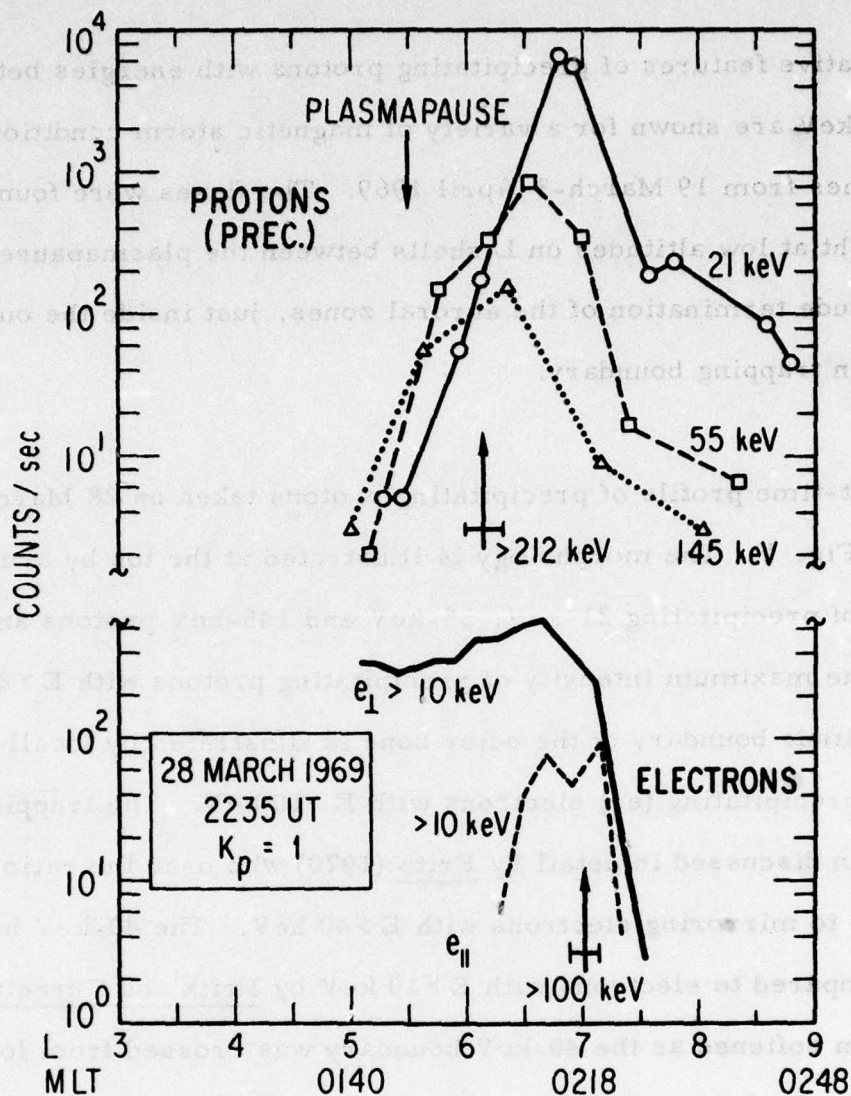


**Fig. 1** Count rate profiles vs L of 21-keV, 55-keV and 145-keV precipitating protons for a quiet time on 28 March 1969. The low-altitude trapping boundary near midnight is shown at the bottom by locally mirroring and precipitating electrons with  $E > 10$  keV. The arrows indicate the plasmopause and the peak of precipitating protons with  $E > 212$  keV and precipitating electrons with  $E > 100$  keV.



lower L shells with the highest energy ( $E > 212$  keV) fluxes observed approximately 0.5 L equatorward of the peak of the 21-keV protons.

The next two examples illustrate particle precipitation in this same region of space during moderate magnetic storms. Figure 2 shows measurements taken on 3 April 1969 approximately 4 hours following a maximum field depression of 87Y ( $D_{st}$ ). The trapping boundary had moved down to  $L \approx 5.4$ , again illustrated by isotropic electrons with  $E > 10$  keV. This change in the trapping boundary represents almost  $5^\circ$  in latitude from the observations during the quiescent period, shown in Fig. 1. The 21-keV precipitating protons maximize at a slightly lower latitude with similar average intensities observed on 28 March. However the storm-time intensities of the higher energy protons, illustrated by the 55-keV and 145-keV protons, are higher than the quiescent fluxes by more than a factor of 10.

Figure 3 shows measurements of precipitating protons taken on 20 March 1969 under similar magnetic conditions as the observations of 3 April. The  $D_{st}$  index again reached -87Y some 3 1/2 hours prior to these measurements. The low-altitude trapping boundary is illustrated by 92-keV electrons observed with the OV1-19 satellite. The OV1-19 was in the opposite hemisphere near the conjugate point. Both sets of observations were taken within 5 minutes of each other. The high-latitude outer-zone boundary was found at  $L \approx 4.6$  near midnight MLT. The 21-keV precipitating proton intensity peaks near the trapping boundary, again poleward of the 55-keV and 145-keV proton maximum intensities. As was the case for the measurements taken on 3 April and shown in Fig. 2, the higher energy proton fluxes

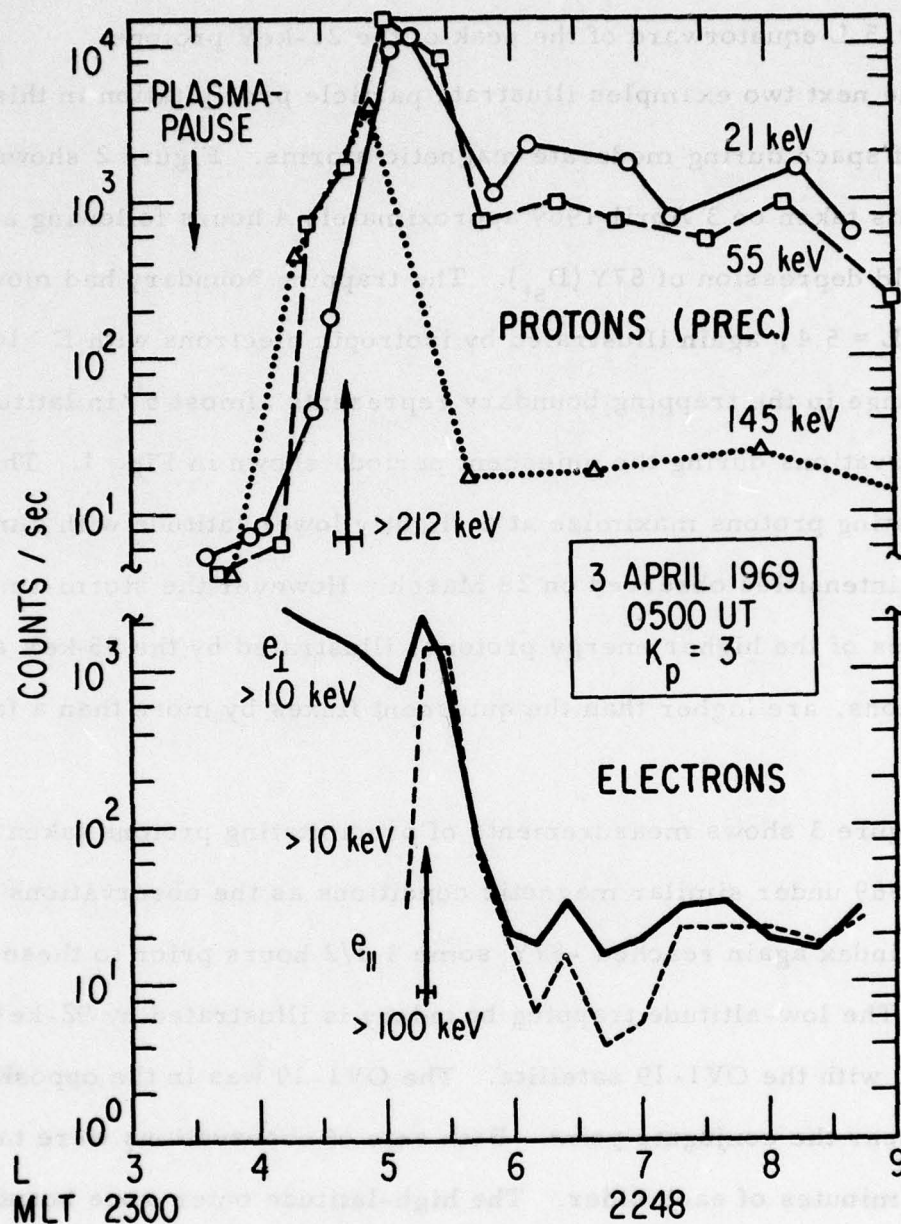


**Fig. 2** Similar observations as shown in Fig. 1 but taken approximately 4 hours into main phase of a moderate magnetic storm on 3 April 1969.

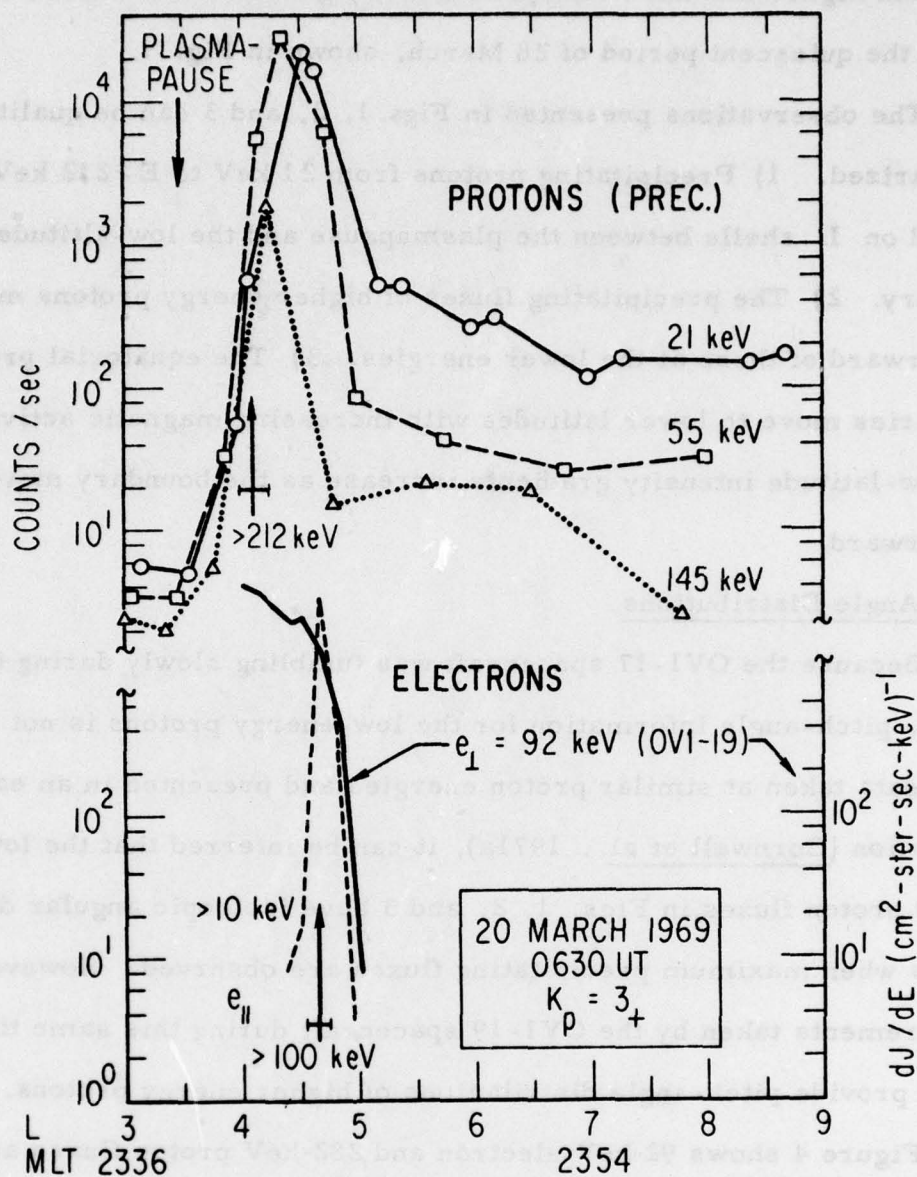


Fig. 3 Similar observations as the previous 2 figures with the exception that 92-keV electron fluxes from OV1-19 are used to illustrate the trapping boundary. The magnetic conditions are almost identical to those on 3 April (Fig. 2).



are much higher and show sharper intensity gradients than those observed during the quiescent period of 28 March, shown in Fig. 1.

The observations presented in Figs. 1, 2, and 3 can be qualitatively summarized. 1) Precipitating protons from 21 keV to  $E > 212$  keV are located on L shells between the plasmapause and the low-altitude trapping boundary. 2) The precipitating fluxes of higher energy protons maximize equatorward of those at the lower energies. 3) The equatorial precipitation boundaries move to lower latitudes with increasing magnetic activity. 4) The low-latitude intensity gradients increase as the boundary moves equatorward.

#### Pitch-Angle Distributions

Because the OV1-17 spacecraft was tumbling slowly during this time period, pitch-angle information for the low-energy protons is not available. From data taken at similar proton energies and presented in an earlier publication (Cornwall et al., 1971a), it can be inferred that the lower energy proton fluxes in Figs. 1, 2, and 3 have isotropic angular distributions when maximum precipitating fluxes are observed. However measurements taken by the OV1-19 spacecraft during this same time period provide pitch-angle distributions of higher energy protons.

Figure 4 shows 92-keV electron and 282-keV proton fluxes as a function of time observed by the OV1-19 satellite on 20 March 1969. The top data set was previously used to define the trapping boundary in Fig. 3. The OV1-19 instruments measure fluxes near  $90^\circ$  pitch angle twice per spin period ( $\sim 8$  sec) and are illustrated by the sharp peaks in Fig. 4. At  $0^\circ$ , the particles are coming down the field line; at  $180^\circ$ , they are reflected. The maximum precipitating flux of 282-keV protons occurs at

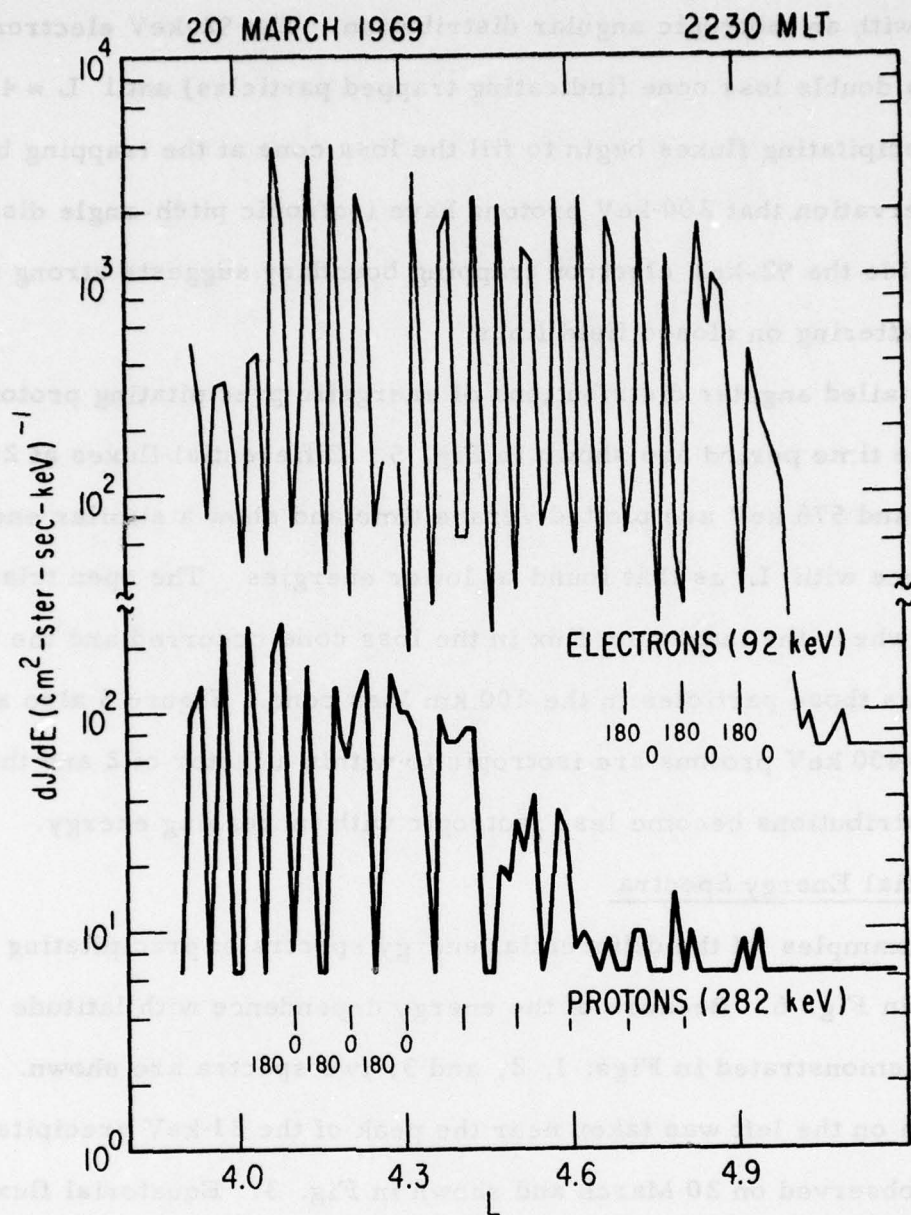


Fig. 4 92-keV electrons and 282-keV protons, measured by OV1-19 on 20 March 1969, illustrate the pitch-angle dependence near the trapping boundary. These data were taken near the conjugate point and within 5 minutes of OV1-17 measurements shown in Fig. 3.

$L = 4.3$  with an isotropic angular distribution. The 92-keV electrons display a double loss cone (indicating trapped particles) until  $L \approx 4.8$  when precipitating fluxes begin to fill the loss cone at the trapping boundary. The observation that 200-keV protons have isotropic pitch-angle distributions inside the 92-keV electron trapping boundary suggests strong pitch-angle scattering on closed field lines.

Detailed angular distributions of energetic precipitating protons for this same time period are shown in Fig. 5. Differential fluxes at 282 keV, 436 keV and 576 keV are plotted versus time and show a similar energy dependence with  $L$  as that found at lower energies. The open triangles indicate where the maximum flux in the loss cone occurred and the width illustrates those particles in the 100 km loss cone. Figure 5 also shows that 200-400 keV protons are isotropic to within a factor of 2 and the pitch-angle distributions become less isotropic with increasing energy.

#### Differential Energy Spectra

Examples of the differential energy spectra of precipitating protons are given in Fig. 6. Because of the energy dependence with latitude previously demonstrated in Figs. 1, 2, and 3; two spectra are shown. The spectrum on the left was taken near the peak of the 21-keV precipitating protons observed on 20 March and shown in Fig. 3. Equatorial fluxes measured by Williams et al. (1973), prior to a magnetic storm and a typical auroral spectrum (Eather and Carovillano, 1971) are shown for comparison.

The spectrum shown at the right of Fig. 6 was taken near the peak of the 200-keV precipitating protons on 20 March. These data include the



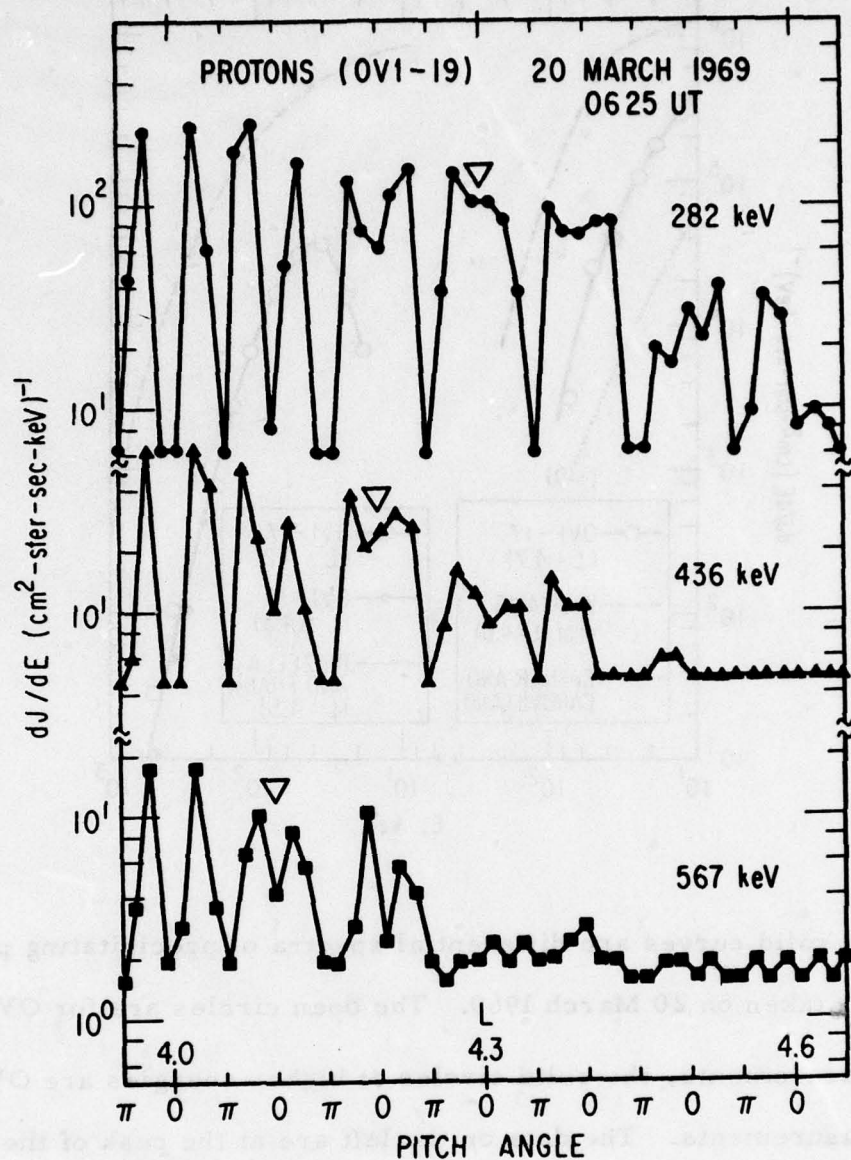


**Fig. 5** Flux vs time plots at all pitch angles for 282-keV, 436-keV and 567-keV protons. This is an expanded plot of the proton trapping boundary shown in Fig. 4. The triangles mark where maximum proton precipitation occurs in the 100 km loss cone illustrated by the width of the symbols.

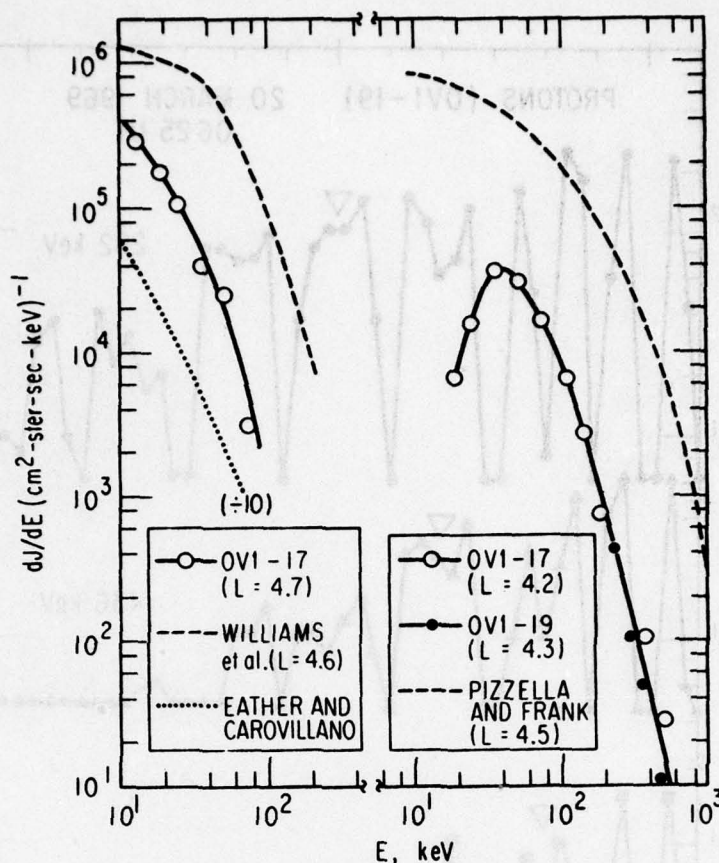


Fig. 6 The solid curves are differential spectra of precipitating protons taken on 20 March 1969. The open circles are for OV1-17 measurements, the solid circles at higher energies are OV1-19 measurements. The data on the left are at the peak of the 21-keV protons at  $L \approx 4.7$ . The data on the right are at the peak of the  $E > 212$  keV protons at  $L \approx 4.2$ . Also shown are equatorial distributions taken by Williams et al. (1973) for a storm-time ring current, by Pizzella and Frank (1971) for averaged quiet-time measurements and a typical auroral precipitation distribution given by Eather and Carovillano (1971).

measurements from the OV1-19 satellite shown in Fig. 5. Implicit in this analysis is the assumption of constant pitch-angle scattering on conjugate field lines over a 5 minute time period. The agreement shown between OV1-17 and OV1-19 data suggests this assumption is valid. Averaged quiet time equatorial fluxes, taken from Pizzella and Frank (1971), are shown for comparison.

#### Conjugate Observations

The data taken on 20 March showed that proton precipitation was relatively constant over a 5 minute time period, at least for  $E > 200$  keV. Figure 7 shows that these conjugate properties at the trapping boundary are apparent over a period of 1 hour. The measurements in the southern hemisphere were previously shown in Fig. 2. The top curves in Fig. 7 illustrate mirroring fluxes measured by the thin-window geiger tubes and the lowest energy channel of solid-state detectors on the OV1-17 satellite. The bottom curves are similar outputs from sensors looking up away from the earth. Both the trapped and precipitating count-rate profiles taken in opposite hemispheres are virtually mirror images of each other suggesting relatively constant pitch-angle scattering of  $E > 10$ -keV electrons and  $E > 200$ -keV protons over a 1 hour time period.

This example also illustrates the comparison of the standard 40-keV trapping boundary with the measurements presented here. The electron spectrum shows an obvious softening toward the high latitude termination of the trapping boundary. This feature has been observed by Fritz and Gurnett (1965) to occur at the standard 40-keV trapping boundary.



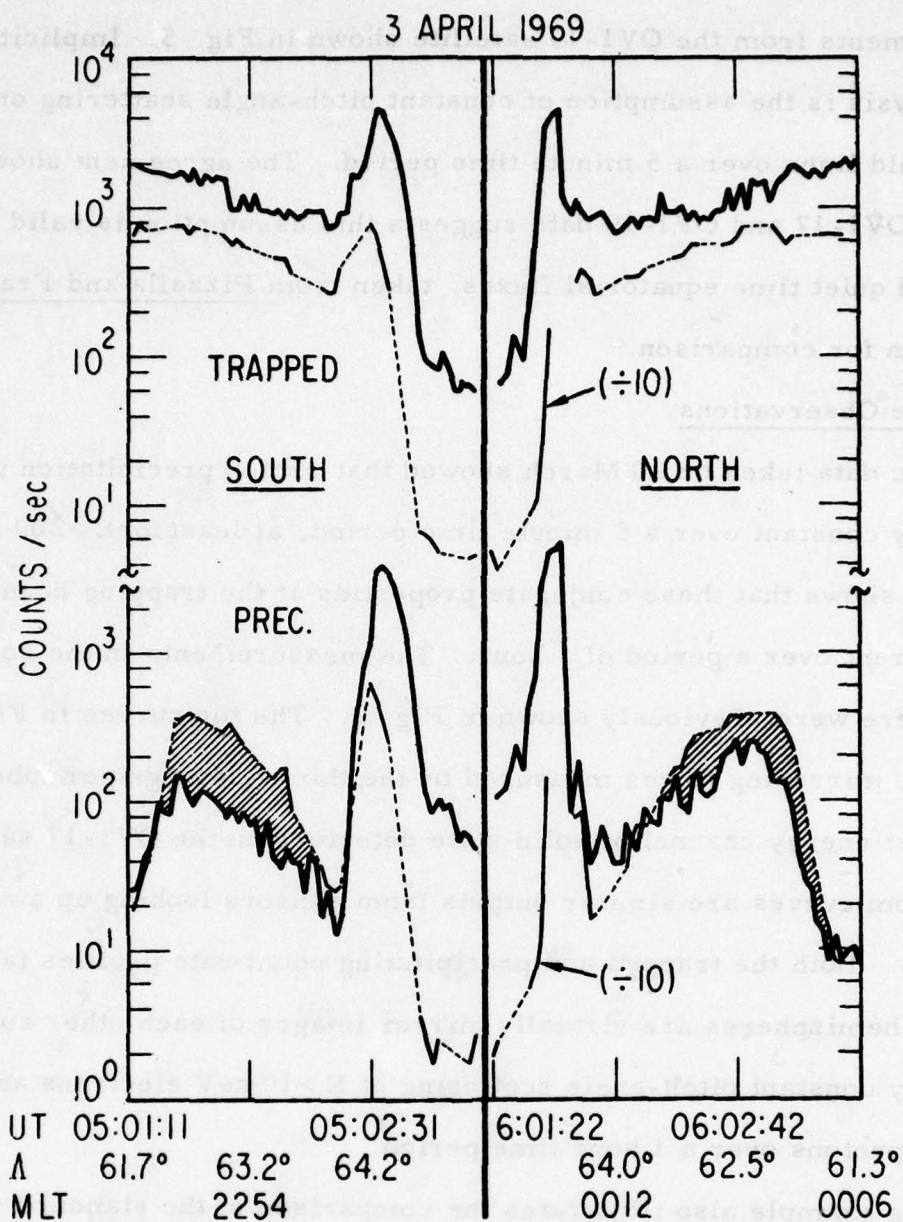


Fig. 7 Count rate profiles of  $E > 10$ -keV (solid curves) and  $E > 100$ -keV (solid - dashed curves) electrons taken in opposite hemispheres on 3 April 1969. The top are trapped particles, the bottom are precipitating particles. The shaded regions show protons with  $E > 212$  keV.

## SUMMARY AND DISCUSSION

A summary of the salient features presented in the previous section is listed below:

1) Precipitating protons with  $12.4 \text{ keV} < E < 500 \text{ keV}$  are observed inside the low-altitude electron trapping boundary near local midnight during all phases of magnetic activity.

2) The count-rate profiles of these protons display a steep low-latitude boundary which moves equatorward during magnetic storms. The peak precipitating fluxes of 21-keV protons usually occur just inside the low-altitude electron trapping boundary delineated by sharp isotropic enhancements of electrons with  $E > 10 \text{ keV}$ . Higher energy protons maximize on lower L shells and with increased intensity during these times. For example, the ratio of 12-keV to 55-keV fluxes was approximately 40 for  $K_p \leq 1$  and approached 1 for  $K_p \leq 3$ . The absolute intensity near 55-keV also increased during moderate magnetic storms by factors of 20-30. However the 12 to 21-keV protons did not show the same large enhancements with increased magnetic activity.

3) The higher energy protons ( $E > 200 \text{ keV}$ ) show pitch-angle distributions which tend toward isotropy over the zenith hemisphere at the peak of the precipitation. The results from Cornwall et al. (1971a) also suggest that isotropy is characteristic of lower-energy angular distributions at the peak of the precipitation.

4) Precipitating protons with  $E > 200 \text{ keV}$  were found simultaneously (Fig. 3 and 4) on the same L shells with similar intensities in opposite hemispheres and with a 1 hour delay (Fig. 7). The protons are found inside

the trapping boundary which suggests that a relatively constant source of precipitating protons was operating on closed field lines for at least 1 hour.

5) The differential spectra of precipitating protons presented here and shown in Fig. 6 are compared with equatorial data. The OV1-17 distribution at low energies agrees well with a precipitation spectrum calculated from an average equatorial ring-current distribution taken from Pizzella and Frank (1971). A disturbed ring-current spectrum taken by Williams et al. (1973) on the  $S^3$ -A satellite is also shown. Both the OV1-17 and  $S^3$ -A data were taken well outside of the midnight plasmapause. Since the OV1-17 proton data were obtained during an injection event, a disturbed equatorial ring-current distribution is probably more appropriate for comparison. However, either a disturbed ring-current distribution with reduced intensity or a quiescent ring current with pitch-angle diffusion compares favorably with OV1-17 data. Higher energy protons ( $E > 40$  keV) show a spectrum similar in shape to the average equatorial distribution given in Pizzella and Frank (1971). At high and low energies, the precipitating intensities are about a factor of 10 lower than those mirroring at the equator.

6) Precipitating protons were observed on L shells poleward of the midnight plasmapause; examples were given in Figs. 1, 2 and 3. Figure 8 shows all OV1-17 low-energy precipitating proton observations from 19 March to 3 April 1969. The  $K_p$  and  $D_{st}$  indices are given for this time period and the arrows between the two indices indicate the times of the OV1-17 measurements presented in Figs. 1, 2 and 3. The L value and the local time of the maximum 55-keV precipitating flux is plotted with the



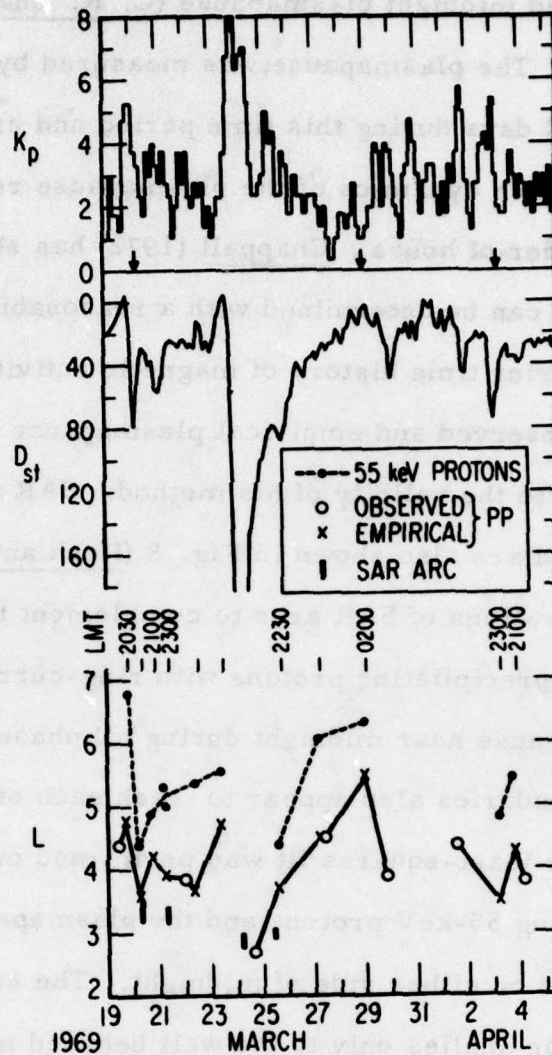


**Fig. 8** All of the 55-keV precipitating proton observations from OV1-17 taken during 19 March to 3 April 1969. The numbers at the top of these circles indicate the hours away from local midnight. The Xs are empirical and Os are measured plasmapause boundaries from Chappell (private communication 1972). SAR arc sightings are shown by vertical bars (Hoch and Smith, 1971b). Also shown are  $K_p$  and  $D_{st}$ .

measured and predicted midnight plasmapause (C. R. Chappell, private communication 1972). The plasmapause was measured by the Ogo-5 spacecraft every 2 1/2 days during this time period and crossed local midnight near  $L = 4$ . The dynamics of the plasmapause require temporal correlations of the order of hours. Chappell (1972) has shown that the midnight plasmapause can be determined with a reasonable degree of confidence using the prior time history of magnetic activity reflected in  $K_p$ . Comparison of observed and empirical plasmapause boundaries in Fig. 8 further attests to the validity of his method. SAR arcs reported during this time period are also shown in Fig. 8 (Hoch and Smith, 1971b).

Using the observations of SAR arcs to complement the plasmapause data, it is shown that precipitating protons with ring-current energies lie outside of the plasmapause near midnight during all phases of magnetic activity. The two boundaries also appear to track each other during this time period. A linear least-squares fit was performed on the low-latitude edge of the precipitating 55-keV protons and the plasmapause for local times within two hours on either side of midnight. The empirical determination of the plasmapause applies only to the well behaved nightside region (Chappell, 1972). However the shape of the plasmapause is known to change slightly with local time over this four-hour interval. The computed plasmapause was corrected from midnight to the local time of the OV1-17 measurements using the average plasmapause profile of Chappell (1972). The maximum correction was  $\approx 0.7L$ .

The above analysis gave a slope of 1, an intercept of  $0.8L$  and a standard deviation of 0.12. The inner boundary of electrons with  $E > 10$  keV was also fit to the plasmapause in the same way. The best fit was obtained with a slope of 1, an intercept of  $1.1L$  and a standard deviation of 0.09. In



the framework of this limited data set, these results mean that the cold plasma boundary of the plasmasphere and the hot plasma precipitation boundaries are well correlated during all phases of magnetic activity. In addition, the average low-latitude boundaries of precipitating ring-current protons and 10-keV electrons are 0.8L and 1.1L poleward of the evening plasmapause.

Hoch et al. (1971a) reported separations of  $0.5 < \Delta L / Re < 1.1$  between a SAR arc and H arcs during a particularly large magnetic storm on 24 March 1969. More typical separations of 1.6L were found over a 4 year study (Kleckner and Hoch, 1973). Ichikawa et al. (1969) reported a good correlation of the relative motion of the earthward termination of visual auroral forms and SAR arcs. These and other related observations suggest that the class of precipitating protons presented here are responsible for the diffuse H arcs commonly observed at the lowest latitudes of the auroral zones (Belon et al., 1969). This observation is further substantiated by the comparison of the high-latitude differential spectrum in Fig. 6 with an average proton auroral spectrum (Eather and Carovillano, 1971). The term H arcs is perhaps more appropriate to describe the OV1-17 observations than proton aurora. The spatial extent of our observations has been shown to be much more localized at lower latitudes and the average energy is higher than is usually associated with proton aurora.

One of the most interesting properties of similar observations presented in Cornwall et al. (1971a) was the delineation of the omnidirectional differential flux into two categories by a single function with a  $L^{-4}$  dependence. The two classes were determined from the pitch-angle distributions of the



low-altitude fluxes measured by the OV1-15 satellite in 1968. From that study, 40-keV protons were observed with isotropic angular distributions when a flux threshold of  $6.3 \times 10^7 \text{ L}^{-4} (\text{cm}^2 \text{-sec-keV})^{-1}$  was exceeded.

For a comparison with the OV1-17 observations, we convert from the omnidirectional to a directional flux threshold by dividing by  $2\pi$ . For example at  $L = 4.5$  the predicted isotropic directional flux threshold at 40 keV is  $\approx 2.5 \times 10^4 (\text{cm}^2 \text{-ster-sec-keV})^{-1}$ . The 40-keV precipitating flux observed near  $L = 4.5$  on 20 March 1969 was  $\approx 4 \times 10^4 (\text{cm}^2 \text{-ster-sec-keV})^{-1}$ , almost a factor of 2 higher than the empirical flux threshold which separated weak from strong pitch-angle scattering (Cornwall et al., 1971a).

An indepth discussion of pitch-angle scattering of ring-current protons is beyond the scope of this presentation. However there has been a great deal of interest recently in proton ion-cyclotron wave instabilities (Cornwall et al., 1970; Eather and Carovillano, 1971; Williams et al., 1973; Coroniti et al., 1972). These instabilities are predicted when the particle energy exceeds the magnetic energy per particle (Cornwall et al., 1970). Figure 9 shows how the energy threshold varies with  $L$  for a moderately disturbed time (Thorne and Kennel, 1971). Ring-current protons and ion cyclotron wave interactions are predicted to occur at the plasmopause ( $L \approx 4$ ) and  $L$  values greater than 6.

Precipitating protons measured by OV1-17 on 3 April and 20 March (Figs. 2 and 3) are found on  $L$  shells where the energy threshold is well above the energy of the precipitating protons and also display the incorrect energy dependence. Figure 9 shows that the higher energy protons are equatorward of the lower energy protons; the precipitating protons have a steeper energy gradient and the maximum precipitation occurs well outside of the plasmopause.

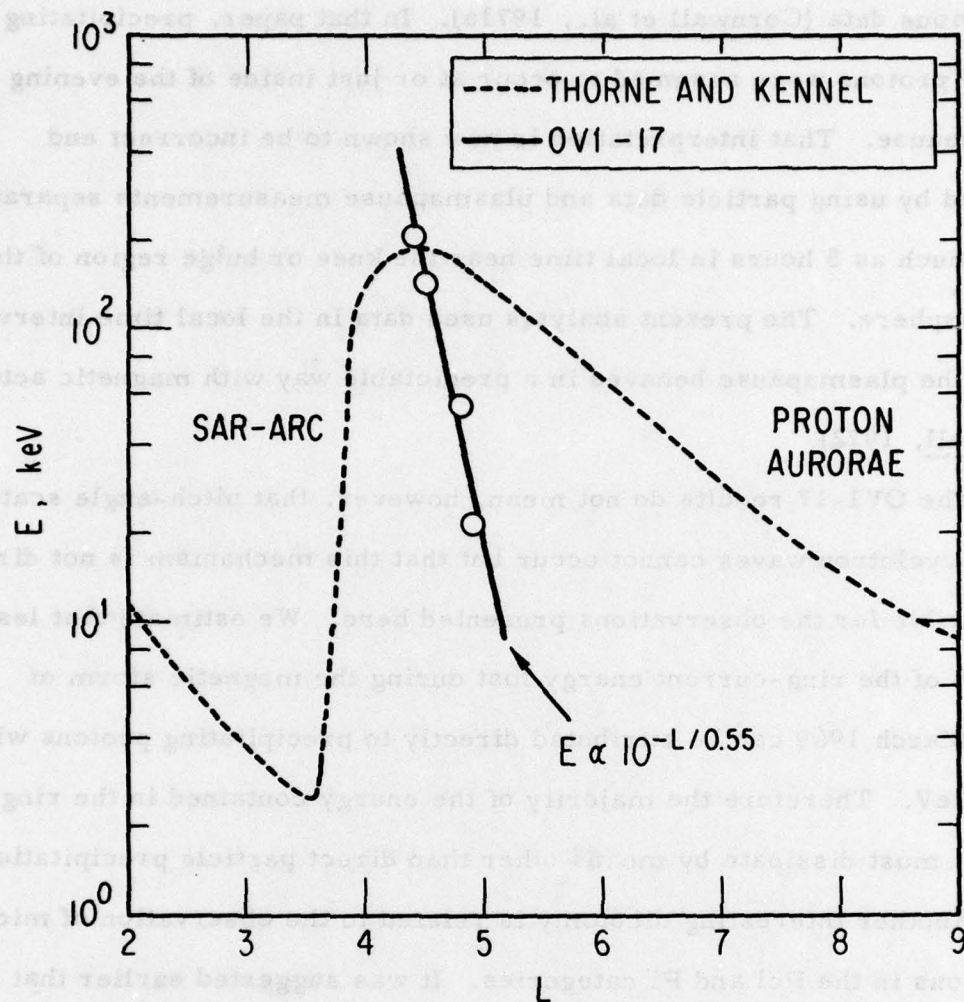


**Fig. 9** The critical energy threshold for ion-cyclotron instabilities is shown for a moderately disturbed time (Thorne and Kennel, 1971). The open circles are OV1-17 measurements taken on 20 March and 3 April 1969. Both data sets are for similar magnetically disturbed times as that used for the calculated threshold.

These present results are in disagreement with the interpretation of previous data (Cornwall et al., 1971a). In that paper, precipitating 40-keV protons were assumed to occur at or just inside of the evening plasmopause. That interpretation is now shown to be incorrect and resulted by using particle data and plasmopause measurements separated by as much as 5 hours in local time near the knee or bulge region of the plasmasphere. The present analysis used data in the local time interval where the plasmopause behaves in a predictable way with magnetic activity (Chappell, 1972).

The OVI-17 results do not mean, however, that pitch-angle scattering by ion-cyclotron waves cannot occur but that this mechanism is not directly responsible for the observations presented here. We estimate that less than 1% of the ring-current energy lost during the magnetic storm of 19-20 March 1969 can be attributed directly to precipitating protons with  $E > 12$  keV. Therefore the majority of the energy contained in the ring current must dissipate by means other than direct particle precipitation.

Another interesting dicotomy is related to the observation of micropulsations in the Pcl and Pi categories. It was suggested earlier that Pcl events, measured inside the plasmopause, are the result of proton ion-cyclotron waves (Mullen and Heacock, 1972). Similar ground measurements showed that Pi observations are found outside the plasmopause and are possibly related to the inner edge of the plasmasheet (Heacock et al., 1971). It is in this region, between the plasmopause and the trapping boundary, where precipitating ring-current protons, with equatorial gyrofrequencies near those of Pi micropulsations, are found with the higher energy fluxes peaking equatorward of those at lower energy.



# ACKNOWLEDGMENTS

The author wishes to thank Drs. J. F. Fennell and M. Schulz for many helpful discussions throughout this investigation.

# References

- Amundsen, R., F. Soraas, H. R. Lindalen, and K. Aarsnes, Pitch-Angle Distributions of 100 to 300 keV Protons Measured by the Esro IB Satellite, J. Geophys. Res., 77, 556 (1972).
- Belon, A. E., J. E. Maggs, T. N. Davis, K. B. Mather, N. W. Glass, and G. F. Hughes, Conjugacy of Visual Auroras during Magnetically Quiet Periods, J. Geophys. Res., 74, 1, (1969).
- Berg, L. E. and F. Soraas, Weak Pitch Angle Diffusion of Protons, J. Geophys. Res., 77, 6708 (1972).
- Brown, J. W. and E. C. Stone, High-Energy Electron Spikes at High Latitudes, J. Geophys. Res., 77, 3384 (1972).
- Burch, J. L., High latitude Proton Precipitation and Light Ion Density Profiles During the Magnetic Storm Initial Phase, J. Geophys. Res., 78 (1973).
- Chappell, C. R., K. K. Harris and G. W. Sharp, Ogo-5 Measurements of the Plasmapause during Observations of Stable Red Arcs, J. Geophys. Res., 76, 2357 (1971).
- Chappell, C. R., Recent Satellite Measurements of the Morphology and Dynamics of the Plasmasphere, Rev. Geophys. Space Phys., 10, 951 (1972).
- Cole, K. D., Stable Auroral Red Arcs, Sinks for Energy of  $D_{st}$  Main Phase, J. Geophys. Res., 70, 1689 (1965).
- Cole, K. D., Relationship of Geomagnetic Fluctuations to Outer Magnetospheric Phenomena, J. Geophys. Res., 75, 4216 (1970).
- Cornwall, J. M., F. V. Coroniti and R. M. Thorne, Turbulent Loss of Ring-Current Protons, J. Geophys. Res., 75, 4699 (1970).
- Cornwall, J. M., H. H. Hilton and P. F. Mizera, Observations of Precipitating Protons in the Energy Range  $2.5 \text{ keV} \leq E \leq 200 \text{ keV}$ , J. Geophys. Res., 76, 5220 (1971a).

- Cornwall, J. M., F. V. Coroniti and R. M. Thorne, Unified Theory of SAR Arc Formation at the Plasmapause, J. Geophys. Res., 76, 4428 (1971b).
- Coroniti, F. V., R. W. Fredricks and Roscoe White, Instability of Ring Current Protons beyond the Plasmapause during Injection Events, J. Geophys. Res., 77, 6243 (1972).
- Eather, R. H., and R. L. Carovillano, The Ring Current as the Source Region for Proton Auroras, Cosmic Electrodyn., 2, 105 (1971).
- Frank, L. A., Direct Detection of Asymmetric Increases of Extraterrestrial Ring Current Proton Intensities in the Outer Radiation Zone, J. Geophys. Res., 75, 1263 (1970).
- Frank, L. A., Relationship of the Plasma Sheet, Ring Current, Trapping Boundary, and Plasmapause near the Magnetic Equator and Local Midnight, J. Geophys. Res., 76, 2265 (1971).
- Fritz, T. A., and D. A. Gurnett, Diurnal and Latitudinal Effects Observed for 10-keV Electrons at Low Satellite Altitudes, J. Geophys. Res., 70, 2485 (1965).
- Fritz, T. A., Study of the High-Latitude, Outer-Zone Boundary Region for  $\geq 40$ -keV Electrons with Satellite Injun 3, J. Geophys. Res., 75, 5387 (1970).
- Heacock, R. R., A. J. Mullen, V. P. Hessler, C. Sucksdorff, M. Kivinen and E. Kataja, Correlations of Ogo-5 Plasmapause Crossing with Observations of type Pi Micropulsations on the Ground, Ann. Geophys., 27, 477 (1971).
- Hoch, R. J., C. R. Batishko and K. C. Clark, Simultaneous Spectrographic Triangulation of a SAR Arc and a Hydrogen Arc, J. Geophys. Res., 76, 6185 (1971a).
- Hoch, R. J., and L. L. Smith, Location in the Magnetosphere of Field Lines Leading to SAR Arcs, J. Geophys. Res., 76, 3079 (1971b).
- Ichikawa, T., T. Old and J. S. Kim, Relationship Between a Monochromatic Auroral Arc of 6300Å and a Visible Aurora, J. Geophys. Res., 74, 5819 (1969).



- Kleckner, E. W. and R. J. Hoch, Simultaneous Occurrences of Hydrogen Arcs and Mid-Latitude Stable Auroral Red Arcs, J. Geophys. Res., 78, 1187 (1973).
- Koons, H. C., A. L. Vampola and D. A. McPherson, Strong Pitch-Angle Scattering of Energetic Electrons in the Presence of Electrostatic Waves Above the Ionospheric Trough Region, J. Geophys. Res., 77, 1771 (1972).
- Mizera, P. F., J. F. Fennell and J. B. Blake, Polar-Cap Measurements of Solar-Flare Protons with Energies down to 12.4 keV, J. Geophys. Res., 77, 4845 (1972).
- Mullen, A. J. and R. R. Heacock, Correlation of Ground-based Measurements of Structured Pcl Micropulsations with Ogo -5 Plasmopause Observations, Ann. Geophys., 28, 519 (1972).
- Paulikas, G. A., The Patterns and Sources of High-Latitude Particle Precipitation, Rev. Geophys. Space Phys., 9, 659 (1971).
- Pizzella, G. and L. A. Frank, Energy Spectrums for Proton ( $200\text{eV} \leq E \leq 1\text{ MeV}$ ) Intensities in the Outer Radiation Zone, J. Geophys. Res., 76, 88 (1971).
- Russell, C. T. and R. M. Thorne, On the Structure of the Inner Magnetosphere, Cosmic Electrodyn., 1, 67 (1970).
- Smith, P. H. and R. A. Hoffman, Ring Current Particle Distributions During the Magnetic Storms of December 16-18, J. Geophys. Res., 78, 4731 (1973).
- Stevens, J. R., E. F. Martina and R. S. White, Proton Energy Distributions from 0.060 to 3.3 MeV at 6.6 Earth Radii, J. Geophys. Res., 75, 5373 (1970).

Thorne, R. M. and C. F. Kennel, Locating the Magnetospheric Ring Current,  
Comments on Astrophys. and Space Phys. III, 115, (1971).

Vampola, A. L., Access of Solar Electrons to Closed Field Lines, J. Geophys.  
Res., 76, 36 (1971).

Williams, D. J., T. A. Fritz and A. Konradi, Observations of Proton Spectra  
( $1.0 \leq E_p \leq 300$  keV) and Fluxes at the Plasmopause, J. Geophys. Res., 78,  
4751 (1973).



## THE IVAN A. GETTING LABORATORIES

The Laboratory Operations of The Aerospace Corporation is conducting experimental and theoretical investigations necessary for the evaluation and application of scientific advances to new military concepts and systems. Versatility and flexibility have been developed to a high degree by the laboratory personnel in dealing with the many problems encountered in the nation's rapidly developing space and missile systems. Expertise in the latest scientific developments is vital to the accomplishment of tasks related to these problems. The laboratories that contribute to this research are:

**Aerophysics Laboratory:** Launch and reentry aerodynamics, heat transfer, reentry physics, chemical kinetics, structural mechanics, flight dynamics, atmospheric pollution, and high-power gas lasers.

**Chemistry and Physics Laboratory:** Atmospheric reactions and atmospheric optics, chemical reactions in polluted atmospheres, chemical reactions of excited species in rocket plumes, chemical thermodynamics, plasma and laser-induced reactions, laser chemistry, propulsion chemistry, space vacuum and radiation effects on materials, lubrication and surface phenomena, photo-sensitive materials and sensors, high precision laser ranging, and the application of physics and chemistry to problems of law enforcement and biomedicine.

**Electronics Research Laboratory:** Electromagnetic theory, devices, and propagation phenomena, including plasma electromagnetics; quantum electronics, lasers, and electro-optics; communication sciences, applied electronics, semiconducting, superconducting, and crystal device physics, optical and acoustical imaging; atmospheric pollution; millimeter wave and far-infrared technology.

**Materials Sciences Laboratory:** Development of new materials; metal matrix composites and new forms of carbon; test and evaluation of graphite and ceramics in reentry; spacecraft materials and electronic components in nuclear weapons environment; application of fracture mechanics to stress corrosion and fatigue-induced fractures in structural metals.

**Space Sciences Laboratory:** Atmospheric and ionospheric physics, radiation from the atmosphere, density and composition of the atmosphere, aurorae and airglow; magnetospheric physics, cosmic rays, generation and propagation of plasma waves in the magnetosphere; solar physics, studies of solar magnetic fields; space astronomy, x-ray astronomy; the effects of nuclear explosions, magnetic storms, and solar activity on the earth's atmosphere, ionosphere, and magnetosphere; the effects of optical, electromagnetic, and particulate radiations in space on space systems.

THE AEROSPACE CORPORATION  
El Segundo, California

. . .